

**USING DRONES TO MONITOR CROP HEALTH, WATER  
STRESS, AND CROP WATER REQUIREMENTS FOR  
IMPROVING CROP WATER PRODUCTIVITY IN THE  
CONTEXT OF PRECISION AGRICULTURE IN  
SMALLHOLDER CROPLANDS**

Report to the  
**WATER RESEARCH COMMISSION**

by

**T Mabhaudhi, M Sibanda, A Clulow, S Gokool, VGP Chimonyo,  
O Mutanga, J Odindi, J Magidi and V Naiken**

Centre for Transformative Agricultural and Food Systems  
School of Agricultural, Earth and Environmental Sciences  
University of KwaZulu-Natal, Pietermaritzburg, South Africa

**WRC Report No. 2971/1/23**

**ISBN 978-0-6392-0480-2**

**June 2023**



**WATER  
RESEARCH  
COMMISSION**

**Obtainable from**

Water Research Commission  
Bloukrans Building, 2<sup>nd</sup> Floor  
Lynnwood Bridge Office Park  
4 Daventry Street  
Lynnwood Manor  
PRETORIA

[orders@wrc.org.za](mailto:orders@wrc.org.za) or download from [www.wrc.org.za](http://www.wrc.org.za)

**DISCLAIMER**

This report has been reviewed by the Water Research Commission (WRC) and approved for publication. Approval does not signify that the contents necessarily reflect the views and policies of the WRC, nor does mention of trade names or commercial products constitute endorsement or recommendation for use.

## EXECUTIVE SUMMARY

Remote sensing and earth observation facilities have emerged as the most optimal non-invasive method of monitoring crops, and they offer fast methods of monitoring and estimating crop productivity parameters. Remote sensing (RS) provides spatial and temporal information on crop responses to dynamic environmental conditions or information that relates directly to LAI. RS data has helped derive important crop parameters such as LAI, water use efficiency, chlorophyll, and biomass fraction of photosynthetically active radiation. However, most freely available Earth observation datasets, such as Landsat and Sentinel 2 multispectral images, are too coarse for mapping heterogeneous, fragmented smallholder croplands. They tend to mask out critical information required to characterise crop attributes.

Meanwhile, unmanned aerial vehicle systems offer invaluable remotely sensed data suitable for estimating crop health, productivity, and water use in smallholder croplands. UAV remote sensing technologies offer maximum flexibility in terms of temporal resolution since the flying times are user-determined. Their ability to fly at low altitudes, portability and generation of very high spatial resolution data of up to 5 cm makes them more suitable for farm-scale research than satellite remotely sensed data. Drones, therefore, can play an important role in reducing risk and vulnerability while ensuring sustained crop-water productivity. The application of drones in agriculture in South Africa could contribute to food and water security and help the country achieve the Sustainable Development Goals (SDG) on alleviating hunger and poverty and providing enough clean water and sanitation to all by 2030, SDGs 1, 2 and 6 respectively. The focus is to use drones to systematically monitor crop development at the field level and provide agro-met information in real-time, improve water use efficiency and productivity and irrigation scheduling in smallholder farming. The project will assess crop health through high spatial resolution drones and NDVI analysis, monitor crop evapotranspiration, and develop high-resolution irrigated maps and datasets on water use, water productivity, potential yield, and potential yield evapotranspiration. These will benefit farmers in making on-field decision-making and preparedness.

The project aimed to systematically monitor crop development and provide agro-met information in real-time using drones. Specifically, to assess crop health by analysing real-time NDVI derived from drone imagery and monitor crop evapotranspiration at the field scale for the farmer to make on-field decisions. The study was conducted in a maize crop field on a smallholder farm in Swayimane within the KwaZulu-Natal province, South Africa (29°31'24''S and 30°41'37'' E), covering an area of 2699.005 m<sup>2</sup>. Maize seedlings were sown on 8 February 2021 and harvested on 26 May 2021, having a total growth cycle of 108 days. The study was conducted throughout the phenological stages of maize. Maize phenology is generally divided into vegetative stages (which range from emergence to tasselling according to the number of fully expanded leaves) and reproductive stages (which range from silking to physiological maturity according to the degree of kernel development).

Pre-sampling of the maize smallholder field was conducted in Google Earth Pro, where the experimental field's polygon was digitized. The digitized polygon was then imported into ArcGIS 10.5, where it was used to generate sampling points. Sixty-three sample points were generated based on stratified random sampling within the digitized field boundary. These points were then uploaded into a handheld Trimble Global Positioning System (GPS) with sub-

meter accuracy (1-100 cm). These locations were used to navigate to each sample point for field data collection. The maize plants at each sampling point were marked for consistent bi-weekly measurement. Crop attributes, including chlorophyll content, leaf area index, stomatal conductance, equivalent water thickness, specific leaf area, and yield were measured from each sampling point. For image acquisition, A Mica Sense multi-spectral camera (Altum) was mounted on a UAV (DJI Matrice 300) to acquire multi-spectral images of the study area. The Altum consists of five spectral bands (Blue, Green, Red, Red Edge and NIR) with a radiometric thermal camera for the thermal region of the EMS, hence acquiring multi-spectral and thermal imagery in a single flight.

In leveraging Google Earth Engine (GEE) with ultra-high spatial resolution data acquired using UAVs for mapping LULC in smallholder farms, with a specific focus on cultivated areas, results demonstrated that field boundaries could be accurately mapped based on random forest ensemble combined with the red edge and NIR derivatives. Furthermore, the UAV-derived LULC map is comparable to publicly available landcover maps for the region at capturing the spatial heterogeneity within the study area.

In testing the use of UAV-derived multispectral data in the estimation of maize chlorophyll content over the various stages of phenotyping, results showed that optimal chlorophyll content prediction accuracies were produced during early vegetative growth stages (V5-V10 and V12), late vegetative growth stages (V14-VT), and early reproductive growth stages (R1-R3). It was also observed that maize chlorophyll content was optimally estimated through UAV-derived NIR and red-edge wavelengths.

Meanwhile, in evaluating the utility of UAV-derived VIs in concert with the Random Forest (RF) algorithm in estimating maize LAI across the growing season, results showed that the optimal stage for estimating maize LAI using UAV-derived VIs in concert with the RF ensemble was during the vegetative stage. The findings also showed that UAV-derived traditional, red edge-based, and new VIs could reliably predict maize LAI across the growing season. The electromagnetic spectrum's blue and red edge and NIR sections were critical in predicting maize LAI. Furthermore, combining traditional, red edge-based, and new VIs was useful in attaining high LAI estimation accuracies.

In evaluating the utility of multispectral and thermal infrared UAV imagery in combination with a random forest machine learning algorithm to estimate the maize foliar temperature and stomatal conductance as indicators of potential crop water stress and moisture content over the entire phenological cycle, results illustrated that the thermal infrared waveband was the most influential variable during the vegetative growth stages. In contrast, the red-edge and near-infrared-derived vegetation indices were fundamental during the reproductive growth stages for temperature and stomatal conductance. Maize foliar temperature was best predicted during the mid-vegetative growth stage and stomatal conductance during the early reproductive growth stage.

The project also comparatively evaluated the utility of UAV-derived multispectral imagery and machine learning techniques in estimating maize leaf moisture indicators, equivalent water thickness (EWT), fuel moisture content (FMC), and specific leaf area (SLA) as proxies of crop moisture stress. This section conducted a comparative analysis between the support vector

regression, random forest regression, decision trees regression, artificial neural network regression, and the partial least squares regression algorithms in predicting leaf moisture content indicators (i.e. EWT, FMC, and SLA). The results illustrated that NIR and red-edge-derived spectral variables were critical in characterising maize moisture indicators on smallholder farms. Furthermore, the best models for estimating EWT, FMC, and SLA were derived from the random forest regression (RFR) algorithm. Additionally, EWT and FMC yielded the highest predictive performance and were the most optimal indicators of maize leaf moisture.

The project also evaluated the utility of UAV-based multispectral datasets for quantifying maize EWT and FMC throughout the phenological growth cycle of maize at five different phenological periods using the random forest (RF) regression algorithm. The findings illustrated that the NIR and red-edge wavelengths were influential in characterising maize moisture variability with the best models for estimating maize EWT and FMC resulting in a relative root mean squared error (rRMSE) of 2.27% and 1%, respectively.

Regarding exploring the prospects of using UAV-derived multispectral data, Landsat, SEBS, METRIC-Efflux models and a cloud computing infrastructure in estimating maize evapotranspiration ( $ET_c$ ). Findings illustrated that maize daily  $ET_c$  increases gradually from the beginning of the growing season to the peak season, then decreases gradually in the late season.  $ET_c$  estimates from both models were within an acceptable range, although SEBS had the highest estimates throughout the growing season compared to METRIC-Efflux. Furthermore, METRIC-Efflux and FAO-56 potential ET were almost equal.

### **New knowledge and innovation**

The application of drone technology for crop management and monitoring is a relatively new field in South Africa. Thus, the project contributed toward the emerging use of drone technologies in South Africa for mapping field boundaries, health and crop water use, and efficiency. The project also assessed the prospects of converting and interpreting the information collected through drones into knowledge useful for decision-making, such as irrigation scheduling precision farming in the context of precision agriculture in smallholder croplands. Finally, the project contributed five articles published in high-impact factor journals.

### **Capacity Building**

The project adequately addressed institutional and individual capacity building. The project recruited five master's students and five postdoctoral fellows. Of these five master's students, three completed, while two were continuing with their MSc studies during the writing of this report. Through this project, one honours student from UWC was supported. The Post-doctoral fellows were actively engaged in student supervision. They were also trained in conceptualization and project management skills. Some Post-doctoral fellows developed further the concept of drone applications in smallholder croplands. In this regard, three Post-doctoral fellows were awarded new drone-based projects as New Project leaders by WRC. Furthermore, a technician and four post-doctoral fellows were being trained to attain their Remote Piloted Aircraft Pilot Licences (RPLs) through this project. Furthermore, a workshop to train the youth from the Swayimane community on drone applications.

## **Conclusion**

As a flagship project on utilising UAVs in agriculture, the project's findings underscore that these technologies can effectively map field boundaries and monitor crop health in heterogeneous smallholder croplands at optimal accuracies. Specifically, proxies of crop health (i.e. Chlorophyll content and leaf area index), as well as proxies of water use (i.e. stomatal conductance, foliar temperature, equivalent water thickness, fuel moisture content, specific leaf area, and evapotranspiration), were optimally estimated using drone acquired red-edge and NIR bands and their spectral derivatives. However, there is still a need to extend the research evaluating the relative contribution of drone technologies in monitoring other climate-smart crops in smallholder croplands. Specifically, there is limited literature on the utilisation of drones in mapping and monitoring neglected and under-utilised crop species, the impact of weeds, and water quality and quantity assessments in smallholder croplands. The successful implementation of drone technologies is a pathway towards offering detailed and spatially explicit information to smallholder farmers on local variations of cropland characteristics and facilitating on-field decisions for optimising productivity.

## **Recommendations**

Numerous gaps remain regarding using drone remotely sensed data in mapping and monitoring crop health and water use efficiency.

- More efforts must be exerted towards assessing the integration of UAV-derived data with Google Earth Engine and ancillary data in characterising farm boundaries.
- There is a need to assess the utility of UAV-derived multispectral data in estimating crop health parameters and ecophysiological attributes such as the canopy chlorophyll content and crops' structural attributes about the fields' environmental attributes.
- Following the exploratory nature of this project, there is a need to exert more efforts toward the estimation of evapotranspiration of crops using UAV-derived data.
- Future studies could assess other techniques, such as the sap flows and atmometers on-site measurement of evapotranspiration in evaluating water use efficiency.
- Research efforts are still needed to estimate water use and productivity, potential yield and evapotranspiration using drone remotely sensed data.
- Variables such as soil moisture and precipitation need to be integrated into the characterisation of crop health and water use efficiency models.
- Above all, future studies could evaluate the fusion of freely available remotely sensed data sets and UAV-acquired data in mapping and monitoring crop attributes in smallholder croplands.

## ACKNOWLEDGMENTS

The research reported here formed part of an unsolicited project initiated, funded and managed by the Water Research Commission (WRC) in Key Strategic Area 4 (Water Utilisation in Agriculture). The project team sincerely thanks the WRC for funding and managing the project. The project team also wishes to sincerely thank the following members of the Reference Group for their valuable contributions and guidance:

Prof S Mpandeli	:	Water Research Commission (Chairman)
Ms RL Lutchman	:	Water Research Commission
Ms IN Masilela	:	Water Research Commission
Dr L Nhamo	:	Water Research Commission
Dr S Hlophe-Ginindza	:	Water Research Commission
Prof A van Niekerk	:	Stellenbosch University
Mr TS Newby	:	Private Consultant
Dr M Wallace	:	Western Cape Department of Agriculture
Mr IY Lavangee	:	DRobotics
Mrs C Cuénod	:	(Committee Secretary)

We would also like to thank the following:

- The uMgeni Resilience Project, funded by the Adaptation Fund, for supporting much of the fieldwork as part of building the resilience of smallholder farmers to climate change
- The postgraduate students who participated in the project: KR Brewer, HS Ndlovu, S Buthelezi and A Nyawose
- The administrative staff from the Centre for Transformative Agricultural and Food Systems (CTAFS) and the Centre for Water Resources Research for supporting the project
- The community members from Swayimane for allowing the field trials to be conducted on their land
- The many stakeholders whose contributions laid the groundwork for the data used in the report.

This page was intentionally left blank

## TABLE OF CONTENTS

<b>EXECUTIVE SUMMARY .....</b>	<b>III</b>
<b>ACKNOWLEDGMENTS .....</b>	<b>VII</b>
<b>TABLE OF CONTENTS .....</b>	<b>IX</b>
<b>LIST OF FIGURES .....</b>	<b>XIV</b>
<b>LIST OF TABLES.....</b>	<b>XVII</b>
<b>LIST OF ACRONYMS AND ABBREVIATIONS.....</b>	<b>XIX</b>
<b>REPOSITORY OF DATA.....</b>	<b>XX</b>
<b>1 INTRODUCTION.....</b>	<b>1</b>
1.1 MAIN OBJECTIVE.....	2
1.1.1 General objective.....	2
1.1.2 Specific Objectives .....	2
1.2 SCOPE OF THE REPORT .....	2
<b>2 LITERATURE REVIEW.....</b>	<b>5</b>
2.1 INTRODUCTION.....	5
2.2 MATERIALS AND METHODS .....	7
2.2.1 Methodological framework.....	7
2.2.2 Types of agricultural UAVs .....	9
2.2.3 Regulations governing drone use in South Africa.....	10
2.3 RESULTS AND DISCUSSIONS .....	10
2.3.1 Mapping agriculture fields using UAVs.....	10
2.3.2 Assessing crop water stress and health using UAV-derived indices.....	12
2.3.3 Estimating crop yield through UAVs.....	14
2.3.4 Modelling crop evapotranspiration (ET) using UAV remote sensing.....	16
2.3.5 Use of UAVs in estimating crop water productivity .....	17
2.3.6 Use of UAVs in agriculture disaster risk reduction.....	19
2.4 RECOMMENDATIONS .....	19
2.5 CONCLUSIONS .....	20
<b>3 DEVELOPMENT OF HIGH-RESOLUTION MAPS OF AGRICULTURAL FIELD BOUNDARIES.....</b>	<b>22</b>
3.1 INTRODUCTION.....	22
3.2 MATERIALS AND METHODS .....	24
3.2.1 Study site description.....	24
3.2.2 Data acquisition and processing .....	26
3.3 RESULTS .....	28
3.3.1 Identifying the best-performing classifier for the original UAV image.....	28
3.3.2 Comparison of the best-performing classifiers at different spatial resolutions ..	29
3.3.3 Comparison of optimal spatial resolution classification against publicly available LULC maps for the region.....	30
3.4 DISCUSSION .....	32

3.5	CONCLUSIONS .....	34
<b>4</b>	<b>PREDICTING CHLOROPHYLL CONTENT OF MAIZE USING UAV-DERIVED MULTISPECTRAL REMOTELY SENSED DATA .....</b>	<b>35</b>
4.1	INTRODUCTION.....	35
4.2	MATERIALS AND METHODS .....	37
4.2.1	Study site description.....	37
4.2.2	Maize phenotyping.....	39
4.2.3	Field data collection, sampling, and survey.....	40
4.2.4	UAV multispectral-thermal camera and platform .....	42
4.2.5	Image acquisition and processing.....	43
4.2.6	Statistical analysis .....	45
4.2.7	Accuracy assessment.....	46
4.3	RESULTS .....	46
4.3.1	Descriptive analysis of UAV-derived data and ground-based maize data .....	46
4.3.2	Evaluation of UAV-derived data against ground-based NDVI and chlorophyll data .....	47
4.3.3	Descriptive statistics of chlorophyll content from SPAD .....	48
4.3.4	Random forest models of maize chlorophyll content .....	49
4.3.5	Mapping the spatial distribution of maize chlorophyll content over the various growth stages .....	50
4.4	DISCUSSION .....	51
4.4.1	Estimating maize chlorophyll content across the growing season .....	52
4.4.2	Implications of the study .....	53
4.5	CONCLUSION .....	54
<b>5</b>	<b>REMOTE SENSING FOLIAR TEMPERATURE AND STOMATAL CONDUCTANCE USING DRONE-ACQUIRED OPTICAL AND THERMAL IMAGES.....</b>	<b>55</b>
5.1	INTRODUCTION.....	55
5.2	MATERIALS AND METHODS .....	57
5.2.1	Study site description.....	57
5.2.2	The maize growth cycle and characteristics.....	59
5.2.3	Field data collection, temperature, and stomatal conductance measurements.....	59
5.2.4	UAV: DJI Matrice 300 and MicaSense Altum .....	61
5.2.5	Image acquisition and processing.....	63
5.2.6	Statistical Analysis .....	65
5.2.7	Accuracy assessment.....	66
5.3	RESULTS .....	66
5.3.1	Descriptive analysis of UAV-derived data and SI-111 IRR maize temperature data .....	66
5.3.2	Descriptive statistics of in-situ maize temperature and stomatal conductance measurements.....	68
5.3.3	UAV-derived data: estimation of maize temperature and stomatal conductance .. .....	70
5.3.4	Mapping the spatial distribution of maize temperature and stomatal conductance over the various phenological stages.....	74
5.4	DISCUSSION .....	75

5.4.1	Prediction of maize water stress using foliar temperature and stomatal conductance .....	76
5.4.2	Implications of the study .....	78
5.5	CONCLUSION .....	79
<b>6</b>	<b>ESTIMATION OF MAIZE LEAF WATER CONTENT USING MACHINE LEARNING TECHNIQUES AND UNMANNED AERIAL VEHICLE (UAV)-BASED PROXIMAL AND REMOTELY SENSED DATA .....</b>	<b>80</b>
6.1	INTRODUCTION.....	80
6.2	MATERIALS AND METHODS .....	83
6.2.1	Description of the study area .....	83
6.2.2	Field Sampling and moisture content measurements.....	85
6.2.3	Model development and statistical analysis .....	86
6.2.4	Spatial analysis.....	86
6.2.5	Accuracy assessment of derived maize moisture content models.....	88
6.3	RESULTS .....	89
6.3.1	Descriptive analysis of maize crop moisture indicators and measured biophysical variables.....	89
6.3.2	Evaluation of maize moisture indicators and optimized regression models .....	90
6.3.3	Optimal models for estimating maize moisture content indicators .....	90
6.3.4	Mapping the spatial distribution of maize leaf moisture content indicators.....	93
6.4	DISCUSSION .....	93
6.4.1	Estimating maize moisture content indicators .....	94
6.4.2	The performance of machine learning algorithms in predicting maize moisture content indicators.....	95
6.5	CONCLUSION .....	96
<b>7</b>	<b>A MULTITEMPORAL ESTIMATION OF MAIZE LEAF EQUIVALENT WATER THICKNESS AND FUEL MOISTURE CONTENT VARIABILITY USING UNMANNED AERIAL VEHICLE (UAV) DERIVED MULTISPECTRAL DATA AS A PROXY TO MOISTURE STRESS .....</b>	<b>98</b>
7.1	INTRODUCTION.....	98
7.2	MATERIALS AND METHODS .....	101
7.2.1	Study site description.....	101
7.2.2	Experimental design and crop management.....	102
7.2.3	Field survey and measurements of maize moisture content.....	104
7.2.4	Selection of vegetation indices.....	104
7.2.5	Model development and statistical analysis .....	105
7.2.6	Accuracy assessment and model validation.....	106
7.3	RESULTS .....	106
7.3.1	Descriptive statistics and temporal variation in EWTleaf and FMCleaf during the maize phenological cycle .....	106
7.3.2	Estimating maize EWTleaf and FMCleaf throughout the maize growing season ..	108
7.4	DISCUSSION .....	115
7.4.1	The influence of precipitation on maize moisture content variability .....	115

7.4.2	Estimation of maize moisture indicators from UAV-derived spectral reflectance ..	116
7.4.3	Implications of the findings.....	118
7.5	CONCLUSION .....	118
<b>8</b>	<b>ASSESSING THE PROSPECTS OF UAV ACQUIRED REMOTELL SENSED DATA IN MAPPING LEAF AREA INDEX AS A PROXY OF YIELD IN SMALLHOLDER CROPLANDS .....</b>	<b>119</b>
8.1	INTRODUCTION.....	119
8.2	MATERIALS AND METHODS .....	121
8.2.1	Study site.....	121
8.2.2	LAI measurements.....	124
8.2.3	Data analysis .....	124
8.2.4	Maize LAI prediction .....	126
8.2.5	Accuracy assessment.....	126
8.3	RESULTS .....	126
8.3.1	Descriptive statistics .....	126
8.3.2	Derived Maize LAI prediction models and their accuracies .....	127
8.4	DISCUSSION .....	130
8.4.1	Predicting maize LAI.....	130
8.4.2	The performance of combining UAV-derived traditional, red edge-based and new VIs in predicting maize LAI .....	132
8.5	CONCLUSION .....	133
<b>9</b>	<b>PREDICTING MAIZE YIELD IN SMALLHOLDER CROPLANDS USING UAVS-DERIVED MULTI-TEMPORAL REMOTELY SENSED DATASETS .....</b>	<b>134</b>
9.1	INSTRODUCTION.....	134
9.2	MATERIALS AND METHODS .....	136
9.2.1	Study area .....	136
9.2.2	Agricultural practices .....	136
9.2.3	Sampling strategy for yield measurements .....	137
9.2.4	Calculation of VIs.....	137
9.2.5	Data Analysis.....	138
9.3	RESULTS .....	139
9.3.1	Descriptive statistics .....	139
9.3.2	Derived maize yield prediction models and their accuracies .....	139
9.4	DISCUSSION .....	143
9.4.1	Maize yield prediction models.....	143
9.4.2	Determining the most optimal growth stages and variables for yield prediction ....	145
9.5	CONCLUSION .....	146
<b>10</b>	<b>EXPLORING THE PROSPECTS OF USING LANDSAT, SEBS AND METRIC-EFFLUX MODELS AND A CLOUD COMPUTING INFRASTRUCTURE IN THE ESTIMATION OF ET<sub>c</sub> USING UAV MULTI-SPECTRAL IMAGERY.....</b>	<b>147</b>
10.1	INTRODUCTION.....	147
10.2	MATERIALS AND METHODS.....	150

10.2.1	Description of the study area.....	150
10.2.2	Daily $ET_C$ estimation using UAV imagery, Landsat data, SEB models, and GEE .....	152
10.2.3	Calculation of EF to NDVI ratio using SEBS.....	154
10.2.4	Calculation of ETrF to NDVI ratio using METRIC-Efflux .....	154
10.2.5	Data Validation .....	155
10.3	RESULTS .....	155
10.3.1	Spatial distribution of $ET_C$ across the growing season.....	155
10.3.2	Comparison of SEBS and METRIC-Efflux daily $ET_C$ estimates with FAO-56 potential ET for maize. ....	156
10.4	DISCUSSION.....	158
10.4.1	Comparison of SEBS and METRIC-Efflux daily $ET_C$ estimates with FAO-56 potential ET for maize. ....	159
10.4.2	Variability of estimated daily $ET_C$ across different plots .....	160
10.4.3	Implications of the Study .....	160
10.4.4	Limitations and recommendations.....	161
10.5	CONCLUSION .....	161
<b>11</b>	<b>GENERAL DISCUSSION, CONCLUSION AND RECOMMENDATIONS.....</b>	<b>163</b>
11.1	GENERAL DISCUSSION.....	163
11.2	LIMITATIONS OF THE STUDY.....	166
11.3	CONCLUSION .....	167
11.4	RECOMMENDATIONS.....	167
	<b>REFERENCES .....</b>	<b>169</b>
	<b>APPENDICES.....</b>	<b>212</b>
	APPENDIX A: LIST OF PUBLICATIONS .....	212
	APPENDIX B: LIST OF CONFERENCES PRESENTATIONS .....	213
	APPENDIX C: LIST OF POST DOCTORAL FELLOWS AND GRADUATED STUDENTS.....	214
	APPENDIX D: LIST OF CONTINUING STUDENTS .....	215

## LIST OF FIGURES

Figure 2-1: A methodological framework to explore the importance of UAVs in agricultural water management.....	8
Figure 2-2: Examples of (a) fixed-wing UAVs and rotary (b) winged UAVs. Fixed-wing UAVs have wider coverage, which could be 10 times bigger than rotary winged, but image quality is poor due to flying speed, and cannot stay stationary in flight mode.....	9
Figure 2-3: Comparing the (a) UAV and, (b) satellite imagery-derived crop maps. Figure (a) shows the real shape of the agricultural while (b) resembles the whole scheme area as cultivated, overestimating the cultivated area. (a) was developed by the authors using a drone and (b) was derived from the irrigated area map developed by IWMI in 2015, (IWMI, 2015).....	12
Figure 3-1: Location of the study site within the KwaZulu-Natal province of South Africa ....	25
Figure 3-2: A conceptual representation of the process followed to develop and test the LULC classification model. ....	28
Figure 3-3: A comparison of the classification results for the study area at different spatial resolutions. ....	31
Figure 3-4: Results of the C2 classification used to distinguish crops from other LULC classes within the study area. ....	31
Figure 3-5: A comparison of the C1 classification for the study area against the 2020 ESRI and South African National Landcover map. ....	32
Figure 4-1: Location of the Swayimane study area, study site, and smallholder maize field.	38
Figure 4-2: Swayimane weather conditions throughout maize phenotyping .....	39
Figure 4-3: (a) Automated in-field meteorological tower in the maize field, (b) meteorological tower mounted with SRS-NDVI and SRS-PRI sensors held 4-meters above the ground, (c) CR1000 data logger, Em50 datalogger and 12 V battery.....	41
Figure 4-4: (a) DJI Matrice 300 platform and, (b) MicaSense Altum multispectral-thermal camera. ....	43
Figure 4-5: (a) DJI M-300 flight plan, (b) MicaSense Altum calibration reflectance panel ....	44
Figure 4-6: Daily SRS-NDVI values of maize throughout the phenological cycle. Red points indicate the days we visited the field to conduct UAV flights. The blue point indicates the day of crop disturbance due to a hailstorm. ....	47
Figure 4-7: Correlation of (a) in-field sensor SRS-NDVI and UAV-derived NDVI (b) measured maize chlorophyll content and UAV-derived NDVI across the maize growth stages.	48
Figure 4-8: Linear relationships between measured and predicted maize chlorophyll content for vegetative stages (a) V5-V10, (b) V12, (c) V14 to VT, and reproductive stages (d) R1-R3, (e) R3-R4, (f) R5-R6.....	49
Figure 4-9: Variable importance scores of optimal chlorophyll content VIs and bands for vegetative stages (a) V5-V10, (b) V12, (c) V14 to VT, and reproductive stages (d) R1-R3, (e) R3-R4, (f) R5-R6.....	50
Figure 4-10: Spatial distribution of chlorophyll content over the maize field for vegetative stages (a) V5-V10, (b) V12, (c) V14 to VT, and reproductive stages (d) R1-R3, (e) R3-R4, (f) R5-R6. ....	51
Figure 5-1: Location of the Swayimane study area, study site, and smallholder maize field.	58
Figure 5-2: Daily weather conditions in Swayimane throughout maize phenotyping.....	59

Figure 5-3: (a) Automated in-field meteorological tower in the maize field, (b) meteorological tower mounted with SI-111 Apogee IRR sensors held 4-meters above the ground, (c) CR1000 data logger, Em50 datalogger and 12 V battery.....	60
Figure 5-4: (a) DJI Matrice 300 UAV platform and, (b) MicaSense Altum multispectral-thermal camera .....	62
Figure 5-5: (a) DJI M-300 flight plan, (b) MicaSense Altum calibration reflectance panel ....	63
Figure 5-6: Daily average T <sub>c</sub> -T <sub>a</sub> , solar radiation, and rainfall throughout the maize phenological cycle. Red points indicate field visits to conduct data collection. The blue point indicates the day of the hailstorm. ....	67
Figure 5-7: Correlation of in-field IRR sensors and UAV-derived temperature throughout the maize phenological cycle.....	68
Figure 5-8: Correlation of foliar temperature and stomatal conductance throughout the maize phenological cycle .....	70
Figure 5-9: Regression models displaying the relationships between measured and predicted IRT foliar temperature and stomatal conductance throughout the maize phenological cycle: (a) V5-V10, (b) V12, (c) V14 to VT, (d) R1-R3, (e) R3-R4, (f) R5-R6 .....	72
Figure 5-10: Variable importance scores of optimal foliar temperature and stomatal conductance bands and VIs throughout the phenological cycle: (a) V5-V10, (b) V12, (c) V14 to VT, (d) R1-R3, (e) R3-R4, (f) R5-R6.....	73
Figure 5-11: Foliar temperature of maize over the smallholder field for vegetative stages (a) V5-V10, (b) V12, (c) V14 to VT, and reproductive stages (d) R1-R3, (e) R3-R4, (f) R5-R6.....	74
Figure 5-12: Maize stomatal conductance over the smallholder field for vegetative stages (a) V5-V10, (b) V12, (c) V14 to VT, and reproductive stages (d) R1-R3, (e) R3-R4, (f) R5-R6.....	75
Figure 6-1: (a) Location of the study area and (b) maize crop field in Swayimane, South Africa.....	84
Figure 6-2: Relationship between the predicted and observed (a) EWT <sub>leaf</sub> , (b) FMC <sub>leaf</sub> and (c) SLA <sub>leaf</sub> of maize derived using optimal predictor variables and the model variable importance scores .....	92
Figure 6-3: Spatial distribution of (a) EWT <sub>leaf</sub> , (b) FMC <sub>leaf</sub> , and (c) SLA <sub>leaf</sub> of smallholder maize crops .....	93
Figure 7-1: Location of the study area in Swayimane, South Africa.....	102
Figure 7-2: Biophysical conditions of maize across the phenological growth period.....	103
Figure 7-3: Bioclimatic condition of maize across the phenological growth period.....	103
Figure 7-4: Temporal variation of maize EWT <sub>leaf</sub> and FMC <sub>leaf</sub> during the maize growing season.....	107
Figure 7-5: Relationship between the predicted and observed maize EWT <sub>leaf</sub> at (a), V8-V10, (b) V14-Vt, (c) R1-R2, (d) R2-R3 and (e) R3-R4 phenological growth stage and the optimal model variable importance scores.....	111
Figure 7-6: Relationship between the predicted and observed maize FMC <sub>leaf</sub> at (a), V8-V10, (b) V14-Vt, (c) R1-R2, (d) R2-R3 and (e) R3-R4 phenological growth stage and the optimal model variable importance scores.....	113
Figure 7-7: Spatial distribution of modelled maize EWT <sub>leaf</sub> across the different stages of the growing season .....	114

Figure 7-8: Spatial distribution of modelled maize FMCleaf across the different stages of the growing season .....	115
Figure 8-1: a) Location of study site in Swayimane, KwaZulu-Natal, South Africa and b) The maize plot.....	122
Figure 8-2: Relationship between field-measure Yield and average LAI estimates of maize. ....	127
Figure 8-3: Relationship between measured and estimated LAI based on the combination of traditional, red edge-based and new VIs using the RF Model for the a) V8-V10 b) V12-V14 c) VT-R1 d) R2-R3 and e) R3-R4 maize growth stages. ....	128
Figure 8-4: The variable importance scores of selected variables that exhibited the highest scores in predicting maize LAI for the a) V8-V10, b) V12-V14, c) VT-R1 d) R2-R3 and e) R3-R4 maize growth stages .....	129
Figure 8-5: The distribution of modelled maize LAI for the a) V8-V10, b) V12-V14, c) VT-R1 d) R2-R3, and e) R3-R4 growth stages based on the RF models. ....	130
Figure 9-1: a) Location of the experimental field plot in Swayimane, KwaZulu-Natal, South Africa, and b) & c) The maize field.....	136
Figure 9-2: Correlation between the grain yield and biomass at the R3-R4 stage using all samples.....	139
Figure 9-3: Relationship between observed and predicted i) biomass, ii) grain yield and iii) proportional yield based on the combination of bands and VIs using the RF Model for a) V8-V10 b) V12-V14 c) VT-R1 d) R2-R3 and e) R3-R4 maize growth stages. ....	141
Figure 9-4: The variable importance of the i) biomass, ii) grain yield and iii) proportional yield models for a) V8-V10, b) V12-V14, c) VT-R1, d) R2-R3 and e) R3-R4 maize growth stages.....	142
Figure 9-5: The spatial distribution of modelled maize a) biomass, b) grain yield and c) proportional yield based on the most optimal RF models.....	143
Figure 10-1: Study area and maize fields (A, B, and B).....	152
Figure 10-2: Daily distribution of $ET_c$ across the growing season .....	156
Figure 10-3: Comparison of maximum $ET_c$ estimates of SEBS, METRIC-Efflux, with FAO-56 across different maize growth stages. ....	157
Figure 10-4: Relationship between SEBS & FAO-56 $ET_c$ estimates and METRIC-Efflux & FAO-56 estimates in (a) February, (b) March and (c) April. ....	158

## LIST OF TABLES

Table 3-1: A description of the LULC classes identified and categorized for mapping. ....	26
Table 3-2: Classification accuracies for the original spatial resolution (0.07 m) based on various classification algorithms available in GEE. ....	29
Table 3-3: Classification accuracies for the UAV images at differing spatial resolutions classified using the GTB classification algorithm. ....	30
Table 4-1: Maize growth stages and characteristics .....	40
Table 4-2: MicaSense Altum camera specifications. ....	43
Table 4-3: UAV flight specifications .....	44
Table 4-4: Spectral UAV-derived vegetation indices used to predict chlorophyll content. ....	45
Table 4-5: Descriptive statistics of maize chlorophyll content throughout the various growth stages.....	48
Table 5-1: MicaSense Altum camera specifications. ....	62
Table 5-2: UAV flight specifications .....	63
Table 5-3: Spectral vegetation indices utilized to predict the foliar temperature and stomatal conductance .....	64
Table 5-4: Descriptive statistics of IRR and IRT foliar temperature throughout the maize growth stages .....	69
Table 5-5: Descriptive statistics of stomatal conductance throughout the maize phenological cycle .....	69
Table 6-1: Bioclimatic conditions of Swayimane during the maize growing season .....	85
Table 6-2: List of vegetation indices (VIs) used in the modelling of crop moisture content and related source references .....	86
Table 6-3: Descriptive statistics of crop moisture indicators and biophysical variables .....	89
Table 6-4: Prediction accuracies of $EWT_{leaf}$ , $FMC_{leaf}$ and $SLA_{leaf}$ were derived using optimal models based on the RFR, DTR, ANNR, PLSR and SVR regression models.....	90
Table 7-1: Selected vegetation indices (VIs) used for maize moisture content estimations	105
Table 7-2: Descriptive statistics of $EWT_{leaf}$ and $FMC_{leaf}$ at the different phenological stages .....	107
Table 7-3: Estimation accuracies of $EWT_{leaf}$ and $FMC_{leaf}$ derived using UAV bands, vegetation indices and the combination of both .....	109
Table 8-1: Maize growth stages. ....	123
Table 8-2: UAV-derived VIs were used in this study .....	125
Table 8-3: Descriptive statistics of the actual maize LAI .....	127
Table 9-1: VIs used in this study. ....	138

Table 10-1: Maize growth stages ..... 151

## LIST OF ACRONYMS AND ABBREVIATIONS

CART	Classification and Regression Tree
CSA	Climate Smart Agriculture
ET	Evapotranspiration
ET <sub>c</sub>	Crop evapotranspiration
EWT	Leaf Equivalent Water Thickness
FMC	Fuel Moisture Content
GEE	Google Earth Engine
GPS	Global Positioning System
GTB	Gradient Tree Boost
LiDAR	Light Detection and Ranging
LULC	Land Use Land Cover
METRIC	Mapping Evapotranspiration at high Resolution with Internalized Calibration
MODIS	Moderate Resolution Imaging Spectroradiometer
NDVI	Normalised Difference Vegetation Index
RF	Random Forest
RGB	Red Green Blue
RPL	Remote Pilot License
SEBAL	Surface Energy Balance Algorithm for Land
SEBI	Surface Energy Balance Index
SEBS	Surface Energy Balance System
SLA	Specific Leaf Area
SPOT	Pour l'Observation de la Terre
SSA	sub-Saharan Africa
SVM	Support Vector Machine
UAV	Unmanned Aerial Vehicle
Vis	Vegetation Indices
VIS	Visible section of the electromagnetic spectrum
WRC	Water Research Commission

## REPOSITORY OF DATA

For details related to the project's data, please contact:

Prof Tafadzwa Mabhaudhi (Project Leader and Principal Researcher)  
Centre for Transformative Agricultural and Food Systems  
School of Agricultural, Earth and Environmental Sciences  
University of KwaZulu-Natal  
Private Bag X01, Scottsville 3209  
Pietermaritzburg, South Africa  
Email: [mabhaudhi@ukzn.ac.za](mailto:mabhaudhi@ukzn.ac.za)

# 1 INTRODUCTION

The demand for agricultural products has significantly increased, with the estimated aggregate agricultural consumption anticipated to rapidly upsurge by 69% by 2050 (Alexandratos and Bruinsma, 2012; Nhamo, Matchaya et al., 2019). A global population surge will induce this, estimated to reach 9 billion people in 2050 (Alexandratos and Bruinsma, 2012; Nhamo, Matchaya et al., 2019). Meanwhile, agricultural production in sub-Saharan Africa has been threatened by water scarcity, unpredictable weather, and arid conditions (Lickley and Solomon, 2018; Nhamo, Matchaya et al., 2019). In South Africa, smallholder agriculture (less than two hectares) is predominantly rainfed, often resulting in crops experiencing water stress and moisture shortages due to inadequate rainfall (Rockstrom, 2000; Ubisi, Mafongoya et al., 2017; Adisa, Botai et al., 2018). However, there are limited, spatially explicit, evidence-based frameworks and instruments for monitoring crop water stress in smallholder croplands, especially in those cultivating maize (*Zea mays* L.), predominantly for subsistence (Andersson, Zehnder et al., 2009; Lu, Xue et al., 2017). Since maize is a staple grain crop and one of the most widely cultivated crops in South African smallholder farms (Walker and Schulze, 2006), there is a need for spatially explicit methods to characterise the extent of fields, water and health deficiencies, yield and water use efficiency of maize to prevent yield losses and optimise the productivity of smallholder farmers (Brewer, Clulow et al., 2022).

Optimisation of maize crop production in smallholder croplands could be enhanced by adopting modern technologies into the agricultural production system. For instance, unmanned aerial vehicles (UAVs), popularly known as drones, could offer advanced crop image data analytics and crop monitoring in real-time (Nhamo, Magidi et al., 2020). Unmanned aerial vehicles are remotely controlled aircraft mounted with GPS and specialised sensors to collect referenced and high-resolution images without cloud interference (Yao, Qin et al., 2019). Using UAVs at the field or farm scale allows accessing near-real-time information spatially reference data suitable for monitoring crops at different stages throughout the cropping cycle (Yao, Qin et al., 2019; Nhamo, Magidi et al., 2020). Systematic crop monitoring offered by drones provides agrometeorological (agro-met) information to farmers (particularly smallholder farmers) in real-time, enabling them to make informed on-field decisions, such as when to plant, irrigate, apply nutrients and chemicals, etc., bringing climate-smart agriculture (CSA) and precision agriculture to the smallholder sector (an important sector for food security).

The advantage of drones is that they offer low-cost imaging at high resolution and offer user-determined revisit periods (Barbedo, 2019; Nhamo, Magidi et al., 2020). Thus, drones are appropriate and affordable tools for assessing crop phenology, stress assessment and crop health in near real-time (Barbedo, 2019; Nhamo, Magidi et al., 2020). Sequential monitoring of crops at the field level allows farmers to get information on crop status, allowing them to detect subtle changes that are not easily identified by the human eye (Tian, Wang et al., 2020). Subsequently, adopting drones in the South African agricultural sector, especially the smallholder farmlands, could optimise food production and address the serious water and food insecurity challenges exacerbated by the recurrence of extreme weather events, mainly drought (Nhamo, Mabhaudhi et al., 2019).

## **1.1 Main Objective**

The contractually specified objectives of the project were:

### **1.1.1 General objective**

In this regard, the main objective of this project was to assess the utility of drone technology for monitoring the state of crops to improve water use productivity with precision agriculture and improved irrigation scheduling in smallholder croplands for four years.

### **1.1.2 Specific Objectives**

- Specific objective 1: Review the literature on specialist drones for crop monitoring and crop-water models that use drone products. This included analysing drones' use to monitor crops, modelling yield and water use, and irrigation scheduling.
- Specific objective 2: To assess crop health by analysing real-time NDVI derived from drone imagery.
- Specific objective 3: To monitor crop evapotranspiration at the field scale for a farmer to make on-field decisions.
- Specific objective 4: To develop high-resolution maps of agriculture fields and irrigated areas and datasets on water use, productivity, potential yield, and evapotranspiration.
- Specific objective 5: To assess the impact of drones on water use, crop nutrition, and water productivity (yield and quality) for improved livelihoods of smallholder farmers.

The contractual objective of this project was initially “to systematically monitor crop development and provide agro-met information in real-time using drones for improving water productivity and irrigation scheduling in selected irrigated farms of KwaZulu-Natal, South Africa”. Most smallholder farmers generally do not have irrigation systems in KwaZulu-Natal. In this regard, the project mostly covered the rainfed maize crop in smallholder crops. Generally, all contractual objectives were adequately addressed and, in some instances, exceeded. Specifically, specific objectives 1 to 3 are well exceedingly addressed. Although objectives 4 and 5 were satisfactorily addressed, numerous setbacks were encountered, specifically concerning the ground-truthing data in estimating evapotranspiration, water use and water productivity. This section was regarded as an exploratory study to assess the prospects of drone remotely sensed data in estimating evapotranspiration. We provide a detailed recommendation for future studies on estimating evapotranspiration, water use, and water productivity that could be conducted in data-scarce regions.

## **1.2 Scope of The Report**

The report comprises a series of self-contained chapters with different authors. Each Chapter addresses at least one of the project's specific objectives as set out after consultations with the technical reference group members and the WRC project managers. The general methodology chapter was not included because the report is presented in a paper format. Each chapter is presented with its specific methodology. Due to the paper format followed, the report does not have a general methodology section since each Chapter has its specific

methodology. In that regard, there are inevitably overlaps or repetitions, especially in the methodology sections, within the ambit of the project report. This is because a seamless flow of methodological principles underpins the current scientific setting. This was considered trivial because some chapters are adapted from published articles critically peer-reviewed by international journals.

The report is structured to address the project objectives of the study in a logical framework. Chapters 1 and 2 address the definition of the scope of the study and the first objective related to conducting state-of-the-art literature. Chapters 3-10 report on acquiring and using drone-derived multispectral remotely sensed data in developing high-resolution maps of agriculture field boundaries, maize crop health, water stress and evapotranspiration throughout the growing season.

A general overview of the report is provided below.

Chapter 1 provides a general introduction, background, and conceptualisation of the entire study. It motivates the broad study as set out in terms of reference. It also sets out the project's aims and specific objectives defined in the contract.

Chapter 2 is a state-of-the-art literature review on prospects of Improving Agricultural and Water Productivity through Unmanned Aerial Vehicles. The chapter synthesises the use of UAVs in smallholder agriculture in the smallholder agriculture sector in developing countries. The review highlights the role of UAV-derived normalised difference vegetation index (NDVI) in assessing crop health, evapotranspiration, water stress and disaster risk reduction. This Chapter addresses the. This chapter addressed contractual-specific objective number 1.

Chapter 3 explores and demonstrates the utility of using the advanced image processing capabilities of the Google Earth Engine (GEE) geospatial cloud computing platform to process and analyse a very high spatial resolution multispectral UAV image to map land use land cover (LULC) within smallholder farms. This chapter addressed contractual-specific objective 4.

Chapter 4 predicted the chlorophyll content of maize over phenotyping as a proxy for crop health in smallholder farming systems. Specifically, crop chlorophyll content is assessed as one of the best-known and reliable indicators of crop health due to its biophysical pigment and biochemical processes that indicate plant productivity. In this regard, the study evaluated the utility of multispectral UAV imagery using the random forest machine learning algorithm to estimate the chlorophyll content of maize through the various growth stages. This chapter addressed contractual objective number 2.

Chapter 5 estimated maize foliar temperature and stomatal conductance as indicators of water stress based on optical and thermal imagery acquired using a UAV platform. Specifically, this chapter evaluated the utility of optical and thermal infrared UAV imagery, combined with a random forest machine-learning algorithm, to estimate the maize foliar temperature and stomatal conductance as indicators of potential crop water stress and moisture content over the entire phenological cycle. This addressed specific objectives two and partly, 4.

Chapter 6 is a comparative analysis which sought to (1) evaluate the performance of five regression techniques in predicting maize water content and (2) determine the most suitable

indicator of smallholder maize water content variability based on multispectral UAV data. This chapter specifically evaluated the utility of UAV-derived multispectral imagery and machine learning techniques in estimating maize leaf water indicators: equivalent water thickness (EWT), fuel moisture content (FMC), and specific leaf area (SLA). This chapter addressed specific objectives 3, 4 and 5.

Chapter 7 assessed the prospects of monitoring multi-temporal maize leaf equivalent water thickness and fuel moisture content variability using UAV-derived multispectral data. Specifically, the chapter evaluated the utility of UAV-based multispectral datasets and random forest regression in quantifying maize EWT and FMC throughout the phenological growth cycle of maize. This chapter addressed specific objectives 3, 4, and partially, 5.

Chapter 8 estimated maize leaf area index using UAV-derived multi-spectral data in smallholder farms as a proxy for productivity. To address this objective, UAV-derived VIs, in concert with the Random Forest (RF) algorithm, were utilised in estimating maize LAI across the growing season in a smallholder farm. This chapter addressed contractual-specific objectives 4 and 5.

Chapter 9 sought to predict maize yield in smallholder croplands using UAVs derived from multi-temporal remotely sensed datasets in concert with the RF regression ensemble. The value of using the grain biomass, absolute plant biomass, grain biomass as a proportion of the absolute maize plant biomass, VIs and combined spectral data were evaluated. This chapter addressed contractual-specific objectives 4 and 5.

Chapter 10 explore and assess the prospects of using Landsat, SEBS and METRIC-Efflux models and a cloud computing infrastructure in estimating  $ET_c$  using UAV multi-spectral imagery. A comparative of the SEBS and the METRIC-Efflux model combined with UAV-derived multispectral data and Landsat-derived VIs as a proxy of albedo was used to estimate maize crop  $ET_c$  in smallholder croplands. FAO-56 potential ET was then used to assess the estimated  $ET_c$  in this study.

Chapter 11 provides a holistic discussion of the entire project and links all the separate studies to achieving the project objectives. The chapter also provides the conclusion and recommendations for future studies.

## 2 LITERATURE REVIEW

Nhamo L, Magidi J, Nyamugama A, Clulow AD, Sibanda M, Chimonyo VGP & Mabhaudhi T

### 2.1 Introduction

Although agricultural production has increased substantially in recent years, the demand for agricultural products has also risen significantly, with estimates that aggregate agricultural consumption is expected to increase by 69% by 2050 (Tilman, Balzer et al., 2011; Alexandratos and Bruinsma, 2012). A surge in the global population mostly fuels the demand for food, fibre and feed, estimated to reach 9 billion by 2050 (Godfray, Beddington et al., 2010). The need to feed a growing population has resulted in the intensification and extensification of agricultural land, resulting in agriculture consuming about 70% of the available freshwater resources worldwide (Pimentel, Berger et al., 2004; Cosgrove and Loucks, 2015). One of the urgent challenges currently facing sub-Saharan Africa (SSA) is to increase crop yields and at the same time reduce the amount of water used in crop production, that is, 'more crops per drop' (Morison, Baker et al., 2008; Fan, Shen et al., 2011). The approach is more urgent in smallholder farming areas, which experience marginal production due to biophysical and management-related factors (Mungai, Snapp et al., 2016). In most arid and semi-arid regions, water is a scarce resource needing improved crop water productivity in agriculture (Du, Kang et al., 2015). Improved agricultural water management requires innovative and evidence-based solutions throughout the agriculture system (Levidow, Zaccaria et al., 2014; Nhamo, Mabhaudhi et al., 2016). Unmanned Aerial Vehicles (UAVs), also known as drones, offer advanced crop image data analytics at high spatial and temporal resolution and crop monitoring in real-time, important elements in agriculture water management (Nhamo, van Dijk et al., 2018).

Unmanned Aerial Vehicles are remotely controlled aircraft mounted with Global Positioning System (GPS) and specialised sensors to collect geo-referenced and high-resolution images without cloud interference (Watts, Ambrosia et al., 2012; Yang, Liu et al., 2017). Their use at the field or farm scale allows access to real-time agro-meteorological (agro-met) information and crop monitoring at different stages throughout the cropping cycle. Using drones in smallholder agriculture, particularly in regions facing water scarcity, could prove worthwhile as they allow improved water and food security (Nhamo, Mabhaudhi et al., 2019). Real-time monitoring of crops at the field scale and timely intervention throughout the growing cycle results in improved crop and water productivity. Systematic crop health monitoring and availability of agro-meteorological information in real-time would enable smallholder farmers to make informed, tactical and operational decisions, such as when to plant, irrigate, apply nutrients and chemicals, etc. The opportunities offered and made available by UAVs bring climate-smart agriculture (CSA) and precision agriculture to smallholder farmers (Adão, Hruška et al., 2017). The advantage of UAVs over satellites is that drones offer low-cost imaging at high spatial resolution and user-determined revisit periods (Manfreda, McCabe et al., 2018). Thus, UAVs are appropriate for assessing rapid changes in crop phenology,

stress assessment and crop health in real-time (Ballesteros, Ortega et al., 2014). Collective ownership of UAVs and the use of extension services could be an effective way to use drones by smallholder farmers who may not have the resources to own and maintain a drone, as well as the technical expertise required to operate, collect, process and interpret drone data.

Sequential monitoring of crops allows farmers to detect subtle changes that are not easily identified by the human eye (Pongnumkul, Chaovalit et al., 2015). For example, multispectral drone imagery can assess crop health through NDVI (Normalized Difference Vegetation Index) or NDRE (Normalised Vegetation Red Edge) indices. NDVI enables an analysis of the intensity of solar radiation absorption in specific bands and the health condition of the monitored crops (Ishihara, Inoue et al., 2015). Traditionally, NDVI has been derived from imageries from satellite sensors such as Landsat, Pour l'Observation de la Terre (SPOT) and Moderate Resolution Imaging Spectroradiometer (MODIS), but the temporal and spatial resolutions of the resulting products have been too low for continuous crop monitoring. Unmanned Aerial Vehicles offer NDVI analysis of crops at 0.05 to 1 metre resolution, suitable for monitoring the condition of individual plants with optimal accuracy. Multispectral drones generally come with a complete crop scouting kit, including software, at a reasonable cost of US\$10 000. The multispectral camera captures RGB, NIR NDVI, and NDRE indices, offering spectral capabilities that make UAV important and suitable for monitoring crop health and density, water stress and weed detection.

Accurate and detailed geospatial drone data is also useful in disaster situations, where crop damage occurs due to extreme weather events. They precisely estimate the level of crop loss by comparing the pre-disaster and post-disaster imagery (Chou, Yeh et al., 2010). The pre and post-disaster information is important for insurance companies as they move towards ensuring smallholder farmers against extreme weather events (Greatrex, Hansen et al., 2015). Drones can provide evidence of damage through the development of index-based crop insurance, thereby reducing risk and vulnerability while contributing towards achieving the 2030 Global Agenda on Sustainable Development (Carter, de Janvry et al., 2014).

Satellite and UAV imagery serve the same purpose but differ significantly in spatial and temporal resolution. The scale and accuracy determine the choice of the two the user requires to achieve (Nhamo, van Dijk et al., 2018; Ruwaimana, Satyanarayana et al., 2018). Unlike satellite images taken at high altitudes, the high spatial resolution offered by UAVs at low altitudes allows plant analyses and the detection of anomalies. Although there are also high-resolution satellites like QuickBird, RapidEye, WorldView and IKONOS, and hyperspectral and Light Detection and Ranging (LiDAR) remote sensing, these are very expensive and generally time-consuming in terms of processing (Sylvester, 2018). Their high costs and temporary low resolution are the major factors limiting their use in smallholder agriculture. The high altitudes and low temporal resolution of satellites make them only suitable over large areas where changes occur slowly (Huang, Chen et al., 2018), significantly limiting their use in smallholder agriculture, which is characterised by small land tenure that averages about 2 ha (Graeub, Chappell et al., 2016). Although the high level of spectral detail in hyperspectral images provides better capabilities to detect crop anomalies, they are very complex due to the high number of bands (Adão, Hruška et al., 2017). Although LiDAR imaging could offer similar services as drones, it samples positions without RGB and thus only creates monochromatic datasets, which could be difficult to interpret (Sevara, Wieser et al., 2019).

Furthermore, high-altitude sensors are susceptible to atmospheric energy attenuation and impurities. Meanwhile, UAVs can acquire images even during cloudy days at short flight preparation times, which has not been possible previously (Torres-Sánchez, Peña et al., 2014). Drones are reducing the cost of remote sensing as new and affordable models are being introduced (Salamí, Barrado et al., 2014). This review discusses the importance of UAVs in agricultural water management and crop health as an alternative to improve productivity.

## **2.2 Materials and Methods**

### **2.2.1 Methodological framework**

Figure 2-1 is a graphical representation of the methodological framework developed to explore the importance of UAVs in enhancing smallholder productivity and water management, focusing on smallholder agriculture. The increasing frequency and intensity of drought recurrence, as well as rising temperatures that result in increased evapotranspiration (ET) (climate change), are causing many regions and particularly arid and semi-arid regions, to experience worsening water scarcity challenges (Naumann, Alfieri et al., 2018; Nhamo, Mabhaudhi et al., 2019). In turn, water scarcity results in increased aridity and shifts in agro-ecological zones and thus, affecting crop yields (Solh and van Ginkel, 2014). The challenge of depleting water resources requires innovative technologies to improve agricultural water management and enable smallholder farmers to improve productivity under water-limited conditions without increasing pressure on already strained water resources. Agriculture consumes about 70% of the available freshwater resources, which has become unsustainable (Cosgrove and Loucks, 2015).

Firstly, we consulted the literature on the types, costs and effectiveness, opportunities and obstacles of utilising UAVs concerning established agricultural remote sensing techniques. A database consisting of published articles was created using the Web of Science, Scopus and Google Scholar using keywords such as “drones”, “unmanned aerial vehicles (UAVs)”, “UAVs application in agriculture”, “UAVs applications in agricultural water management”, “UAVs and remote sensing”, “UAVs and precision agriculture”, and “UAVs in disaster management”. To cover a wide range of relevant research, we supplemented papers about irrigated area mapping, irrigation scheduling, crop water stress, crop health detection, crop ET, water productivity and weed detection. Irrelevant papers were excluded by reading abstracts and conclusions.

We note that the use of drones in science and research is growing exponentially. Publications related to drones started picking up in 2010, and since then, the drone industry has grown. As of 2016, the drone market revenue was US\$6.8 billion and is projected to grow to US\$36.9 billion by 2022 (Gonzalez-Aguilera and Rodriguez-Gonzalvez, 2017; Shakhathreh, Sawalmeh et al., 2019). We also consulted the literature on regulations controlling the use of UAVs worldwide. We noted that most countries have or are developing laws governing the use of drones, and therefore relevant authorities need to be consulted before their use (Jones, 2017).

Secondly, within the consulted literature, we identified thematic areas on how UAVs are used to improve agricultural water management. The aim was to explore the opportunities offered by UAVs in enhancing agriculture and water productivity by identifying the limitations of current remote sensing products and methods. We looked into how UAVs can enhance mapping agricultural fields (particularly small-scale irrigated areas), crop stress and health at the field level, crop yield and evapotranspiration (ET) estimation, and crop water productivity. We gave detailed examples of how UAVs enhance different agriculture research fields from existing literature. The overall goal was to explore the role of UAVs in ensuring water and food security in the advent of climate change.

While there have been previous studies on UAV applications, this review offers detailed and practical insights, from multidisciplinary perspectives, on how UAVs can enhance agricultural productivity and water management among smallholder rural farmers in times of water scarcity and the advent of climate change. The review further provides detailed comparisons between satellite and UAV-sensed products, highlighting how UAVs can particularly improve the accuracy of these products. The review emphasises how several UAV applications could be deployed to promote precision farming and climate change adaptation among often-poor smallholder farmers. This group of farmers is characterised by low access to climate information and services and technologies that enhance productivity and adaptive capacities.

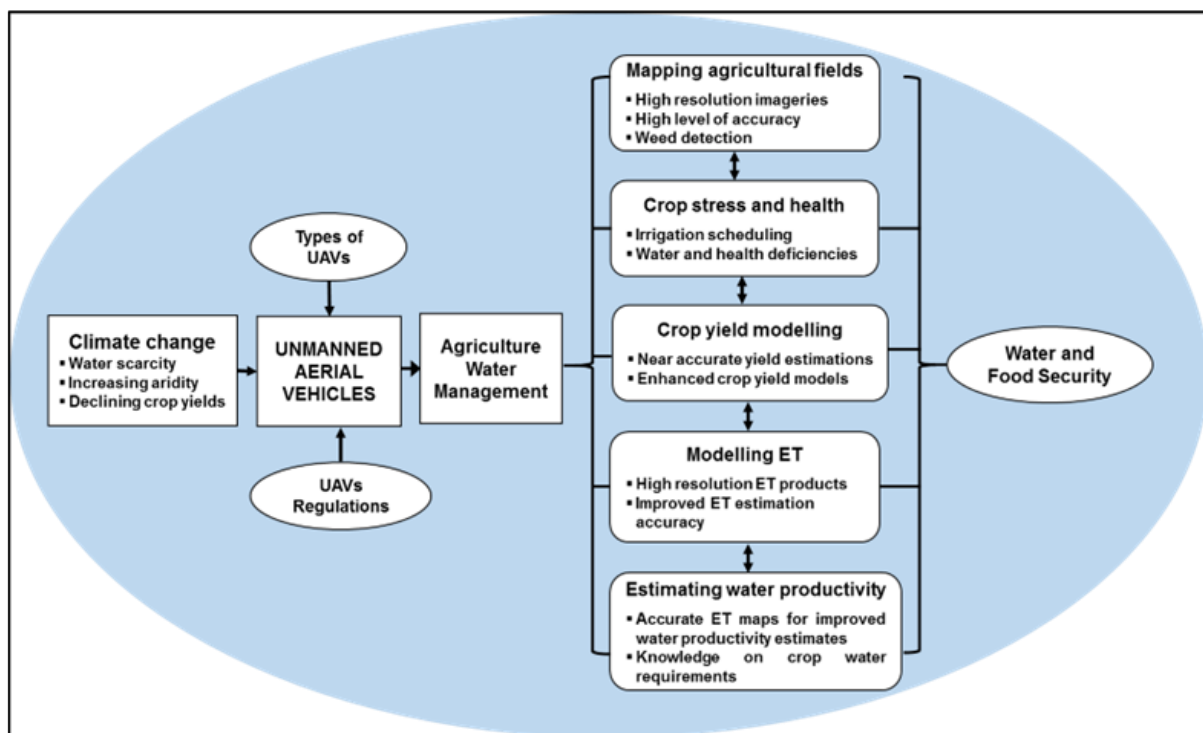


Figure 2-1: A methodological framework to explore the importance of UAVs in agricultural water management.

## 2.2 Types of agricultural UAVs

There are two types of UAVs, fixed wing and multi-rotor or rotary wing (Figure 2-2), equipped with the necessary software, sensors and hardware to monitor crop health and conduct field surveys. The advantage of fixed-wing UAVs is that they have wider coverage, which could be ten times bigger than rotary-winged UAVs (Sandbrook, 2015; McEvoy, Hall et al., 2016). However, image quality is compromised due to the flying speed. Also, fixed-wing UAVs have a much simpler structure making them less complicated to maintain and repair (Sandbrook, 2015). The simple structure of fixed-wing UAVs ensures more efficient aerodynamics that allows longer flight durations at high speeds, natural gliding capabilities with no power and the capability to carry greater payloads for longer distances on less power (Çetinsoy, Dikyar et al., 2012). However, fixed-wing UAVs may require a runway or launcher for take-off and landing. They cannot stay stationary in flight mode like rotary-winged UAVs, making them unsuitable for stationary applications like crop inspection (McEvoy, Hall et al., 2016).

Rotary-winged UAVs are best suited for close range and detailed surveying as the pilot can control its movements and functions, allowing it to hover over plants at a low altitude (Hackney and Clayton, 2015). The capability of a rotary-winged UAV to fly low and slowly allows the production of more accurate and high-resolution imageries for site-specific assessments (Hunt Jr and Daughtry, 2017). The main limiting factor of the rotary-winged UAVs is the small coverage per flight and low flight duration. However, these can be overcome by undertaking several flights per survey and changing batteries at intervals to allow for more time coverage (Sandbrook, 2015). One important advantage of rotary UAVs is their ability to take-off and land vertically, allowing them to be operated anywhere. The capacity of rotary UAVs to hover around a single place makes them well-suited for agricultural surveying and research (Shakhatreh, Sawalmeh et al., 2019). However, their complicated nature makes them more expensive to maintain and repair.



Figure 2-2: Examples of (a) fixed-wing UAVs and rotary (b) winged UAVs. Fixed-wing UAVs have wider coverage, which could be 10 times bigger than rotary winged, but image quality is poor due to flying speed, and cannot stay stationary in flight mode.

### **2.2.3 Regulations governing drone use in South Africa**

Most countries are passing regulations and laws governing the use of drones. Before flying a drone for any purpose, users are advised to inquire about their use with the authorities. In South Africa, for example, the responsible body for regulating drone use is the South African Civil Aviation Authority (SACAA), which requires that all UAVs weighing above 7 kg be registered (whatever the purpose) and that the pilot has aviation training from an approved training organisation (ATO) and have a Remote Pilot Certificate. UAVs weighing below 7 kg do not need to be registered for private use. However, all drone users must steer clear from and within 10 km of airports and other No Fly Zones and respect private property ([www.caa.co.za/Pages](http://www.caa.co.za/Pages)). The most important things to note about drone use in South Africa, according to part 101 of Civil Aviation regulations, include:

- a) Must be SACAA approved and have a valid remote pilot licence and a letter of approval to operate the drone.
- b) The letter is valid for 12 months. These are not important for purchasing, but the dealer must highlight the regulations at the time of sale.
- c) Drones cannot fly more than 120 m above the ground nor within 10 km of an aerodrome.
- d) Drones cannot be flown within 50 m above or close to a person or crowd of people, structure or building without SACAA approval. Drones cannot be flown above security areas like power plants, prisons, police stations, national parks, etc.
- e) Drones cannot be used to transport cargo or make deliveries.

## **2.3 Results and Discussions**

### **2.3.1 Mapping agriculture fields using UAVs**

Accurate geospatial information on agriculture is a critical requirement for planning and decision-making, particularly in countries intending to increase and improve smallholder irrigated agriculture (Cai, Magidi et al., 2017; Scott and Rajabifard, 2017). Satellite imageries have been used to produce coarse land use/cover maps. However, the advent of UAVs has improved mapping accuracy because of their high resolution and low cost, although at a smaller coverage (Sandbrook, 2015). The use of UAVs in mapping land use makes it possible to monitor smallholder farming fields that are generally too small to be detected by readily available moderate to low-resolution satellite imageries (Nhamo, van Dijk et al., 2018). Smallholder farming plots measure about two hectares in area per farmer (Graeub, Chappell et al., 2016).

Smallholder farming areas are generally detected as one massive agricultural land (Figure 2-3 (b)) by low to moderate-resolution satellites. Yet, their mapping accuracy is important as, for example, in southern Africa, they occupy about 80% of the cultivated land, contributing about 90% of the agricultural produce (Livingston, Schonberger et al., 2011). Therefore, mapping accurate and detailed agricultural fields is important for decision-making, especially

for addressing the climate resilience of agricultural livelihoods. High-resolution satellite imageries that could offer the same accuracy as UAV imagery are costly, which limits their use (Boyle, Kennedy et al., 2014). Unlike satellite imagery, UAV imagery is not limited by cloud cover. The temporal resolution (acquisition time) is user-defined and can be adjusted to local weather conditions (Ruwaimana, Satyanarayana et al., 2018). Unmanned Aerial Vehicles can be deployed repeatedly at flexible mission times and altitudes to acquire data on agricultural fields. Images acquired by UAVs offer an observation of single plants, patches and ultimately, patterns over the fields, something that was not possible previously with satellite imageries (Xiang and Tian, 2011). These advantages and ultra-high spatial resolutions make UAVs best suited for mapping crops planted in narrow rows at optimal accuracies. The main limiting factor of UAV imagery as compared to satellite imagery is their small coverage area per image.

As the resolution of UAVs can be as high as 0.05 m depending on the flight altitude, they are appropriate for mapping small agricultural fields accurately. Figure 2-3 compares the accuracy of irrigated area maps derived from UAV imagery (Figure 3a) and satellite imagery (Figure 2-3 (b)). The maps are part of the Taung Irrigation Scheme in the North West Province, South Africa. Figure 3b was extracted from the irrigated area map for Africa developed by the International Water Management Institute (IWMI) from the MODIS satellite at 250 m spatial resolution (IWMI, 2015). Figure 3a is a map of the same area developed by authors from UAV imagery taken in 2018. The irrigation scheme is dominated by centre pivots, as shown in Figure 2-3 (a) (derived UAV imagery), yet Figure 2-3 (b) resembles the whole scheme area as cultivated. The irrigated area calculated from the UAV map is 40 647 ha, 17 000 ha less than the area calculated from the satellite map, which is 57 803 ha. Thus, satellite imagery overestimates land use areas. Although accuracy may improve with high-resolution satellites, there is always an overestimation of land use area, especially at the field scale. Overestimating irrigated areas has the disadvantage of misinforming policy and decision-making. Accurate estimates are important for understanding the ecological footprint of food production and assessing the potential of irrigation development with limited land and water resources.

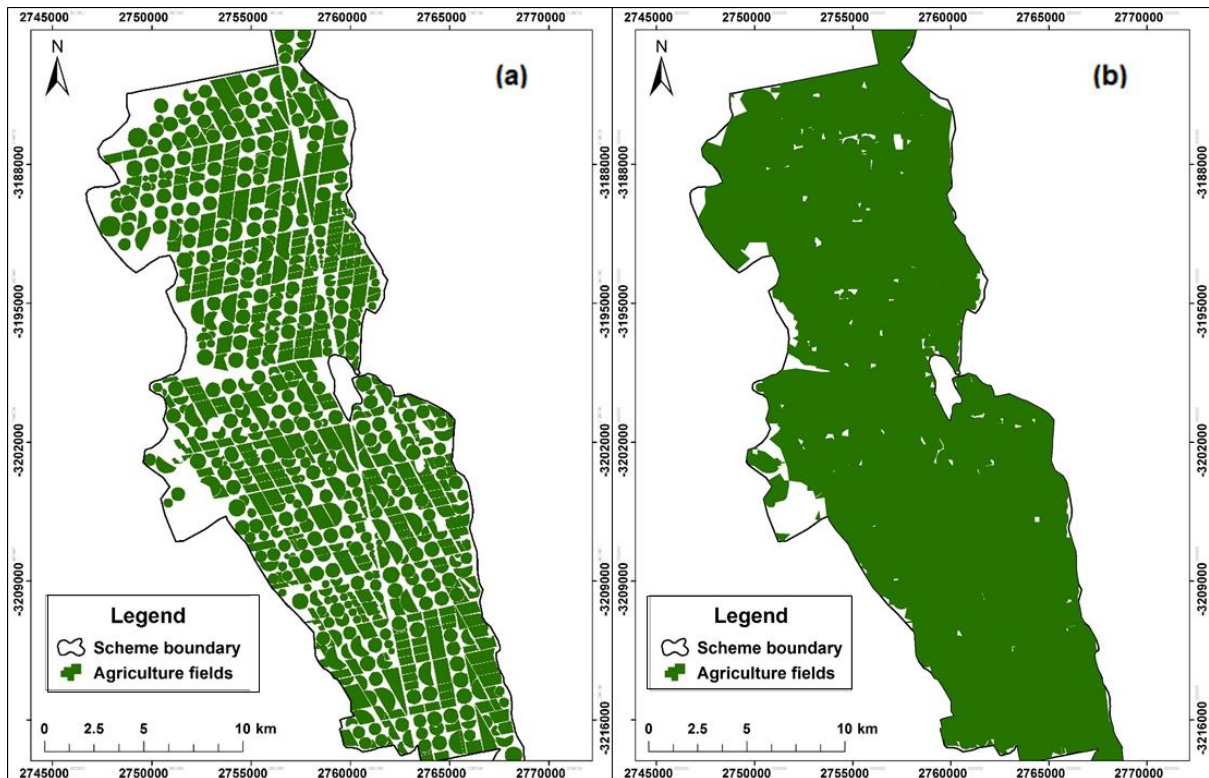


Figure 2-3: Comparing the (a) UAV and, (b) satellite imagery-derived crop maps. Figure (a) shows the real shape of the agricultural while (b) resembles the whole scheme area as cultivated, overestimating the cultivated area. (a) was developed by the authors using a drone and (b) was derived from the irrigated area map developed by IWMI in 2015, (IWMI, 2015)

Various studies have also illustrated the robustness and capabilities of UAVs in mapping croplands (Torres-Sánchez, Peña et al., 2014; de Castro, Peña et al., 2017; Ma, Fu et al., 2017; de Castro, Torres-Sánchez et al., 2018; Liu, Zhang et al., 2018; Mink, Dutta et al., 2018; Wahab, Hall et al., 2018). For instance, a study done in Córdoba and Seville in Spain illustrated the accuracy and capability of UAVs' remotely sensed data in characterising weeds between and within rows of sunflower and cotton crops across the growing season (de Castro, Torres-Sánchez et al., 2018). In a related study, de Castro *et al.* illustrated the utility of UVAs in discriminating *Cynodon dactylon* grassweeds in the vineyards of Lleida in Spain (de Castro, Peña et al., 2017). These studies discriminated the weeds from crops with overall classification accuracy ranging between 71-80%. Thus, using UAV imagery at the field scale helps farmers make timely on-field decisions on when to apply pesticides and weeding. Although UAVs have been useful in agriculture, their use in Africa is still low, mainly due to scarce resources, as well as the dearth of skilled human resources to take up the utilisation and maintenance of UAVs (Mutanga, Dube et al., 2017; Wahab, Hall et al., 2018).

### 2.3.2 Assessing crop water stress and health using UAV-derived indices

Water Stress Indices (WSI) are useful crop parameters for mitigating drought impacts and irrigation scheduling. Remote sensing provides various products for acquiring ecological information from interpreting and analysing multi-spectral and hyperspectral image bands. The

interaction between electromagnetic energy and plants or vegetation differs depending on chlorophyll content, type of plant, and leaf area index (Fang and Ramasamy, 2015). Interpretation of spectral reflectance can reveal water and nutrient deficiencies, as well as information on plant health. During the growing process, a plant requires water, carbon dioxide and light for photosynthesis to produce sugar and oxygen (Mee, Balasundram et al., 2017). Besides these requirements, plants also need nutrients for plant cell and tissue development (Mee, Balasundram et al., 2017). Lack of these components leads to plant stress, and the symptoms are mainly observed through the defoliation of older leaves and a decrease in biomass.

Therefore, one indicator of a healthy plant is the chlorophyll content in the leaves (Pavlovic, Nikolic et al., 2015). Chlorophyll absorbs visible light and reflects Near Infrared (NIR). Healthy plants with good photosynthetic activities can be analysed by comparing the reflectance of NIR and visible light (Mee, Balasundram et al., 2017; Xue and Su, 2017). These plant characteristics can be assessed through vegetation indices, which are the mathematical transformation of image bands used to qualitatively and quantitatively extract certain spectral properties such as vegetation cover, vigour and growth dynamics (Xue and Su, 2017). These vegetation indices are tailor-made to specific applications, each of which has its advantage. Thus, vegetation indices can enhance plant health classification and assessment algorithms (Hatfield and Prueger, 2010; Amani and Mobasheri, 2015). Vegetation indices also provide information on plant growth as healthy plants absorb more visible light and reflect more NIR (Hatfield and Prueger, 2010). Many vegetation indices use NIR and Red bands, and these are the Normalised Difference Vegetation Index (NDVI), Soil Adjusted (SAVI), Ashburn Vegetation Index (AVI), and Enhanced Vegetation Index (EVI), among others (Xue and Su, 2017). The commonly used vegetation index is the NDVI, which monitors and characterises canopy growth and plant vigour (Xue and Su, 2017). The NDVI is expressed as (Townshend and Justice, 1986):

$$NDVI = \frac{NIR - Red}{NIR + Red} \quad \text{Equation 2-1}$$

where NIR is the Near Infrared band, and Red is the red band.

NDVI values range between -1 and 1, with high NDVI values indicating healthy crops while low NDVI values indicating unhealthy crops and less vegetative vigour or more stressed crops (Boken and Shaykewich, 2002; Huang, Wang et al., 2014). Thus, NDVI is important for providing information on the variability of the health of crops, as well as in large-scale monitoring of plantations, assessing changes in the field, quantifying crop acreage and analysing crop loss (Boken and Shaykewich, 2002). NDVI also estimates plant attributes such as physiological status, yield production, crop distribution and irrigation mapping (Filella, Serrano et al., 1995; Aparicio, Villegas et al., 2000; Nhamo, van Dijk et al., 2018). Another modification of the NDVI used to assess changes in plant health is the SAVI (Soil Adjusted Vegetation Index) (Costa, Coelho et al., 2019). SAVI takes into consideration the variations in soil properties. SAVI tends to minimize soil brightness, and therefore, it introduces the soil calibration factor in the NDVI equation (Equation 2.1) to account for the first-order soil-vegetation optical interactions. SAVI is defined as (Huete, 1988):

$$SAVI = \left( \frac{NIR-Red}{NIR+Red} \right) \times (1 + L) \quad \text{Equation 2-2}$$

where L is a constant surrogate for the leaf area index (LAI) (Panda, Ames et al., 2010; Xu, Lacey et al., 2018).

To monitor changes in plant physiology, the NDVI-based crop growth curve is used where the data is captured at regular intervals. NDVI values are plotted on the graph to show temporal variations (Govaerts and Verhulst, 2010). Thus, spatio-temporal NDVI profiles show plant phenology (Huang, Wang et al., 2014). Time-series satellite images from UAVs acquired at short and constant intervals provide the necessary information on crop growth variation and water and nutrient deficiencies, as their temporal resolution is user-defined. They provide high spatial resolution at low altitudes, and adequate information to analyse individual plants or croplands (Govaerts and Verhulst, 2010; Yang, Liu et al., 2017; Khan, Rahimi-Eichi et al., 2018).

The crop water stress index (CWSI) is another index for assessing the level of stress in a plant by using the temperature extracted from the thermal band, as there is a correlation between CWSI and transpiration rate and soil water moisture (Fuentes, De Bei et al., 2012; Dalezios, Dercas et al., 2018). High-resolution UAV-derived NDVI can be combined with other indices, such as the CWSI and the Canopy-Chlorophyll Content Index (CCCI), to accurately delineate agricultural fields and monitor crop health (Cammarano, Fitzgerald et al., 2014).

An analysis of crop water deficit or water stress monitoring is the basis for effective irrigation scheduling (Jones, 2004; Möller, Alchanatis et al., 2006; Ihuoma and Madramootoo, 2017). The CWSI identifies water stress in crops within 24-48 hrs before stress detection by visual observation (Ihuoma and Madramootoo, 2017). The water deficit index (WDI) is another water stress index which works the same way as the CWSI (Tanriverdi, Atilgan et al., 2017). In water stress indices, 0 indicates no water stress, and 1 represents maximum water stress (Tanriverdi, Atilgan et al., 2017). The crop water stress that signals the need for irrigation varies from crop to crop and is determined by factors of yield response to water stress, probable crop price, and water cost (Tilling, O'Leary et al., 2007).

The accuracy of satellite-based remote sensing techniques has been hampered by the low resolution of satellite images that are readily and freely available (Pinter Jr, Hatfield et al., 2003; Nhamo, van Dijk et al., 2018). However, the advent of multispectral UAVs has transformed and enhanced the accuracy of crop water stress estimates due to the high-resolution and low-cost UAV images (Gago, Douthe et al., 2015).

### **2.3.3 Estimating crop yield through UAVs**

High costs have generally limited the use of high-resolution satellite images to assess crop vigour and yields, particularly for hyperspectral images (Wahab, Hall et al., 2018). Other limitations of satellite remote sensing in crop yield estimation include the noise from cloud cover on images and the complex and heterogeneous nature of farming systems in smallholder farming areas, which are difficult to detect with low-resolution images. The application of UAVs has bridged the gap between satellites and the use of remotely sensed products in smallholder farmlands, and the high cost, labour-intensive, and time-consuming

conventional field surveys of crops on the other hand (Yang, Liu et al., 2017). Thus, the availability of low costs UAVs has opened up new possibilities to remotely sense crop status and yields even on complex smallholder farms.

As already alluded to, high-resolution multi-temporal UAV images have enabled monitoring of crop development throughout the crop growing period, important information for farmers to plan and make crucial decisions (Shamshiri, Hameed et al., 2018). High-resolution UAV images provide more accurate information on crop biomass, yield and cropped area with acceptable accuracy for farmers and decision-makers to manage and monitor crops for optimum benefits (Shi, Thomasson et al., 2016; Hunt Jr and Daughtry, 2018). Studies have shown a high correlation between the vegetation spectral index extracted from satellite images and the green biomass and yield (Jin, Liu et al., 2017; Zhou, Zheng et al., 2017). Thus, combining vegetation spectral indices and green biomass can be used to estimate yield before harvesting. Crop yield is defined as crop production per unit area, and it is a product of the complex interaction between soil conditions (physical and chemical conditions), management (cultivar and spacing), and meteorological conditions (water and thermal) (Fan, Shen et al., 2011). Crop yield estimation enhances preparedness, as it is part of early warning, providing decision-makers with timely information on crop deficit or surplus (Nhamo, Mabhaudhi et al., 2019).

Remote sensing has shown to be an alternative tool to estimate crop yield to traditional methods, as it offers more accurate and high-resolution crop data in a cost and time-effective manner. Traditional methods are costly, time-consuming and prone to errors, often resulting in poor crop yield assessment (Tilly, Hoffmeister et al., 2014). There are three remote sensing methods used to estimate crop yield: (i) based on empirical statistical models, (ii) based on water consumption balance models, and (iii) based on biomass estimation models (Basso, Cammarano et al., 2013; Meroni, Marinho et al., 2013). UAVs provide accurate crop height and biomass information timeously and at user-defined temporal resolution as they can fly at low altitudes, providing high-resolution multispectral imageries. Crop height and biomass are important components for assessing crops' growth rate and health (Vriet, Russinova et al., 2012; Tumlihan, 2017). Plant height and biomass data are important to assess the effect of genetic variation on crops, crop development, and crop yield potential (Govindaraj, Vetriventhan et al., 2015). Thus, plant height and biomass are essential for optimising site-specific crop management and yield predictions (Hunt Jr and Daughtry, 2018).

The most used model for estimating crop yield is the Penman-Monteith equation, which uses biomass accumulation as a proportion of accumulated absorbed photo-synthetically active radiation (APAR) (Monteith, 1972). According to Monteith, crop yield is expressed as (Monteith, 1972):

$$CY = \varepsilon \sum(APAR)(t)(t)(Kgm^{-2}) \quad \text{Equation 2-3}$$

where CY is the crop yield, which is the accumulated biomass ( $kg m^{-2}$ ) in period t,  $\varepsilon$  in  $g M/J$  is the light use efficiency, t is the period over which accumulation occurs, and APAR is the absorbed photosynthetically active radiation.

Variability in plant light use efficiency ( $\epsilon$ ) is caused by varying nutrient and water levels (Craine and Dybzinski, 2013). Studies show that when crops are not water stressed, and temperature is optimal,  $\epsilon$  is a relatively constant property of plants (Haxeltine and Prentice, 1996; Onoda, Saluñga et al., 2014; Slattery, Walker et al., 2018). UAVs mounted with multispectral sensors produce more accurate and reliable biomass and light use efficiency indices for accurately estimating crop yields.

#### **2.3.4 Modelling crop evapotranspiration (ET) using UAV remote sensing**

Crop ET or crop water use is the largest water loss from agriculture. Its accurate quantification is critical for improved agricultural water management, irrigation scheduling and knowledge of crop water requirements (Fereres and Soriano, 2006). Evapotranspiration has historically been estimated using various field techniques such as the soil water balance, weighing lysimetry, Bowen ratio, eddy Covariance and surface renewal. These techniques rely on theoretical derivations and major assumptions (Burba, 2013). In addition, they represent a point measurement and require footprint estimates to determine the surface area that the measurement represents (Burba, 2013). Scintillometry has recently overcome the difficulties to some extent by estimating ET over wider, heterogeneous landscapes but still relies on the other components of the energy balance, which are difficult to measure directly in heterogeneous landscapes (Perez-Priego, El-Madany et al., 2017).

With the advent of satellite sensors and multispectral imagery of the earth's surface, remote sensing has evolved as a technique that allows ET to be measured more efficiently and economically on a large spatial scale or field scale using the shortened energy balance equation (Allen, Irmak et al., 2011; Nouri, Beecham et al., 2013). Several models have been developed that include the Surface Energy Balance Index (SEBI), the Surface Energy Balance Algorithm for Land (SEBAL), the Mapping Evapotranspiration at high Resolution with Internalized Calibration (METRIC) and Surface Energy Balance System (SEBS). These models vary in their specific methodologies but generally use the visible, red and infrared bands of the earth's surface reflectance together with terrain and vegetation properties to determine ET, which is extrapolated between consecutive satellite overpasses using representative meteorological data.

SEBI is a single-sourced energy balance model based on the difference between the dry and wet limits used to derive pixel-by-pixel ET from the relative evaporative fraction (Li, Tang et al., 2009). SEBAL uses visible, near-infrared and thermal-infrared reflectances to determine the instantaneous fluxes of the shortened energy balance equation (Jovanovic and Israel, 2012). The SEBS model estimates the atmospheric turbulent fluxes and evaporative fraction through satellite earth observation and meteorological data (Su, 2002). The SEBS model requires three sets of data to run (Su, 2002); the first set consists of the land surface albedo, emissivity, temperature, fractional vegetation coverage, leaf area index and the height of the vegetation cover. The second set includes the air pressure, temperature, relative humidity and wind speed at a reference height. The third is longwave and shortwave downward radiation. These parameters can be derived by direct measurement, modelling, or parameterization. These input data for the model are incorporated into three-sub models to determine the components needed for the shortened energy balance, the stability factors and the roughness

length of heat transfer. The sub-models are then used to estimate the evaporative fraction, which is assumed constant for the entire day, as with the other models.

The METRIC algorithm is a successor of the SEBAL model, but with slope and aspect influences included (Allen, Tasumi et al., 2007; Gokool, Chetty et al., 2016). The algorithm uses weather data (air temperature, wind speed, solar radiation, and relative humidity) and satellite radiance data at various bands as inputs for this model. Previous studies have shown that the METRIC algorithm produces more accurate results than any other ET model (Gibson, Jarman et al., 2013; Mokhtari, Ahmad et al., 2013; Madugundu, Al-Gaadi et al., 2017). The algorithm is calculated as residual energy of the surface energy balance equation and expressed as (Allen, Tasumi et al., 2007):

$$LE = R_n - G - H \quad \text{Equation 2-4}$$

where LE is latent energy consumed by ET,  $R_n$  is net radiation, G is the energy consumed by soil, and H is sensible heat flux (energy consumed in heating of air (all units are in  $W/m^2$ ))

Initially, the METRIC model was developed using Landsat satellite imageries, but the advent of high-resolution UAV imagery has the potential to further improve the accuracy of ET estimation (Thorp, Thompson et al., 2018). The METRIC-UAV approach uses the thermal band sensed directly from the UAV's multispectral camera. The thermal band is used to calculate surface energy balance, and the thermal information is used to estimate sensible heat flux (H), soil heat flux (G), and net radiation ( $R_n$ ).  $R_n$  uses surface temperature to estimate longwave thermal emission by the surface. The approach uses high-resolution UAV images and is the same METRIC model developed by Allen et al (Allen, Tasumi et al., 2007).

High-resolution UAVs are best positioned for estimating more accurate ET as they are equipped with sensors that provide multispectral reflectance of the earth's surface as a substitute for satellite data (Thorp, Thompson et al., 2018). Many problems associated with satellite data used for ET models, such as course resolution, fixed satellite overpass times and cloud cover, are addressed using UAVs. ET changes rapidly according to microclimatic variables and soil water availability. The benefit of being able to determine ET at variables, or when required, intervals, using UAVs is a significant benefit over satellites, and it is potential for UAVs to become useful tools in monitoring crop water use (Elarab, Torres-Rua et al., 2015; Thorp, Thompson et al., 2018).

### **2.3.5 Use of UAVs in estimating crop water productivity**

UAVs are transforming the agriculture sector by providing more accurate and precise data that was not readily available before. UAVs show their worth by providing the previously unavailable spatially explicit information required to understand and improve crop and water productivity. Improvements in agricultural water management, particularly crop water productivity, allow the agriculture sector to share water equitably with other competing sectors. Water productivity (WP) is a quantitative term which refers to the relationship between the volume of water utilised in crop production and the amount of crop produced expressed in  $kg/m^3$  (Igbadun, Mahoo et al., 2006; Liu, Williams et al., 2007). Thus, crop WP is a measure

of output from a given agricultural system in relation to the water it consumes and is expressed as (Kijne, Barker et al., 2003):

$$WP = \frac{\text{Agriculture benefit}}{\text{Water consumed}} \quad \text{Equation 2-5}$$

where the agriculture benefit is the actual harvested yield expressed in units of mass like kilograms ( $\text{kg/m}^3$ ) or monetary value (income) of that yield expressed in dollars ( $\text{US\$/m}^3$ ) or nutritional value ( $\text{kcal/m}^3$ ). Water consumed (the denominator of Equation 2-5) refers to water directly consumed by crops (Mabhaudhi, Chibarabada et al., 2016). WP is critical in understanding food and water relations while offering a footstool for assessing water use efficiency and water footprint integrated into the global food trade (Liu, Williams et al., 2007). Thus, WP can efficiently be determined through accurate crop evapotranspiration ( $ET_c$ ) measurements. There are other methods used to estimate WP, such as the quantity of water supplied to a field, but all water supplied to a field is not consumed by crops in its entirety as part of it will always find its way into the drainage system or is evaporated (Nhamo, Mabhaudhi et al., 2016). Water directly consumed by crops is efficiently measured through actual or crop ET ( $ET_c$ ) (Nhamo, Mabhaudhi et al., 2016). As already alluded to,  $ET$  is a better measure of water consumed by crops and is measured through  $ET_c$ . Crop ET is the consumption of water through ET, which is incorporated into a product and cannot be readily reused (Molden, Oweis et al., 2010).

UAVs are important in mapping accurate agriculture fields because of their high spatial resolution (Figure 2-3). The exclusion of other landuses provides accurate estimates of  $ET_c$ . UAVs could provide adequate spatial and temporal detail for estimating ET, ultimately offering a plausible understanding of WP (DeBell, Anderson et al., 2015). The Land Surface Heat Flux model and drone-measured land surface temperature (LST) at high resolution are used to estimate ET. A drone mounted with a thermal camera and flown on a field of heat fluxes and hydrology by concatenating thermal images into mosaics of Land surface temperature (LST) and using these as input for the Two-Source Energy Balance (TSEB) modelling scheme, which partitions the fluxes into soil and canopy (soil evaporation and canopy transpiration) (Park, Ryu et al., 2017).

Thus, UAV imageries can build high spatial resolution ET maps of up to 1 m. More accurate  $ET_c$  is derived from ET maps developed using data acquired by UAVs at the field scale. The results of UAV-derived ET are then compared with measured ET to assess the accuracy of the modelled ET. Existing ET datasets have presented challenges when estimating crop ET because of their low resolution compared to small agriculture fields. For example, the ET data derived from the Global Land Evaporation Amsterdam Model (GLEAM) has a spatial resolution of 25 km. In comparison, those derived from the MODIS 16 and Satellite Application Facility on Land Surface Analysis (LSA-SAF) at a spatial resolution of 1 km are too coarse for characterising  $ET_c$  and WP in smallholder plots of about two hectares in area (Graeub, Chappell et al., 2016). Also, studies have shown that most of these ET datasets tend to either overestimate or underestimate ET (Kim, Hwang et al., 2012; Ramoelo, Majozi et al., 2014).

### **2.3.6 Use of UAVs in agriculture disaster risk reduction**

Twenty-two percent of economic damage caused by natural disasters occurs in the agriculture sector, often resulting in yield reductions of about 20-40% every year (FAO, 2015). Most of the disasters that affect agriculture are climate-induced, including hailstorms, fires caused by heatwaves, cyclonic floods and winds, and droughts. The impact of these disasters can be reduced by systematically applying disaster risk reduction practices (Jayanthi, Husak et al., 2013). For example, UAVs could be important in assessing pre-disaster conditions, immediate impacts after a disaster and post-disaster analysis. Coupled with satellite images, which do not depend on ground infrastructure, UAVs can be used to develop index-based weather insurance that targets smallholder farmers (Castillo, Boucher et al., 2016).

The Food and Agriculture Organisation (FAO) has used drones in The Philippines to reduce the impacts of drought and flooding (Sylvester, 2018). UAVs mounted with multispectral cameras can relay information about upland agricultural risks such as landslides and erosion, inform agricultural communities of the risks, and reduce the impacts. As already alluded, remotely sensed data from drones is important in estimating crop yield to precisely warn about the food situation (Singha and Swain, 2016). Such advanced information provides enough lead time for decision-makers to prepare.

## **2.4 Recommendations**

The following recommendations are suggested based on the advantages of adopting drone use, particularly by smallholder farmers. Using drones can increase agricultural production, improve crop water productivity and build resilience.

- The use of UAVs in smallholder agriculture could offer detailed and spatially explicit information to smallholder farmers by availing information on local variations of cropland characteristics and facilitating on-field decisions such as when to apply chemicals and irrigate, bringing precision agriculture to disadvantaged farming communities. Furthermore, UAVs-derived remotely sensed data could potentially be used together with freely available satellite remotely sensed data for designing robust methods of characterising croplands (Mutanga, Dube et al., 2017).
- As individual ownership of UAVs by smallholder farmers could be beyond the reach of many because of limited financial resources, communal ownership could be an option, particularly for irrigation schemes. The operation of the UAVs can be done through an extension officer who could be trained to operate the UAVs and pass on the information to the smallholder farmers.
- The availability of multispectral UAV images enhances the development of high-resolution ET datasets. Existing satellite-derived ET datasets, such as GLEAM and MOD16, have coarse resolutions of more than 25 km and 1 km, respectively, which is not suitable for use in smallholder farming areas, which have an average

land tenure of about 2 ha (Cousins 2010, Nhamo; van Dijk et al., 2018). UAVs' user-defined spatial and temporal resolution offers significant benefits over satellites when estimating ET.

- Multispectral UAVs are poised to revolutionise smallholder agriculture by tackling agricultural challenges and other tasks collectively, thereby bringing precision agriculture to previously disadvantaged farming households. Using UAVs in smallholder agriculture is an opportunity to empower women and the youth as they dominate the smallholder agriculture sector.
- The operational flexibility of UAVs, their high efficiency and image quality, as well as high economic benefits and returns, make their application in agriculture not only conducive to resource conservation and environmental application but also very useful in agricultural applications for increasing crop yield and improving crop water productivity (Di Gennaro, Rizza et al., 2018; Simic Milas, Sousa et al., 2018). Increasing crop yield and improving crop water productivity are key factors to ensure food and water security in a drying environment and increasing demand from a growing global population.
- With limited land for agricultural expansion and water resources, UAVs can turn smallholder farms that currently lack technology into smart farmlands by inspecting crops and generating data within a short space of time and at low costs, and surveying fields in near real-time to enable the precise application of inputs and irrigation scheduling (Wang, Lan et al., 2019). Three niche areas for UAV applications that allow converting farms into small but effective smart enterprises include: scouting for problems, monitoring to prevent yield losses, and planning crop management operations (Hunt Jr and Daughtry, 2017).
- The impact of extreme weather events on smallholder agriculture demands urgent insurance mechanisms to enhance resilience to climate change. The high accuracy of UAV imagery and user-defined temporal resolution suits them to develop precise index-based crop insurance for the benefit of smallholder farmers and insurers.

Some disadvantages of using UAVs include (i) the limited time and flight range which is a big disadvantage for large farms, (ii) High-end agricultural UAVs are usually costly for individual ownership, (iii) UAV use is highly controlled in most countries; and most cases need to be registered, (iv) UAV are weather dependant as they cannot be used during windy or rainy days, and (v) they require certain skills to operate them and use the imagery for any productive means (Hunt Jr and Daughtry, 2017).

## **2.5 Conclusions**

Unmanned aerial vehicles have become important smallholder farming and agricultural water management tools. They are a source of high-resolution images acquired at user-defined temporal resolution at low altitudes, sufficient to effectively monitor crops in near real-time.

However, a lack of resources and skills to acquire and operate UAVs has limited their use in smallholder farming. This review recommends communal ownership of UAVs by smallholder farmers to reduce operational costs, as they have the potential to improve agriculture and water productivity. UAV remote sensing can transform smallholder agriculture by improving the mapping of small croplands, assessing crop water-nutrient deficiencies, improving crop water productivity and yield estimation, and improving crop evapotranspiration estimation with high accuracy. Applications of UAVs in smallholder agriculture could significantly improve input efficiency, environmental sustainability, and nutrition of farmers, as well as farm income and livelihoods. Although UAVs have the disadvantage of low coverage, this could be an important attribute for smallholder farmers as they can monitor the state of individual crops in real-time and act before the damage can spread, which is an effective way to maximise crop yield and quality. Water stress indices are not only important for irrigation scheduling, but they are also important for drought assessment and mitigation. As a result, water stress indices (CWSI and WDI) provide a better option for agricultural water management and climate change adaptation. The application of UAVs in smallholder agriculture would advance the importance of remote sensing in previously disadvantaged smallholder farmers by providing high-resolution images at the user-defined temporal resolution and by automating data collection, processing and analysis at low cost. This improves mapping accuracy, stress classification, irrigation scheduling and yield prediction for small croplands. UAVs are fast becoming key components of agriculture research and industry by being an important source of information of previously unavailable agro-meteorological data at the field scale. They are improving smallholder farmers' farming practices and, in the long term, could contribute to climate change adaptation and building resilience.

### **3 DEVELOPMENT OF HIGH-RESOLUTION MAPS OF AGRICULTURAL FIELD BOUNDARIES.**

Gokool S, Brewer K, Naiken V, Clulow A, Sibanda M and Mabhaudhi T

#### **3.1 Introduction**

The rapid expansion of the human population coupled with the impacts of climate and land-use land-cover (LULC) changes are significant factors presently contributing to global food insecurity (Hall, Dawson et al., 2017). Since this situation is projected to progressively worsen in the future, improving food security with a focus on providing nutritious food that is produced in an environmentally sustainable manner is high on the political agenda of governments worldwide (Gomez y Paloma, Riesgo et al., 2020). Fan and Rue (2020) state that agricultural practices must undergo a major overhaul over the next few decades to meet the targets above.

Smallholder farms which are typically less than 2 hectares in size, contribute an inordinate amount to food production relative to the area they occupy and, therefore, can play a pivotal role in tackling food security challenges (Wolfenson, 2013; Lowder, Skoet et al., 2014; Kamara, Conteh et al., 2019; Kpienbaareh, Sun et al., 2021). In many developing countries worldwide, smallholder farms are not only major contributors to agricultural production and food security but are also one of the main drivers of socio-economic growth (Kamara, Conteh et al., 2019). Despite their relative importance, smallholder farms generally lack the resources of their larger-scale commercial counterparts. Subsequently, their agricultural productivity potential is often not realized, resulting in these farms not effectively contributing to addressing food security and socio-economic challenges (Department of Agriculture and Fisheries, 2012; Kamara, Conteh et al., 2019; Nhamo, Magidi et al., 2020). To remedy this situation, smallholder farmers in developing countries require innovative, evidence-based, and low-cost solutions that can assist them in optimizing their productivity (Agidew and Singh, 2017; Nhamo, Magidi et al., 2020).

Several studies have demonstrated the potential of using remote sensing technologies for agricultural applications. However, these applications typically use satellite-earth observation or manned aerial vehicles (Manfreda, McCabe et al., 2018). Satellite-earth observation datasets and associated products can provide information at various spatial, spectral and temporal resolutions. However, their application in smallholder farm settings is limited. The spatial resolution of open-access datasets or products is too coarse to capture the spatial heterogeneity generally found within smallholder farms. Whereas more advanced satellite-earth observation systems and manned-aerial vehicles, which can capture data at finer spatial resolutions (metre to sub-metre spatial resolution), are often too costly for widespread smallholder agricultural applications (Cucho-Padin, Loayza et al., 2020).

Furthermore, satellite revisits and repeat cycles coupled with the influence of cloud cover reduce the frequency at which data can be captured and processed (Manfreda, McCabe

et al., 2018; Nhamo, Magidi et al., 2020). Recently, precision agricultural practices facilitated by unmanned aerial vehicles (UAVs) have gained traction in the agricultural sector (Cucho-Padin, Loayza et al., 2020; Radoglou-Grammatikis, Sarigiannidis et al., 2020; Delavarpour, Koparan et al., 2021). UAVs have been shown to hold vast potential for agricultural applications, as relatively low-flying UAVs can potentially capture very-high spatial resolution data at various spectral resolutions (depending on the optical properties of the onboard camera). Moreover, data can be captured at user-determined intervals with this data being less severely impacted by the effects of cloud cover, thus allowing for data to be captured more frequently than satellite-based approaches (Torres-Sánchez, Peña et al., 2014; Manfreda, McCabe et al., 2018; Bennett, Younes et al., 2020; Cucho-Padin, Loayza et al., 2020).

The features mentioned above and the relatively lower costs of UAVs have seen them emerge as a promising tool for smallholder agricultural applications (Salamí, Barrado et al., 2014, Cucho-Padin, Loayza et al., 2020). While there is a great deal of potential in using UAVs for smallholder agricultural applications, processing UAV data to derive meaningful outputs can prove challenging. UAV data processing can be computationally intensive and may require expensive specialised software and user expertise, which are not always readily available (Bennett, Younes et al., 2020). Advancements in geospatial cloud computing platforms such as Google Earth Engine (GEE) have provided a means to address these limitations by providing users with inter-alia high-level computational power and sophisticated image analysis techniques (Gorelick, Hancher et al., 2017).

According to Bennett, Younes et al. (2020), with the increased use of UAVs for various applications and the growing popularity of utilizing cloud-based computing platforms for image analysis, it is important to develop reproducible and adaptable techniques that can be easily shared to facilitate more efficient analysis of UAV imagery for future applications. To this end, in this study, we aim to explore and demonstrate the utility of using GEE and multi-spectral UAV imagery to map LULC within smallholder rural farms situated within the KwaZulu-Natal (KZN) province of South Africa. The ability to accurately map the location and spatial distribution of crops and monitor their growth over time plays a pivotal role in agricultural management (Nhamo, Magidi et al., 2020).

Quantifying spatio-temporal LULC dynamics within smallholder farms can play an important role in more effectively managing resources and enhancing the productivity of these farms, as changes in agricultural crop types, management practices, climatic influences, water use, efficiency, and vegetation health can be assessed in near-real time which can allow for quick and decisive management actions to be taken (Ketema, Wei et al., 2020; Kpienbaareh, Sun et al., 2021).

## **3.2 Materials and Methods**

### **3.2.1 Study site description**

The study site is located within Ward 8 of the rural community of Swayimane, which forms part of the uMshwati municipality situated within the KwaZulu-Natal province of South Africa (Figure 3.1). Swayimane is approximately 880 m.a.s.l and covers a geographic extent of 32 km<sup>2</sup>. A generally warm climate with cooler, dry winters and warm wet summers is experienced within the study area (Lembede, 2017; Lucas, 2018). Mean annual precipitation ranges between 500 and 800 mm, with most rainfall received during the summer months as high-intensity thundershowers (Basdew, Jiri et al., 2017). Mean annual temperatures range between 11.80 and 24.0°C.

The community of Swayimane are largely dependent on subsistence farming to support their livelihoods. Farming consists of cropping and animal husbandry, with crops dominating the agricultural system, while animals are primarily used for land preparation. Farmers grow various crops with the most common including maize, amadumbe (taro), sugarcane and sweet potato. Although the study area is characterised by good rainfall and deep soils, these soils are depleted in some mineral elements essential to good and sustained crop production. Further compounding this situation is the influence of short-term droughts on crop performance. Due to the projected increases in the frequency of extreme events, threats to food security and livelihoods are an ever-present challenge that surrounding communities face.

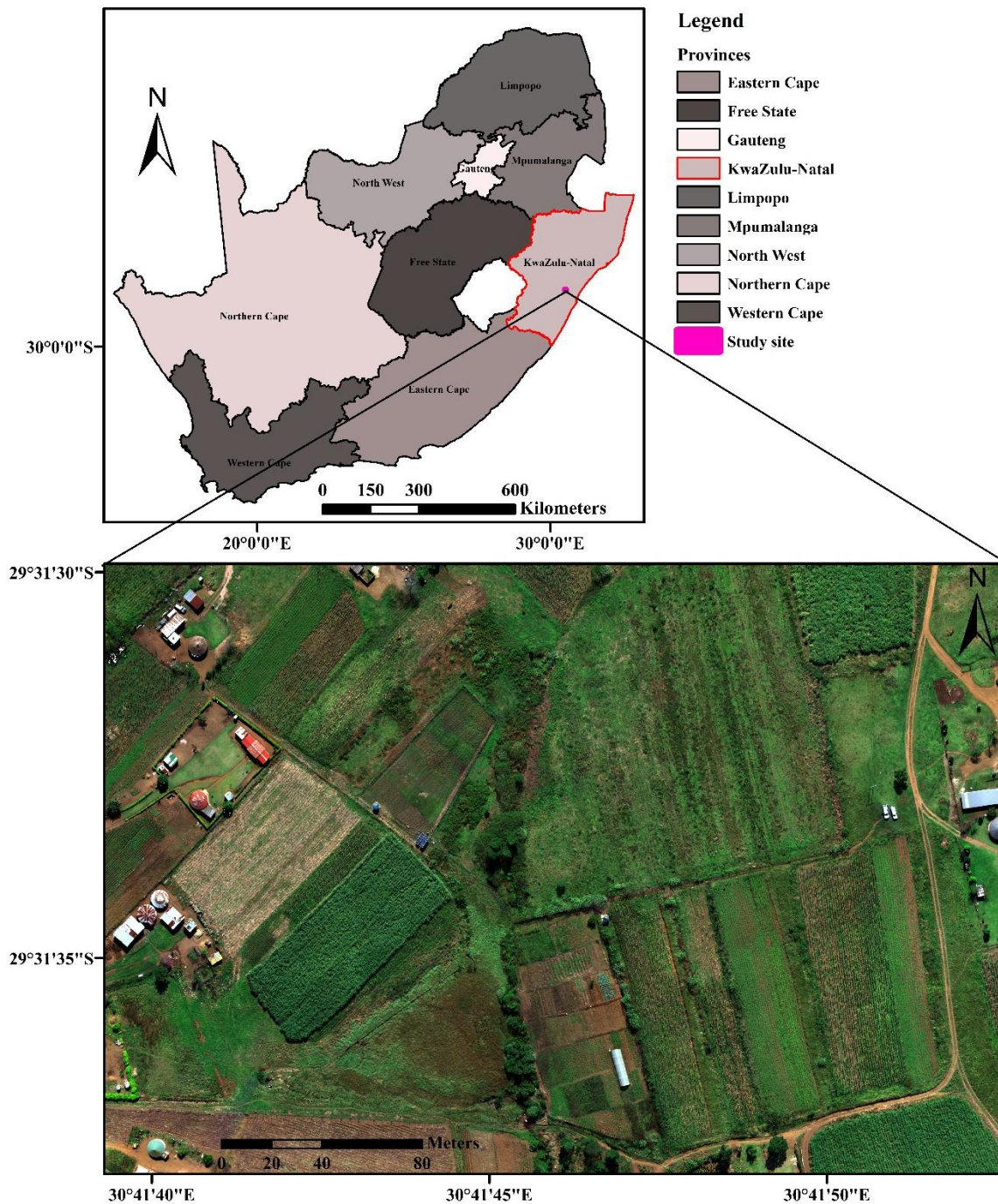


Figure 3-1: Location of the study site within the KwaZulu-Natal province of South Africa

Considering the socio-economic circumstances of this community in concert with the biophysical factors which influence crop production, this study site provides the ideal opportunity to demonstrate how the use of UAVs can be utilized to provide a relatively cost-effective approach to provide spatially explicit information in near-real time, which can then be used to inform and guide operational decision making at a localised level to enhance crop production and mitigate the risk of crop failure in the future.

### 3.2.2 Data acquisition and processing

The image for the study area was collected using a consumer-grade DJI Matrice 300 (M-300) UAV fitted with a Micasense Altum multispectral sensor and Downwelling Light Sensor 2 (DLS-2). The Altum imaging sensor captures data in the electromagnetic spectrum's blue, green, red, red-edge and near infra-red regions (<https://micasense.com/altum/>). The Altum imaging sensor was configured to capture images with a 75% overlap across the study area. The study area boundary was digitised within Google Earth and saved as a “kml” file which was then imported into the DJI smart controller that had been connected to the internet following the creation of a DJI user account. The “kml file” was used to design an optimal flight path to acquire images covering the entire study area.

The DJI Matrice 300 was configured to fly at an altitude of 100 m, sufficient to capture data at a 0.07 m pixel resolution for the entire study area. Light intensity changes during the day were accounted for through calibration before and after each flight mission using the MicaSense Altum calibrated reflectance panel (CRP). All captured images were then pre-processed using Pix4d software before further analysis. The UAV image pre-processing involved performing radiometric corrections and mosaicking the multiple images captured during the flight into a single orthomosaic.

The orthomosaic image was then uploaded and imported into GEE for further processing. Training data for the image classification was acquired through visual inspection of the orthomosaiced UAV image captured on the 28<sup>th</sup> of April 2021. Five broad LULCs were identified, and training data was collected by identifying pixels containing one of these classes (Table 3-1). A total of 150 points were captured for each class, with 70% of this data being randomly selected for the training of the classification algorithm and the remaining 30% being reserved for validation of the classification accuracy.

Table 3-1: A description of the LULC classes identified and categorized for mapping.

<b>Broad LULC class</b>	<b>LULC present in each Broad LULC</b>
1. Buildings and Infrastructure	Buildings, roads, water tanks and solar panels
2. Bareground	Bare soil, harvested crops, dirt roads
3. Crops	Maize, sugarcane, amadumbe, sweet potato and butternut
4. Grassland	Grassland
5. Trees and Shrubs	Intermediate and tall trees or shrubs

All the spectral bands captured by the UAV on-board sensor, as well as nine indices (NDVI, greenNDVI, Red-edge NDVI, EVI, SAVI, Simple Blue and Red-edge Ratio, Simple NIR and Red-edge Ratio, Simple NIR ratio and Green chlorophyll index) for each of the training and validation points, were extracted and used as covariates to train the classification algorithm (Midekisa et al., 2017). To model and predict the five broad LULC, some of the commonly used machine learning classification algorithms i) Classification and Regression Tree (CART), ii) Support Vector Machine (SVM), iii) Random Forest (RF) and iv) Gradient Tree Boost (GTB)

available in GEE were deployed. Accuracy assessments (Overall accuracy, User accuracy, Producer accuracy, kappa coefficient) were then performed for each classifier using the training and validation datasets. The best-performing classifier was then selected to classify the image by combining the training and validation data into a single dataset (Shelestov, Lavreniuk et al., 2017).

Once the best-performing classifier had been established and applied to the original image (0.07 m), the spatial resolution of the image was resampled in GEE using bilinear interpolation to produce lower-resolution images (0.50, 1.00 and 2.00 m). The classification process was then repeated using the best-performing classifier and these images to identify the optimal resolution (C1) for mapping LULC within the study area (Zhao et al., 2019). An additional feature of GEE is the ability to utilize certain classifiers to perform probabilistic classifications to determine the likelihood of a pixel belonging to a particular LULC class (Rebelo, Gokool et al., 2021). Considering the availability of this feature and ease of application within GEE, we also performed a probabilistic classification (C2) using the RF classifier and optimal spatial resolution image to distinguish agriculture from all other classes.

The C2 classification provides less detail regarding the various LULC classes in the study area and is therefore limited in its potential applications (Rebelo, Gokool et al., 2021). However, distinguishing crops from other LULC classes can be quite useful, particularly when there is limited knowledge of the variety of classes present. To perform the C2 classification, the previously collected training data points were divided into two classes, i.e. crops and other (including all other LULC classes). These were then used to train the classification algorithm to determine the probability of a pixel being a crop within the optimal spatial resolution UAV image. Following the UAV image classification, pixels with a greater than 50% probability of being a crop were identified and used to separate crops from other LULC classes. A conceptual representation of the entire methodological process is provided in Figure 3 2 to better understand how the proposed methodology was executed.

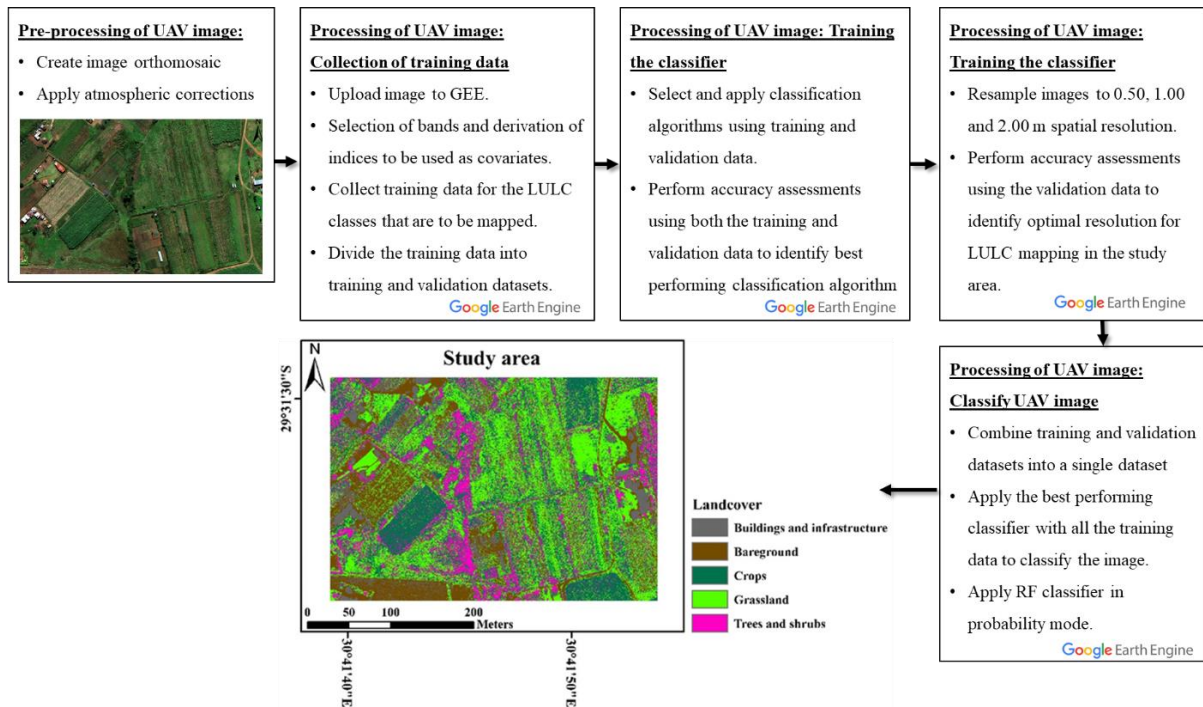


Figure 3-2: A conceptual representation of the process followed to develop and test the LULC classification model.

### 3.3 Results

#### 3.3.1 Identifying the best-performing classifier for the original UAV image

The best-performing classification algorithm was the GTB classifier, marginally outperforming the RF classifier. The LULC classification using the GTB model achieved an overall accuracy (OA) of 87%, as shown in Table 3-2. The average class-specific producer (PA) and user (UA) accuracies for the GTB classification were 87.40% ( $\pm 8.35$ ) and 87.00% ( $\pm 9.03$ ). The buildings, infrastructure, and bareground classes were most accurately predicted within the GTB classification, whereas crops were the least accurately predicted.

Table 3-2: Classification accuracies for the original spatial resolution (0.07 m) based on various classification algorithms available in GEE.

Accuracy Assessment								
	CART		SVM		RF		GTB	
<b>Overall Accuracy (%)</b>	80.00		82.00		87.00		87.00	
<b>Kappa Coefficient</b>	0.75		0.77		0.84		0.84	
	PA (%)	UA (%)	PA (%)	UA (%)	PA (%)	UA (%)	PA (%)	UA (%)
Buildings and Infrastructure	92.00	90.00	92.00	98.00	92.00	98.00	96.00	96.00
Bare ground	94.00	94.00	100.00	91.00	98.00	90.00	96.00	96.00
Crops	68.00	71.00	60.00	83.00	80.00	83.00	78.00	85.00
Grassland	74.00	65.00	95.00	59.00	80.00	77.00	86.00	75.00
Trees & Shrubs	69.00	75.00	67.00	82.00	83.00	83.00	81.00	83.00
GTB Confusion Matrix								
	Buildings and Infrastructure	Bare ground	Crops	Grassland	Trees & Shrubs	UA (%)		
Buildings and Infrastructure	46	2	0	0	0	96.00		
Bare ground	1	48	0	0	1	96.00		
Crops	0	0	39	1	6	85.00		
Grassland	1	0	7	30	2	75.00		
Trees & Shrubs	0	0	4	4	39	83.00		
<b>PA (%)</b>	96.00	96.00	78.00	86.00	81.00			
<b>OA (%)</b>	87.00							
<b>Random Accuracy (%)</b>	20.00							
<b>Kappa coefficient</b>	0.84							

### 3.3.2 Comparison of the best-performing classifiers at different spatial resolutions

The classification results for each of the different spatial resolution UAV images that were classified using the GTB classification algorithm are shown in Table 3-2 and Figure 3-3. The overall classification accuracy and kappa coefficient for each of these classifications were relatively high. However, the highest level of accuracy was achieved using a spatial resolution of 1.00 m (C1), whereas the lowest classification accuracy was obtained at a spatial resolution of 5.00 m.

The C1 classification achieved an OA of 95%, with an average PA and UA of 95.20%. Buildings and infrastructure were most accurately predicted within the C1 classification, whereas crops were least accurately predicted. Since the 1.00 m spatial resolution UAV image was identified as the optimal resolution for mapping LULC within the study area, this image was then used to perform the C2 classification (Figure 3-4).

Table 3-3: Classification accuracies for the UAV images at differing spatial resolutions classified using the GTB classification algorithm.

Accuracy Assessment								
Spatial resolution	0.07 m		0.50 m		1.00 m		5.00 m	
OA (%)	87.00		90.00		95.00		84.00	
Kappa Coefficient	0.84		0.87		0.94		0.80	
	PA (%)	UA (%)						
Buildings and Infrastructure	96.00	96.00	100.00	98.00	100.00	98.00	89.00	88.00
Bare ground	96.00	96.00	98.00	100.00	98.00	98.00	68.00	89.00
Crops	78.00	85.00	78.00	82.00	90.00	94.00	96.00	80.00
Grassland	86.00	75.00	86.00	84.00	96.00	94.00	91.00	80.00
Trees & Shrubs	81.00	83.00	87.00	85.00	92.00	92.00	80.00	84.00

GTB Confusion Matrix for 1.00 m spatial resolution UAV image						
	Buildings and Infrastructure	Bare ground	Crops	Grassland	Trees & Shrubs	UA (%)
Buildings and Infrastructure	43	1	0	0	0	98.00
Bare ground	0	42	0	0	1	98.00
Crops	0	0	46	1	2	94.00
Grassland	0	0	2	46	1	94.00
Trees & Shrubs	0	0	3	1	44	92.00
PA (%)	100.00	98.00	90.00	96.00	92.00	
OA (%)	95.00					
Random Accuracy (%)	20.00					
Kappa coefficient	0.94					

### 3.3.3 Comparison of optimal spatial resolution classification against publicly available LULC maps for the region

The C1 and C2 classification results were compared against the 2020 ESRI and 2020 South African National Landcover (SANLC) maps, among the most recent (moderate spatial resolution) publicly available LULC maps for the region. Comparisons between the C1 classification and these maps (Figure 3-5) showed differences in the total number of LULC classes that are mapped and the area which they occupy within the study area. Focusing specifically on crops, the total area classified as crops for classifications C1 (0.03 km<sup>2</sup>) and C2 (0.02 km<sup>2</sup>) was relatively similar, occupying approximately 30 and 20% of the study area, respectively.

Whereas the total area classified as crops within the 2020 ESRI (0.08 km<sup>2</sup>) and 2020 South African National Landcover (0.07 km<sup>2</sup>) datasets is relatively similar and more than two-fold larger than the area classified as crops for classifications C1 and C2.

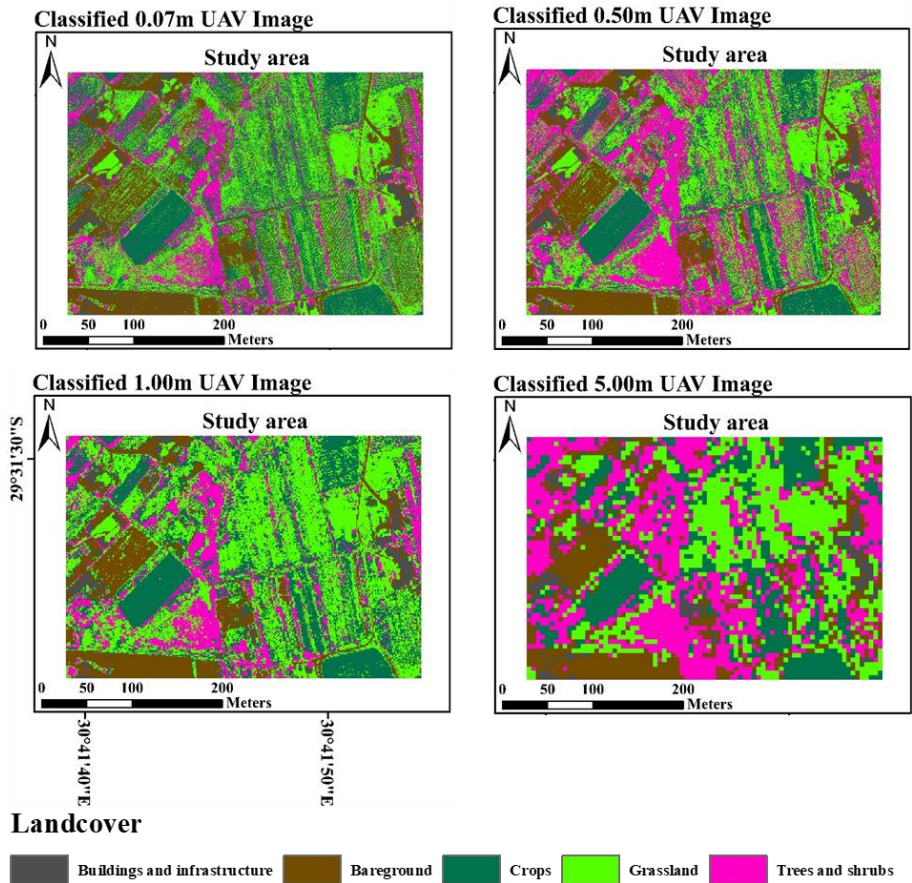


Figure 3-3: A comparison of the classification results for the study area at different spatial resolutions.

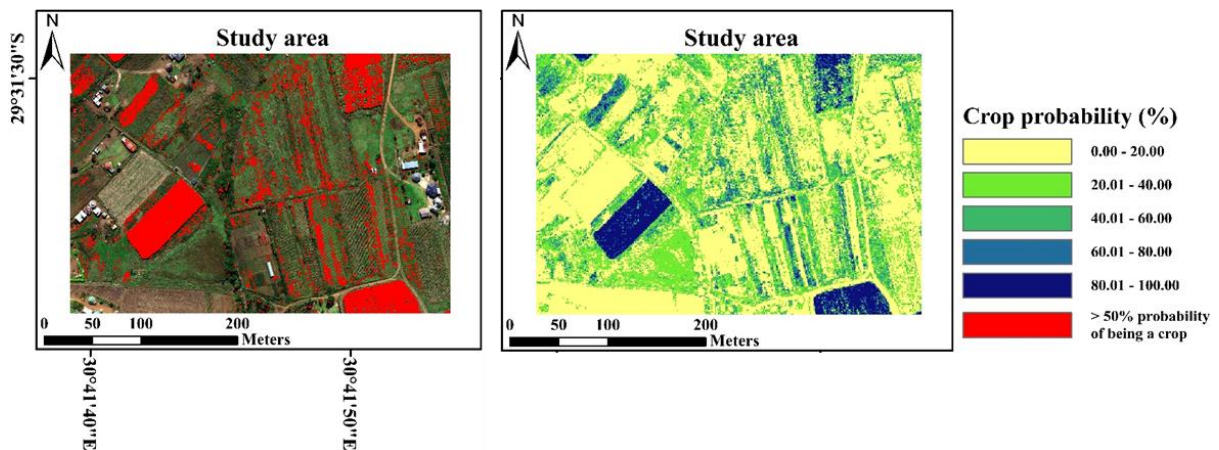


Figure 3-4: Results of the C2 classification used to distinguish crops from other LULC classes within the study area.

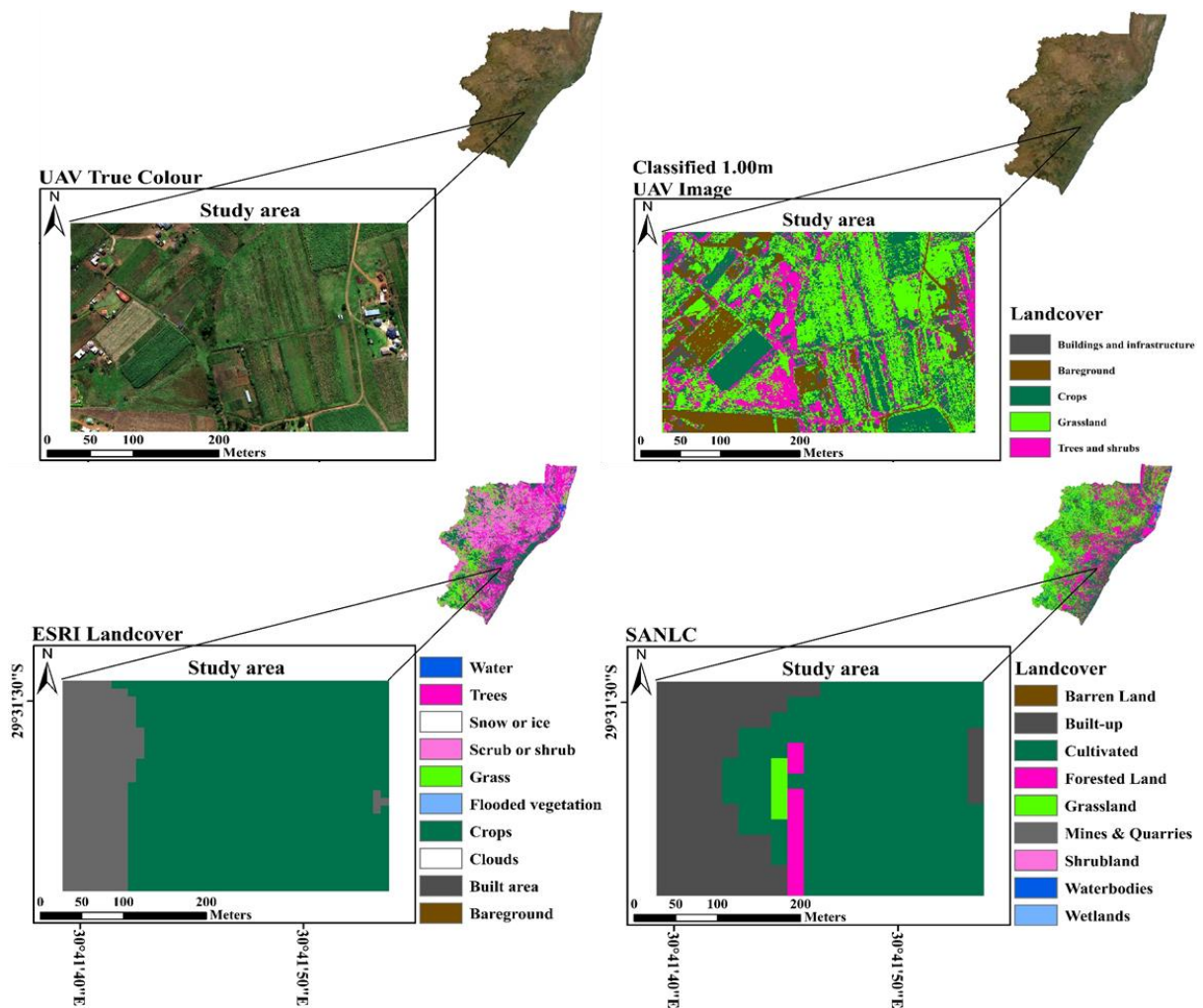


Figure 3-5: A comparison of the C1 classification for the study area against the 2020 ESRI and South African National Landcover map.

### 3.4 Discussion

The machine learning algorithms available within GEE performed relatively well at mapping LULC within the study area. However, it should be noted that the training and evaluation of these algorithms were performed using a limited sample size that was collected entirely from visual inspection of the UAV True colour image. The collection of training data from visual inspection of the UAV image does promote ease of application and expedites the classification process. However, this may have contributed to misclassification, as some of the data points may have been incorrectly identified or may not have adequately represented the unique spectral properties for each mapped class.

Subsequently, it is recommended that the sample size is increased and ground truth data be included in the training and evaluation process where possible so that a more accurate and objective assessment of the performance of these classification algorithms can be ascertained. Comparisons between the various classification algorithms showed that the

ensemble machine learning algorithms (RF and GTB) performed the best. This occurrence may have been due to the ability of these ensemble-machine learning methods to combine several predictive models to create a single model that can improve predictive performance by decreasing variance as well as bias and producing a model with greater accuracy than the single machine learning models (Abdi, 2020).

Although the RF and GTB models performed better than the SVM and CART models, the accuracies presented here may not represent the maximum possible. These values will largely be influenced by the user-specified parameter choices for each algorithm (Abdi, 2020). While it was not within the scope of this study, Abdi (2020) recommends that an unbiased evaluation of each algorithm's performance is undertaken through an equally robust hyper-parameter selection where possible so as not to introduce bias into the model's performance. During this process, these algorithms should be evaluated with respect to their overall accuracy and ability to adequately represent each LULC class (Abdi, 2020).

The classification accuracy of all LULC classes was generally greater than 75% across the different spatial resolution UAV images classified using the GTB classification model. The major source of inaccuracy in these classifications was the confusion between Crops, Grasslands and Trees and Shrubs. The confusion in this instance was largely unidirectional as a greater proportion of Crops were misclassified as either Grassland or Trees and Shrubs. This confusion may be a combined consequence of the training data used during the classification process and the relatively low spectral resolution of the UAV on-board sensor, making it difficult to distinguish between certain spectrally similar (Böhler, Schaepman et al., 2018).

Using higher spectral resolution data may allow for the unique spectral characteristics of the various LULC classes to be more adequately represented. Furthermore, this may also present an opportunity to map LULC within the study area in greater detail than the broad LULC classes mapped in this study. This, in turn, may allow the resultant landcover map to apply to a wider range of applications.

Although the acquisition and use of higher spectral resolution imaging sensors may help address the spectral resolution limitations of this study, this is generally accompanied by higher costs. The fusion of high spatial resolution UAV imagery with freely available higher spectral resolution satellite imagery does present an alternate and more pragmatic approach to potentially address the challenges above. However, further testing is advocated before these are readily implemented (Adão, Hruška et al., 2017; Böhler, Schaepman et al., 2018).

Despite the misclassification errors observed, the classification accuracy of crops for the 1.00 and 5.00 m spatial resolution UAV images was greater than the 85% target accuracy specified by (McNairn, Champagne et al., 2009). The classified 1.00 m spatial resolution image produced the highest classification accuracies overall and for individual classes. While this image was not the highest spatial resolution image that could be used for the mapping of LULC within the study area, this spatial resolution was still unrivalled in its ability to capture the spatial heterogeneity within the study area when compared against the publicly available LULC maps for the region (Figure 3-5).

The results of the comparisons between the classification accuracies for the different spatial resolution UAV images that were classified were consistent with the findings of Zhao et al. (2019). They showed that using a higher spatial resolution image does not necessarily translate into improved classification accuracy. While the 1.00 m spatial resolution image produced the highest overall and individual class accuracies, this spatial resolution should not be viewed as a generalized optimal spatial resolution as this may vary for specific LULC classes or agricultural applications (Zhao, 2019). Instead, this spatial resolution can be used as a reference point for selecting an optimal resolution for future UAV-based applications within the study area.

### **3.5 Conclusions**

Smallholder farms are major contributors to agricultural production, food security and socio-economic growth in many developing countries worldwide. However, these farms generally lack the resources to maximize their agricultural potential. They cannot effectively contribute to addressing the food security and socio-economic challenges that many of these regions face.

Recently, UAVs have been gaining traction in the agricultural sector. With the emergence of geospatial cloud computing platforms, there are now greater opportunities for many smallholder farmers in developing nations worldwide to integrate technological advances into their agricultural practices to optimize their productivity. The synergistic application of these technologies offers the opportunity to develop bespoke, innovative, low-cost solutions that can facilitate improved agricultural management within smallholder farms.

Considering these developments, in this study, we aimed to demonstrate how GEE can be leveraged to maximize the potential of UAVs for mapping LULC in smallholder farms, with a specific focus on cultivated areas. The results of these investigations demonstrated that LULC could be mapped accurately using UAV imagery and GEE's image classification procedures. Furthermore, the UAV-derived LULC map outperforms the region's publicly available landcover maps in capturing the spatial heterogeneity within the study area. While these investigations could have benefited from the availability of more training data or higher spectral resolution data, the overall results were quite promising. They can serve as a foundation for the development of improved land cover maps for the study area in the future, which in turn can facilitate improved agricultural management.

Notwithstanding the limitations of the study, the use of GEE is particularly useful for processing and analysing UAV imagery for applications such as LULC mapping, as it seamlessly tackles computationally intensive tasks and provides a wide range of users with a repeatable and flexible approach that can be easily adapted and shared for various applications. The availability of such approaches is particularly beneficial to data-scarce and resource-poor regions, as it provides users with a powerful tool to guide support and decision-making.

## 4 PREDICTING CHLOROPHYLL CONTENT OF MAIZE USING UAV-DERIVED MULTISPECTRAL REMOTELY SENSED DATA

Brewer K, Clulow A, Sibanda M, Gokool S, Naiken V and Mabhaudhi T

### 4.1 Introduction

Smallholder agricultural systems contribute significantly to agricultural production, livelihood sustenance, and socioeconomic growth in developing nations (Kamara, Conteh et al., 2019). Specifically, in sub-Saharan Africa, smallholder farming practices are threatened by a decline in productivity and profitability due to climatic variability's recent and ongoing effects (Salami, Kamara et al., 2010; Vanlauwe, Coyne et al., 2014; Adisa, Botai et al., 2018). Maize (*Zea mays L.*) is one of the staple grain crops grown in South Africa and is extensively cultivated at a subsistence scale for household economic gain, food security, and feedlots (Tefera, Kanampiu et al., 2011; Adisa, Botai et al., 2018). Smallholder farmers typically cultivate maize under rainfed conditions to maximize production and produce healthy crop yields. Despite the goals of smallholder farmers to optimize yields, small-scale farming systems often face various challenges (Unganai and Murwira 2010; Adisa, Botai et al., 2018). Their dependence on rainfall poses a significant threat to crop yields, as reduced seasonal rainfall and severe weather impact the overall crop health, biochemical processes, and physical development of crops (Muzari, Gatsi et al., 2012; Okonya, Syndikus et al., 2013). Smallholder farms also lack the resources required to maximize their potential and are often faced with low unproductive yields significantly lower than the potential of the land (Walker and Schulze, 2006). Hence, it is imperative to provide smallholder farmers with innovative, effective, low-cost solutions to assist them in optimizing their productivity to produce increased and healthy yields (Shi, Thomasson et al., 2016; Nhamo, Magidi et al., 2020). Therefore, a deeper understanding of crop dynamics could assist smallholder farmers in identifying crop health issues at an early stage, allowing them to implement the necessary remedial solutions to ensure productivity.

Literature has documented various indicators of crop health (Whitford, De Soyza et al., 1998; Nicholls, Altieri et al., 2004; Hernández-Clemente, Hornero et al., 2019); however, chlorophyll content has been identified as one of the most important and reliable health and productivity indicators (Flynn, Frazier et al., 2020). This is due to the biophysical pigment in the leaves and biochemical photosynthetic processes that suggest plant productivity (Terashima, Fujita et al., 2009, Tahir, Naqvi et al., 2018). Hence, monitoring its concentration and variability in plants could aid in evaluating crop productivity through time (Zhang, He et al., 2019), which is significant towards detecting subtle crop changes and optimizing healthy yields in smallholder farming practices (Afzal and Mousavi 2008; Li, Liu et al., 2015).

Advanced and objective tools such as remote sensing have been utilized for estimating and monitoring agricultural vegetative health and productivity for several years (Pinter Jr, Hatfield et al., 2003; Wu, Meng et al., 2014). For example, Sibanda, Mutanga et al. (2020) estimated the foliar chlorophyll content of grasses using field-based hyperspectral data, Delegido,

Verrelst et al. (2011) estimated the chlorophyll content of multiple crops using Sentinel-2 red-edge bands, and Kooistra and Clevers (2016) estimated the chlorophyll content in potato leaves using vegetation indices derived from RapidEye satellite imagery. Such studies have illustrated remote sensing as a powerful tool in characterizing chlorophyll concentrations in different vegetation. Thus, at a farm scale, it may be useful to use chlorophyll as a proxy for crop health and productivity (Kanning, Kühling et al., 2018).

Remote sensing techniques obtain the potential to monitor crop productivity and map its spatial distribution based on high-resolution images of varied wavelengths (Miao, Mulla et al., 2009; Duveiller, López-Lozano et al., 2013; Nhamo, Magidi et al., 2020). Conventional applications of earth observation techniques use satellite-borne earth observation or manned aerial vehicles (Nhamo, van Dijk et al., 2018; Berra and Peppas, 2020). However, a major constraint of freely available satellite-borne data is its inability to fulfil the ever-increasing need for high spatial and temporal resolution data, which is necessary for monitoring small-scale crop properties throughout phenotyping (Psirofonis, Samaritakis et al., 2017). Moreover, manned aerial vehicles can overcome the issues of spatio-temporal resolution, but the associated costs are a major limitation to smallholder farms.

In recent years, unmanned aerial vehicles (UAVs) have been globally recognized as innovative, low-cost, and effective precision technology for agricultural applications. UAVs offer state-of-the-art image data throughput analytics at very high resolutions (VHR) and have proven to be effective in overcoming the limitations of satellite imagery (Maes and Steppe, 2019; Nhamo, Magidi et al., 2020). UAVs have great potential in small-scale agriculture as the low-flying altitudes capture VHR spatial and spectral data. High-resolution images are acquired by multispectral cameras mounted onboard UAVs, which offer near real-time data critical for monitoring subtle shifts in crop phenology and vigour. Moreover, UAVs can be deployed frequently at user-determined ground sampling distances and revisit times, impossible with conventional freely accessible satellite-borne sensors such as Landsat 8 Operational Land Imager or Sentinel 2 Multispectral Instrument (Xiang and Tian, 2011). Thus, VHR UAV imagery can detect individual maize plants, canopy patches and, ultimately, phenological growth patterns over the fragmented smallholder fields. Therefore, accurate mapping and analysis of smallholder maize fields using a VHR UAV hold significant potential for providing data that could inform farmers on the health status of their crops through the phenological cycle.

Specifically, multispectral chlorophyll data can be optimally assessed using UAV-derived vegetation indices (VIs) and a robust machine-learning algorithm. VIs are mathematical transformations of image bands used quantitatively to extract spectral properties such as canopy cover, plant vigour and phenological dynamics (Xue and Su, 2017; Khan, Rahimi-Eichi et al., 2018). The most common index used for plant health is the normalized difference vegetation index (NDVI), which is directly used to acquire information on the physiological health status of crops and crop growth changes (Boken and Shaykewich, 2002; Gitelson, Peng et al., 2014). Particularly, chlorophyll-specific VIs have proven to be more valuable than normalized VIs in some instances as they include a variety of combinations from bands which reflect highly in vegetation (Wu, Meng et al., 2014). Such indices include the canopy chlorophyll content index (CCCI) and the modified chlorophyll absorption ratio index (MCARI),

which have shown significant correlations to crop chlorophyll content (Haboudane, Miller et al., 2002; Raper and Varco, 2015).

Furthermore, machine learning algorithms such as random forest, support vector machines and multiple linear regressions have proven to be instrumental in characterizing crop chlorophyll content and health status (Abdel-Rahman, Ahmed et al., 2013; Han, Yang et al., 2019; Guo, Yin et al., 2020; Hassanijalilian, Igathinathane et al., 2020). The random forest ensemble has been widely proven to outperform the other two algorithms above (Yao, Yang et al., 2013; Ramos, Osco et al., 2020). Hence it is anticipated that using UAV-derived data (spectral bands and VIs) with the robust random forest regression could produce accurate results to quantitatively assess the chlorophyll content of maize as an indicator of health in smallholder farms.

Thus, with maize being one of the dominant food crops grown across South Africa, it is necessary to assess its health in smallholder agricultural systems through a robust multispectral sensor. A multispectral sensor enables proximal remote sensing analysis of maize and can potentially predict chlorophyll content, which informs the crop's health status. In this regard, this study aims to investigate the potential of multispectral UAV-derived data to assess maize crop chlorophyll content using the random forest model simulation for an improved understanding of crop health and productivity in smallholder agricultural systems. Therefore, the objectives of the study were to (1) estimate chlorophyll content variations across the different maize phenological stages using UAV-derived data and (2) determine the optimal maize growth stage(s) for chlorophyll model prediction.

## **4.2 Materials and Methods**

### **4.2.1 Study site description**

The research was conducted over four months from February 2021 to May 2021 in the rural area of Swayimane, KwaZulu-Natal (29°31'24"S; 30°41'37" E) (Figure 4-1). Swayimane is in the uMshwathi Local Municipality, located approximately 55 km northeast of Pietermaritzburg. The small communal area covers a geographical extent of approximately 36 km<sup>2</sup>, and smallholder farming systems of the local community dominate land use. Common crops cultivated in the area include white and yellow maize, sugarcane, amadumbe (*taro*), and sweet potato. The smallholder farmers follow traditional farming methods of planting, maintenance, and manual harvesting of crops. Farm plots are rainfed, fertilized using livestock manure and hand-weeded by farmers. Alternatively, herbicide backpack sprayers are used by small growers to control weeds and grasses. The area is predominantly characterized by semi-subsistence farming, which is a form of food security and livelihood sustenance. The produce is sold at local markets for economic benefits, which sustains farmers' livelihoods.

The favourable environmental conditions of the region support agriculture and crop production in Swayimane. The climate is characterized by warm wet summers and cool, dry winters, with an annual average air temperature of approximately 18°C. The mean annual rainfall ranges between 600 and 1200 mm, with the most rain occurring during the summer as thunderstorms.

During the research period, Swayimane had a maximum average air temperature of 24°C and total rainfall of 242.8 mm, amongst other weather data (Figure 4-2). Weather conditions were continuously monitored by the Automatic Weather Station installed at a Swayimane high school. Weather data was downloaded from the Swayimane weather website. The weather station is approximately 2 km from the smallholder maize farm, and as such, it is proximally adequate in capturing the weather conditions of the study site. The research was conducted on a 30 × 96 (2850 m<sup>2</sup>) smallholder maize field (Figure 4-1). The field was located on a slope with a ranging field elevation of approximately 850 m to 839 m.

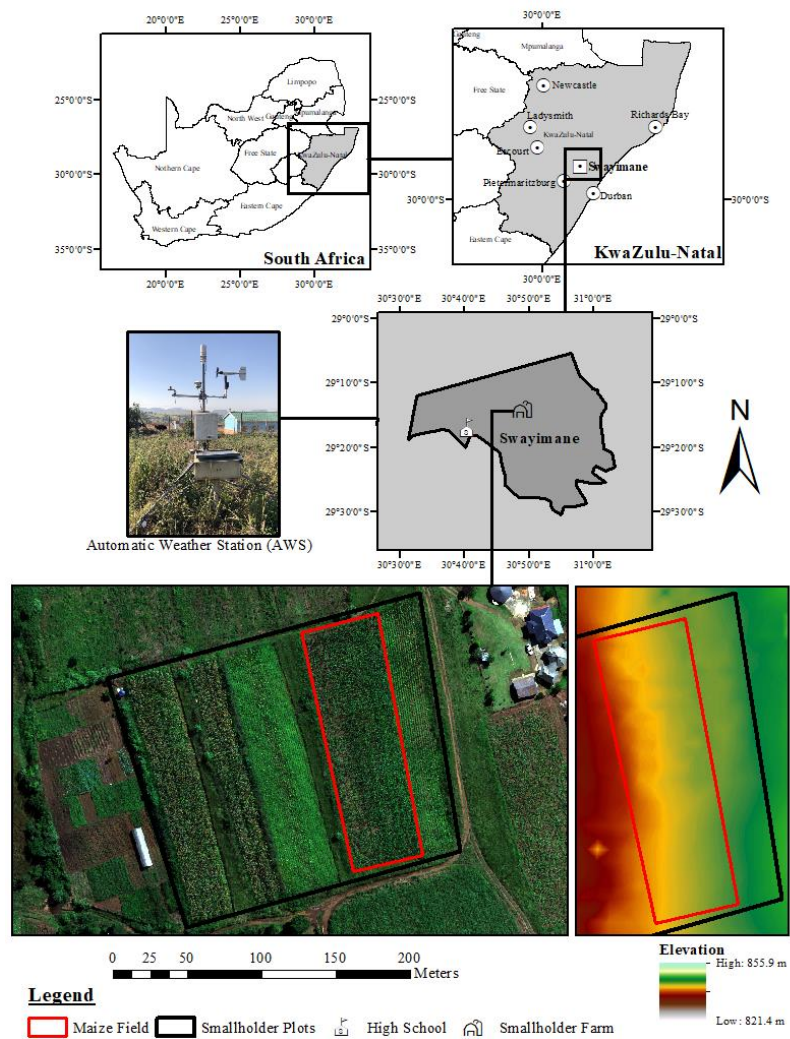


Figure 4-1: Location of the Swayimane study area, study site, and smallholder maize field.

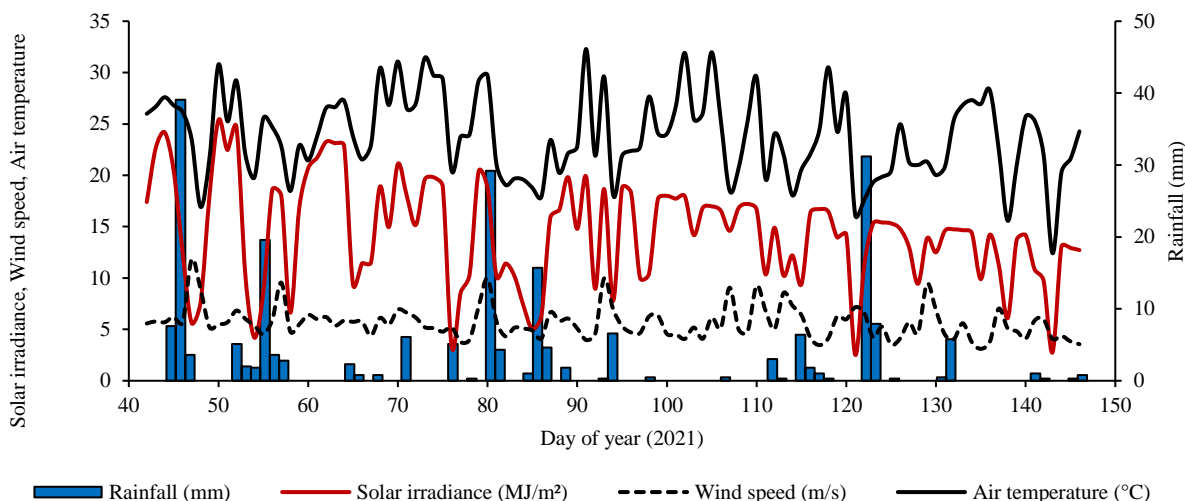


Figure 4-2: Swayimane weather conditions throughout maize phenotyping

#### 4.2.2 Maize phenotyping

Maize seedlings were sown on the 8<sup>th</sup> of February 2021 and harvested on the 26<sup>th</sup> of May 2021, having a total growth cycle of 108 days (Table 4-1). Chlorophyll was examined at different growth stages of the maize phenological cycle. Maize growth is divided into vegetative stages (which range from emergence to tasseling based on the number of fully expanded leaves) and reproductive stages (which range from silking to physiological maturity based on kernel development) (Cakir, 2004; Zhao, Tong et al., 2012). Certain transitions are important for monitoring and informing smallholder farmers within the various stages. These are crop vegetative emergence (date of onset photosynthetic activity, termed VE), tasseling (date when maximum leaf area is recorded and maize tassels emerge, termed VT), the beginning of senescence (date when green leaf visibly begins to become brown-toned) (Table 4 1) (Du Plessis, 2003).

It is worth mentioning that during the mid-vegetative stage, the field's western portion (lower elevation) appeared unhealthy. This may have been because this portion of the field was not weeded with the rest of the field during the early vegetative growth stage. However, the farmer applied herbicide during the mid-vegetative growth stage to remove grasses and weeds found between maize rows. Consequently, the herbicide impacted the health status of these crops and the maize suffered herbicide burn.

Table 4-1: Maize growth stages and characteristics

Days after emergence	Growth stage	Description	Pictures
0	VE	Germination and emergence. Planting depth 5-8 cm.	
7	V2		
21	V5	Plant population established. Growth point 20-25 mm below the surface. Leaf-sheath and blades. Tassel initiation.	
32	V8		
38	V10	Ear initiation and early cob development.	
44	V12		
49	V14	Tassel, at the growth point, begins to develop rapidly. Active growth of lateral shoots and cob development from the sixth to the eighth node above the surface. Brace root development.	
56	VT		
63	R1	Tasseling stage. Silks are developing. The demand for water and nutrients is high. All leaves are present. Pollination 5-10 days.	
70	R2-R3		
77	R3-R4	Kernel development. Silking stage.	
84			
91			
98	R5 R6	Grain filling. Nutrients are transported to the cob. Sugars are converted into starch.	
105			
112	R+	Physiological maturity and drying of kernels. Starch in kernels. End of mass gain.	
119			
160		Ready for harvest. Optimal moisture and nutrients.	

Vegetative Growth Stages

Reproductive Growth Stages

#### 4.2.3 Field data collection, sampling, and survey

Field data collection was conducted throughout the maize phenological cycle. A meteorological tower (Figure 3a) was installed in the centre of the maize field monitoring NDVI through spectral reflectance sensors (SRS) (SRS sensors, Decagon Inc, Pullman, WA, USA). The SRS-NDVI sensors consist of a downward-facing and an upward-facing sensor. The upward-facing hemispherical sensor provided reference values of the sky radiance, which

normalized the downward-facing sensor values of maize foliar canopy irradiance. The SRS-NDVI measured wavelengths of 630 nm (red) and 800 nm (NIR) continuously at 10-minute intervals and 30-minute intervals (EM50G, Decagon, Pullman, WA, USA). To calculate upward reflected NDVI, the two-band radiometer measurements of incident radiation within a 36° field of view (FOV), were used to measure the maize canopy reflected radiation (Figure 4-3). The SRS data was calibrated using the information from the incident red and NIR radiation collected by the hemispherical SRS and used to calculate a calibration constant  $\alpha$ :

$$\alpha = I_r / I_n \quad \text{Equation 4-1}$$

where,  $I_r$  is the incident red radiation (630 nm) from above and  $I_n$  the incident NIR radiation (800 nm) from above, both obtained from the hemispherical sensor. Calibration of the values recorded by the Decagon sensors was then calculated:

$$\text{SRS NDVI} = \frac{\alpha R_n - R_r}{\alpha R_n + R_r} \quad \text{Equation 4-2}$$

where,  $R_n$  is the reflected NIR radiation and  $R_r$  the reflected red radiation (Anderson, Nilsen et al., 2016).

The data collected was downloaded from the data logger to a laptop computer (ECH<sub>2</sub>O Utility, Decagon, Pullman, WA, USA) (Figure 4-3 (c)). The SRS-NDVI data was used to monitor maize NDVI values through phenotyping. Importantly, the SRS-NDVI measurements of maize were used in conjunction with the multispectral UAV-derived NDVI imagery to assess the accuracy and reliability of the UAV-derived data. Since the SRS-NDVI sensor measures the NDVI of maize within its FOV, the average NDVI value of the same FOV was clipped and extracted from the multispectral UAV image. The SRS-NDVI measurements used for comparative correlation were taken simultaneously as the UAV flight. Thus, the environmental variance was assumed to be negligible.

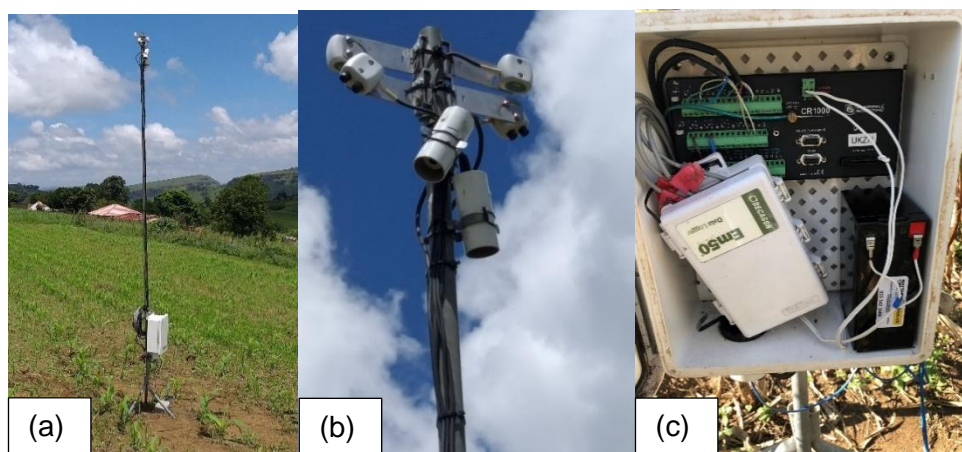


Figure 4-3: (a) Automated in-field meteorological tower in the maize field, (b) meteorological tower mounted with SRS-NDVI and SRS-PRI sensors held 4-meters above the ground, (c) CR1000 data logger, Em50 datalogger and 12 V battery.

At two-week intervals, in-field chlorophyll measurements of maize were collected from the early vegetative (V5) growth stage to the late reproductive growth stages (R6). Pre-sampling

of the maize smallholder field was conducted in Google Earth Pro, where a polygon of the experimental field was digitized. The digitized polygon was then imported into ArcGIS 10.5, where it was used to generate sampling points. A total of 63 sample points were generated based on stratified random sampling within the digitized field boundary. These points were then uploaded into a handheld Trimble Global Positioning System (GPS) with sub-meter accuracy. These locations were used to navigate to each sample point for field data collection. The maize plants at each sampling point were marked for consistent bi-weekly measurement.

A Konica Minolta soil plant analysis development (SPAD) 502 chlorophyll meter (Minolta Corporation, Ltd., Osaka, Japan) was used to measure the chlorophyll content of maize leaves. SPAD meter readings are portable, non-destructive measurements of the red (650 nm) and infrared (940 nm) radiation leaf transmittance. The device instantly calculates a unitless SPAD value proportional to the chlorophyll concentration within the sample leaf (Uddling, Gelang-Alfredsson et al., 2007; Sibanda, Mutanga et al., 2020). Field measurements were conducted between 10:00 am and 2:00 pm, corresponding with the optimal day period for crop photosynthetic activity. During the early growth stages (where a six-leaf was present), the SPAD readings were measured on the newest fully expanded leaf with an exposed collar. After tasseling, the ear leaf (i.e. the leaf attached to the same node as the primary ear shank) was measured (Costa, Frigon et al., 2003). Readings were taken on one leaf per plant. The different locations of leaf measurement included: (a) the midpoint of each leaf blade, next to the main leaf vein, (b) approximately 1/3 down from the leaf tip, and (c) approximately 1/3 of the way down from the leaf tip. The three measurements were averaged per leaf and subsequently recorded. The SPAD meter was shielded from direct sunlight when conducting the chlorophyll readings. SPAD meter measurements were conducted simultaneously with UAV image acquisition. SPAD measurements were converted into chlorophyll content values using the equation derived by Markwell, Osterman et al. (1995) that achieved an  $R^2 = 0.94$ :

$$Chl = 10^{M(0.265)} \quad \text{Equation 4-3}$$

Chl represents the chlorophyll per unit leaf area in  $\mu\text{mol}/\text{m}^2$  and the S is the unitless SPAD value (Ling, Huang et al., 2011). The chlorophyll data was added to the 63-sampling points map in a geographical information system (GIS). The point map was overlaid with the multispectral UAV image of each sampling point's derived spectral reflectance values.

#### 4.2.4 UAV multispectral-thermal camera and platform

The DJI Matrice 300 (DJI M-300) platform mounted with a MicaSense Altum camera and Downwelling Light Sensor 2 (DLS-2) was used to conduct aerial-based flights over the smallholder farms. The rotary-wing DJI M-300 series has vertical take-off and landing (VTOL) technology, making it well-suited for small-scale agricultural crop imaging (Figure 4-4 (a)). The DJI M-300 platform novelties include its 15 km transmission range, 7000 m maximum altitude, obstacle avoidance, flightpath planning and locational position tracker. The maximum flight time of the M-300 is 55 minutes (without payload), and it can reach a maximum speed of 27 m/s, which surpasses most drone platforms on the market. Moreover, the MicaSense Altum camera is a multispectral and thermal imaging sensor that integrates five spectral high-resolution narrow bands (blue, green, red, red-edge, near-infrared) with a radiometric longwave infrared thermal camera (Figure 4-4 (b)). The high-performance camera offers

synchronized multispectral and thermal image capture and uses a global shutter that provides a one-second capture rate for precise and aligned imagery (Hutton, Lipa et al., 2020). The multispectral bands have a sensor resolution of 2064 × 1544 at 120 m (3.2 megapixels per multispectral band) and a ground sample distance (GSD) of 5.2 cm per pixel at the height of 120 m, suggesting the optimum flight altitude above the crop to receive high-resolution images (Table 4-2). The camera also has a 48° × 37° FOV, with an 8 mm focal length.

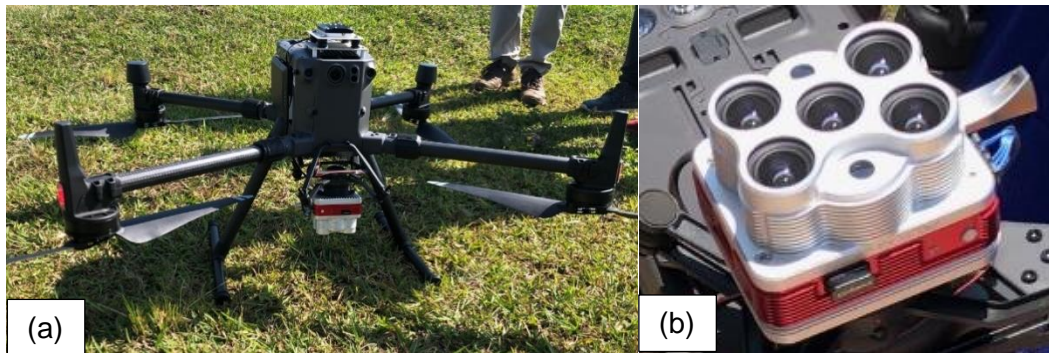


Figure 4-4: (a) DJI Matrice 300 platform and, (b) MicaSense Altum multispectral-thermal camera.

Table 4-2: MicaSense Altum camera specifications.

Band	Spectral colour	Band centre/range	Ground sampling distance at a flying height of 120 m
1	Blue	475 nm	5.2 cm per pixel
2	Green	560 nm	5.2 cm per pixel
3	Red	668 nm	5.2 cm per pixel
4	Red-edge	717 nm	5.2 cm per pixel
5	Near-infrared	842 nm	5.2 cm per pixel
6	Thermal infrared	8000-14 000 nm	81 cm per pixel

Source : (<https://micasense.com/altum/>)

#### 4.2.5 Image acquisition and processing

A shapefile of the maize field was digitized in Google Earth Pro and imported into the DJI M-300 smart console, which was used to design a flight plan covering the study area (Figure 4-5 (a)). The flight plan enabled a hands-free drone flight mission over the study field and adjacent areas. Before and after the flight, the UAV was calibrated using the MicaSense Altum calibrated reflectance panel (CRP). This included the user manually taking an unshaded image directly over the CRP to discern the lighting conditions of the specific flight date, time, and location (Figure 4-5 (b)). We conducted UAV flights every 2-weeks on selected days with clear sky conditions. UAV flights were conducted between 10:00 am and 12:00 pm as this is the time of optimal solar irradiance. This period also coincided with chlorophyll content measurements. Detailed flight conditions are presented in Table 4-3.

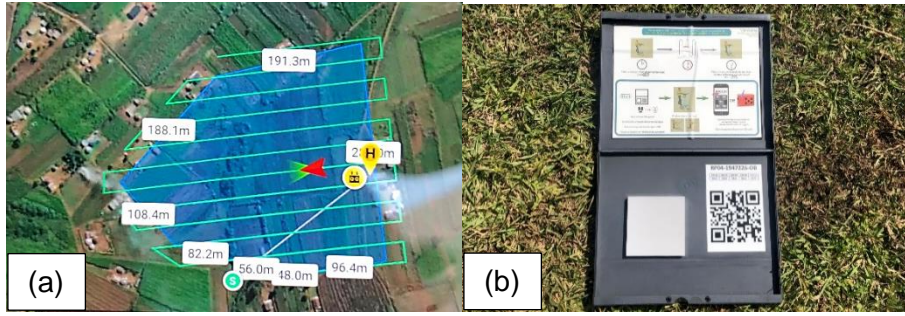


Figure 4-5: (a) DJI M-300 flight plan, (b) MicaSense Altum calibration reflectance panel

Table 4-3: UAV flight specifications

Parameters	Specifications
Altitude	100 meters
Ground sampling distance	7 cm
Speed	16 m/s
Flight duration	14 minutes 36 seconds
Composite images	321
Image overlap	80%

A total of 3576 images were stitched together and radiometrically corrected (Pix4Dfields 1.8.0, Pix4d Inc., San Francisco, CA, USA). The radiometric correction was conducted in Pix4Dfields using all the captured images, including the before and after flight CRP images. The radiometric calibration target (CRP) is a white balance card that provides the card's reflectance properties across the camera's electromagnetic spectrum wavelengths. This enabled the software to calibrate and correct the reflectance of the images accordingly in line with the prevalent atmospheric conditions during the image acquisition. The CRP also had an absolute reference, which obtained the absolute reflectance values and made comparing data from several flights possible. Once processed, a final orthomosaic and a digital elevation model (DEM) GeoTIFF image were generated. The orthomosaic was georeferenced in ArcGIS 10.5 using ground reference points from Google Earth Pro. Images were referenced to the Universal Transverse Mercator (UTM zone 36S) projection.

The maize reflectance data was extracted from the multispectral Altum image. This was done by overlaying the ground-truthed maize chlorophyll measurements and their GPS coordinates as a point map with the UAV multispectral image. The reflectance values were extracted for each coordinate and each UAV spectral band. The image was then used to compute vegetation indices (VIs) detailed in Table 4-4. VIs selected included various combinations of the multispectral bands specific to vegetation health and chlorophyll, such as the NDVI, the canopy chlorophyll content index (CCCI) and the red-edge chlorophyll index ( $CI_{rededge}$ ). These vegetation indices were derived from their performance in the research literature (Zhang and Zhou 2015; Naito, Ogawa et al., 2017; Xue and Su, 2017; Haghighian, Yousefi et al., 2020).

Table 4-4: Spectral UAV-derived vegetation indices used to predict chlorophyll content.

Vegetation Index	Abbreviation	Equation	Reference
Normalized difference vegetation index	NDVI	$(\text{NIR} - \text{RED}) / (\text{NIR} + \text{RED})$	Xue and Su (2017)
Green normalized difference vegetation index	GNDVI	$\frac{\text{NIR} - \text{GREEN}}{\text{NIR} + \text{GREEN}}$	Naito, Ogawa et al. (2017)
Red-green ratio index	RGR	$\frac{\text{RED}}{\text{GREEN}}$	Qiu, Xiang et al. (2020)
Normalized difference red-edge index	NDRE	$\frac{\text{NIR} - \text{RED EDGE}}{\text{NIR} + \text{RED EDGE}}$	Fitzgerald, Rodriguez et al. (2010)
Corrected transformed vegetation index	CTVI	$\frac{\text{NDVI} + 0.5}{\text{NDVI} + 0.5} * (\sqrt{\text{NDVI} + 0.5})$	Naito, Ogawa et al. (2017)
Infrared percentage vegetation index	IPVI	$\left( \frac{\text{NIR} + \text{RED}}{2} \right) * (\text{NDVI} + 1)$	Haghighian, Yousefi et al. (2020)
Soil adjusted vegetation index	SAVI	$\left( \frac{\text{NIR} - \text{RED}}{\text{NIR} + \text{RED} + \text{L}} \right) * (1 + \text{L})$ L is a constant between 0 and 1.	Xue and Su (2017)
Optimized soil adjusted vegetation index	OSAVI	$\frac{\text{NIR} - \text{RED}}{\text{NIR} + \text{RED} + 0.16}$	Xue and Su (2017)
Green chlorophyll index	Cl <sub>green</sub>	$(\text{NIR}/\text{GREEN}) - 1$	Zhang and Zhou (2015)
Red-edge chlorophyll index	Cl <sub>rededge</sub>	$(\text{NIR} - \text{RED EDGE}) - 1$	Zhang and Zhou (2015)
Canopy chlorophyll content index	CCCI	$\frac{\text{NIR} - \text{RED EDGE}}{\text{NIR} + \text{RED EDGE}} / \frac{\text{NIR} - \text{RED}}{\text{NIR} + \text{RED}}$	Fitzgerald, Rodriguez et al. (2010)
Chlorophyll vegetation index	CVI	$\text{NIR} * \left( \frac{\text{RED}}{\text{GREEN}^2} \right)$	Vincini and Frazzi (2011)
Modified chlorophyll absorption ratio index	MCARI	$\frac{1.5[2.5(\text{NIR} - \text{RED}) - 1.3(\text{NIR} - \text{GREEN})]}{\sqrt{[2\text{NIR} + 1]^2 - (6\text{NIR} - 5\sqrt{(\text{RED})})} - 0.5}$	Wu, Niu et al. (2008)

#### 4.2.6 Statistical analysis

The random forest algorithm was used to predict maize chlorophyll content since it is renowned for its simplicity, robustness, and ability to perform well regardless of sample size (Dye, Mutanga et al., 2011; Luan, Zhang et al., 2020). The random forest ensemble is a machine learning algorithm that uses bootstrap aggregation to construct multiple trees on a subset of samples derived from the training data (Abdel-Rahman, Ahmed et al., 2013). Decision trees are grown to maximum capacity with a randomized subset of predictors (UAV-

derived spectral data). Each node is split using random subsets of input variables (Adam, Mutanga et al., 2012). Furthermore, the random forest regression can identify predictor variables that are influential in the prediction model based on the sum of the reduction in Gini impurity across the feature nodes (Sibanda, Onisimo et al., 2021).

Specifically, the RGtk2 and rattle packages in RStudio software version 1.4.1564 were used to develop the random forest regression model through numerical inputs. The outputs of the random forest model were optimized using the variable importance as they determine the most influential bands and VIs in prediction. Variables of low importance were removed throughout the analysis, and the random forest model was continuously modified for optimal prediction. The variable selection process reduces variable redundancy and multicollinearity issues, which affect the regression model's performance. The model was user-defined and fine-tuned to an optimal 500 trees and eight variables. These hyper-parameters were attained for numerous iterations.

#### **4.2.7 Accuracy assessment**

Accuracy assessments were performed to evaluate the predicted chlorophyll regression models. The accuracy metrics used were the coefficient of determination ( $R^2$ ), root-mean-squared error (RMSE), and relative root-mean-squared error (RRMSE). The  $R^2$  measured the variation between the measured and predicted: foliar temperature and stomatal conductance. The RMSE assessed the magnitude of error between the field measurements and modelled outputs of foliar temperature and stomatal conductance. At the same time, the RRMSE evaluated the model's accuracy and was used to compare the performance of regression models across maize phenotyping. The RRMSE is calculated by normalizing each variable RMSE value's mean and expressed as a percentage, where lower percentages are considered more accurate (Taghizadeh-Mehrjardi, Mahdianpari et al., 2020).

### **4.3 Results**

#### **4.3.1 Descriptive analysis of UAV-derived data and ground-based maize data**

The automated time series of daily SRS-NDVI data over the phenological cycle was generally a smooth curve with fluctuations during the various vegetative growth stages and a significant decline in NDVI values after an unanticipated hailstorm (Figure 4-6). NDVI values increased rapidly from 0.1 in the early vegetative growth stages (DOY 42) to a peak of approximately 0.7 in the early reproductive development stages (DOY 102). After that, a strong decline in NDVI was observed from the early reproductive growth stage (DOY 102) to the mid-reproductive growth stage (DOY 118), declining from an NDVI of 0.7 to 0.5 respectively. During the transition from the early to mid-reproductive stages, a hailstorm damaged the crop and resulted in a slight NDVI increase the day after the weather occurrence but was subsequently followed by a rapid decrease in NDVI values for the following days. Subsequently, the NDVI during the late reproductive growth stages fluctuated between 0.5 and 0.6. The SRS-NDVI data shows significant changes through the growth cycle of the maize crop, with increases corresponding to a time when rapid vegetative growth occurred and decreases corresponding to mid-to-late maize productivity.

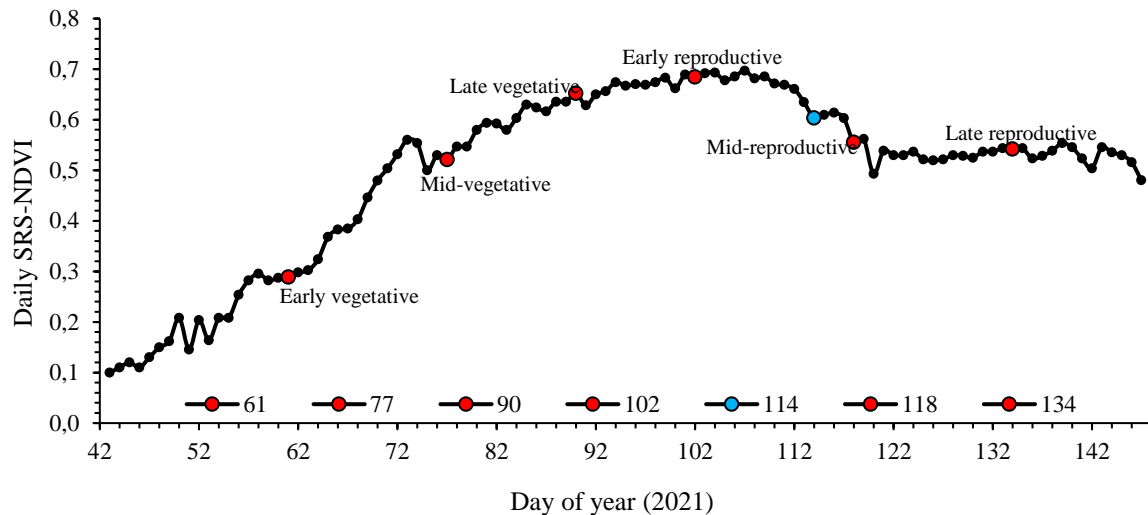


Figure 4-6: Daily SRS-NDVI values of maize throughout the phenological cycle. Red points indicate the days we visited the field to conduct UAV flights. The blue point indicates the day of crop disturbance due to a hailstorm.

#### 4.3.2 Evaluation of UAV-derived data against ground-based NDVI and chlorophyll data

The relationship between the ground-based SRS-NDVI data and the UAV-derived NDVI data for the various maize growth stages was linear (Figure 4-7 (a)). A strong positive correlation existed between the SRS-NDVI and UAV-derived NDVI ( $R^2 = 0.98$ ;  $p = 0.001$ ). At low NDVI values, such as 0.30, the UAV-derived NDVI was higher than the SRS-NDVI. At mid-range NDVI values, i.e. 0.50, the UAV-derived NDVI and SRS-NDVI were almost identical. At higher NDVI values, such as 0.70, the SRS-NDVI was higher than the UAV-derived NDVI. Similarly, the average chlorophyll content measurements for each trip were compared against the UAV-derived NDVI data to better understand the relationship of NDVI with maize chlorophyll concentration. Figure 4-7 (b) illustrates that SRS-NDVI values correlate well with chlorophyll content values, attaining an  $R^2 = 0.78$ . High UAV-derived NDVI values generally corresponded with high chlorophyll concentrations.

Specifically, the early maize growth stages yielded low NDVI values of approximately 0.30-0.45 for a day of the year (DOY) 61. Similarly, the low NDVI value correlated with a low chlorophyll concentration of  $74.5 \mu\text{mol}/\text{m}^2$  on DOY 61. However, as the maize developed, the measured and UAV-derived NDVI values progressively increased to 0.54 on DOY 77, followed by 0.65 on DOY 90 and 0.67 on DOY 102. Likewise, maize chlorophyll concentrations increased to  $461 \mu\text{mol}/\text{m}^2$  on DOY 77,  $573.6 \mu\text{mol}/\text{m}^2$  on DOY 90, and  $651.8 \mu\text{mol}/\text{m}^2$  on DOY 102. After that, the measured and UAV-derived NDVI values in the mid and late reproductive stages decrease to 0.55-0.57 on DOY 118 and 0.49-0.54 on DOY 134, respectively. Similarly, the measured chlorophyll concentrations in these stages decreased to  $331.4 \mu\text{mol}/\text{m}^2$  on DOY 118 and  $183.5 \mu\text{mol}/\text{m}^2$  on DOY 134.

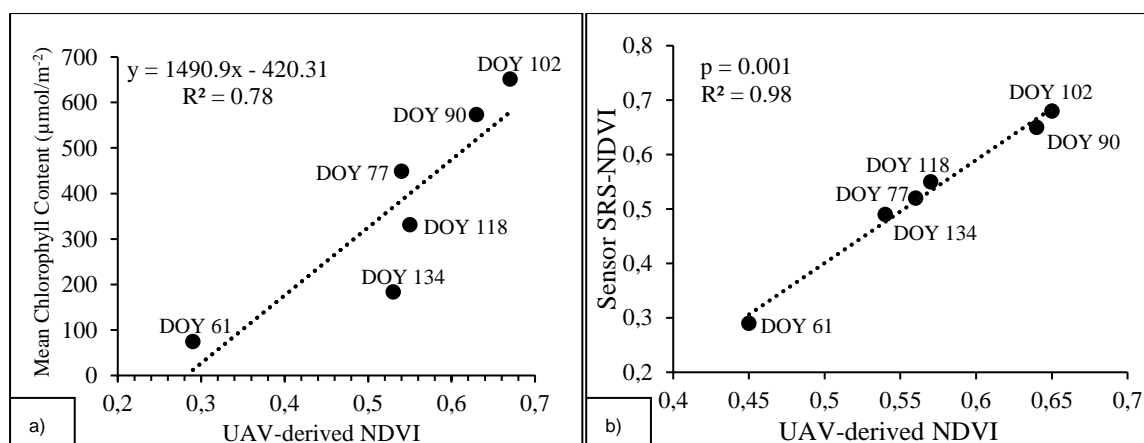


Figure 4-7: Correlation of (a) in-field sensor SRS-NDVI and UAV-derived NDVI (b) measured maize chlorophyll content and UAV-derived NDVI across the maize growth stages.

### 4.3.3 Descriptive statistics of chlorophyll content from SPAD

The lowest chlorophyll concentration was attained during the early vegetative growth stage (V5-V10) at 13.5  $\mu\text{mol}/\text{m}^2$  (Table 4-5). The highest chlorophyll concentration was recorded during the early reproductive stage (R1-R3) at 3765.4  $\mu\text{mol}/\text{m}^2$ . On average, the maize chlorophyll ranged from 58.85  $\mu\text{mol}/\text{m}^2$  to 2043.5  $\mu\text{mol}/\text{m}^2$ . The average and median of maize chlorophyll across the growth stages were 362.9  $\mu\text{mol}/\text{m}^2$  and 259  $\mu\text{mol}/\text{m}^2$ , respectively. The average standard deviation of chlorophyll values was 342.6, which indicated a large deviation of the measurements from the mean value of 362.9.

Table 4-5: Descriptive statistics of maize chlorophyll content throughout the various growth stages

Day of year (DOY)	Chlorophyll content at various growth stages	Minimum ( $\mu\text{mol}/\text{m}^2$ )	Maximum ( $\mu\text{mol}/\text{m}^2$ )	Mean ( $\mu\text{mol}/\text{m}^2$ )	Median ( $\mu\text{mol}/\text{m}^2$ )	Standard deviation
61	V5-V10	13.51	255.5	74.5	60.2	54.2
77	V12	61.7	3242.6	461	331.8	466.7
90	V14-VT	130.4	2792.4	573.6	390.2	497.7
102	R1-R2	104.2	3765.4	651.8	476.2	641.8
118	R2-R4	26.8	1555	331.4	234.1	301.8
134	R4-R5	16.5	650.2	183.5	61.7	93.6
<b>Average value</b>		<b>58.85</b>	<b>2043.5</b>	<b>362.6</b>	<b>259</b>	<b>342.6</b>

#### 4.3.4 Random forest models of maize chlorophyll content

The relationship between measured (SPAD-derived) and modelled (UAV-derived) chlorophyll content varied across the various maize growth stages. The model could optimally estimate the chlorophyll content throughout the various growth stages; however, the prediction of chlorophyll proved more accurate during the vegetative growth stages. During the early vegetative growth stage (V5-V10), the highest RMSE accuracy for the growth cycle achieved was  $13.9 \mu\text{mol}/\text{m}^2$ , with an  $R^2 = 0.80$  and  $\text{RRMSE} = 11\%$  (Figure 4-8 (a)). The mid-vegetative growth stage (V12)  $\text{RMSE} = 78.2 \mu\text{mol}/\text{m}^2$ ,  $R^2 = 0.79$  and  $\text{RRMSE} = 14\%$  (Figure 4-8 (b)). Whereas the late vegetative growth stage (V14-T) produced the lowest  $\text{RMSE} = 96.2 \mu\text{mol}/\text{m}^2$ ,  $R^2 = 0.85$  but obtained an  $\text{RRMSE}$  model accuracy of  $8\%$  (Figure 4-8 (c)). Similarly, the early reproductive development stage (R1-R2) obtained a low  $\text{RMSE} = 87.4 \mu\text{mol}/\text{m}^2$ ,  $R^2 = 0.89$  but produced the highest  $\text{RRMSE}$  accuracy of  $7\%$  (Figure 4-8 (d)). The  $\text{RMSE}$  accuracies improved during the mid-reproductive (R2-R4) and late reproductive (R4-R5) growth stages to  $76.2 \mu\text{mol}/\text{m}^2$  and  $31.3 \mu\text{mol}/\text{m}^2$ , respectively. However, the model produced the lowest  $\text{RRMSE}$  and  $R^2$  accuracies during the R2-R4 and R4-R5 stages at an  $\text{RRMSE}$  of  $28\%$ ,  $R^2 = 0.75$  (Figure 4-8 (e)) and an  $\text{RRMSE}$  of  $25\%$ ,  $R^2 = 0.78$  (Figure 4-8 (f)), respectively.

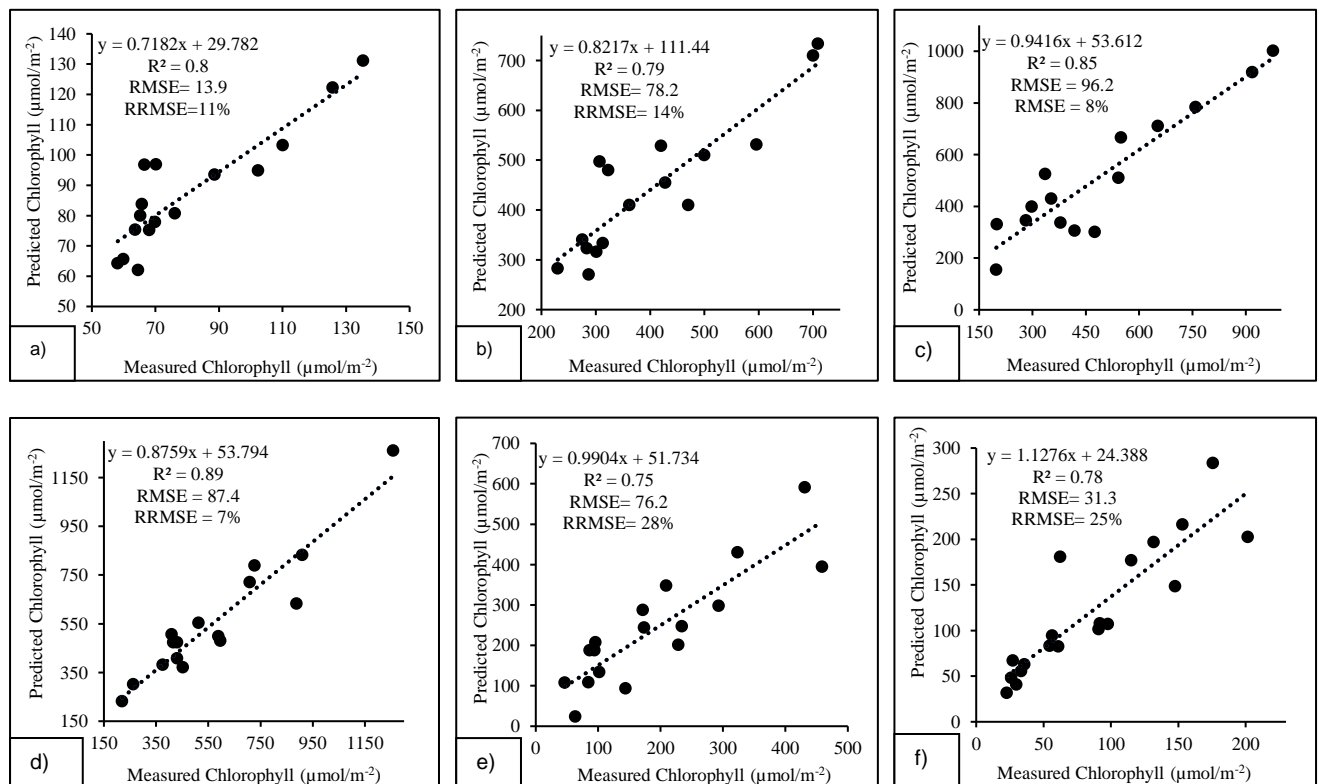


Figure 4-8: Linear relationships between measured and predicted maize chlorophyll content for vegetative stages (a) V5-V10, (b) V12, (c) V14 to VT, and reproductive stages (d) R1-R3, (e) R3-R4, (f) R5-R6

The early reproductive (R1-R3) growth stage generally produced the most optimal model performance, with an RRMSE = 7% and  $R^2 = 0.85$ . The top VIs and spectral bands selected by the model for the early reproductive growth stage were the NDRE, NIR band,  $CI_{rededge}$  and NDVI (Figure 4-9 (d)). The late vegetative (V14-T) growth stage also yielded a high model RRMSE = 8% and  $R^2 = 0.89$  based on the NIR band, CCCl, red-edge band and NDVI amongst others, in order of importance (Figure 4-9 (c)). The variables above of importance for the R1-R3 and V14-T stages were major contributors to modelling chlorophyll content, as there was a major step down in the importance of the other VIs and bands. Similarly, the mid-vegetative (V12) and mid-reproductive (R4-R5) have major stand-out importance variables of CCCl, red-edge, green, NIR and NDVI, NIR, red-edge and  $CI_{rededge}$ , amongst others, respectively. On the other hand, the early vegetative (V5-V10) and late reproductive (R5-R6) stages gradually decrease variable importance scores based on the  $CI_{rededge}$ , NDVI, NDRE, NIR and red-edge, NIR, MCARI, OSAVI, amongst others, respectively. The variables obtaining the highest importance scores were generally derived from the NIR, red-edge and red wavebands.

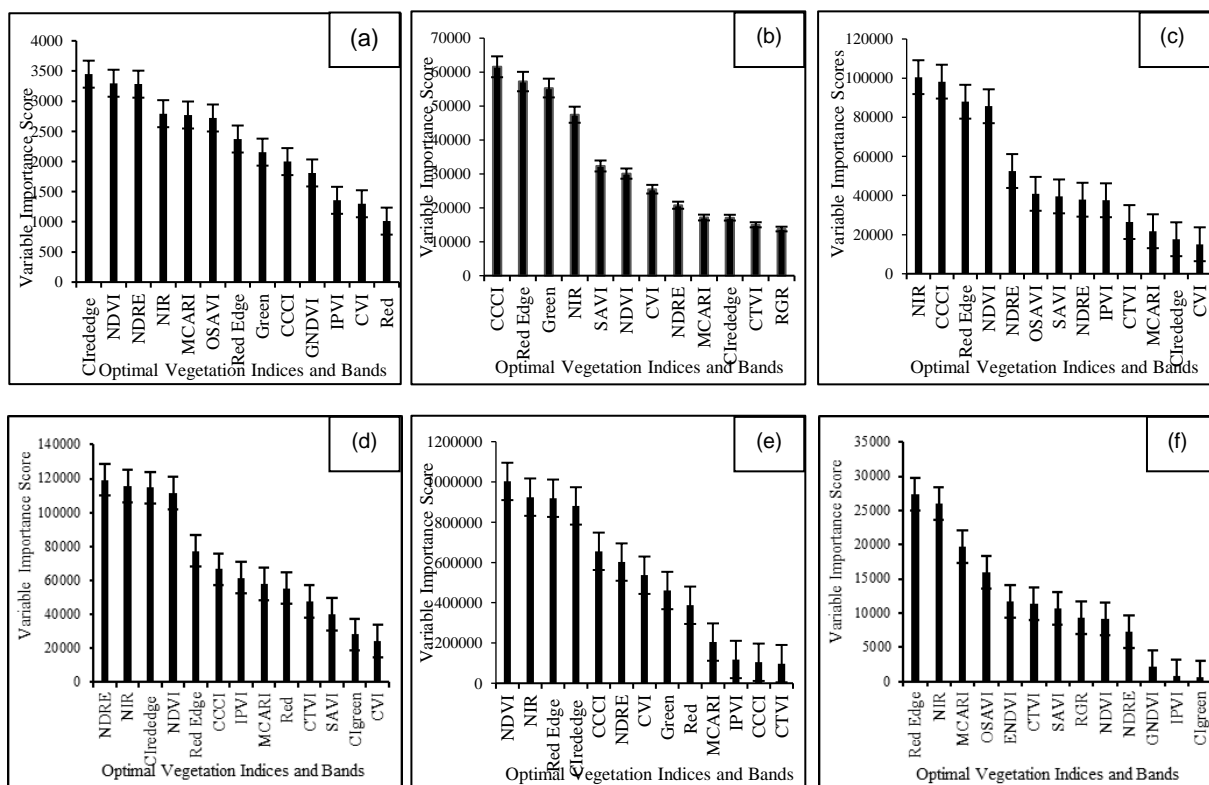


Figure 4-9: Variable importance scores of optimal chlorophyll content VIs and bands for vegetative stages (a) V5-V10, (b) V12, (c) V14 to VT, and reproductive stages (d) R1-R3, (e) R3-R4, (f) R5-R6

#### 4.3.5 Mapping the spatial distribution of maize chlorophyll content over the various growth stages

The modelled chlorophyll concentrations ranged from  $33 \mu\text{mol}/\text{m}^2$  to  $126 \mu\text{mol}/\text{m}^2$  (Figure 4-10). The chlorophyll content of maize was low during the early vegetative growth stage

(V5-V10) and then progressively increased throughout the various growth stages. In the late vegetative (V14-T), early reproductive (R1-R3), and mid-reproductive (R4-R5) growth stages, the chlorophyll concentrations were the highest. Subsequently, chlorophyll content was depleted during the late reproductive stage (R5-R6).

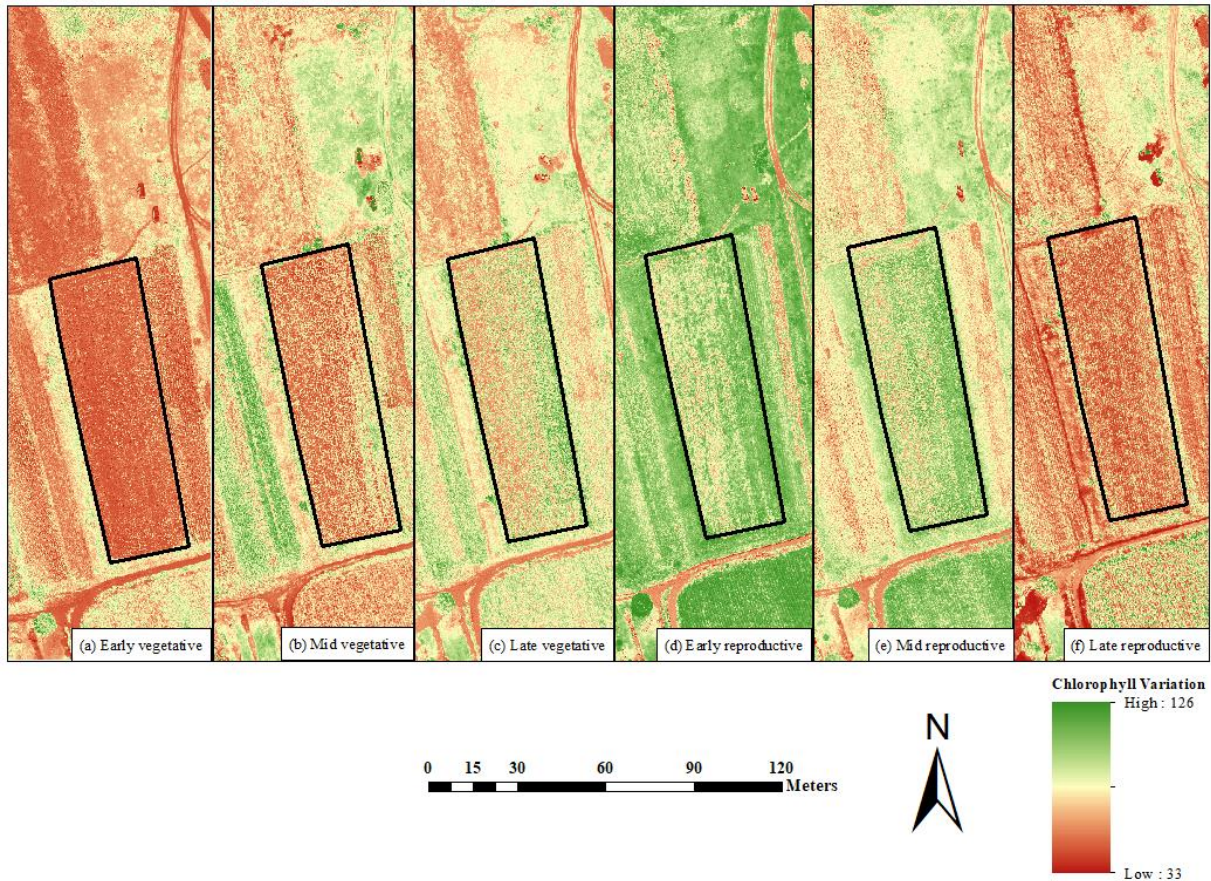


Figure 4-10: Spatial distribution of chlorophyll content over the maize field for vegetative stages (a) V5-V10, (b) V12, (c) V14 to VT, and reproductive stages (d) R1-R3, (e) R3-R4, (f) R5-R6.

#### 4.4 Discussion

This study aimed to predict chlorophyll content variations across maize phenological stages using UAV-derived VIs and the random forest algorithm. In doing so, we attempted to determine the optimal maize growth stage(s) for chlorophyll prediction. Clearly, chlorophyll concentrations varied over the phenological stages, and the model could discern the optimal chlorophyll growth stages. The chlorophyll variations of maize over the growing season are useful for estimating the health and productivity status of the smallholder field.

#### 4.4.1 Estimating maize chlorophyll content across the growing season

The findings of the study model performed well throughout the vegetative growth stages. They showed that the earliest vegetative growth stage yielded the highest RMSE accuracy of 13.9  $\mu\text{mol}/\text{m}^2$ ,  $R^2 = 0.80$  (RRMSE = 11%) based on the  $CI_{\text{rededge}}$ , NDVI, NDRE, NIR as the most influential variables (in order of importance). Specifically, due to their association with healthier plants, the red-edge and NIR regions were detected as crucial wavelengths in the model's prediction of chlorophyll content. This is because the red-edge wavelength is sensitive to plants with a high chlorophyll content, nitrogen content, and biomass, and thus are better predicted using the red-edge (Delegido, Verrelst et al., 2011; Clevers and Gitelson, 2013; Sibanda, Mutanga et al., 2020). Additionally, the NIR region strongly influences the prediction of chlorophyll content, as it is sensitive to the high foliar reflectance induced by the pigment concentrations of plant canopy structures (Broge and Leblanc, 2001; Sankaran, Maja et al., 2013). The studies of Sibanda, Mutanga et al. (2020), and Singhal, Bansod et al. (2019) demonstrated a similar association between the red-edge and NIR regions with chlorophyll content by achieving an  $R^2$  of 0.91 and 0.90, respectively. In this study, strong chlorophyll concentrations were associated with crop emergence and development, as the leaf area index was low, resulting in more dynamic photosynthetic rates of the crop, facilitating high reflectance in the red-edge and NIR sections. Furthermore, red-edge and NIR-derived VIs are notable regions that surpass the effects of atmospheric interferences, visible irradiance, variable background effects, and geometrical arrangement of a scene when compared to conventional bands (Curran et al., 1990; Goodbody et al., 2020). Thus, the red-edge and NIR wavelengths facilitated optimal maize chlorophyll prediction, as the low foliage density of the early vegetative growth stage did not saturate and cause spectral confusion of the sensor during image acquisition.

Meanwhile, high chlorophyll concentrations are associated with the late vegetative and early reproductive growth stages, as maize reaches photosynthetic maturity and requires high productivity to begin fruit production (Rostami, Koocheki et al., 2008). Results from this study showed a similar trend, and the model prediction accuracies were most optimal during the late vegetative and early reproductive with an RRMSE accuracy of 8% and 7% and  $R^2$  values of 0.85 and 0.89, respectively. Such results are attributed to the fact that the reflectance of maize leaf chlorophyll content during the late vegetative and early reproductive stages are stronger than other stages of phenotyping due to the high leaf area index and full canopy closure characterized by these stages (Walker and Schulze, 2006; Walker, Drewry et al., 2018). It has been documented in studies by Walker, Drewry et al. (2018), Dahms, Seissiger et al. (2016) and Costa, Dwyer et al. (2001) that during the stages of tasseling, silking and pollination, maize is characterized by a fully developed leaf canopy structure with a high leaf area index that promotes the detection of higher chlorophyll contents. Hence, the dense canopy architecture and absence of soil background effect created a homogenous scene of green pigment reflectance, which was optimal in the prediction of chlorophyll content over the smallholder field.

Similarly to the early vegetative stages, the NIR and red-edge bands were significant variables of maize chlorophyll prediction due to these regions' favourable detection of high chlorophyll reflectance. The biochemical properties of a dense foliar canopy, the thick waxy cuticle, air

cavities, chloroplasts and mesophyll cell thickness all contribute to the high NIR and red-edge reflectance, which is directly correlated with chlorophyll content (Mutanga, Adam et al., 2012; Sibanda, Onesimo et al., 2021). Thus, the high chlorophyll concentrations associated with these stages in the study are also associated with a healthier crop and further coincided with the SRS-NDVI values of approximately 0.65. In this regard, the high levels of chlorophyll content were favourable in model prediction. Hence these stages are the most accurate estimation.

During the mid-reproductive and late reproductive stages, the model prediction accuracies were lowest, with an RRMSE of 28% and 25% and  $R^2$  values of 0.75 and 0.78, respectively. The low model prediction accuracies could be attributed to the adverse effects of a hailstorm that damaged the maize canopy structure, resulting in a lower crop chlorophyll content. The physical damage to the maize canopy exposed the underlying soil surface of damaged and decayed leaves. This resulted in spectral confusion due to the hybrid of soil and senescing leaf reflectance imaged by the MicaSense Altum camera, failing the model to discern the apparent chlorophyll variations. This is because the predominant brown tone of the senescing leaves and soil resulted in most bands and VIs being absorbed due to the low chlorophyll concentrations.

In contrast, wavelengths such as the red band reflected much higher. Nevertheless, an apparent decline in NDVI values before the hailstorm was evident and associated with a decline in chlorophyll. This may be because, at this point in phenotyping, the crop channels its nutritional resources and energy towards fruit production (Walker, Drewry et al., 2018), resulting in a reduction of chlorophyll concentration which is also apparent in the results.

#### **4.4.2 Implications of the study**

Smallholder farmers constantly strive to maximize their small-scale crop production and produce healthy and productive yields. However, they are seldom the focus of innovation and lack resources, as it is always assumed that their scale of operations does not necessitate such. Thus, such findings demonstrate using precision agricultural technologies (i.e. UAVs), which can facilitate improved smallholder agricultural management. Specifically, UAV-derived data is near real-time, enabling quick and effective management that may improve crop health and productivity. Moreover, near real-time data is particularly useful when erratic weather conditions, such as hailstorms, occur. Such agrometeorological effects prove how South African smallholder farmers are subjected to the variability of weather and climate, which has consequences on crop growth, health, and the overall productivity of their farms. In such instances, UAV-derived could be used to perform rapid assessment of likely hail damage in near real-time, allowing farmers to make informed and effective decisions on agricultural management and provide early warnings for food insecurity. Therefore, near real-time UAV technology benefits smallholder agricultural systems as it allows for rapid and informed decisions to limit further crop health issues.

## 4.5 Conclusion

Smallholder farming systems lack the resources to maximize their productivity and monitor croplands for healthy growth and development. In recent years, the synergistic use of UAV remotely sensed technology and crop health proxies such as chlorophyll content had facilitated a deeper understanding of crop dynamics. In this regard, the study tested the use of UAV-derived multispectral data by estimating maize chlorophyll content over the various stages of phenotyping. This was done using a random forest prediction model, which estimated the chlorophyll concentrations of maize in smallholder farms of Swayimane. Therefore, premised on the findings of the study, it is concluded that:

- Optimal chlorophyll content prediction accuracies were produced during early vegetative growth stages (V5-V10 and V12), late vegetative growth stages (V14-T) and early reproductive growth stages (R1-R3),
- Maize chlorophyll content was optimally estimated through UAV-derived NIR and red-edge wavelengths.

Since chlorophyll content has been widely illustrated as a proxy of crop health, the study's findings imply that UAV-derived data could be optimally utilized to characterize the general state of maize health in smallholder cropping lands, with significantly improved spatial accuracies. Such precision technology advancements are a low-cost, objective, and accurate technique that smallholder farmers can adapt to inform decision-making and agricultural management. Specifically, multispectral UAV technology is spatially explicit and provides near real-time data for understanding crop health through the biochemical indicator of chlorophyll. This technology potentially overcomes some of the limitations associated with satellite imagery. However, the study could have benefitted from higher spectral resolution data and additional testing data to improve the model performance.

Nevertheless, the random forest model performed relatively well at predicting the chlorophyll content in smallholder farms. Therefore, multispectral UAV technology is a beneficial solution to smallholder agriculture. It provides farmers information on crop dynamics at user-defined spatial and temporal scales for improved management and productivity.

## 5 REMOTE SENSING FOLIAR TEMPERATURE AND STOMATAL CONDUCTANCE USING DRONE-ACQUIRED OPTICAL AND THERMAL IMAGES

Brewer K, Clulow A, Sibanda M, Gokool S, Odindi J, Mutanga O, Naiken V, Chimonyo VGP and Mabhaudhi T

### 5.1 Introduction

In recent decades, agricultural production in sub-Saharan Africa has been threatened by water scarcity, unpredictable weather, and arid conditions (Lickley and Solomon, 2018; Nhamo, Matchaya et al., 2019). In South Africa, smallholder agriculture (less than two hectares) is predominantly rainfed, which often results in crops experiencing water stress and moisture shortages due to inadequate rainfall (Rockstrom, 2000; Ubisi, Mafongoya et al., 2017; Adisa, Botai et al., 2018). However, there are limited spatially explicit evidence-based frameworks and instruments for monitoring crop water stress in smallholder croplands, especially in those cultivating maize (*Zea mays L.*) predominantly for subsistence (Andersson, Zehnder et al., 2009; Lu, Xue et al., 2017). Since maize is a staple grain crop and one of the most widely cultivated crops in South African smallholder farms (Walker and Schulze, 2006), there is a need for spatially explicit methods to characterize maize water stress to prevent yield losses and optimize the productivity of smallholder farmers.

Maize requires 450 to 600 mm of water per season as it is sensitive to water stress, especially during the tasseling, silking, and pollination stages (Taghvaeian, Chávez et al., 2014). At physiological maturity, a single maize crop requires approximately 250 litres of water to produce approximately 15 kilograms of grain per millimetre of water consumed (Du Plessis, 2003). Although additional factors like soil nutrients, light and humidity may affect growth, water stress is often the major limiting factor. The high variability of rainfall in South Africa often results in less water to sustain optimal crop growth and productivity (Carroll, Hansen et al., 2017; Haarhoff, Kotzé et al., 2020). These water deficits result in stomatal closure to reduce moisture loss through transpiration, increasing leaf temperatures due to limited moisture conductance to cool the leaf surface (Saseendran, Trout et al., 2015; Zhang and Zhou, 2019). Hence, the determination of foliar temperature and stomatal conductance are often used as proxies for near real-time detection of crop water stress (Jackson, Idso et al., 1981; Dai, Dickinson et al., 2004; González-Dugo, Moran et al., 2006; Gerhards, Schlerf et al., 2019; Yun, Kim et al., 2020). Accurate quantification of maize foliar temperature and stomatal conductance across the growing season can assist smallholder farmers in adopting measures to mitigate losses and optimize yield.

Traditionally, crop water stress has been determined using in-situ plant measurements, soil moisture content or meteorological variables (González-Dugo, Moran et al., 2006). However, these approaches are time-consuming, costly, and laborious (Jackson, Idso et al., 1981). South Africa is prone to vandalism and theft and thus unsuitable for continuous and real-time monitoring of crop water stress. Recently, studies have demonstrated that remote sensing

techniques using multispectral or thermal imagery can be used to monitor crop water stress (Sepulcre-Cantó, Zarco-Tejada et al., 2005; Veysi, Naseri et al., 2017; Zhang, Niu et al., 2019; Zhang, Zhang et al., 2019; Jamshidi, Zand-Parsa et al., 2021). According to El-Hendawy, Al-Suhaibani et al. (2019), several multispectral sections of the electromagnetic spectrum are indirect water stress indicators. They are useful for quantifying crop water content through leaf biochemical attributes (El-Hendawy, Al-Suhaibani et al., 2019). Specifically, the visible (blue, green, red) and the near-infrared (NIR) wavelengths hold great potential for the prediction of water due to their absorption of water through leaf pigments such as chlorophyll (Pasqualotto, Delegido et al., 2018). Moreover, the thermal infrared portion of the spectrum is directly correlated to water content proxies, such as temperature and stomatal activity. It is thus proficient in the analysis of temperature attributes. The thermal infrared radiation ranges from 8  $\mu\text{m}$  to 14  $\mu\text{m}$  on the electromagnetic spectrum. Its utility in remote sensing enables water stress detection due to its non-destructive and low labour inputs (Gerhards, Schlerf et al., 2019).

While traditional satellite-based remote sensing techniques have proven useful in quantifying water stress, several constraints limit their suitability for monitoring temperature and stomatal conductance at a farm scale. The spatial resolution of satellite earth observation data is generally too coarse to capture the spatial heterogeneity within smallholder farms. Moreover, broad-band thermal satellite imagery results in geometrical inaccuracies when co-registering to other portions of the electromagnetic spectrum with higher spatial resolutions (Prakash, 2000). Thus, alternate approaches that can adequately capture spatial heterogeneity at localized levels are required to facilitate precision agricultural applications within smallholder farms.

In recent years, unmanned aerial vehicles (UAVs) have become a popular farm phenotyping platform for precision agricultural applications (Hoffmann, Jensen et al., 2016; Messina and Modica 2020; Hu, Chapman et al., 2021). Very high-resolution (VHR) cameras attached to UAV platforms offer advanced crop image throughput analytics. They effectively overcome satellite imagery's limitations (Maes and Steppe, 2019; Nhamo, Magidi et al., 2020). The spatially explicit UAV images acquired by VHR cameras offer near real-time spectral information useful for detecting changes in crop phenology, foliar temperature, and moisture content (Park, Ryu et al., 2017; Zhang, Niu et al., 2019). UAV images can be continuously acquired under user-defined ground sampling distances and temporal intervals, which limit atmospheric perturbations such as cloud cover (Cucho-Padin, Loayza et al., 2020, Nhamo, Magidi et al., 2020). Therefore, accurate mapping and analysis of agricultural maize fields using a multispectral and thermal infrared UAV hold significant potential for providing data that informs smallholder farmers on potential crop water stress.

Foliar temperature and stomatal conductance can be optimally assessed using a robust machine-learning algorithm that can derive a relationship using spectral bands and vegetation indices (VIs) to predict temperature and conductance. VIs are mathematical combinations of image bands that are ratioed for extracting spectral properties such as canopy cover, plant vigour and phenology dynamics (Kayet, Pathak et al., 2016; Xue and Su, 2017). VIs, such as the normalized difference water index (NDWI) and the normalized difference vegetation index (NDVI), have been identified as particularly useful in directly or indirectly quantifying water stress within vegetation (Zarco-Tejada, González-Dugo et al., 2012; Liang, Di et al., 2018; El-

Hendawy, Al-Suhaibani et al., 2019; Zhang and Zhou, 2019). Furthermore, using these VIs in combination with machine learning algorithms has proven useful in characterizing crop temperature and water stress (Noi, Degener et al., 2017; Liang, Di et al., 2018). Considering the potential of utilizing UAV-derived data with machine learning, in this study, we aimed to analyze the utility of the UAV-derived data to predict foliar temperature and stomatal conductance. Specifically, we sought to predict maize foliar temperature and stomatal conductance using UAV-derived spectral variables (bands and VIs) to quantify potential water stress throughout the growing season within a smallholder farm.

## 5.2 Materials and Methods

### 5.2.1 Study site description

Data for this study were collected over four months from February 2021 to May 2021 in the rural area of Swayimane, KwaZulu-Natal, South Africa (29°31'24''S; 30°41'37'' E) (Figure 5-1). Swayimane is located in the uMshwathi Local Municipality and approximately 55 km northeast of Pietermaritzburg. The small communal area covers a geographical extent of approximately 36 km<sup>2</sup>. Common crops cultivated in the area include white and yellow maize, sugarcane, amadumbe (*taro*), and sweet potato. The smallholder farmers follow traditional farming methods of planting, maintenance, and manual harvesting of crops. Farm plots are rainfed, fertilized using livestock manure, and hand weeded. Weeds and grass are also controlled using backpack herbicide sprayers. This study examined a 30 × 96 (2850 m<sup>2</sup>) smallholder maize field located on a slope, with a field elevation ranging from 850 m to 839 m.

The area is predominantly characterized by semi-subsistence farming, which is a form of food security and livelihood sustenance. The favourable environmental conditions of the region support agriculture and crop production in Swayimane. The climate is characterized by warm wet summers and cool, dry winters, with an average temperature ranging between 12°C and 24°C. Mean annual rainfall ranges between 600 and 1200 mm, with the most rain occurring during the summer occasioned by thunderstorms. During data collection, Swayimane had a maximum daily average air temperature of 24°C and total rainfall of 242.80 mm, amongst other weather data (Figure 5 2). Weather conditions were monitored continuously by the Automatic Weather Station installed at a Swayimane high school. Weather data was downloaded from the Swayimane weather website. The weather station was situated approximately 2 km from the smallholder maize farm. It was considered proximally adequate in capturing the weather conditions of the study site.

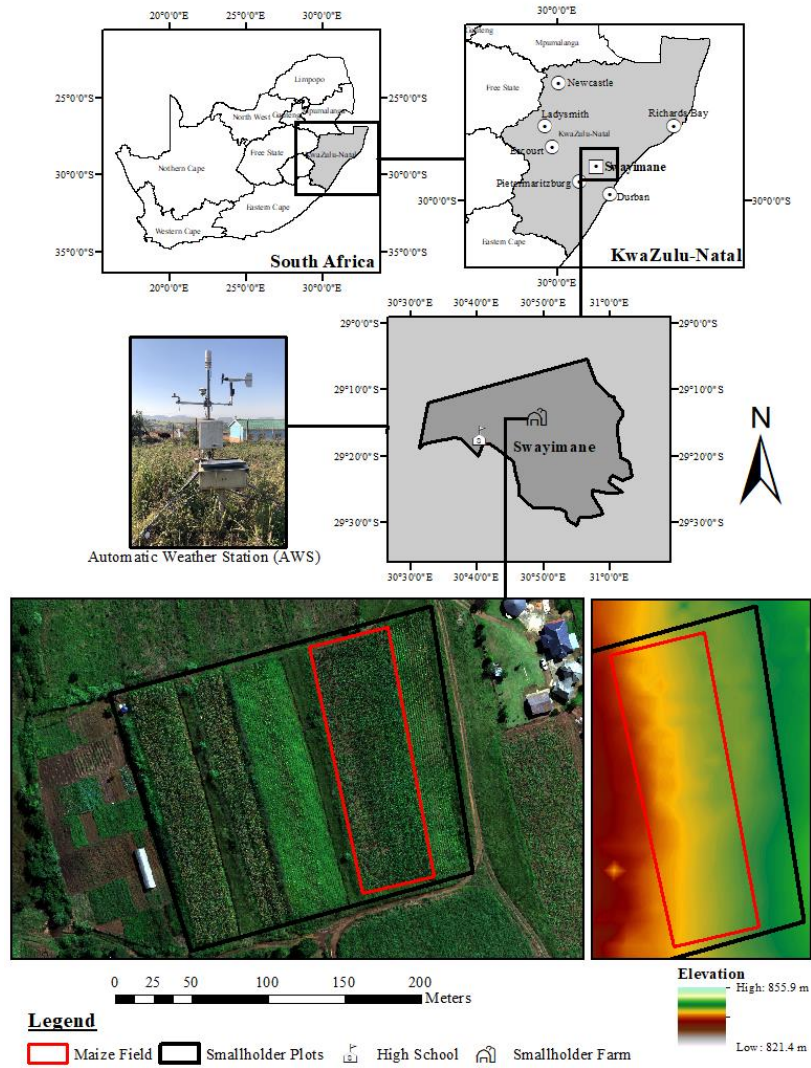


Figure 5-1: Location of the Swayimane study area, study site, and smallholder maize field.

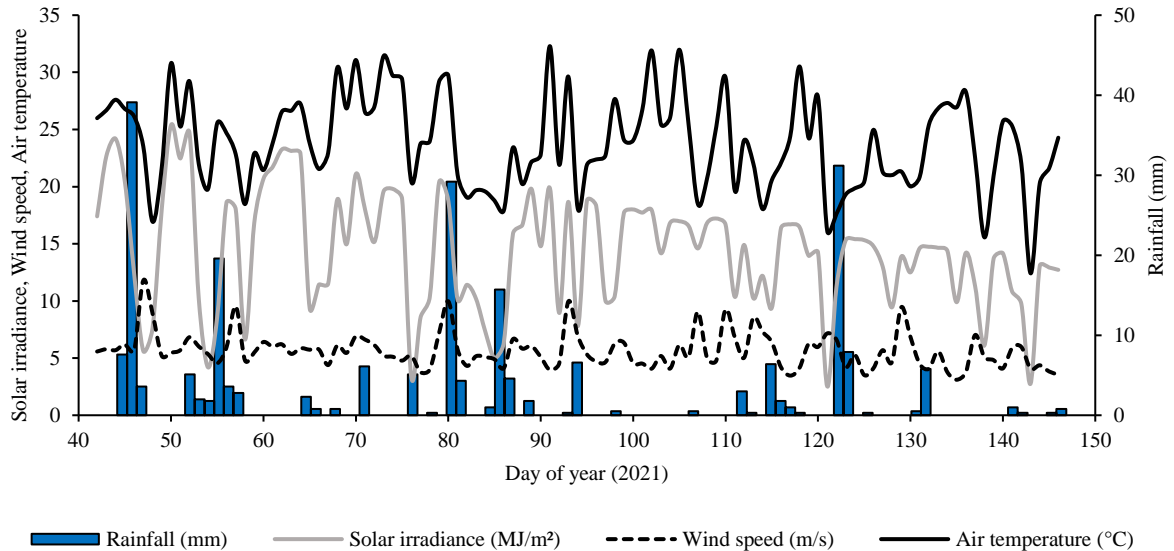


Figure 5-2: Daily weather conditions in Swayimane throughout maize phenotyping

### 5.2.2 The maize growth cycle and characteristics

Maize seedlings were sown on the 8<sup>th</sup> of February 2021 and harvested on the 26<sup>th</sup> of May 2021 (see Table 4-1), having a total growth cycle of 108 days and temperature and stomatal conductance examined at the various stages of phenotyping. The maize growth cycle is split into vegetative stages (emergence to tasseling based on the number of fully developed leaves) and reproductive stages (silking to physiological maturity based on the degree of kernel growth) (Cakir, 2004; Zhao, Tong et al., 2012). Within the various stages, certain transitions are significant for monitoring the potential occurrence of water stress. These are the emergence of crop growth (the first day of photosynthetic activity, termed VE), tasseling (the day when maximum leaf area is recorded and tassels appear, termed VT) and the commencement of senescence (the day when green leaf visibly loses colour) (Du Plessis, 2003).

It is worth mentioning that during the mid-vegetative stage, the field's western portion (lower elevation) appeared unhealthy. This may have been because this portion of the field was not weeded with the rest of the field during the early vegetative growth stage. However, the farmer applied herbicide during the mid-vegetative growth stage to remove grasses and weeds between maize rows. Consequently, the herbicide impacted the health status of these crops and the maize suffered herbicide burn.

### 5.2.3 Field data collection, temperature, and stomatal conductance measurements

Field data was collected throughout the maize phenological cycle. A 4-meter meteorological tower was installed at the centre of the maize field with two infrared radiometers (IRR) (Apogee SI-111, Apogee Instruments Inc., Logan, UT, USA) (Figure 5-3). The SI-111 IRR measures

surface temperature by converting the thermal energy radiated from the surface. The SI-111 IRR obtains a spectral range from 8  $\mu\text{m}$  to 14  $\mu\text{m}$ , with measurement ranges from  $-60^{\circ}\text{C}$  to  $110^{\circ}\text{C}$ , and a manufacturer accuracy of  $\pm 0.5^{\circ}\text{C}$  (Aragon, Johansen et al., 2020). The two IRR sensors were attached at a  $23^{\circ}$  and  $45^{\circ}$  half-angle field of view (FOV), with one centred on maize and the other obtaining an azimuth view perpendicular to the row direction. We programmed the datalogger (CR1000, Campbell Scientific, Logan, Utah, USA) to output average foliar canopy temperature, from 10-second measurements, at the following intervals: 5-minutes, 10-minutes, 30-minutes, and 60-minutes. IRR measurements were also aggregated to acquire daily average temperature using the 10-minute data.

The SI-111 radiometers were calibrated in a temperature-controlled chamber with a blackbody cone for the radiation source. This was conducted by holding the SI-111 IRRs in a fixture at the opening of the blackbody cone. The IRR sensors were thermally insulated from the cone, and each temperature was independently controlled. The IRRs are held at a constant temperature while the cone was controlled at temperatures below  $12^{\circ}\text{C}$ , above  $18^{\circ}\text{C}$  and equal to the IRR temperature. IRR temperature data were collected every  $10^{\circ}\text{C}$  until the IRRs and blackbody cone reached constant temperatures. IRR measurements of maize temperature were used to calibrate the handheld infrared thermometer (IRT) measurements that were used to develop the prediction model. Moreover, the IRR measurements were used to assess the thermal infrared UAV-derived temperature.

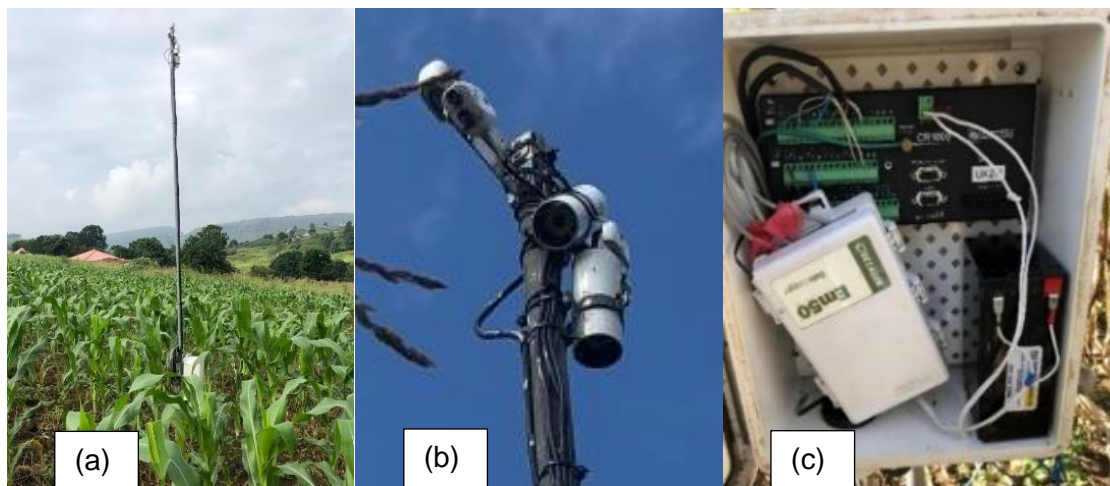


Figure 5-3: (a) Automated in-field meteorological tower in the maize field, (b) meteorological tower mounted with SI-111 Apogee IRR sensors held 4-meters above the ground, (c) CR1000 data logger, Em50 datalogger and 12 V battery

At two-week intervals, in-field maize temperature and stomatal conductance measurements were collected from the early vegetative (V5) growth stage to the late reproductive growth stages (R6). Pre-sampling of the maize smallholder field was conducted in Google Earth Pro, where a polygon of the experimental field was digitized. The digitized polygon was imported into ArcGIS 10.5 and used to generate sampling points. A total of 63 sample points were generated based on stratified random sampling within the digitized field boundary. These points were then uploaded into a handheld Trimble Global Positioning System (GPS) with sub-meter accuracy. These locations navigated the field to each sample point during data

collection. The maize plants at each sampling point were marked for consistent bi-weekly measurement. The 63 maize points were sampled on six occasions over phenotyping.

A digital laser infrared GM320 handheld thermometer (IRT) was used to measure selected maize foliar temperatures. IRT measurements can range from approximately  $-50^{\circ}\text{C}$  to  $330^{\circ}\text{C}$ . During the vegetative growth stages (where a sixth leaf was present) and the tasseling stage, the IRT temperature readings were measured on the newest fully expanded leaf with an exposed collar. After the tasseling stage, the ear leaf (i.e. the leaf attached at the same node as the primary ear shank) was measured (Costa, Frigon et al., 2003). Three foliar temperature measurements were taken and subsequently averaged per sampling point.

Stomatal conductance was measured using an SC-1 leaf porometer (Decagon Devices, Inc., Pullman, WA, USA). Stomatal conductance is the measure of gaseous exchange (i.e. carbon dioxide intake) and transpiration (i.e. water vapour loss) through the leaf stomata and is a function of the size, density and opening of leaf stomata (Handiganoor, Patil et al., 2018). Leaves with open stomata allow for higher conductance levels and indicate productive photosynthetic and transpiration rates. While closed leaf stomata indicate potential plant stress.

The SC-1 leaf porometer calibration was done before measurements under field conditions, as the leaf clip must be in thermal equilibrium with the environment. This included wetting filter paper with the distilled water provided in the sensor kit and then placing filter paper over the hole of the calibration plate. The sensor head was then attached to the calibration plate, where a 30-second measurement started. After the measurement, the sensor was equilibrated, and the sensor head was re-attached for another measurement.

Calibration measurements were repeated up to 10 times until a stable measurement was achieved. Leaf porometer readings were carried out on the same leaf as the IRT temperature readings. During the mid and late reproductive stage, a fully matured maize leaf in full exposure to sunlight was selected. The sensor was placed in the middle of the leaf blade perpendicular to the midrib when conducting measurements. The SC-1 leaf porometer automatically measured the leaf stomatal conductance (in  $\text{mmol}/\text{m}^2\text{s}$ ) for a measurement period of 30 seconds whilst providing measurements of air temperature and relative humidity. Stomatal measurements approaching  $0 \text{ mmol}/\text{m}^2\text{s}$  indicate stress, whereas values close to  $500 \text{ mmol}/\text{m}^2\text{s}$  indicate no stress.

IRT (temperature) and SC-1 leaf porometer (stomatal conductance) measurements were consistently taken between 10:00 am to 2:00 pm throughout the various stages of the maize phenological cycle. The temperature and stomatal conductance data were added to the 63 sampling points map in a geographical information system (GIS). The point map was then overlaid with the multispectral and thermal UAV imagery of each sampling point's derived spectral reflectance values.

#### **5.2.4 UAV: DJI Matrice 300 and MicaSense Altum**

The DJI Matrice 300 (DJI M-300) platform, mounted with a MicaSense Altum camera and Downwelling Light Sensor 2 (DLS-2), was used for aerial-based flights over the smallholder

farms. The rotary-wing DJI M-300 series has vertical take-off and landing (VTOL) technology, making it well-suited for small-scale agricultural crop imaging (Figure 5-4 (a)).

The DJI M-300 platform novelties include its 15 km transmission range, 7000 m maximum altitude, obstacle avoidance, flightpath planning and locational position tracker. The maximum flight time of the M-300 is 55 minutes (without payload), and it can reach a maximum speed of 27 m/s, which surpasses most drone platforms on the market. Moreover, the MicaSense Altum camera is a multispectral and thermal imaging sensor that integrates five spectral high-resolution narrow bands (blue, green, red, red-edge, and near-infrared) with a radiometric longwave infrared thermal camera (b). The high-performance camera offers synchronized multispectral and thermal image capture and uses a global shutter of up to a one-second capture rate for precise and aligned imagery (Hutton, Lipa et al., 2020). The multispectral bands have 2064 × 1544 at 120 m (3.2 megapixels per multispectral band) sensor resolution and a ground sample distance (GSD) of 5.2 cm per pixel at the height of 120 m. The thermal infrared camera has a 160 × 120 sensor resolution and a GSD of 81 cm per pixel at 120 m. The multispectral camera has a 48° × 37° FOV with an 8 mm focal length. While the thermal camera has a 57° × 44° FOV with a 1.7 mm focal length.

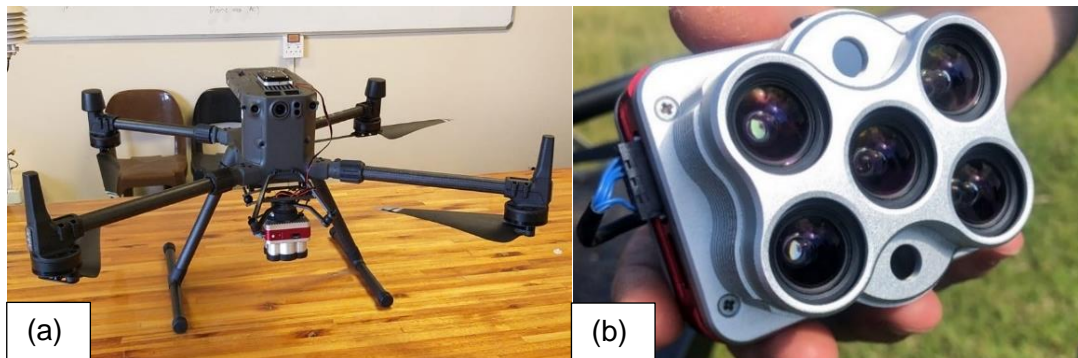


Figure 5-4: (a) DJI Matrice 300 UAV platform and, (b) MicaSense Altum multispectral-thermal camera

Table 5-1: MicaSense Altum camera specifications.

<b>Band</b>	<b>Spectral colour</b>	<b>Band centre/range</b>	<b>Ground sampling distance at a flying height of 120 m</b>
1	Blue	475 nm	5.2 cm per pixel
2	Green	560 nm	5.2 cm per pixel
3	Red	668 nm	5.2 cm per pixel
4	Red-edge	717 nm	5.2 cm per pixel
5	Near-infrared	842 nm	5.2 cm per pixel
6	LWIR thermal infrared	8000-14000 nm	81 m per pixel

## 5.2.5 Image acquisition and processing

A shapefile of the maize field was created in Google Earth Pro and imported into the DJI M-300 smart console, where it was used to design a flight plan covering the study area (Figure 5-6 (a); Table 4 3). The flight plan enabled a hands-free drone flight mission over the study field and adjacent areas. Before and after the flight, the UAV was calibrated using the MicaSense Altum calibrated reflectance panel (CRP). This included the user manually taking an unshaded image directly over the CRP to discern the lighting conditions of the specific flight date, time, and location (Table 5-5). We conducted UAV flights every 2-weeks on days with clear sky conditions. UAV flights were conducted between 10:00 am and 12:00 pm as this was the time of optimal solar irradiance. This period also coincided with the measurements of temperature and stomatal conductance.

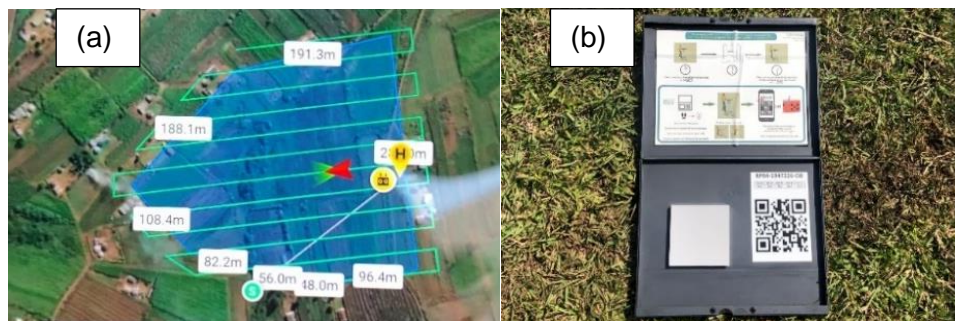


Figure 5-5: (a) DJI M-300 flight plan, (b) MicaSense Altum calibration reflectance panel

Table 5-2: UAV flight specifications

Parameters	Specifications
Altitude	100 meters
Ground sampling distance (multispectral)	7 cm
Ground sampling distance (thermal infrared)	109 cm
Speed	16 m/s
Flight duration	14 minutes 36 seconds
Composite images	321
Image overlap	80%

A total of 3576 images (per flight) were collected, mosaicked and radiometrically corrected (Pix4Dfields 1.8.0, Pix4d Inc., San Francisco, CA, USA). A radiometric correction was conducted in Pix4Dfields using all the captured images, including the before and after flight CRP images. The radiometric calibration target (CRP) is a white balance card that provides the reflectance properties of the card across the electromagnetic spectrum wavelengths captured by the camera. This enabled the software to calibrate and correct the reflectance of the images accordingly in line with the prevalent atmospheric conditions during the image acquisition. The CRP also obtained an absolute reflectance, making comparing data from several flights possible. Once processed, a final orthomosaic and a digital elevation model

(DEM) GeoTIFF image were generated. The orthomosaic was georeferenced in ArcGIS 10.5 using ground reference points from Google Earth Pro and referenced to the Universal Transverse Mercator (UTM zone 36S) projection.

The LWIR thermal infrared band was converted to absolute temperature values in Pix4Dfields, using the following equation:

$$\text{Temperature} = \frac{\text{LWIR Thermal Infrared (B6)}}{100} - 273.15 \quad \text{Equation 5-1}$$

The maize reflectance data was extracted from the multispectral and thermal infrared Altum image. This was done by overlaying the ground-truthed maize IRT temperature, stomatal conductance measurements, and their GPS coordinates in a point map with the UAV multispectral-thermal image. The reflectance values were extracted for each coordinate and each UAV band. The image was then used to compute vegetation indices (VIs) detailed in Table 5-3. VIs selected included direct and indirect water-related indices. These VIs were chosen based on their performance in the research literature (Yang and Du, 2017; Panigrahi and Das, 2018; Zhang and Zhou, 2019).

Table 5-3: Spectral vegetation indices utilized to predict the foliar temperature and stomatal conductance

Vegetation Index	Abbreviation	Equation	Reference
<b>Direct water-related indices</b>			
Normalized difference water index	NDWI	$\frac{\text{GREEN} - \text{NIR}}{\text{GREEN} + \text{NIR}}$	Yang and Du (2017) and Gao (1996)
<b>Indirect water-related indices</b>			
Normalized difference vegetation index	NDVI	$\frac{\text{NIR} - \text{RED}}{\text{NIR} + \text{RED}}$	Panigrahi and Das (2018)
Transformed normalized difference vegetation index	TDVI	$\sqrt{\frac{\text{NIR} - \text{RED}}{\text{NIR} + \text{RED}} + 0.5}$	Castellanos-Quiroz, Ramírez-Daza et al. (2017)
Normalized difference red-edge index	NDRE	$\frac{\text{NIR} - \text{RED EDGE}}{\text{NIR} + \text{RED EDGE}}$	Song, Birch et al. (2010)
Normalized green-red difference index	NGRDI	$\frac{\text{GREEN} - \text{RED}}{\text{GREEN} + \text{RED}}$	Song, Birch et al. (2010)
Green chlorophyll index	Clgreen	$\left(\frac{\text{NIR}}{\text{GREEN}}\right) - 1$	Zhang and Zhou (2019)
Red-edge chlorophyll index	Clrededge	$\left(\frac{\text{NIR}}{\text{RED EDGE}}\right) - 1$	Zhang and Zhou (2019)

Vegetation Index	Abbreviation	Equation	Reference
Green NDVI	GNDVI	$\frac{\text{NIR} - \text{GREEN}}{\text{NIR} + \text{GREEN}}$	Song, Birch et al. (2010)
Canopy chlorophyll content index	CCCI	$\frac{\text{NIR} - \text{RED EDGE}}{\text{NIR} + \text{RED EDGE}}$ $\frac{\text{NIR} - \text{RED}}{\text{NIR} + \text{RED}}$	Fitzgerald, Rodriguez et al. (2010)
Chlorophyll vegetation index	CVI	$\text{NIR} * \left(\frac{\text{RED}}{\text{GREEN}^2}\right)$	Vincini and Frazzi (2011)
Enhanced vegetation index	EVI	$\frac{2.5(\text{NIR} - \text{RED})}{\text{NIR} + 6\text{RED} - 7.5\text{BLUE} + 1}$	Wiratmoko, Prasetyo et al. (2018)
Soil-adjusted vegetation index	SAVI	$\frac{(\text{NIR} - \text{RED})(1 + L)}{\text{NIR} + \text{RED} + L}$	Sishodia, Ray et al. (2020)
Optimized soil-adjusted vegetation index	OSAVI	$\frac{1.16 (\text{NIR} - \text{RED})}{\text{NIR} + \text{RED} + 0.16}$	Sishodia, Ray et al. (2020)

### 5.2.6 Statistical Analysis

The sampled data were randomly partitioned into training (70%) and testing (30%) datasets used to develop the predictive regression models. A random forest regression algorithm was used to predict maize foliar temperature and stomatal conductance (from spectral bands and VIs) since it is renowned for its simplicity, robust nature, and ability to perform well regardless of sample size (Dye, Mutanga et al., 2011; Luan, Zhang et al., 2020). The random forest ensemble is a machine learning algorithm that uses bootstrap aggregation to construct multiple trees on a subset of samples derived from the training data (Abdel-Rahman, Ahmed et al., 2013). Decision trees are grown to maximum capacity with a randomized subset of predictors (UAV-derived spectral data). Each node is split using random subsets of input variables (Adam, Mutanga et al., 2012). Furthermore, the random forest regression can identify predictor variables that are influential in the prediction model based on the sum of the reduction in Gini impurity across the feature nodes (Sibanda, Onisimo et al., 2021).

Specifically, the RGtk2 and rattle packages in RStudio software version 1.4.1564 were used to develop the random forest regression model through numerical inputs. The outputs of the random forest model were optimized using the variable importance scores as they determine the most influential bands and VIs in prediction. Variables of low importance were removed throughout the analysis, and the random forest model was continuously modified for optimal prediction. The variable selection process reduces variable redundancy and multicollinearity issues, which affect the regression model's performance. The user optimised and fine-tuned the model to hyper-parameters of 500 trees, six variables for temperature and 500 trees, and

10 for stomatal conductance. These hyper-parameters were attained after numerous iterations.

### **5.2.7 Accuracy assessment**

Accuracy assessments were conducted to assess the regression model's predicted foliar temperature and stomatal conductance performance. The accuracy metrics used were the coefficient of determination ( $R^2$ ), root-mean-squared error (RMSE), and relative root-mean-squared error (RRMSE). The  $R^2$  measured the variation between the measured and predicted: foliar temperature and stomatal conductance. The RMSE assessed the magnitude of error between the field measurements and modelled outputs of foliar temperature and stomatal conductance. While the RRMSE evaluated the accuracy of the model and was used to compare the performance of regression models across maize phenotyping. The RRMSE was calculated by normalizing the mean of each variable RMSE value and expressing it as a percentage, where lower percentages are considered more accurate (Taghizadeh-Mehrjardi, Mahdianpari et al., 2020).

## **5.3 Results**

### **5.3.1 Descriptive analysis of UAV-derived data and SI-111 IRR maize temperature data**

The IRR time-series data was used to plot the difference between IRR foliar canopy temperature ( $T_c$ ) and air temperature ( $T_a$ ) (Figure 5-6). The foliar canopy to air temperature difference ( $T_c - T_a$ ) fluctuated throughout maize phenotyping, as ambient conditions of air temperature, solar radiation, and the influence of rainfall influenced foliar canopy temperatures. Hence, solar radiation and  $T_c - T_a$  followed a similar fluctuation trend. Days of low solar radiation or rainfall were associated with a lower  $T_c - T_a$ , and days of high solar radiation were generally associated with a higher  $T_c - T_a$ .

The trendline through  $T_c - T_a$  over the maize growing season shows that a higher  $T_c - T_a$  was associated with the early vegetative stages, such as DOY 43 at 3.1°C, as well as mid-reproductive and late reproductive growth stages, such as DOY 115 at 3°C and DOY 130 at 2.7°C, respectively. The maximum  $T_c - T_a$  was recorded during the mid-reproductive stage on DOY 116 at 3.4°C. This was after a hailstorm that occurred on DOY 113, which increased the  $T_c - T_a$  and resulted in  $T_c - T_a$  remaining relatively high for the duration of phenotyping at approximately 1.9°C. A lower  $T_c - T_a$  was associated with the mid-vegetative and late vegetative growth stages, such as DOY 85 at -0.8°C and DOY 90 at -7.3°C, respectively. The lowest  $T_c - T_a$  was recorded during the late vegetative stage on DOY 92 at -8.6°C.

Generally, the solar radiation and air temperature decreased as winter approached. However, the  $T_c - T_a$  increased as the winter season approached, suggesting reduced transpiration due to water stress during the mid-reproductive and senescence in the late reproductive growth stages.

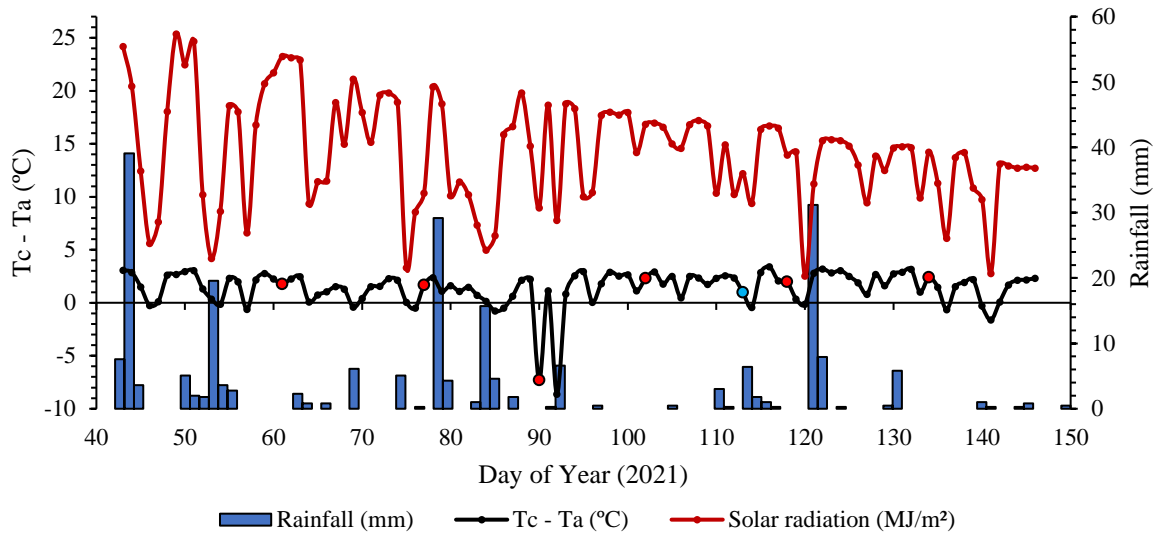


Figure 5-6: Daily average Tc-Ta, solar radiation, and rainfall throughout the maize phenological cycle. Red points indicate field visits to conduct data collection. The blue point indicates the day of the hailstorm.

A strong positive linear relationship ( $R^2 = 0.94$ ;  $p = 0.001$ ) between temperature derived from the UAV-acquired thermal band and that measured in-field using the IRR temperature sensors (Figure 5-7) across all sampling dates. During the early vegetative growth stage, DOY 61, the IRR and UAV temperatures recorded a satisfactory correlation of approximately 29.7°C to 30.8°C, respectively. The mid-vegetative stage, DOY 77, obtained a significant correlation of 22.2°C and 21.2°C for IRR and UAV temperatures.

Moreover, during the late vegetative stage (DOY 90) and the early reproductive stage (DOY 102), maize IRR and UAV temperatures correlated substantially and were recorded at approximately 27°C and 24°C, respectively. However, the correlation during the mid-reproductive and late reproductive stages, DOY 118 and DOY 134, deviated from the trendline due to the maize canopy disturbance by the hailstorm on DOY 113. Hence, IRR and UAV temperatures were recorded at 24°C and 26°C for the mid-reproductive stage and 24°C and 23°C for the late reproductive stage.

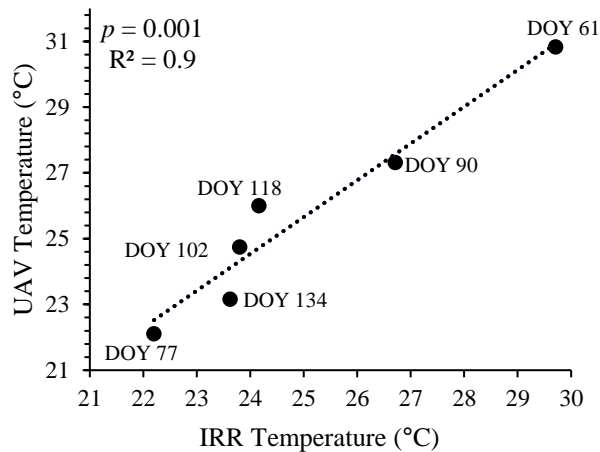


Figure 5-7: Correlation of in-field IRR sensors and UAV-derived temperature throughout the maize phenological cycle

### 5.3.2 Descriptive statistics of in-situ maize temperature and stomatal conductance measurements

The IRR and IRT minimum and maximum temperatures of the 63 sampling points were used to illustrate the descriptive temperature statistics (Table 5-5). The average maximum IRR temperature for the entire phenological cycle was 32.2°C, and the average IRT temperature for the maize growth cycle was 32.6°C. This suggested an average temperature offset of 0.4°C between the IRR and IRT temperature measurements. The highest recorded IRR temperature occurred during the late vegetative growth stage of V14-T at 35°C, and the maximum IRT temperature was 39.1°C recorded during the V14-T growth stage. The average minimum IRR temperature for the entire phenological cycle was 18.3°C, and the average IRT temperature for the maize growth cycle was 20.9°C. This suggested an average temperature offset of 2.6°C between the IRR and IRT temperature measurements.

The lowest IRR temperature value occurred during the R3-R4 growth stage at 16°C, whereas the lowest IRT temperature value occurred during the V12 growth stage at 15.5°C. The IRR maximum values were within 1.7 standard deviations of the mean, whereas the IRT maximum values were within 5.1 standard deviations of the mean. Similarly, with the minimum values, the standard deviation of the IRR and IRT temperatures were 1.9 and 3.2, respectively. The total mean coefficient of variation for the maximum IRR was 5.2%, whereas the maximum coefficient of variation for the IRT was 15.7%. Moreover, the minimum IRR and IRT temperatures had co-efficient variations of 10.4% and 15.5%, respectively. The IRR values suggest precise temperature estimates close to the mean value.

Table 5-4: Descriptive statistics of IRR and IRT foliar temperature throughout the maize growth stages

Maize foliar temperature at the various growth stages		Maximum (°C)		Minimum (°C)	
		IRR	IRT	IRR	IRT
DOY 61	V5-V10	34	32.7	17	21.5
DOY 77	V12	33	23.4	20.5	15.5
DOY 90	V14-T	35	39.1	17.1	23.1
DOY 102	R1-R3	34	33.7	18.9	21.4
DOY 118	R3-R4	33	34.3	16	19.3
DOY 134	R5-R6	30	32.3	20.4	24.8
<b>Mean</b>		33.2	32.6	18.3	20.9
<b>Median</b>		33.5	33.2	18	21.5
<b>Standard deviation</b>		1.7	5.1	1.9	3.2
<b>Co-efficient of variation</b>		5.2	15.7	10.4	15.5

The measured maize stomatal conductance varied at the different stages of maize phenotyping (Table 5-6). The average stomatal conductance over the maize phenotyping was 206.9 mmol/m<sup>2</sup>. The lowest conductance value occurred during the early vegetative growth stage (V5-V10) at 42 mmol/m<sup>2</sup>, and the highest stomatal conductance occurred during the early reproductive development stage (R1-R3) at 556.5 mmol/m<sup>2</sup>. Higher stomatal conductance values characterized reproductive stages compared to the vegetative stages. However, the average stomatal conductance for the mid-reproductive stage (R2-R4) decreased to 172.6 mmol/m<sup>2</sup> due to the crop stress from the hailstorm on DOY 113. Furthermore, the median value of maize stomatal conductance across the growing season was 194.6 mmol/m<sup>2</sup>, and the average stomatal conductance values were within 79.3 standard deviations of the mean value.

Table 5-5: Descriptive statistics of stomatal conductance throughout the maize phenological cycle

Maize stomatal conductance at the various growth stages	Minimum (mmol/m <sup>2</sup> s)	Maximum (mmol/m <sup>2</sup> s)	Mean (mmol/m <sup>2</sup> s)	Median (mmol/m <sup>2</sup> s)	Standard deviation	
DOY 61	V5-V10	42	245.1	121.8	112.9	49.25
DOY 77	V12	86.6	556.5	248.5	238.1	113.3
DOY 90	V14-T	44.2	404.8	166.5	157.6	73.7
DOY 102	R1-R2	182.7	480.1	298.9	290.1	79.3
DOY 118	R2-R4	100.2	373.6	172.6	160.3	55.6
DOY 134	R4-R5	74.3	483.1	233.3	208.5	104.8
<b>Average value</b>		<b>88.3</b>	<b>423.9</b>	<b>206.9</b>	<b>194.6</b>	<b>79.3</b>

Importantly, foliar temperature and stomatal conductance had a significant inverse relationship, producing an  $R^2 = 0.72$  (Figure 5-8). The negative relationship between stomatal conductance and temperature further enhanced potential crop water stress identification. Such a relationship illustrated that when stomatal conductance was low, foliar temperatures were high, i.e. hot canopy. Furthermore, high stomatal conductance was associated with low foliar temperatures, i.e. cool canopy, suggesting optimal maize water productivity.

For example, on DOY 77, the maize temperature was low at 20°C, and the stomatal conductance was high at 396 mmol/m<sup>2</sup>, illustrating potentially optimal crop conditions. On DOY 61, the maize temperature was higher at 28°C, and the stomatal conductance was low at 122 mmol/m<sup>2</sup>, indicating potential water stress. Thus, the inverse relationship between foliar temperature and stomatal conductance was useful in estimating crop water stress.

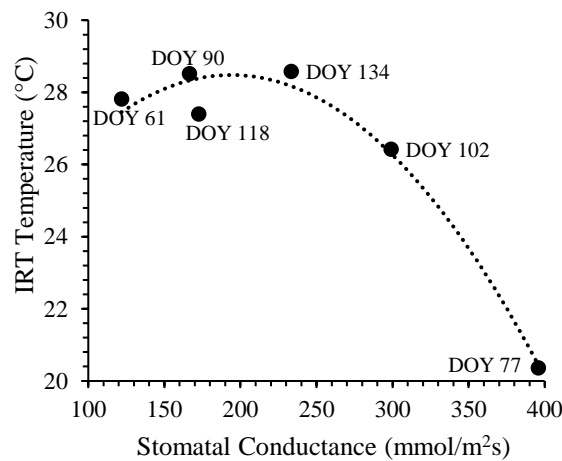


Figure 5-8: Correlation of foliar temperature and stomatal conductance throughout the maize phenological cycle

### 5.3.3 UAV-derived data: estimation of maize temperature and stomatal conductance

For the prediction of maize temperature, the mid-vegetative stage (DOY 77 (V12)) yielded the most optimal modelled RMSE = 0.59°C and  $R^2 = 0.81$  (RRMSE = 2.9%) (Figure 5-9 (b)). The optimal variables for this model were the thermal infrared followed by red, NGRDI, CVI and NDVI, in order of importance (Figure 5-10 (b)). The mid-reproductive stages yielded an RMSE = 1.24°C,  $R^2 = 0.76$  and the poorest maize phenology RRMSE = 6.2%. Model prediction accuracies moderately improved in the late vegetative stages (DOY 90 (V14-T)) and the early reproductive stage (DOY 102 (R1-R3)) to an RMSE = 1.14°C,  $R^2 = 0.79$  (RRMSE = 4%) and RMSE = 1.02°C,  $R^2 = 0.73$  (RRMSE = 3.9%), respectively. The model from the late reproductive stage (DOY 134 (R5-R6)) obtained an RMSE = 0.7°C and  $R^2 = 0.78$  (RRMSE = 2.6%) based on NDRE, OSAVI, CCCI, thermal infrared, and EVI, in order of importance

(Figure 5 10 (e)). The early vegetative stage (DOY 61(V5-V10)) exhibited a RMSE = 1.29 and  $R^2 = 0.69$  (RRMSE = 4.7%).

In estimating stomatal conductance, the early reproductive stage (DOY 102 (R1-R3)) produced the most accurate model with an RMSE = 25.9 mmol/m<sup>2</sup>, the highest  $R^2 = 0.85$  (and the best RRMSE = 11.5%) based on NIR, NDRE, Thermal,  $CI_{rededge}$ , and red-edge, in order of importance (Figure 5-10 (d)). Poor stomatal conductance accuracies were attained during the late reproductive stage (DOY 134 (R5-R6)) with an RMSE = 52.6 mmol/m<sup>2</sup> and  $R^2 = 0.78$  (RRMSE = 23.8%) using the thermal infrared, CCCI, blue,  $CI_{rededge}$ , and CVI in order of importance (Figure 5-10 (f)). In addition, the late vegetative stages (DOY 90 (V14-T)) also yielded a poor model with an RMSE = 51.2 mmol/m<sup>2</sup> and  $R^2 = 0.64$  (poorest RRMSE = 28.7%). The mid-reproductive stage (DOY 118 (R3-R4)) model produced a RMSE = 44.6 mmol/m<sup>2</sup> and  $R^2 = 0.7$  (RRMSE = 25.6%). The mid-vegetative stage (DOY 77 (V12)) yielded improved model accuracies with an RMSE = 34.8 mmol/m<sup>2</sup>, the poorest  $R^2 = 0.58$  (RRMSE = 20.1%), whereas the early vegetative stage (DOY 61 (V5-V10)) produced an optimal RMSE = 26.5 mmol/m<sup>2</sup> and  $R^2 = 0.73$  (RRMSE = 22.9%). The early and mid-reproductive stages were characterized by the red-edge band and the  $CI_{rededge}$ , respectively. The red-edge and NIR bands were clear stand-out and optimal model contributors. However, the model achieved higher  $R^2$  values during the reproductive stages and more optimal RMSE values during the vegetative stages.

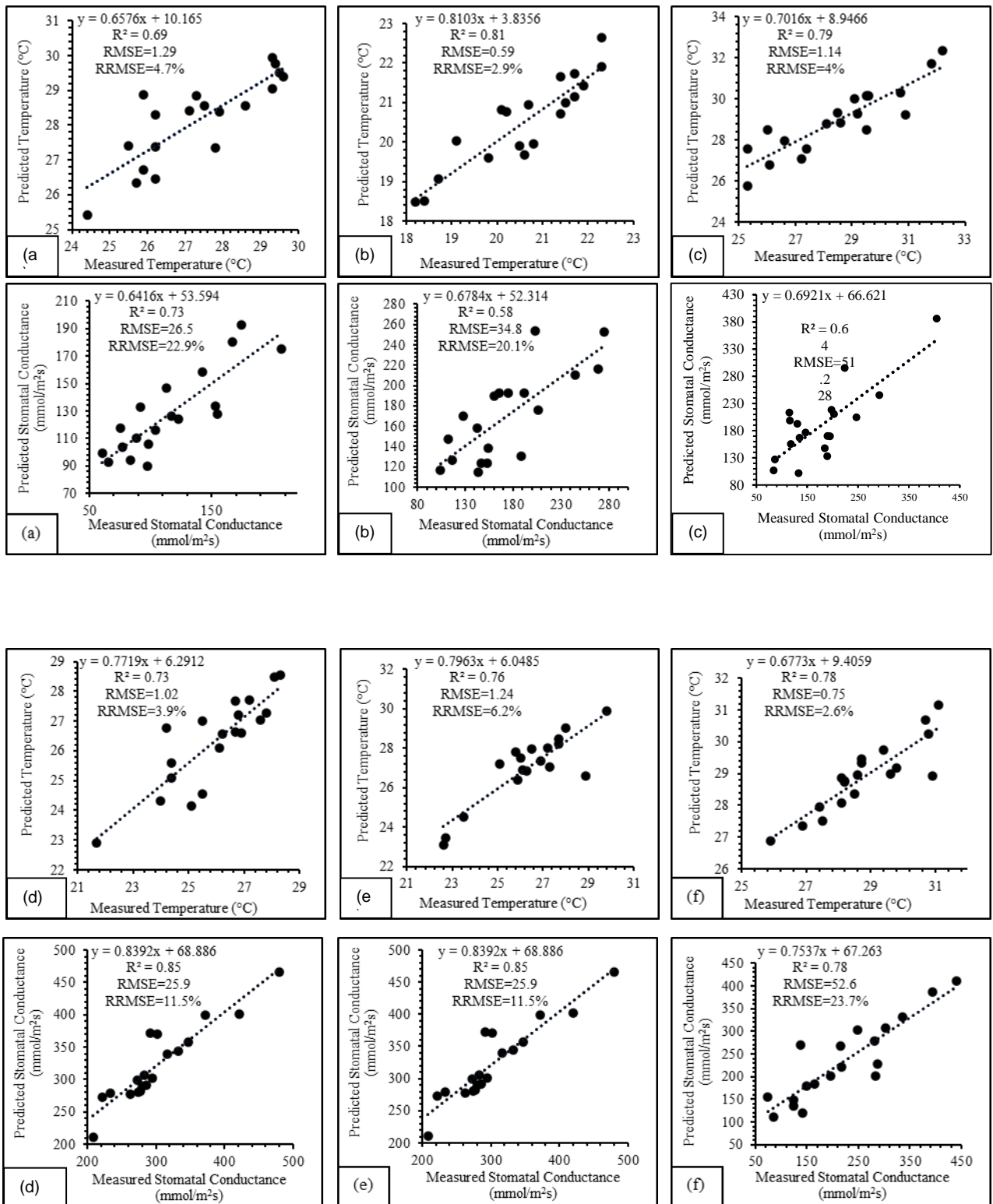


Figure 5-9: Regression models displaying the relationships between measured and predicted IRT foliar temperature and stomatal conductance throughout the maize phenological cycle: (a) V5-V10, (b) V12, (c) V14 to VT, (d) R1-R3, (e) R3-R4, (f) R5-R6

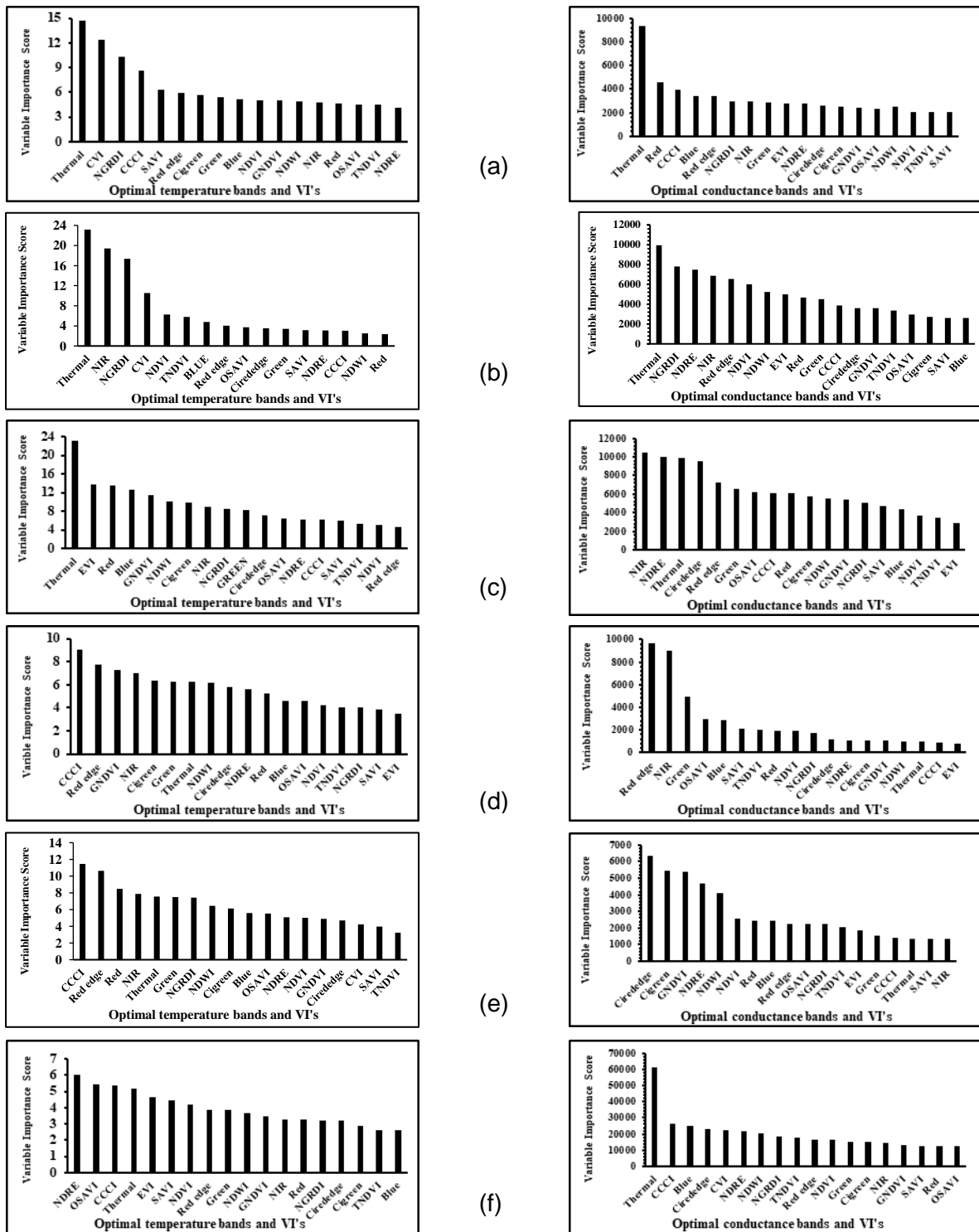


Figure 5-10: Variable importance scores of optimal foliar temperature and stomatal conductance bands and VIs throughout the phenological cycle: (a) V5-V10, (b) V12, (c) V14 to VT, (d) R1-R3, (e) R3-R4, (f) R5-R6

### 5.3.4 Mapping the spatial distribution of maize temperature and stomatal conductance over the various phenological stages.

The modelled maize temperature ranged from 8 to 57°C (Figure 5-11). The maize field temperatures were high during the early vegetative growth stage. Subsequently, during the mid-vegetative growth stage, the field temperature moderately decreased and further decreased during the late vegetative stage to have the lowest field foliar temperatures. Likewise, in the early reproductive stage, the field was characterized by a generally low temperature, except for the field's eastern edge (high elevation). The maize temperature during the mid-reproductive stage increased due to the hailstorm damage. During the late reproductive stage, the hailstorm effects increased and further escalated field temperatures.

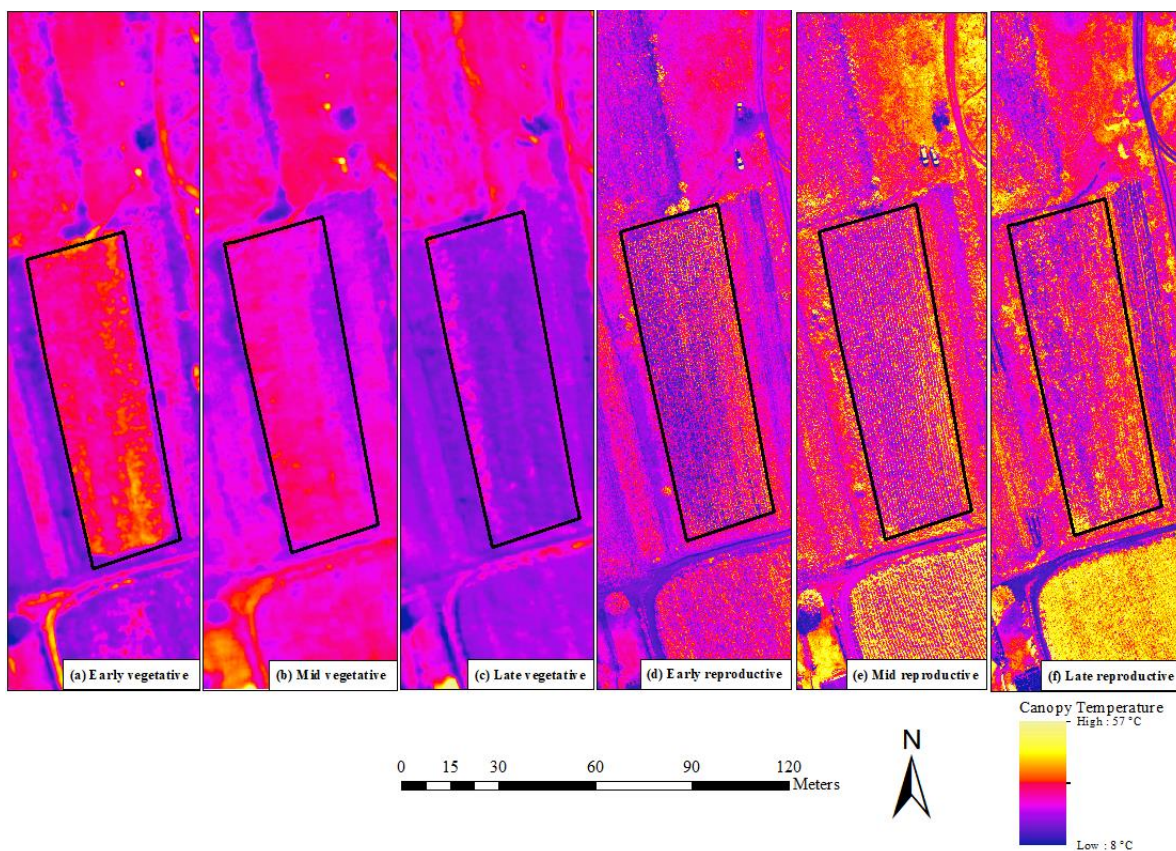


Figure 5-11: Foliar temperature of maize over the smallholder field for vegetative stages (a) V5-V10, (b) V12, (c) V14 to VT, and reproductive stages (d) R1-R3, (e) R3-R4, (f) R5-R6.

The spatial distribution of stomatal conductance was estimated based on the optimal models for each maize phenological stage. The stomatal conductance values ranged from 82.2 mmol/m<sup>2</sup> to 683.4 mmol/m<sup>2</sup> (Figure 5-12). It can be observed that the stomatal conductance of maize was relatively low throughout the maize fields. However, high levels of stomatal conductance were identified during the early vegetative stage towards the southern portion of the field, the eastern part of the field during the late vegetative stage, and the eastern section during the mid-reproductive stage. The remainder of the stages, being the mid-vegetative, early reproductive, and late reproductive, were characterized by lower levels of stomatal

conductance. The late reproductive stage had the lowest conductance due to the hailstorm stress and crop senescence.

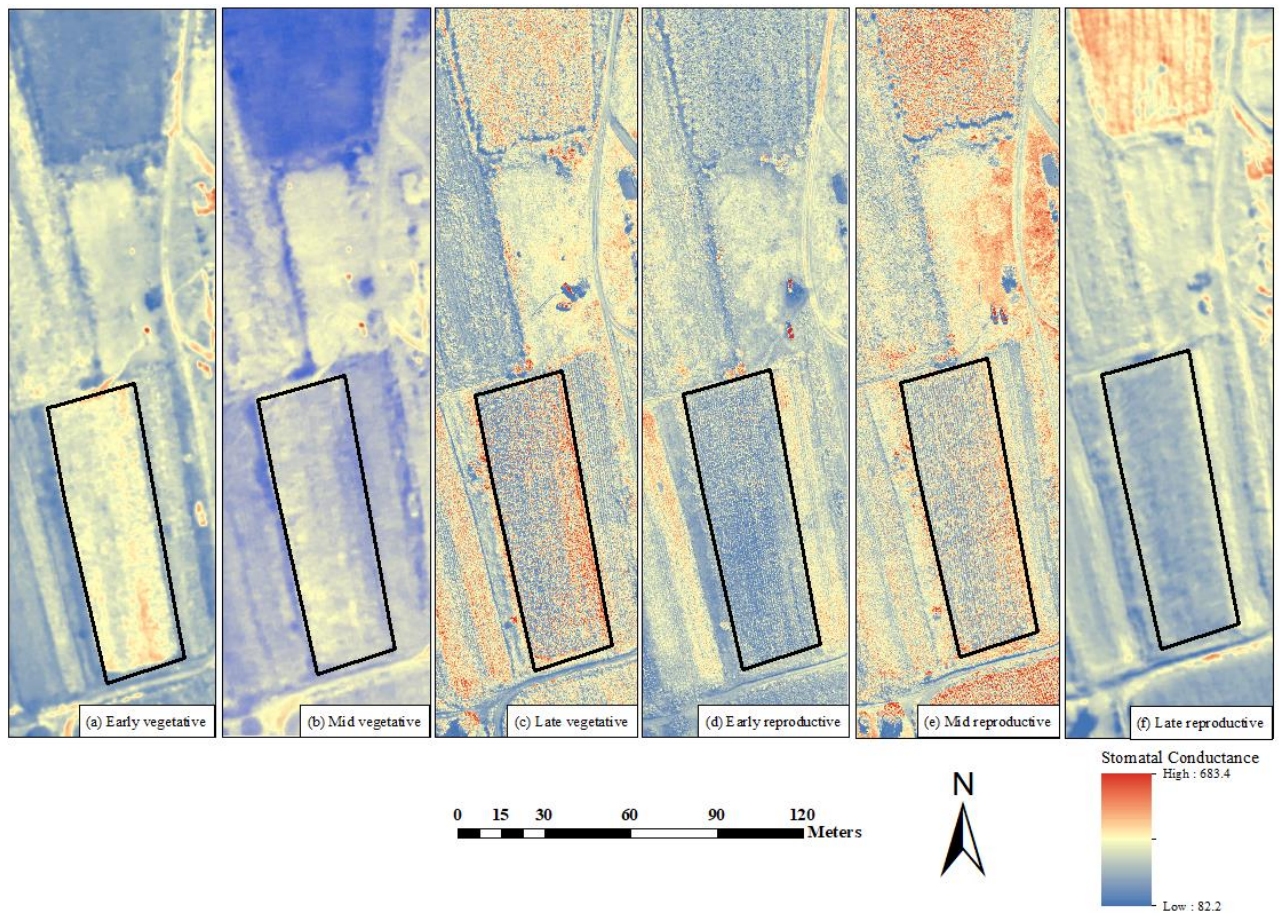


Figure 5-12: Maize stomatal conductance over the smallholder field for vegetative stages (a) 5-V10, (b) V12, (c) V14 to VT, and reproductive stages (d) R1-R3, (e) R3-R4, (f) R5-R6.

## 5.4 Discussion

This study aimed to predict maize temperature and stomatal conductance over the various maize growth stages using UAV-derived data in combination with the random forest algorithm. We aimed to determine the most optimal maize growth stage(s) for temperature and stomatal conductance model estimation. It was evident that maize foliar temperatures and stomatal conductance differed throughout phenotyping. The UAV-derived data could discern the optimal growth stages for characterising temperature and stomatal conductance as proxies for crop water stress. For this purpose, the foliar temperature and stomatal conductance data were used to understand the smallholder field's potential crop water stress and moisture status throughout the growing stages.

#### 5.4.1 Prediction of maize water stress using foliar temperature and stomatal conductance

The regression models were set to predict maize foliar temperature and stomatal conductance using the thermal infrared and multispectral UAV data. Generally, the random forest model performed relatively well in predicting maize foliar temperature and stomatal conductance over the various growth stages. Specifically, the random forest model achieved stronger prediction accuracies for foliar temperature than stomatal conductance over maize phenotyping.

The maize foliar temperature was optimally predicted during the mid-vegetative growth stage (RMSE = 0.59°C,  $R^2 = 0.81$  and RRMSE = 2.9%) based on the thermal infrared, followed by the NIR, NGRBI, EVI and NDVI, in order of importance. It has been illustrated in the literature that crop leaves' water content is directly associated with foliar reflectance across the electromagnetic spectrum (Mangus, Sharda et al., 2016; Gerhards, Schlerf et al., 2019). Specifically, the foliar temperature was strongly detected by the thermal infrared as it can sense emitted radiant energy; hence, it is commonly used for evaluating crop water stress (Prakash, 2000; Zarco-Tejada, González-Dugo et al., 2012; Brenner, Thiem et al., 2017). Moreover, the NIR region was valuable in quantifying crop water status due to its strong water absorption ability to detect crop water stress based on reflectance variation (Das, Sahoo et al., 2021). Thus, the thermal infrared and NIR wavebands strongly detected the crop surface temperatures, hence their crucial role in predicting the maize temperature variability during vegetative growth stages.

Specifically, during the vegetative stages, the maize canopy structure develops, thus exposing the underlying soil surface, which absorbs and retains thermal radiation (Zhang, Niu et al., 2019). As a result, the high ambient soil temperatures influence the maize temperature, especially during early vegetative growth when there is maximum soil exposure. However, soil influence is reduced as the canopy structure develops, and crops generally experience lower leaf temperatures. Since stomata are generally more numerous on the underside of the leaf, they are influenced by the heat of soil, which reaches the underside due to convection (Nejad 2011; Göbel, Coners et al., 2019). This reduces the stomatal conductance levels as the crop closes the stomata to retain moisture and subsequently experiences higher foliar temperatures (van der Vyver and Peters, 2017). Hence, the thermal infrared section was a strong predictor variable of foliar temperature due to its ability to overcome the influence of soil temperature during the stages of minimal canopy closure.

Nevertheless, the temperature of a leaf, relative to the surrounding air temperature, is primarily influenced by the plant's photosynthetic capacity, as well as the productivity of the internal structural leaf components such as the air cavities, chloroplasts, and mesophyll cell thickness (Peñuelas, Filella et al., 1993; Ustin and Jacquemoud, 2020). Thus, when a crop is water-stressed, the molecular leaf networks transmit a signal to initiate physiological and biochemical changes that regularly result in increased foliar temperatures relative to the air temperatures (Bonada, Sadras et al., 2013; Hasanuzzaman, Nahar et al., 2013; Osakabe, Osakabe et al., 2014). However, when optimal water is present, the Tc-Ta remains low as there are productive rates of transpiration and photosynthesis. Therefore, the sustained influence of the thermal infrared and chlorophyll-based VIs during vegetative growth stages suggested that the crop was optimally transpiring with no water stress. However, the relatively high maize leaf

temperatures measured in combination with the high Tc-Ta during the early vegetative stage suggested slight water stress at crop emergence.

During the reproductive stages, the importance of the thermal infrared waveband decreased, and spectral wavelengths such as the red edge and NIR, as well as VIs derived from these sections, were found to be more important in facilitating the prediction of foliar temperature. This could be attributed to the fact that there was minimal soil exposure due to the fully developed canopy structure. More specifically, the red edge borders the absorption of photosynthetic pigments such as chlorophyll, which tend to be more vigorous in fully developed canopies (Ciganda, Gitelson et al., 2012; Bano, Aslam et al., 2015). Generally, the change in chlorophyll affects the photosynthetic rates, which indirectly alters the temperature tolerance and further the stomatal conductance of the crop, inherently indicating crop water productivity (Yordanov, Tsonev et al., 1997). Additionally, during these stages, a higher leaf area index facilitates multiple leaf scattering and reduced transmittance through the leaf due to stronger chlorophyll concentrations optimally identified by the NIR region (Ustin and Jacquemoud 2020; Sibanda, Onisimo et al., 2021). Hence, the significant contribution of chlorophyll-based indices from the red-edge and NIR sections, such as the CCCI, NDRE, and GNDVI, during the reproductive stages of temperature prediction. However, the hailstorm occurrence during the mid-reproductive stage damaged the maize canopy structure and exposed underlying soil, causing poorer model prediction due to the spectral confusion between soil and foliar temperatures. After the hailstorm, the Tc-Ta increased due to the canopy damage that caused increased crop temperatures. This increase indicated potential crop water stress during the mid-reproductive and late reproductive stages.

Meanwhile, based on the red edge, maize stomatal conductance was optimally predicted during the early reproductive stage (RMSE = 25.9 mmol/m<sup>2</sup>, R<sup>2</sup> = 0.85 and RRMSE = 11.5%) followed by the NIR, green, OSAVI and blue band, in order of importance. Literature has confirmed that the red-edge region is renowned for its relation to plant water stress and evapotranspiration (Ballester, Brinkhoff et al., 2019; Niu, Zhao et al., 2019; Vitrack-Tamam, Holtzman et al., 2020). This is because the red edge is layered with physiological and chemical processes that reflect the photosynthetic activity of the crop, which indicate stomatal conductance and the potential of crop water stress (Zarco-Tejada, Pushnik et al., 2003, Dobrowski, Pushnik et al., 2005). Specifically, during photosynthesis, the red edge overlaps the fluorescence emission, which affects the degree of reflection and corroborates the dependence of stomatal conductance on photosynthetic activity (Vitrack-Tamam, Holtzman et al., 2020). Moreover, denser canopies provide increased accuracy in estimates of photosynthetic capacity and stomatal conductance through the NIR region (Carter, 1998, Waring and Landsberg, 2011). Optimal stomatal activities are also associated with rapid chlorophyll development, which reflects highly in the red-edge and NIR (Ballester, Brinkhoff et al., 2019). Hence, the optimal influence of the red-edge and NIR wavebands and indices derived from these sections in estimating the stomatal conductance of maize in smallholder farms, especially during the reproductive stages.

During the early reproductive stage, the crop was almost at peak biomass and obtained a high leaf surface area that promoted faster rates of photosynthesis and conductance to support fruit development (Yordanov, Tsonev et al., 1997; Dai, Dickinson et al., 2004). The measured stomatal activities were most prominent during this stage as a high foliar surface area was

generally associated with more stomata on the leaf (Li, Kang et al., 2004). Hence, transpiration rates are more dynamic, and the leaf stomata open, facilitating high productivity levels through optimal foliar conductance and cooling of crop temperatures (Gerhards, Schlerf et al., 2019). During the early reproductive stage, such processes indicated crop productivity and optimal moisture content, which influence a strong reflectance of the leaf tissue in the red-edge and NIR regions. Even though the crop was undergoing developmental processes during these stages that required high amounts of water (tasseling, silking, and kernel development), the maize measured an optimal foliar temperature and high stomatal conductance, suggesting crop water productivity and minimal crop water stress of the smallholder farm. However, the hailstorm, during the mid-reproductive stage disturbed the maize canopy structure and resulted in low measured stomatal conductance. Subsequently, this resulted in the thermal infrared being an important predictor due to damage of the canopy and exposure of soil. Furthermore, the high  $T_c - T_a$  indicated that the hailstorm damage-initiated crop water stress, as foliar temperatures increased and stomatal conductance was reduced in the mid-reproductive and later reproductive stages. Similarly, this was also the case during the early vegetative stage, as stomatal conductance was low and  $T_c - T_a$  measured high.

Finally, the prediction model proved that a combination of UAV multispectral and thermal wavebands and UAV-derived VIs could accurately predict maize foliar temperature and stomatal conductance. The variables of importance for foliar temperature and stomatal conductance were fairly similar in their contribution to the model development throughout maize phenotyping. Thus, this indicates that foliar temperature and stomatal conductance are independent yet interrelated functions, which holistically can be used to understand the potential of crop water stress. Therefore, timeously predicting maize foliar temperature and stomatal conductance allows smallholder farmers to make near real-time decisions that aid water-related crop productivity.

#### **5.4.2 Implications of the study**

Smallholder farming systems often lack the resources to initiate successful farming practices, as commercial agriculture tends to be the focus of contemporary innovation and development. Thus, the findings of this study imply that incorporating multispectral and thermal infrared UAV technology could facilitate in-depth analysis of near real-time crop water stress through temperature and stomatal conductance as proxies. In this regard, the study's findings are useful for informing smallholder agriculture management by suggesting the potential implementation of irrigation schedules at crucial water stages (i.e. tasseling, silking, and pollination). Moreover, the UAV-derived data identified stages of high temperatures and low stomatal conductance (i.e. early vegetative stage), suggesting a potential moisture deficit and, thus, the need for necessary interventional irrigation schedules to ensure optimal crop productivity and development. Specifically, irrigation during vegetative stages may aid optimal productivity and prevent early crop water stress.

The hailstorm during the mid-reproductive stages caused damage to the maize canopy structure and led to adverse effects on crop growth and premature senescence. Subsequent in-field measurements of stomatal conductance reflected potential stress, as stomatal conductance values were much lower than typical values expected during this growth stage. Additionally, foliar temperature measurements were relatively high and indicated mild stress,

especially during the late reproductive stage. Such agrometeorological effects prove South African smallholder farmers are susceptible to weather events affecting crop water productivity. Thus, using UAV-derived data enables the identification of such occurrences in near real-time, allowing farmers to make rapid, informed, and effective decisions on subsequent crop management. This is crucial as it affects the food security and socio-economic growth of smallholder farmers who rely on healthy and moisture-filled crop yields. Therefore, smallholder farmers benefit from the near real-time analysis of the UAV data and can ensure prompt remedial measures to prevent further crop stress.

## 5.5 Conclusion

Premised on the study's findings, it can be concluded that foliar temperature and stomatal conductance are adequate indicators to quantify proxies of water stress throughout the growing period. Foliar temperature yielded higher prediction accuracies as compared to stomatal conductance. Nevertheless, the random forest regression model optimally predicted both indicators throughout maize phenotyping. Specifically:

- The UAV-derived multispectral data and thermal infrared waveband optimally estimated maize temperature during the mid-vegetative stage to an RMSE = 0.59°C and  $R^2 = 0.81$  (RRMSE = 2.9%) based on the thermal infrared, followed by the NIR, NGRBI, EVI and NDVI, in order of importance,
- The multispectral and thermal infrared data optimally predicted stomatal conductance during the early reproductive stage to an RMSE = 25.9 mmol/m<sup>2</sup> and  $R^2 = 0.85$  (RRMSE = 11.5%) based on the red-edge band, followed by the NIR, green, OSAVI and blue band, in order of importance.

Considering the study results, UAV technology is a plausible, flexible, and accurate earth observation technique useful for small-scale farming applications. This is because UAV-derived data provides information at improved spatial resolutions to help smallholder farmers understand their crop dynamics and make informed farm management decisions. Specifically, using multispectral and thermal infrared UAV-data is a step towards attaining an agroclimatic smart, near real-time and high spatial resolution technology for assessing crop water stress through foliar temperature and stomatal conductance. However, the study could have benefitted from higher spectral resolution data and additional measured testing data for improved model performance. Nevertheless, the random forest model performed relatively well at estimating maize leaf temperature and stomatal conductance in the Swayimane area. Therefore, implementing low-cost, near real-time, and evidence-based solutions to smallholder agriculture facilitates improved interventions in these agricultural systems.

## 6 ESTIMATION OF MAIZE LEAF WATER CONTENT USING MACHINE LEARNING TECHNIQUES AND UNMANNED AERIAL VEHICLE (UAV)-BASED PROXIMAL AND REMOTELY SENSED DATA

Ndlovu HS, Odindi J, Sibanda M, Mutanga O, Clulow A, Chimonyo VGP and Mabhaudhi T

### 6.1 Introduction

Crop moisture stress is one of maize crop production's most drastic limiting factors (Avetisyan and Cvetanova, 2019). Maize (*Zea mays L.*) is an important grain crop mostly grown under rain-fed conditions and consumed by most of Southern Africa's population as a staple food (Ngoune Tandzi and Mutengwa, 2020). Due to high population growth and increased food and nutrition insecurities, smallholder farmers now play a critical role in maize production and foster food security, particularly in developing nations such as South Africa (Sibanda, Mutanga et al., 2019; Agbugba, Christian et al., 2020). Despite their key role, smallholder farms constantly face the challenge of intermittent water stress and drought, resulting in significant yield losses (Gomez y Paloma, Riesgo et al., 2020). When stress occurs from the pre-flowering to late grain-filling stages, it is often difficult to detect the onset and magnitude of intermittent water stress (Daryanto, Wang et al., 2016). In addition, spatial and temporal crop management, cultivar selection, soil and topography affect its extent and impacts on maize yield (Daryanto, Wang et al., 2016). As such, there are no clear cut spatially explicit methods of quantifying its water stress near-real-time in smallholder farms of the global south with limited resources. It is therefore imperative to develop optimal methods for quantifying maize water stress in a spatially explicit manner. This provides a key pathway towards effectively monitoring drought impacts and deriving useful information that can be used to inform irrigation decisions.

When maize crops are in a state of moisture deficit, there is a decrease in leaf photosynthesis, stomatal conductance, leaf expansion and transpiration, resulting in impaired growth (Zhang, Zhang et al., 2019). Lack of water molecules results in the loss of turgor-driven cell expansion and primary productivity of maize crops, which has detrimental impacts on its growth (Pasqualotto, Delegido et al., 2018; Chivasa, Mutanga et al., 2020). Crop water deficits result in a decline in the quantity and quality of maize produce (Afzal and Mousavi, 2008) and considerably affect the phenotype, reproductive system and seed set (Afzal and Mousavi, 2008). Strong and positive correlations have been observed between grain yield and leaf water content (Afzal and Mousavi, 2008; Zhang, Zhang et al., 2019). Therefore, knowledge of estimating maize leaf moisture conditions is necessary for crop monitoring and developing early warning systems to optimise agricultural production in exclusively rain-fed smallholder farms (Davidson, Wang et al., 2006; Zhang and Zhou, 2015).

A variety of physiological indicators have been developed to quantify crop moisture stress. They include equivalent water thickness (EWT), fuel moisture content (FMC) and specific leaf area (SLA) (Liu, Peng et al., 2015; Zhang, Pattey et al., 2017; Zhou, Zhou et al., 2020). EWT

is the ratio between a crop's leaf area and the quantity of water per unit area (Yi, Wang et al., 2014). EWT is an improvement of dry matter content as it takes into account the thickness and area covered by the canopy. FMC represents the quantity of water per unit mass of leaf dry matter. It is an effective indicator of moisture stress or drought conditions and is commonly used in wildfire monitoring (Chivasa, Mutanga et al., 2020). SLA is the leaf area ratio per dry mass unit (Gonzalez, Gallardo et al., 2009). SLA is a fundamental indicator of crop physiology and the variability of the crop's photosynthetic capacity and growth rate (Ali, Darvishzadeh et al., 2017). Although various studies have been conducted in monitoring crop water status (Zhang, Zhang et al., 2019; Zhou, Zhou et al., 2020), there is still a disagreement on the best-suited indicator for maize moisture content prediction at a leaf level in small fields.

Several methods have been developed for quantifying maize moisture content indicators (Ustin, Riaño et al., 2012; Zhang, Liu et al., 2018; Xu, Qu et al., 2020). Conventionally, variations in crop moisture status are measured through conventional methods such as visual assessment or in-situ measurements conducted by trained experts (Chivasa, Mutanga et al., 2020). However, such techniques are laborious, costly and comparatively time-consuming, hence not feasible for continuous and time-efficient crop monitoring (Yue, Feng et al., 2018). Over the decades, satellite-borne earth observation technologies have proven to be effective in monitoring plant water status, variations in the physiology of water-stressed vegetation and indicating crop water requirements for improved irrigation efficiency (Sibanda, Onisimo et al., 2021). For instance, Xu, Qu et al. (2020) used multispectral data derived from Landsat-OLI and MODIS datasets to quantify crop moisture content with an optimal  $R^2$  of 0.78. Additionally, Sibanda, Onisimo et al. (2021) utilized Sentinel-2 MSI to estimate canopy water content and FMC to an rRMSE of 20.8% and 18.45%, respectively, while Krishna, Sahoo et al. (2019) used the combination of hyperspectral sensors and partial least squares regression to estimate rice crop moisture stress with an  $R^2$  of 0.94. However, despite these successes, the application of satellite data in characterising moisture indicators at a farm scale is restricted by their relatively coarser spatial and temporal resolutions (Hussain, Gao et al., 2020). Although some sensors provide very-high-resolution (VHR) remotely sensed data, such as QuickBird and Worldview imagery, they are often costly and not ideal for monitoring maize moisture content on smallholder farms (Chivasa, Mutanga et al., 2020).

In recent years, unmanned aerial vehicles (UAVs), known as drones, have received widespread attention in precision agriculture (Maes, Huete et al., 2018). UAVs, mounted with lightweight multispectral sensors capable of providing spatially explicit near real-time information, are valuable for crop physiology monitoring (Hussain, Gao et al., 2020). Additionally, UAV proximal sensors with a sub-meter resolution deliver rapid, cost-effective and accurate measurements required for detecting maize water status at a plot level (Chivasa, Mutanga et al., 2020). Compared with satellite imagery, UAV-based sensors can provide exceptionally high spatial and temporal resolution datasets. In addition, UAV platforms can hover over a specific area of interest. They can acquire imagery at lower altitudes, allowing for a finer ground sampling distance, hence suitable for better quantifying maize moisture content at a field scale (Chivasa, Mutanga et al., 2020). Various studies have utilized UAV-based proximal sensing in environmental applications (Castaldi, Pelosi et al., 2017; Zhang, Basso et al., 2018; Wijewardana, Alsajri et al., 2019). For example, Han, Yang et al. (2019) used a DJI Spreading Wings UAV mounted with an RGB camera to estimate plant height of maize crops and attained an RMSE of 14.1 cm, while Zhang, Basso et al. (2018) utilised a

Phantom 3 UAV-based RGB image to investigate the optimal flight height for discriminating maize varieties.

Additionally, studies have demonstrated the utility of UAV remote sensing approaches in maize yield prediction (Wahab, Hall et al., 2018), maize pest and disease detection (Castaldi, Pelosi et al., 2017) and crop physiology monitoring (Wijewardana, Alsajri et al., 2019). However, these studies were conducted in controlled experimental plots in the global north. Very few studies have been conducted in the global south, particularly in smallholder croplands with rain-fed maize and other crops. As a result, the potential application of UAVs equipped with high-resolution sensors for monitoring crop dynamics, such as maize moisture content, needs to be further investigated, especially in small, fragmented croplands of Southern Africa.

The prediction of maize moisture content using proximal remote sensing approaches is derived from the reflectance behaviour of water molecules and dry vegetation matter in the near-infrared (NIR) and the shortwave infrared (SWIR) sections of the electromagnetic spectrum (Wijewardana, Alsajri et al., 2019). However, many of the available drone sensors widely used in assessing crop moisture content and health have either covered the visible section of the electromagnetic spectrum or included the NIR. Very few of these studies have assessed the utility of drone sensors covering the red edge, NIR and the thermal sections of the electromagnetic spectrum in characterising crop moisture content. Furthermore, a large and growing body of literature has demonstrated the optimal performance of vegetation indices (VIs) derived from water-sensitive sections of the electromagnetic spectrum as an instrument for the retrieval of crop water status (Colombo, Meroni et al., 2008; Pasqualotto, Delegido et al., 2018; Zhang, Zhang et al., 2019). For example, the Normalized Difference Water Index (NDWI), Normalised Difference Vegetation Index (NDVI), Green Chlorophyll Index ( $CI_{green}$ ) and the Red Edge Chlorophyll Index ( $CI_{rededge}$ ) have demonstrated significant correlations to crop moisture indicators (Zhang and Zhou, 2015; Zhang and Zhou, 2019). In this regard, combining the drone-derived red-edge, NIR and thermal bands with optimal vegetation indices was anticipated to yield accurate estimations of maize moisture content in smallholder farms.

Regression techniques have been proposed for predicting vegetation parameters using remotely sensed data. These may be broadly categorised into conventional regression methods and machine-learning techniques (Yue, Feng et al., 2018). However, an example of a conventional regression technique is multiple linear regression (MLR). A major limitation of conventional techniques, such as linear regression (MLR), is that they assume an explicit relationship between measured biophysical parameters and spectral observations, thus limiting their applicability to spatially complex datasets (Lu and He, 2019). Recently, machine learning regression techniques, such as support vector machines (SVM), random forest (RF), artificial neural network (ANN), partial least squares (PLS) and decision trees (DT), have gained popularity for their high-performance in computing, quantifying and understanding complex processes in agricultural applications (Liakos, Busato et al., 2018). Jin, Shi et al. (2017) applied the SVM model to estimate the leaf moisture content of maiden grass and achieved an exceptional model accuracy ( $R^2 = 0.98$ ). Sibanda, Onesimo et al. (2021) implemented the RF ensemble to predict the canopy moisture content of grasslands obtaining an  $R^2$  of 0.98 and RMSE of  $9.8 \text{ gm}^{-2}$ , while Yue, Feng et al. (2018) applied machine learning

techniques, including DT, PLS and ANN in estimating the above-ground biomass of winter wheat. The above studies illustrate machine learning regression ensembles' robustness and prediction capabilities based on remotely sensed data. Although other algorithms have been used in remote sensing applications, a large and growing body of literature shows that SVM, RF, ANN, PLS and DT are the most widely adopted. This is attributed to their ease of implementation, robustness, especially in dealing with small sample sizes, optimal feature selection abilities, and high accuracies they yield. However, the literature indicates that no specific algorithm is suited for a specific context. There is, therefore, a need to assess and identify the most efficient algorithm that could accurately estimate maize foliar moisture content using UAV derived data in the context of smallholder croplands.

Although UAV-based proximal sensing has become a powerful tool for estimating physiochemical variations in vegetation, only a few studies have been conducted on identifying the best method and moisture indicators to evaluate maize crop moisture stress at a farm scale. Therefore, operational and robust regression algorithms must be identified, tested and validated for their performance in predicting smallholder maize functional traits, such as moisture content. This study sought to investigate the potential of UAV-derived multispectral imagery and machine learning techniques in remotely estimating smallholder maize moisture content. The objectives of this study were to conduct a comparative analysis to (1) evaluate the performance of five regression techniques in predicting maize moisture content and (2) determine the most suitable indicator of smallholder maize moisture content. The anticipated results will help provide a technical approach for quickly and accurately monitoring changes in either EWT, FMC or SLA due to moisture variability to inform irrigation decisions and planning of smallholder maize crops.

## **6.2 Materials and Methods**

### **6.2.1 Description of the study area**

This study was conducted at Swayimane (29° 52' S, 30° 69' E), a communal area within the uMshwathi Municipality, north-east of the city of Pietermaritzburg, South Africa (Figure 6-1). Swayimane is situated within the moist midlands mistbelt bioresource area, characterized by an average temperature ranging between 11.8°C and 24°C and a mean annual temperature of 17°C. The climate in the area is relatively hot, with wet, cool summers and dry winters. The area receives an annual rainfall that varies between 600-1100 mm. Swayimane experienced an average air temperature of 23.94°C and an average rainfall of 25 mm during the maize growing season 2020-2021 (Table 6 1). Swayimane is distinguished by arable clay loam soils and is ranked within the top 2% of the high-potential land in South Africa. Subsequently, such environmental conditions support the production of various grain and legume crops.

Common crops produced within the study area are beans, sweet potato, sugarcane, spinach and maize. Swayimane is dominated by smallholder maize farms cultivated by the local community. Maize farmers depend primarily on traditional farming methods such as manual labour and livestock manure for fertilizer. Maize in Swayimane is cultivated at a subsistence scale and for additional income generation. Moreover, Swayimane is a good example of a

rural setup where organic farming is conducted on a semi-subsistence scale. This highlights the success of utilizing organic farming methods for optimizing maize yield at a minimal cost. Plot-level maize growth experiments were conducted in summer, the optimal growing season. The maize plot covered a spatial extent of 250 m<sup>2</sup> and was primarily rain-fed. The maize crop was sown in mid-November 2020. When the project commenced, the crop was 86 days old, termed the reproductive phase of the growth cycle. Specifically, the maize seedlings were intermediate between the kernel blister stage (growth stage R2) and kernel milk stage (growth stage R3). This stage was selected because the literature confirms that the early reproductive stages of maize are highly influenced by moisture and are most sensitive to water deficits (Ghooshchi, Seilsepour et al., 2008; Mi, Cai et al., 2018).

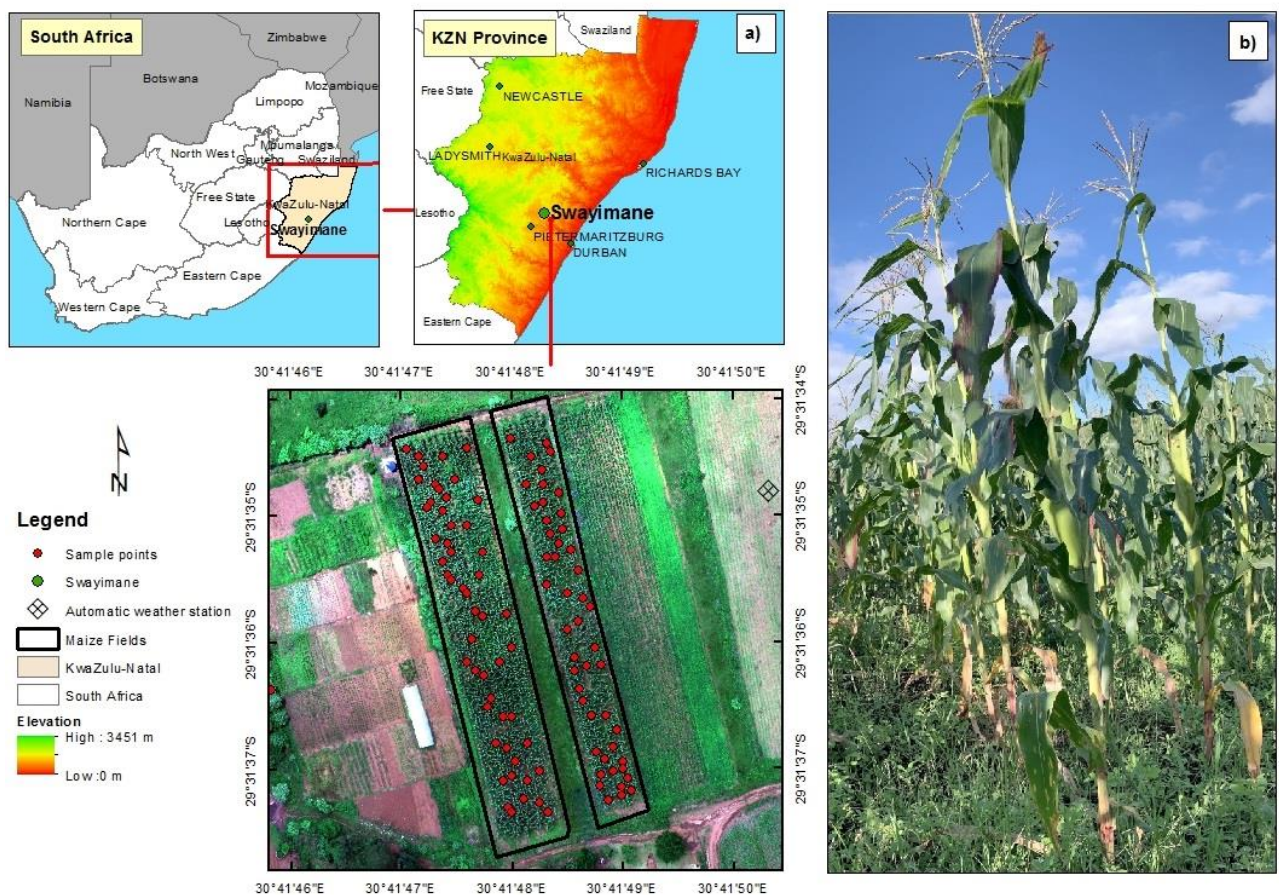


Figure 6-1: (a) Location of the study area and (b) maize crop field in Swayimane, South Africa

Table 6-1: Bioclimatic conditions of Swayimane during the maize growing season

Bioclimatic variable	Data
Total rainfall	25 mm
Average Air temperature	23.94°C
Average wind speed	1.68 m/s
Average vapour pressure	2.55 kPa
Average atmospheric pressure	917.64 mbar

Source: On-site automatic weather station

### 6.2.2 Field Sampling and moisture content measurements

Field data collection was conducted on the 11<sup>th</sup> of February 2021 at the study site. An automatic weather station (AWS) was installed near the maize fields to acquire crop bioclimatic data. The AWS measured air temperature, relative humidity and wind speed. Wind direction sensors and a rain gauge measured the experimental plot's daily wind direction and rainfall. A stratified random sampling approach generated 104 sampling points within the maize field. This technique was selected to provide a representative sample of the study area. A Trimble handheld Global Positioning System (GPS) with a sub-meter accuracy was used to navigate to the randomly generated sample points within the field. Sampling fully developed leaves from the top of the maize canopy ensure reliable measurements of plant physiological characteristics, especially since these leaves receive direct sunlight and have maximum spectral reflectance (Mulla, 2013). Sampling young emerging leaves is unsuitable for plant analysis as it can exacerbate plant stress leading to plant mortality (Wahbi and Avery, 2018; Zhang, Niu et al., 2019). In this regard, the first fully developed leaf (first leaf below whorl) was collected from the top of the maize canopy at each sample point to measure leaf moisture content indicators. An LI-3000C Portable Area Meter combined with an LI-3050C Transparent Belt Conveyer Accessory with one mm<sup>2</sup> resolution was used to measure the leaf area (A) of sampled maize leaves (Li-Cor, USA). The fresh weight (FW) of sampled maize leaves was obtained using a calibrated scale with a 0.5 g measurement error. Field measurements were conducted between 12:00 noon and 14:00 as this is the most optimal period for crop photosynthetic activity (Sade, Galkin et al., 2015). The sampled maize leaves were then dried in an oven at 70° C until a constant dry weight (DW) was reached (approximately 48 hours). The A, FW and DW were then used as input variables to compute maize leaf moisture indicators using the following equations:

$$EWT_{\text{leaf}} (\text{gm}^{-2}) = (\text{FW}-\text{DW}) / A \quad \text{Equation 6-1}$$

$$\text{FMC}_{\text{leaf}} (\%) = (\text{FW}-\text{DW}) / \text{DW} \times 100\% \quad \text{Equation 6-2}$$

$$\text{SLA}_{\text{leaf}} (\text{g}^{-1} \text{m}^2) = A / \text{DW} \quad \text{Equation 6-3}$$

The computed data for each crop moisture indicator was integrated with the GPS location and converted into a point map overlaid with the UAV multispectral images of the study area.

### 6.2.3 Model development and statistical analysis

The UAV imaging platform used in this study measures reflectance in the spectrum's visible, red-edge and NIR regions. Hence we sought to evaluate all possible combinations of UAV spectral bands to accurately predict crop leaf moisture indicators. This study used the reflectance data from the Altum multispectral and thermal bands to derive VIs. Table 6-2 lists VIs selected for this study based on their direct and indirect correlation with plant water status indicators. As aforementioned, the prepared spectral data were then overlaid with the point data associated with measured maize moisture indicators to derive data used for the statistical prediction of maize moisture content.

Table 6-2: List of vegetation indices (VIs) used in the modelling of crop moisture content and related source references

Index	Full Name	Formula	Reference
<b>Direct water-sensitive spectral VI</b>			
NDWI	Normalised Difference Water Index	$\frac{\text{Green} - \text{NIR}}{\text{Green} + \text{NIR}}$	(Ozelkan, 2020)
<b>Indirect water-sensitive spectral VIs</b>			
NDVI	Normalized Difference Vegetation Index	$\frac{\text{NIR} - \text{Red}}{\text{NIR} + \text{Red}}$	(Ali, Darvishzadeh et al., 2017)
NGRDI	Normalized Difference Green/Red Index	$\frac{\text{Green} - \text{Red}}{\text{Green} + \text{Red}}$	(Hoffmann, Jensen et al., 2016)
NDRE	Normalized Difference Red-Edge Index	$\frac{\text{NIR} - \text{Rededge}}{\text{NIR} + \text{Rededge}}$	(Zhang and Zhou, 2019)
$\text{NDVI}_{\text{rededge}}$	Red-Edge Normalised Difference Vegetation Index	$\frac{\text{Rededge} - \text{Red}}{\text{Rededge} + \text{red}}$	(Zhang and Zhou, 2019)
$\text{CI}_{\text{green}}$	Green Chlorophyll Index	$(\text{NIR}/\text{Green}) - 1$	(Zhang and Zhou, 2015)
$\text{CI}_{\text{rededge}}$	Red-edge chlorophyll index	$(\text{NIR}/\text{Rededge}) - 1$	(Zhang and Zhou, 2019)

### 6.2.4 Spatial analysis

The sampled data were randomly split into training (70%) and validation data (30%). The former was used to develop the model, and the latter for assessing the accuracy of predictive models. A comparative analysis was conducted between the support vector regression, random forest regression, decision trees regression, artificial neural network regression and the partial least squares regression algorithms in predicting leaf moisture content indicators (i.e. EWT, FMC and SLA). According to Lary, Alavi et al. (2016), RF SVM, DT, ANN, and PLS are geosciences' most widely used machine learning algorithms. These non-parametric algorithms are robust, efficient, and can be parameterised and implemented easily (Liakos,

Busato et al., 2018; Yue, Feng et al., 2018). Above all, these algorithms have been used in literature and are renowned for their accuracy, facilitated by their ability to optimally select spectral features for accurate predictions (Lary, Alavi et al., 2016; Wang and Singh, 2017). It is in this regard that these algorithms were chosen for this study. Then, the variable selection was performed for each prediction model to identify the most influential variables in the prediction of the named indicators. Variable selection reduces issues associated with variable redundancy and multicollinearity, affecting regression model performance (Chivasa, Mutanga et al., 2021). Details on how each algorithm was used in this study are provided below.

**Support vector regression (SVR):** initially developed for classification problems, it has proven to be an effective tool in regression problems (Wang, Cherkauer et al., 2016). As an intensive supervised learning technique, SVR is less sensitive to noisy inputs; thus, minimal estimation errors make the model more robust (Fan, Zheng et al., 2021). The greatest advantage of SVR is its robustness to outliers and capacity to perform well in high-dimensional datasets. Selecting the optimal hyperparameter settings of SVR is critical for optimising the model's predictive power (Bae, Han et al., 2019). Three parameters were tuned for the SVR model, specifically, penalty parameter ( $C$ ), precision parameter ( $\epsilon$ ) and kernel parameter ( $\gamma$ ). In this study, the grid search and 10-fold cross-validation method, recommended by Shafiee, Lied et al. (2021), was performed on the training data and the SVR model was performed optimally at a  $C$  value of 8,  $\epsilon$  equal to 0.5, and the  $\gamma$  kept at a default of 1.

**Random forest regression (RFR):** is a machine learning ensemble that uses bootstrap aggregation and binary recursive partitioning to grow several independent regression trees (Abdel-Rahman, Ahmed et al., 2013). The strength of RFR lies in its ability to use bootstrap aggregation to build regression trees that are grown to their maximum sizes, with the results being combined by unweighted averaging to make predictions (Jeong, Resop et al., 2016). The RFR algorithm is renowned for producing high prediction accuracies and is easy and simple to implement (Sibanda, Onisimo et al., 2021). The quality of the RFR model depends on the proper setting of the RFR hyperparameters. The RFR model is generally optimized based on two parameters, namely *Ntree*, which is the number of decision trees to be generated and *Mtry*, the number of predictor variables tested for the best split when growing the trees (Belgiu and Dragut, 2016). To determine the *Ntree* and *Mtry* values that best predict maize leaf moisture content, the *Ntree* (the default value is 500 trees) values were tested from 500 to 9500. In contrast, *Mtry* was tested from 1 to 25 using a single interval (Adam, Mutanga et al., 2012; Mutanga, Adam et al., 2012). The optimal hyperparameter values for predicting maize moisture content in the study were *Ntree* equal to 500 and a *Mtry* of 11.

**Decision tree regression (DTR):** uses tree structures to build a regression model based on the structural patterns of the input data (Liang, Di et al., 2018). The DTR formally creates decision rules that guide the prediction of the relationship between the objective and predictor variables. The greatest advantage of the DTR model is its ability to avoid over-fitting, overcome missing data in explanatory and response variables and simple implementation (Pekel, 2020). In DTR, the hyperparameters were tuned using a pre-pruning technique, which stops the generation of a tree before it is fully constructed, to achieve optimal model performance (Bae, Han et al., 2019; Furuya, Aguiar et al., 2020). In this study, the fine-tuning process of the DTR algorithm was performed until no improvements were observed, and the model parameters were specified as follows; the minimum split, which is the minimum number

of values that must exist at a node before the split is attempted (Furuya, Aguiar et al., 2020), was fixed at 20 (Williams, 2011). The maximum depth at which the tree is allowed to grow was set to 30. Finally, the termination criteria for the regression tree was specified at 0.01 (Losing, Wersing et al., 2018). The hyperparameters of the DTR parameters are kept to their default values, except for the maximum depth, which is a fixed parameter for all the models (Williams 2011; Hu, Siala et al., 2020).

**Artificial neural network (ANNR):** has been widely applied in developing regression models. The quality of the ANNR model depends largely on the selection of the network structure, proper assignment of weights, and the training dataset of the model (Wang, Cherkauer et al., 2016). The robustness of the ANNR is derived from the algorithm's ability to imitate the human neural system, allowing it to detect complex trends and patterns often unnoticed by other regression models (Yuan et al., 2017). Furthermore, the ANNR entails one or more hidden layers, in addition to the input and output layers, and discovers prominent features in the input data (Yeganefar, Niknam et al., 2019). As such, the hyperparameters of the optimal ANN model were determined to be ten nodes and two hidden layers.

**Partial least squares regression (PLSR):** is a multivariate statistical technique characterised by robust information recognition and modelling capabilities (Yue, Feng et al., 2018). The algorithm combines the theory of multiple linear regression with the principal component analysis theory to effectively analyse the datasets with high dimensional and collinear predictors (Zhang, Liu et al., 2018). The PLSR is renowned as a powerful modelling technique, particularly in models with a large number of predictor variables and a high level of collinearity (Li, Zhang et al., 2014).

To optimize the outputs of the above models, the variable importance scores were used to determine the most influential bands and indices for estimating leaf moisture content indicators (Ambrosone, Matese et al., 2020). The least important predictor variables were progressively removed, and the model was re-developed (Ambrosone, Matese et al., 2020; Bois, Pauthier et al., 2020). The Caret Package was used to develop the regression models in RStudio software version 1.4.1564.

### **6.2.5 Accuracy assessment of derived maize moisture content models**

An accuracy assessment was conducted to evaluate the performance of regression models in predicting leaf moisture content indicators. The coefficient of determination ( $R^2$ ), the root mean square error (RMSE) and the relative root mean square error (rRMSE) were used to compare the accuracy of different models. Specifically, the  $R^2$  was used to measure the variation between measured and predicted maize leaf moisture content. RMSE was used to assess the magnitude of error between the field measurements and the modelled moisture content. The rRMSE was used to compare the performance of regression models across different algorithms and maize moisture indicators. To compute rRMSE, the RMSEs from each model were normalised using the mean of each variable and then expressed as a percentage (Li, Yang et al., 2021). The rRMSE has been widely used in literature to compare different variable predictions (Wocher, Berger et al., 2018; Sibanda, Onisimo et al., 2021); hence it was adopted in this study. The optimal model for predicting leaf moisture content indicators was characterised by lower RMSE and RRMSE and a high  $R^2$  value. Additionally, the most suitable

indicator of maize moisture content was estimated by comparing the  $R^2$ , RMSE and RRMSE. Similarly, the indicator that produces the highest  $R^2$  and the lowest RMSE and RRMSE will indicate a higher precision and accuracy in predicting maize moisture content.

## 6.3 Results

### 6.3.1 Descriptive analysis of maize crop moisture indicators and measured biophysical variables

A wide range of variations was recorded in both biophysical variables and crop moisture indicators of maize crops. Table 6-3 represents the descriptive statistics of leaf FW, DW, Leaf area, EWT, FMC, and SLA. Averages for FW, DW, and Leaf area were 37.06 g, 6.94 g and 0.09 m<sup>2</sup>, correspondingly, while the averages for crop moisture indicators, particularly EWT<sub>leaf</sub>, FMC<sub>leaf</sub> and SLA<sub>leaf</sub> were 356.52 gm<sup>-2</sup>, 81.27%, 29.86 gm<sup>-2</sup> and 0.01 m<sup>2</sup>g<sup>-1</sup>, respectively. A Kolmogorov-Smirnov normality test revealed that all crop moisture indicators did not deviate significantly from the normal distribution curve.

Table 6-3: Descriptive statistics of crop moisture indicators and biophysical variables

Parameter	Range (min-max)	Mean	Median	Std.	CV%	SEM*
<b>Biophysical variables</b>						
FW (g)	31.02-45.52	37.06	36.73	3.82	10.31	0.53
DW (g)	3.22-8.76	6.94	6.95	1.02	14.69	0.14
Leaf area (m <sup>2</sup> )	0.06-0.10	0.09	0.09	0.01	10.53	0.00
<b>Crop water indicators</b>						
EWT <sub>leaf</sub> (gm <sup>-2</sup> )	290.91-473.18	356.52	344.14	42.42	11.90	5.88
FMC <sub>leaf</sub> (%)	77.84-91.39	81.27	81.24	1.89	2.33	0.26
SLA <sub>leaf</sub> (m <sup>2</sup> g <sup>-1</sup> )	0.0009-0.025	0.01	0.01	0.00	18.16	0.00

\*SEM is the standard error of the mean, Std. is the standard deviation, and CV is the coefficient of variation

### 6.3.2 Evaluation of maize moisture indicators and optimized regression models

Table 6-4 illustrates the model accuracies in predicting leaf EWT, FMC and SLA based on the RFR, DTR, ANNR, PLSR and SVR regression techniques. The accuracies of the prediction models varied greatly for the crop moisture indicators.

For example, when estimating  $EWT_{leaf}$ , the DTR yielded the poorest model accuracy, with an RMSE of  $25.16 \text{ gm}^{-2}$  and  $R^2$  of 0.73. The accuracy in predicting  $EWT_{leaf}$  improved slightly for the PLSR model (RMSE =  $17.1 \text{ gm}^{-2}$  and  $R^2 = 0.74$ ). Similarly, the SVR and the ANNR models predicted  $EWT_{leaf}$  at an improved accuracy of RMSE =  $15.05 \text{ gm}^{-2}$ ,  $R = 0.76$  and RMSE =  $14.29 \text{ gm}^{-2}$ ,  $R^2 = 0.84$ , respectively. The optimal algorithm for estimating  $EWT_{leaf}$  was derived from the RFR model with an RMSE of  $10.28 \text{ gm}^{-2}$  and  $R^2$  of 0.89 (Table 6-4).

Similarly, the ANNR model exhibited the lowest prediction accuracy in estimating  $FMC_{leaf}$  (RMSE = 1.54% and  $R^2 = 0.34$ ). The PLSR followed this with an RMSE of 0.48% and  $R^2$  of 0.45. The prediction accuracy increased significantly with the DTR and the SVR models with a corresponding  $R^2 = 0.65$  and  $R^2 = 0.69$ . The RFR model optimally predicted  $FMC_{leaf}$  with the highest model accuracy of RMSE = 0.45% and  $R^2 = 0.76$  (Table 6 4).

When predicting  $SLA_{leaf}$ , the lowest RMSE of  $0.0008 \text{ g}^{-1} \text{ m}^2$  and  $R^2$  of 0.6 was obtained using the PLSR model. The ANNR model improved the prediction by a magnitude of 8, i.e.  $R^2 = 0.68$ . The accuracy derived from the DTR and SVR in predicting SLA differed slightly with an RMSE =  $0.0009 \text{ m}^2 \text{ g}^{-1}$  and  $R^2 = 0.7$ , and RMSE =  $0.0005 \text{ g}^{-1} \text{ m}^2$  and  $R^2 = 0.71$ . The optimal model for estimating  $SLA_{leaf}$  exhibited an RMSE of  $0.0004 \text{ g}^{-1} \text{ m}^2$  and  $R^2$  of 0.73 (Table).

Table 6-4: Prediction accuracies of  $EWT_{leaf}$ ,  $FMC_{leaf}$  and  $SLA_{leaf}$  were derived using optimal models based on the RFR, DTR, ANNR, PLSR and SVR regression models

Model	$EWT_{leaf} \text{ (gm}^{-2}\text{)}$			$FMC_{leaf} \text{ (%)}$			$SLA_{leaf} \text{ (m}^2 \text{ g}^{-1}\text{)}$		
	$R^2$	RMSE	RRMSE	$R^2$	RMSE	RRMSE	$R^2$	RMSE	RRMSE
RFR	0.89	1028	3.13	0.76	0.45	1.00	0.73	0.0004	3.48
DTR	0.73	25.16	7.67	0.65	1.08	1.35	0.7	0.0009	8.16
ANNR	0.84	14.29	4.35	0,34	1.54	1.92	0.68	0.0007	6.60
PLSR	0.74	17.1	5.15	0.45	0.48	0.60	0.6	0.0008	19.33
SVR	0.78	15.05	4.76	0.69	0.70	0.89	0.71	0.0005	18.82

### 6.3.3 Optimal models for estimating maize moisture content indicators

Figure 6-2 illustrates the results obtained when all maize moisture content indicators were estimated based on the optimal regression models. The  $EWT_{leaf}$  performed optimally to indicate maize moisture content with an rRMSE of 3.13% and an  $R^2$  of 0.89. The most optimal

variables selected in estimating  $EWT_{leaf}$  were NDVI, NIR, NDWI,  $CI_{green}$ ,  $NDVI_{rededge}$ , Red,  $CI_{rededge}$ , NDRE and NGRDI, in order of importance (Figure 6 2 (a)).

Meanwhile, the  $FMC_{leaf}$  based on the PLSR model performed better than the  $EWT_{leaf}$  by 2.53% with an rRMSE of 0.6%. The most suitable predictor variables included NDRE, NIR, NDWI,  $CI_{rededge}$ ,  $NDVI_{rededge}$ , red-edge,  $CI_{green}$ , blue, thermal, NDVI, red and the green band (Figure 6-2 (b)). Additionally, the  $FMC_{leaf}$  SVR model produced a relatively high rRMSE of 0.89%. However, although the rRMSE of these  $FMC_{leaf}$  models was high, there was a high variation between the measured and estimated  $FMC_{leaf}$  values, with an  $R^2$  of 0.45 and 0.69, respectively. In comparison, the  $FMC_{leaf}$  based on the RFR model exhibited an optimally high  $R^2$  of 0.76 and an acceptable rRMSE of 1%, making it the optimal  $FMC_{leaf}$  model.

The optimal model in predicting maize  $SLA_{leaf}$  exhibited an rRMSE of 3.48% and  $R^2 = 0.73$ . The variables with the highest influence in the SLA model were the NDVI, Thermal, NIR, NDRE,  $CI_{green}$ , red-edge,  $NDVI_{rededge}$ ,  $CI_{rededge}$ , NGRDI and the NDWI, in order of descending importance (Figure 6 2 (c)).

The results revealed that the optimal indicators of maize moisture content based on the RFR models were  $FMC_{leaf}$  and  $EWT_{leaf}$ , followed by  $SLA_{leaf}$ . Additionally, the UAV multispectral bands and derived VIs successfully predicted all maize moisture content indicators.

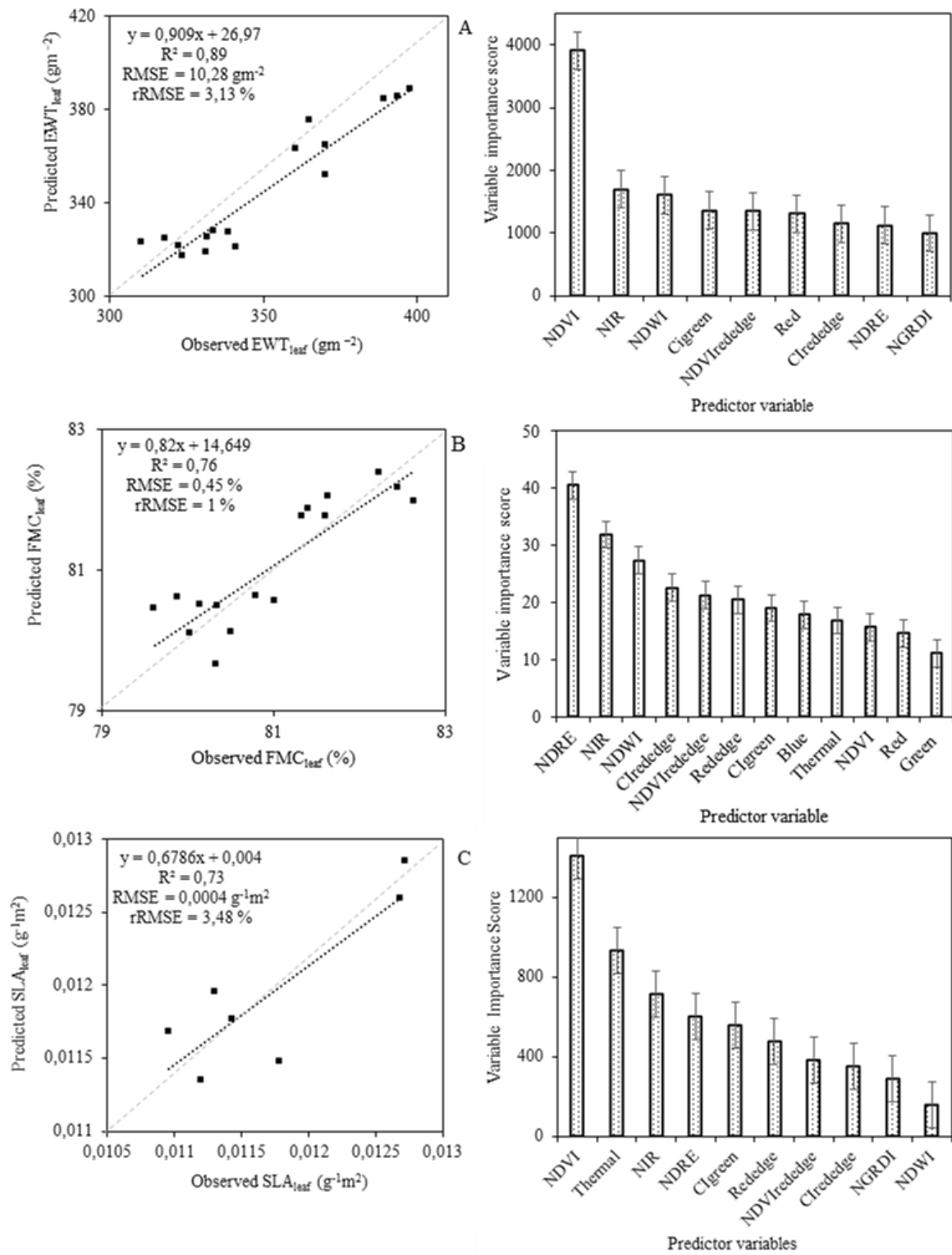


Figure 6-2: Relationship between the predicted and observed (a)  $EWT_{leaf}$ , (b)  $FMC_{leaf}$  and (c)  $SLA_{leaf}$  of maize derived using optimal predictor variables and the model variable importance scores

### 6.3.4 Mapping the spatial distribution of maize leaf moisture content indicators

The spatial distribution of leaf EWT, FMC, and SLA was estimated based on the optimal models. Figure 6-3 illustrates the spatial distribution of maize moisture content indicators. It can be observed that the moisture content of maize is relatively high throughout maize fields and seem to decrease towards the edge of the maize plot, with the exception of the FMC, which revealed small patches of lower maize moisture content within maize fields.

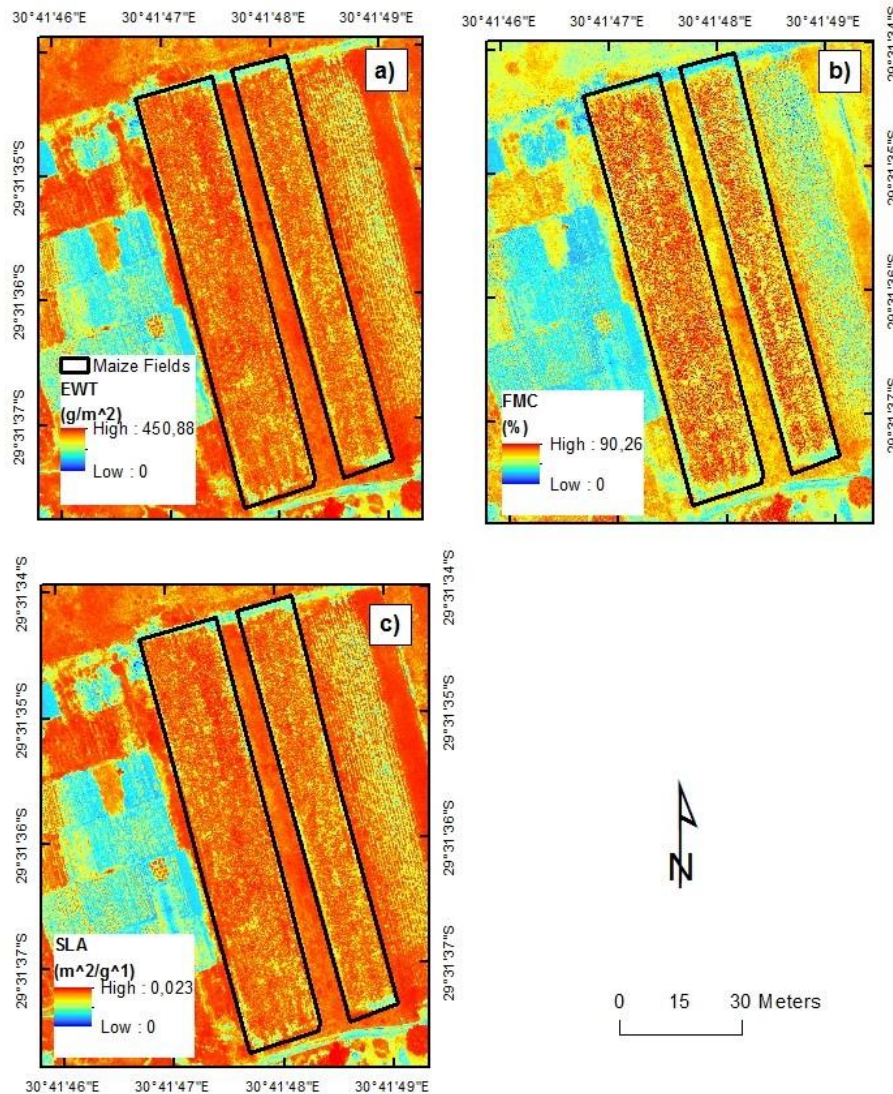


Figure 6-3: Spatial distribution of (a) EWT<sub>leaf</sub>, (b) FMC<sub>leaf</sub>, and (c) SLA<sub>leaf</sub> of smallholder maize crops

### 6.4 Discussion

Smallholder farmers frequently need to optimize maize production; therefore, assessing maize water status through monitoring EWT, FMC and SLA could provide essential information for improving crop water use efficiency and enhancing maize productivity under water-limited conditions (EI-Hendawy, Al-Suhaibani et al., 2019). The essence of this study was to assess

and identify a suitable indicator for maize moisture content and evaluate the predictive performance of robust algorithms in predicting maize moisture status. Thus, this study sought to investigate using UAV-derived remotely sensed data and machine learning techniques in estimating maize EWT, FMC and SLA.

#### 6.4.1 Estimating maize moisture content indicators

Results in this study indicate that when estimating maize equivalent water thickness, an optimal estimation accuracy ( $rRMSE = 3.13\%$  and  $R^2 = 0.89$ ) can be obtained based on spectral variables derived from the NIR section of the electromagnetic spectrum (NDVI, NIR, NDWI, and NDRE). Literature confirms that the quantity of water in crop leaves is statistically correlated with leaf reflectance across the spectrum (Mobasheri and Fatemi 2013; El-Hendawy, Al-Suhaibani et al., 2019; Wijewardana, Alsajri et al., 2019). Specifically, the variation in water molecules present in the leaf cell strongly reflects solar radiation in the NIR region. Hence, this section of the spectrum is commonly used to quantify leaf water status (Pasqualotto, Delegido et al., 2018; El-Hendawy, Al-Suhaibani et al., 2019). Leaves which are characterised by high moisture status reflect highly in the NIR region due to multiple scattering within the leaf cell, which is primarily controlled by leaf cuticles, mesophyll thickness and intercellular air spaces and is directly linked to leaf moisture content (Romero-Trigueros, Nortes et al., 2017; Sibanda, Onisimo et al., 2021).

Furthermore, the NIR section has been widely proven to be related to the leaf water absorption zone, hence its optimal influence in estimating the leaf EWT of maize in smallholder farms. Correspondingly, studies by Mobasheri and Fatemi (2013) and Riaño, Vaughan et al. (2005) successfully illustrated the use of leaf optical reflectance in the NIR section of the electromagnetic spectrum in optimally predicting EWT with an  $R^2$  of 0.95 and 0.75, respectively. EWT also displayed high sensitivity to chlorophyll-based indices, especially  $CI_{green}$  and  $CI_{rededge}$ . This could be explained by the fact that changes in the level of chlorophyll in leaves, which alters crop greenness and leaf pigmentation, are closely related to water status (Jurdao, Yebra et al., 2013; Zhang and Zhou, 2015). As in this study, Zhang and Zhou (2019) noted that these chlorophyll-based indices presented a higher sensitivity to crop water indicators.

Fuel moisture content (FMC) was optimally predicted to a model accuracy of  $rRMSE$  of 1% and  $R^2 = 0.76$ . The results of this study show that FMC is particularly sensitive to the red-edge waveband and associated derivatives of these spectral channels. For instance, there was a significant influence of the red-edge, NDRE,  $NDVI_{rededge}$  and  $CI_{rededge}$  in the prediction of maize FMC. Such sensitivity of the red-edge band in predicting FMC can be explained by its positive association with crop biomass and chlorophyll content, which is also positively correlated with FMC (Sibanda, Onisimo et al., 2021). Generally, the variations in crop moisture content are largely associated with chlorophyll activity and leaf area index, which influence the reflectance of leaf tissue in the red-edge section of the electromagnetic spectrum (García, Chuvieco et al., 2008). This was the case in studies by Bar-Massada and Sviri (2020) and Cao and Wang (2017) that confirmed a variation in the reflectance of green leaves under water-stressed conditions in the red-edge band, making this wavelength a significant predictor of FMC.

Furthermore, NDWI, which is primarily derived from the NIR band, has a significant influence on the prediction of FMC. This VI is particularly important in predicting moisture content as it is sensitive to the variations of leaf reflectance induced by water molecules and dry matter content, hence, strongly correlates to plant water stress (Zhang and Zhou, 2015). A study by Sow, Mbow et al. (2013) demonstrated the importance of the NDWI in predicting FMC by achieving an  $R^2$  of 0.85. In this regard, the literature supports the relationship between FMC and the red-edge and the NIR sections of the electromagnetic spectrum (García, Chuvieco et al., 2008; Sibanda, Onesimo et al., 2021).

Finally, the results of this study show that SLA could be estimated to have an rRMSE of 3.48%.  $R^2$  of 0.73 and SLA were particularly sensitive to the UAV-derived thermal, NIR and red-edge wavelengths. When crops are in a state of water deficit, there is an overall increase in crop surface temperature due to the closure of leaf stoma, which decreases the evaporation cooling effect (Gerhards, Schlerf et al., 2019). The literature notes that the thermal band has been well-established as a key wavelength for early plant moisture stress detection (Mangus, Sharda et al., 2016; Gerhards, Schlerf et al., 2019). Again, NDVI was this study's most influential predictor of maize SLA. This could be explained by the fact that NDVI is proportional to chlorophyll content which is sensitive to changes in crop moisture content (Wang, Cherkauer et al., 2016).

Furthermore, when crops are water-stressed, there is a decrease in chlorophyll absorption at the red wavelength and a decrease in reflectance at the NIR region due to the shrinkage of leaf thickness during the wilting process (Lim, Watanabe et al., 2020). In a similar study, Ali, Darvishzadeh et al. (2017) noted that NDVI was very effective in optimally estimating SLA ( $R^2 = 0.73$  and  $RMSE = 4.68\%$ ). Wijewardana, Alsajri et al. (2019) confirmed that the combination of both the NIR and red wavelengths allows NDVI to be an invaluable predictor of photosynthetic activity and long-term water stress. Also, SLA was sensitive to the NDRE, NDVIrededge, and chlorophyll-based VIs. The influence of these red-edge-based VIs in predicting SLA stems from the fact that the variations in leaf thickness and area and leaf pigmentation due to moisture stress are promptly detected at the red-edge section (Easterday, Kislik et al., 2019). In this regard, the leaf photosynthetic capacity variations provide essential information about maize leaf water vapour and moisture content (Ali, Darvishzadeh et al., 2017).

Furthermore, results illustrate that all maize leaf moisture content indicators were optimally predicted using UAV-derived data. Accordingly, FMC and EWT yielded the highest predictive power of moisture content, while SLA was effectively estimated. The FMC and EWT are the ideal crop water indicators for monitoring moisture stress using field spectroscopy techniques (Yi, Wang et al., 2014; Liu, Peng et al., 2015).

#### **6.4.2 The performance of machine learning algorithms in predicting maize moisture content indicators**

Results in this study show that the RFR approach is the most suitable explorative tool to predict all maize moisture content indicators. For instance, RFR optimally predicted FMC, EWT and SLA, producing the highest prediction accuracy (rRMSE = 1%, 3.13% and 3.48%). The RFR algorithm can effectively establish the relationship between leaf reflectance and maize

moisture at a farm scale. The strength of RFR could be explained by the fact that the algorithm is not highly affected by noise in the data. Hence there is a reduced risk of producing overfitting models (Abdel-Rahman, Ahmed et al., 2013; Zhu, Liu et al., 2017). In a similar study, Sibanda, Onesimo et al. (2021) confirmed the robustness of the RFR model in modelling moisture content elements, particularly FMC, by achieving optimal  $R^2$ s as high as 1 and an RMSE of 16.4%.

The SVR approach was also optimal in predicting maize leaf EWT, FMC and SLA. The strength of the SVR lies in its ability to circumvent outliers and exhibit a high generalization capacity to handle unseen patterns (Liang, Di et al., 2018). The results of this study reveal that the SVR is similar to the RFR in predictive power. This could be explained by the fact that the SVR and RFR ensembles optimally operate with a relatively small number of training samples, which is often the case for data acquired at a field scale after avoiding spatial autocorrelation (Wang, Cherkauer et al., 2016; Zhu, Liu et al., 2017). Research has indicated that the presence of spatial autocorrelation, defined as the systematic spatial variation of the mapped variable, could result in biased and statistically invalid results (Zhu, Liu et al., 2017; Liang, Di et al., 2018; Sinha, Gaughan et al., 2019). Therefore, the results of this study demonstrate that the model properties of RFR and SVR are well-suited for the estimation of smallholder maize moisture content. Generally, DTR did not perform well in predicting maize moisture indicators. This could be explained by the fact that DTR does not have features such as the bootstrapping in RFR and hyperplanes in SVR for effectively encompassing all the samples during the prediction procedure (Liang, Di et al., 2018). This can result in the DTR algorithm being conservative in its prediction procedure, exhibiting lower prediction accuracies. In this regard, very few studies have evaluated its predictive performance in the context of canopy and leaf moisture content.

In comparison, the ANN and PLSR had poorer performance predicting maize moisture content. This could be because the ANN and PLSR are best suited for a large training dataset to produce credible results (Wang, Cherkauer et al., 2016; Yuan, Yang et al., 2017). As such, this study prompts future studies to investigate the optimal sample size required to produce accurate predictions of smallholder maize moisture content when using a combination of UAV imagery and machine learning techniques. Additionally, there are prospects to evaluate the ability of other empirical models and deep learning methods in accurately modelling maize water variability.

## 6.5 Conclusion

The present study tested the utility of UAV-based multispectral data in a comparative approach of estimating moisture content using RFR, SVR, DTR, ANNR and PLSR machine learning techniques and EWT, FMC and SLA of maize crops in smallholder farms. Based on the findings of the study, it can be concluded that:

- EWT, FMC and SLA moisture content indicators of maize could be optimally predicted using NIR and red-edge derived spectral variables

- The RFR and SVR modelling techniques have a more robust capacity to predict moisture content indicators of maize in comparison to the DTR, ANNR and PLSR
- FMC and EWT, in concert with the RFR approach, exhibited the highest predictive performance, therefore, are valid indicators of maize moisture content

This study demonstrates that UAV-derived multispectral data can predict maize moisture variations of smallholder farms with exceptional accuracy, hence can complement and inform farms of drought-related water stress. However, there are research gaps that demand further inquiry, particularly on smallholder maize farms. Future studies should evaluate the utility of UAV-derived data and the optimal moisture indicators in characterising the variation of maize moisture content across different phenological stages. Furthermore, a key limitation of this study is the lack of the SWIR spectrum, which would be valuable as it is an essential water absorption band. Therefore, additional studies are necessary to evaluate whether UAV sensors that measure spectral reflectance along the SWIR section of the electromagnetic spectrum improve smallholder maize moisture content prediction. Finally, this study was site and crop-specific. Therefore, studies conducted across various climates, different smallholder crops and at a multi-temporal scale should be assessed to draw broad conclusions in characterising crop moisture stress.

## **7 A MULTITEMPORAL ESTIMATION OF MAIZE LEAF EQUIVALENT WATER THICKNESS AND FUEL MOISTURE CONTENT VARIABILITY USING UNMANNED AERIAL VEHICLE (UAV) DERIVED MULTISPECTRAL DATA AS A PROXY TO MOISTURE STRESS**

Ndlovu HS, Odindi J, Sibanda M, Mutanga O, Clulow A, Chimonyo VGP and Mabhaudhi T

### **7.1 Introduction**

Maize (*Zea mays L.*) is an important and eminent food security crop that is a valuable source of animal fodder, bio-energy and raw industrial material (Ge, Sui et al., 2012; Sah, Chakraborty et al., 2020). However, due to rainfall scarcity and variability, maize moisture stress is a serious abiotic threat to maize production (Ge, Sui et al., 2012; Ndlovu, Odindi et al., 2021). Literature shows that maize is commonly grown in regions that receive annual average precipitation of 300-500 mm, which is below the critical level of water supply for achieving a good maize yield (Sah, Chakraborty et al., 2020). This is a serious concern, particularly in Southern Africa, a water-scarce region that only receives an average and seasonal precipitation of 450 mm per annum (DAFF, 2017; Nembilwi, Chikoore et al., 2021). Despite a semi-arid climate, more than 85% of Southern Africa's smallholder maize farms are rain-fed (Ngoune Tandzi and Mutengwa, 2020). According to Sah, Chakraborty et al. (2020), climatic conditions, specifically seasonal rainfall variability, are a significant limiting factor of maize moisture status, ultimately regulating maize production. Therefore, there is a need for innovative and sustainable approaches to monitoring maize moisture status throughout the growing season for developing early detection and warning systems of moisture stress for the adoption of relevant mitigation measures.

Maize moisture stress results in numerous physiological and biochemical changes, including a reduction in crop metabolism, increased stomatal closure and decreased dry matter production and leaf area (Song, Jin et al., 2019; Zhang, Zhang et al. Subsequently, water deficit negatively impacts maize productivity, impairs crop growth and development, significantly reducing yield (Ghooshchi, Seilsepour et al., 2008; Ge, Sui et al., 2012). A study by Ge, Sui et al. (2012) and Avetisyan and Cvetanova (2019) noted that crop water status varies with crop development stages as well as the response of environmental conditions, metabolic activity and hydraulic adaptations (Okunlola, Olatunji et al., 2017). Ghooshchi, Seilsepour et al. (2008) indicated that the maize tasselling and silking growth stages are most sensitive to impacts of moisture variability, while Sah, Chakraborty et al. (2020) noted that the earlier phenological stages of maize are less subjected to water stress due to favourable climatic conditions. Therefore, the quantitative assessment of maize moisture content throughout the growth cycle offers valuable knowledge of maize growth and development and is a key pathway towards developing adaptive strategies for increasing smallholder maize resilience to water stress.

The most widely used physiological indicators of maize moisture content are equivalent water thickness (EWT) and fuel moisture content (FMC) (Mobasher and Fatemi, 2013; Yi, Wang et al., 2014; Elsherif, Gaulton et al., 2019; Ndlovu, Odindi et al., 2021). EWT is a leaf water status metric defined as the ratio between the quantity of water and leaf area (Niinemets, 2001; Elsherif, Gaulton et al., 2019). Zhang and Zhou (2019) stated that EWT is closely associated with plant biochemical processes such as photosynthesis, plant metabolism and crop evapotranspiration. Hence it is a suitable indicator of moisture stress. FMC is defined as the proportion of water to dry matter (Matthews, 2013; Yi, Wang et al., 2014) and has been widely used for plant water stress, drought monitoring and as a measure of ignition and fire propagation potential (Yi, Wang et al., 2014; Ndlovu, Odindi et al., 2021; Sibanda, Onesimo et al., 2021). A study by Ndlovu, Odindi et al. (2021) confirms that EWT and FMC are valuable indicators of the maize water content of smallholder farming systems. These indicators demonstrated the highest correlation with spectral data. Therefore, quantifying maize leaf EWT and FMC can provide valuable information for the early detection of maize moisture stress and monitoring of maize physiology throughout the growth period to inform small-scale agricultural decision making.

Conventionally, maize EWT and FMC variations relied on direct measurements and the visual assessment of maize physiology conducted by trained experts (Chivasa, Mutanga et al., 2020). However, these methods are extremely time-consuming, tedious, subject to human error and cannot sufficiently reflect spatial and temporal variability in maize moisture status (Zhang, Zhou et al., 2012; Mobasher and Fatemi 2013; Jin, Shi et al., 2017). Furthermore, field data collection requires continuous measurements throughout the maize growth cycle, making implementation marginally feasible (Yue, Feng et al., 2018; Chivasa, Mutanga et al., 2020). Meanwhile, a large body of literature has explored the potential of satellite remote sensing techniques in quantifying crop productivity, health and water status (Pasqualotto, Delegido et al., 2018; El-Hendawy, Al-Suhaibani et al., 2019; Krishna, Sahoo et al., 2019). For example, a study by Kamali and Nazari (2018) estimated maize water requirement using Landsat-8 data to an rRMSE of 0.73 mm/day, while Ambrosone, Matese et al. (2020) quantified soil moisture content of rain-fed and irrigated fields using Sentinel-2 multispectral imagery and achieved an optimal  $R^2$  of 0.80 and RMSE of  $0.06 \text{ cm}^3\text{cm}^{-3}$ . However, multispectral satellite sensors are restricted in their ability to accurately monitor variations in maize moisture content throughout the growing season as they are limited by coarse spatial resolution and a longer revisit time for plot-level maize observations (Krishna, Sahoo et al., 2019; Chivasa, Mutanga et al., 2020). On the contrary, high-resolution multispectral sensors such as WorldView and new-generation hyperspectral datasets such as QuickBird provide viable options for continuous water stress detection of maize crops at the field scale (Chemura, Mutanga et al., 2017; Easterday, Kislik et al., 2019). Nonetheless, these datasets are limited by the high image acquisition cost and operational complexity for application in smallholder maize crops (Chivasa, Mutanga et al., 2020). Consequently, there is a need for methods that can provide spatially explicit datasets with a high temporal resolution to monitor changes in smallholder maize leaf moisture content throughout the growth period.

Recent technological advances, particularly the Unmanned Aerial Vehicle (UAV), have heralded a new era in remote sensing, mapping and data analytics within precision agriculture (Hoffmann, Jensen et al., 2016; Maes and Steppe, 2019; Tang, Han et al., 2019). Using lightweight multispectral sensors mounted on UAVs offer great possibilities for continuous

near-real-time crop monitoring at a farm level (Chivasa, Mutanga et al., 2020). UAVs are unique in that they can provide high-quality remote sensing data at unprecedented spatial, spectral and temporal resolutions (Maes and Steppe, 2019; Ndlovu, Odindi et al., 2021). In addition, UAVs mounted sensors capture imagery at low altitudes and can hover over areas of interest, making them a desirable tool for monitoring changes in maize moisture content at different phenological stages (Tsouros, Bibi et al., 2019). Furthermore, UAVs provide a cost-effective option to obtain frequent imagery at an ultra-high spatial resolution, often in centimetres, which is necessary for monitoring crop physiology at a plot level (Maes and Steppe, 2019). For example, in a comparative study between UAV-based data and satellite imagery, Matese, Toscano et al. (2015) confirmed that UAV-derived datasets could detect even the most subtle variations in crop physiological characteristics, a challenge even for high-resolution satellite imagery such as RapidEye. A study by Tang, Han et al. (2019) demonstrated the value of UAV-derived multispectral data in predicting maize evapotranspiration with an  $R^2$  of 0.81 and RMSE of 0.95 mm/day. Nonetheless, the ability of UAV imagery to adequately discriminate maize moisture content variability across the growing season remains untested. Therefore, the potential application of UAVs equipped with multispectral sensors in characterising smallholder maize moisture status at different growth stages still requires investigation.

Since the moisture content in leaf tissue is a critical influencer of crop survival, accurately monitoring crop water status using spectral reflectance measurements has been a key objective in environmental research (Pasqualotto, Delegido et al., 2018). The rationality of estimating maize moisture content stems from the fact that literature confirms the existence of a strong relationship between foliar water concentration and spectral absorption at specific near-infrared (NIR) and the shortwave infrared (SWIR) wavelengths of the electromagnetic spectrum (Chemura, Mutanga et al., 2017). For instance, water molecules in leaf tissue produce maximum absorption features along the NIR (750-1300 nm) section of the spectrum as a result of a decrease in leaf reflectance (Pasqualotto, Delegido et al., 2018; Krishna, Sahoo et al., 2019; Wijewardana, Alsajri et al., 2019). Furthermore, there are secondary effects of water absorption in the visible region of the electromagnetic spectrum (blue, green and red), which are influenced by internal leaf structure and water transmissivity (Mobasheri and Fatemi 2013; Chemura, Mutanga et al., 2017). This makes these sections of the spectrum sensitive to changes in water content and, therefore, a plausible proxy for crop water stress detection. To enhance the spectral characteristics of crop leaf reflectance, several studies have demonstrated using empirical models and vegetation indices (VIs) to predict crop moisture content (Xue and Su, 2017; Pasqualotto, Delegido et al., 2018). For example, studies have reported the Normalised Difference Water Index (NDWI) as a water content-sensitive index that can predict crop moisture throughout the growing season (Zhang and Zhou, 2015; Xu, Qu et al., 2020). Krishna, Sahoo et al. (2019) noted that even though the Normalised Difference Vegetation Index (NDVI) is optimal for crop chlorophyll content estimations, the index is highly correlated to the plant water status, hence, is also a valuable predictor of maize moisture content. Therefore, by understanding crop leaf reflectance across the electromagnetic spectrum, UAV-derived spectral datasets provide a viable approach to quantifying intra-species moisture content variability of smallholder maize crops throughout the growth cycle.

Considering that limited studies have evaluated the feasibility of using UAV-based proximal remotely sensed data in accurately monitoring maize moisture content across all phenological stages (Zhang and Zhou, 2019), there is a need to assess the value of UAV-derived data in mapping crop moisture content variability. Therefore, this study sought to evaluate the utility of UAV-derived multispectral imagery in estimating the spatio-temporal variability of smallholder maize leaf EWT and FMC across the growing season.

## **7.2 Materials and Methods**

### **7.2.1 Study site description**

This study was conducted in Swayimane (29° 31' S, 30° 41' E), uMshwati Municipality, KwaZulu-Natal, South Africa (Figure 7-1). The study area experiences a sub-tropical climate, with a mean annual rainfall of 500-800 mm per annum and an average air temperature between 11.8°C and 24°C (Basdew, Jiri et al., 2017). Swayimane is located at an altitude of 886 m above sea level and has a relatively flat topography. The soil of the study area is classified as deep and dark clay loam soils, which indicates high organic matter and soil fertility (Ndlovu, Thamaga-Chitja et al., 2021). The land in Swayimane is predominantly used for commercial and small-scale subsistence agriculture, with several crops including taro, sweet potatoes, spinach, beans, sugarcane and maize (Ndlovu, Thamaga-Chitja et al., 2021). The study area is situated within the moist midlands mistbelt bioclimatic region prone to berg winds, extreme clouds, flash floods, seasonal hail and occasional periods of drought (Mahomed, Clulow et al., 2021). The Umgeni Resilience Project has identified the area as a climate change hot-spot region (Keen and Winkler, 2020). Climate projections of the area indicate an increase in temperature and unpredictable variations in annual precipitation resulting in an increased risk of climate-driven events, including an increase in drought (Mahomed, Clulow et al., 2021). As such, it is an area of interest to climatologists and agronomists studying how to combat climate variability's impacts on smallholder agricultural systems.

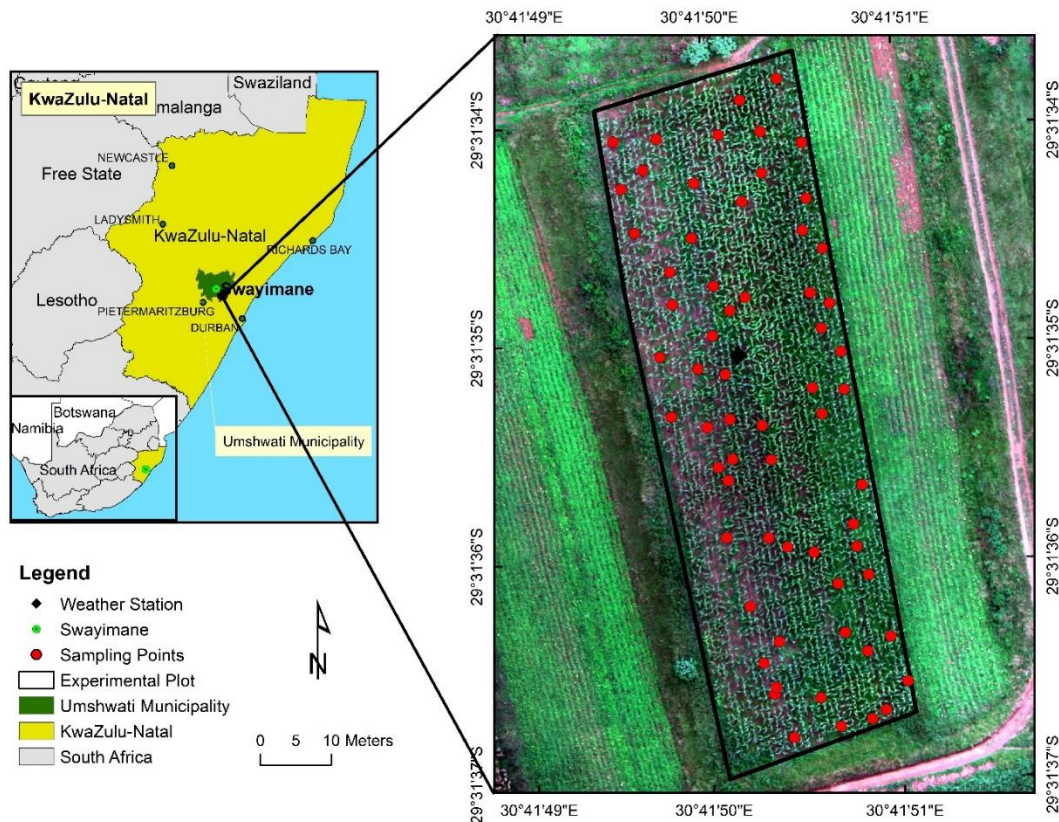


Figure 7-1: Location of the study area in Swayimane, South Africa

## 7.2.2 Experimental design and crop management

The maize moisture content was continuously monitored through the maize phenological stages. Field measurements were conducted at two-week intervals for five growth stages: 8<sup>th</sup> leaf collar – 10<sup>th</sup> leaf collar (V8-V10), 14<sup>th</sup> leaf collar – tasselling (V14-Vt), silking – blister (R1-R2), blister – milk (R2-R3) and dough – dent (R3-R4). Figure 7-2 illustrates the biophysical condition of maize at the various phenological growth stages. The experimental plot was 50 m long and 30 m wide, occupying a gentle topography. Maize crops were sown on the 8<sup>th</sup> of February 2021, and corn kernels were harvested on the 17<sup>th</sup> of May 2021. Cow urea and manure were applied as crop fertilizer before sowing, and a combination of manual hand weeding and herbicide application was conducted when the maize crops were 21 days old. The experimental plot relied primarily on precipitation for water supply. The study plots were not irrigated or applied fertiliser during the growing season. Figure 7-3 presents the bioclimatic conditions of the study plot during the maize growing period, derived from an automatic weather station located approximately 860 m from the experimental plot.

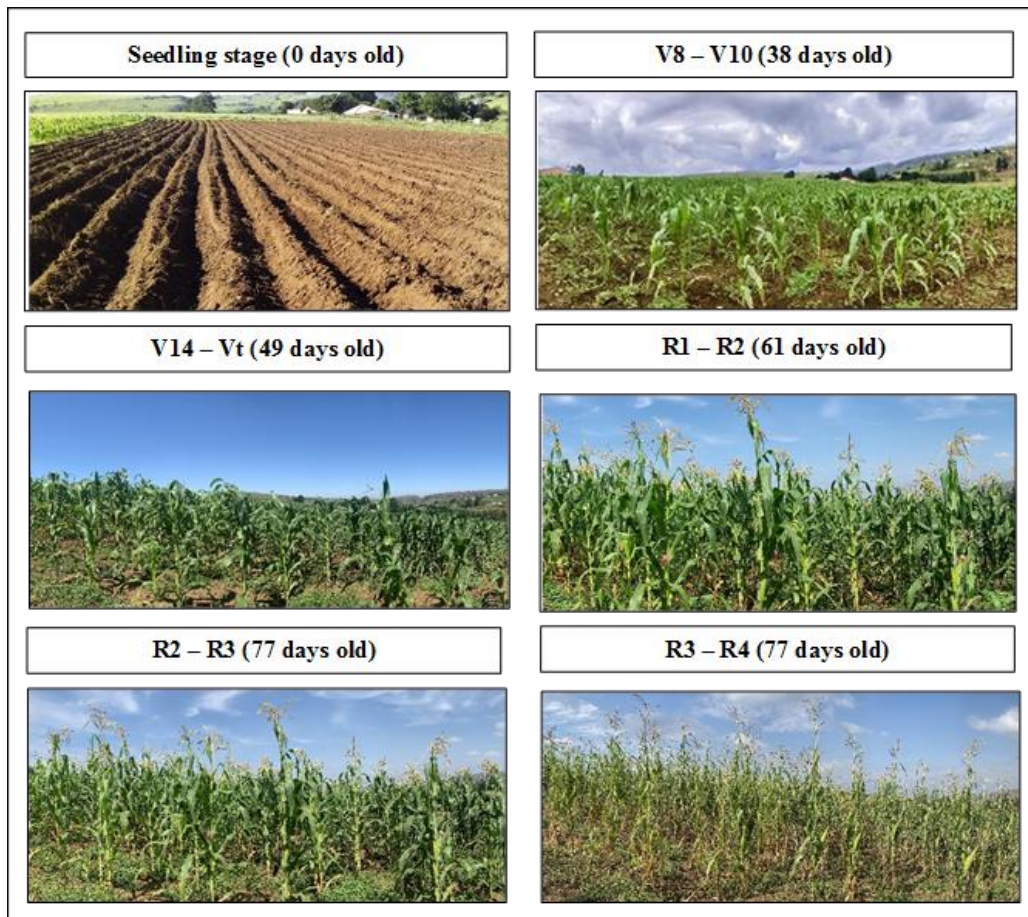


Figure 7-2: Biophysical conditions of maize across the phenological growth period

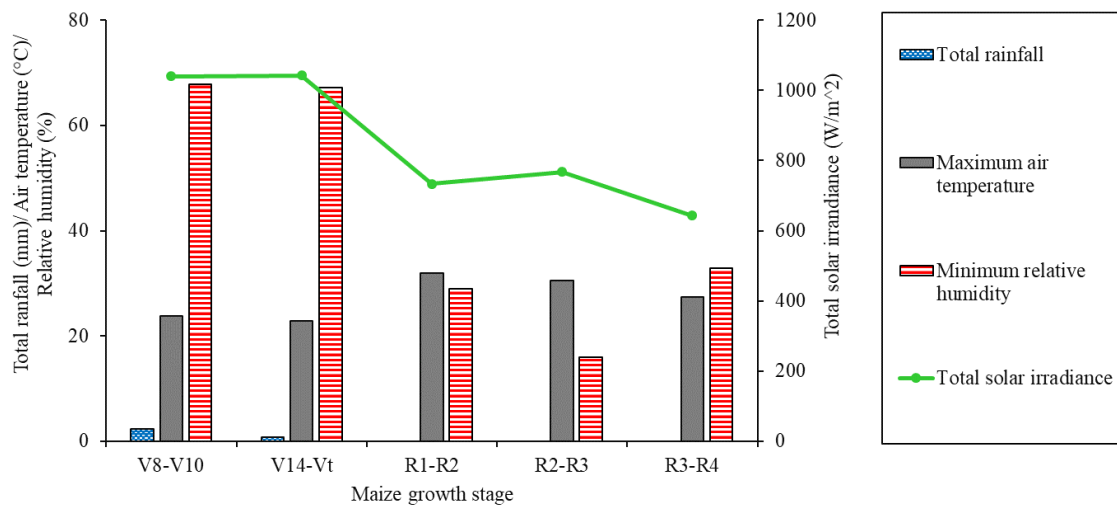


Figure 7-3: Bioclimatic condition of maize across the phenological growth period

### 7.2.3 Field survey and measurements of maize moisture content

Field measurements were conducted on the 18<sup>th</sup> of March (V8-V10), 31<sup>st</sup> of March (V14-Vt), 12<sup>th</sup> of April (R1-R2), 28<sup>th</sup> of April (R2-R3) and 14<sup>th</sup> of May (R3-R4) in 2021. A stratified random sampling procedure generated 65 points within the experimental plot. This method is optimal for acquiring an unbiased representative sample of the experimental maize plot. A Trimble handheld GPS with a sub-meter accuracy was used to navigate these sampling points at each stage of the maize growth period. The third fully developed maize leaf from the top of the stalk was sampled at each sample point. Literature states that to obtain reliable maize physiological measurements, fully developed leaf samples should be taken from the top of the canopy as there is maximum reflectance of light energy.

Meanwhile, the sampling of young crops can lead to plant stress, which can ultimately cease crop growth (Mulla, 2013; Wahbi and Avery, 2018). In this regard, maize leaf sampling was not conducted during the emergence stages, specifically from germination to the 5<sup>th</sup> leaf collar growth stage. Crop moisture content measurements were conducted under near-cloud-free conditions between 12:00 noon and 14:000 as this is the most optimal photosynthetic period of the day with radiation at maximum (Sade, Galkin et al., 2015). A portable leaf area meter (LI-3000C) with one mm<sup>2</sup> resolution was used to measure the leaf area (A) of sampled leaves. A calibrated scale was used to obtain the fresh weight (FW) of maize leaf samples, which were then dried in an oven at 70° C until a constant dry weight (DW) was reached ( $\pm$  48 hours). The leaf equivalent water thickness ( $EWT_{leaf}$  in gm<sup>-2</sup>) and fuel moisture content ( $FMC_{leaf}$  in %) were then computed using the FW, DW and A of maize leaves based on the formula;

$$EWT_{leaf} (gm^{-2}) = \frac{FW-DW}{A} \quad \text{Equation 7-1}$$

$$FMC_{leaf} (\%) = \frac{FW-DW}{DW} \times 100 \quad \text{Equation 7-2}$$

Where FW is the fresh weight, DW is the dry weight, and A is the leaf area. The computed  $EWT_{leaf}$  and  $FMC_{leaf}$  were recorded in an Excel spreadsheet against the coordinate of each sampling point, which was later converted into a point map in ArcMap version 10.3.1.

### 7.2.4 Selection of vegetation indices

The six UAV-derived spectral bands were used to estimate maize  $EWT_{leaf}$  and  $FMC_{leaf}$ . These bands were also used to compute vegetation indices (VIs) to estimate maize moisture indicators. Studies have confirmed the ability of the visible and NIR channels of the electromagnetic spectrum to detect subtle variations in vegetation water characteristics (Chemura, Mutanga et al., 2017; Pasqualotto, Delegido et al., 2018). Based on existing literature, ten moisture content-related VIs were computed based on their correlation with maize moisture content indicators. Table 7-1 details the VI used to estimate maize moisture content.

Table 7-1: Selected vegetation indices (VIs) used for maize moisture content estimations

Vegetation Index	Equation	Reference
NDWI	$(\text{Green} - \text{NIR} / \text{Green} + \text{NIR})$	(Miller, Schieber et al., 2020)
NDVI	$(\text{NIR} - \text{Red} / \text{NIR} + \text{Red})$	(Krishna, Sahoo et al., 2019)
NGRDI	$(\text{Green} - \text{Red} / \text{Green} + \text{Red})$	(Hoffmann, Jensen et al., 2016)
NDRE	$(\text{NIR} - \text{Rededge} / \text{NIR} + \text{Rededge})$	(Zhang, Zhang et al., 2019)
NDVI <sub>rededge</sub>	$(\text{Rededge} - \text{Red} / \text{Rededge} + \text{Red})$	(Zhang, Zhang et al., 2019)
CI <sub>green</sub>	$((\text{NIR}/\text{Green}) - 1)$	(Zhang and Zhou, 2015)
CI <sub>rededge</sub>	$((\text{NIR}/\text{Rededge}) - 1)$	(Zhang and Zhou, 2015)
SR	$(\text{NIR}/\text{Red})$	(Xue and Su, 2017)
OSAVI	$((\text{NIR} - \text{Red})/(\text{NIR} + \text{Red} + 0,16))$	(Xue and Su, 2017)

### 7.2.5 Model development and statistical analysis

The random forest (RF) regression provides a reliable and efficient method for performing complex and multi-dimensional environmental data analysis that would naturally be time-consuming to observe (Lu and He, 2019). This study used the RF regression algorithm to predict maize leaf moisture content indicators (EWT<sub>leaf</sub> and FMC<sub>leaf</sub>) at different phenological growth stages of maize crops because of its simplicity and robustness (Sibanda, Onisimo et al., 2021). The RF ensemble is a machine learning technique that uses bootstrap aggregation and binary recursive partitioning to construct several independent trees using a random subset derived from the training data (Lu and He, 2019). The robustness of RF originates from the capacity of the algorithm to use bootstrap aggregation to build regression trees that are grown to their maximum sizes, which are then used to allocate an input variable (spectral bands and VIs) to a response variable (EWT<sub>leaf</sub> or FMC<sub>leaf</sub>) using unweighted averaging (Jeong, Resop et al., 2016). Additionally, the out-of-bag samples, which are samples that have been excluded from the bootstrap aggregation, are used by the RF ensemble to evaluate the generated regression model (Abdel-Rahman, Ahmed et al., 2013). However, a common challenge with regression models is multicollinearity which results from a high level of correlation between two or more predictor variables (Chivasa, Mutanga et al., 2021). As such, it is advisable to use only the most suitable predictor variables in building regression models (Jeong, Resop et al., 2016). Variable importance selection was adopted to resolve potential collinearity and select the best and the fewest predictor variables for the RF model. RF can compute Gini impurity scores to identify predictor variables most influential in prediction (Sibanda, Onisimo et al., 2021). Therefore, a higher Gini impurity score was identified as the most important predictor variable. The best predictor variables were then used to develop the final RF model of maize

moisture content at each growth stage. Before the analysis, the dataset was randomly split into training data (70%:46 samples) and validation data (30%:19 samples). The former was used to develop the regression model, and the latter to evaluate the model's predictive performance.

## 7.2.6 Accuracy assessment and model validation

The prediction accuracy of the derived RF models was assessed based on the coefficient of determination ( $R^2$ ), the root mean square error (RMSE) and the relative root mean square error (rRMSE). The  $R^2$  is a statistical measure of the variation between measured and predicted output. It also measures how well the response variable fits into the regression line. The RMSE assesses the error magnitude between field measurements and the modelled maize moisture content. Meanwhile, the rRMSE was used as a metric to compare the performance of  $EWT_{leaf}$  to  $FMC_{leaf}$  at the different maize growth stages. The optimal model for estimating maize moisture content indicators at different phenological stages was determined based on the highest  $R^2$  and the lowest RMSE and rRMSE.

$$RMSE = \sqrt{\frac{\sum(\text{predicted}-\text{actual})^2}{n}} \quad \text{Equation 7-3}$$

$$rRMSE = \frac{RMSE}{\text{Mean (actual)}} \times 100 \quad \text{Equation 7-4}$$

where *predicted* is the modelled variables and *actual* is the measured variables. Lastly, a map was generated illustrating the spatial and temporal distribution of the predicted maize  $EWT_{leaf}$  or  $FMC_{leaf}$  at every growth stage. The RMSE and the rRMSE were calculated based on the above formulas.

## 7.3 Results

### 7.3.1 Descriptive statistics and temporal variation in $EWT_{leaf}$ and $FMC_{leaf}$ during the maize phenological cycle

Figure 7 4 illustrates the temporal variation of measured  $EWT_{leaf}$  and  $FMC_{leaf}$  throughout the maize growing season. As expected, there was a variation in maize  $EWT_{leaf}$  and  $FMC_{leaf}$  measured across the maize phenological season. Both maize  $EWT_{leaf}$  and  $FMC_{leaf}$  displayed a decreasing trend in moisture content as the growing season progressed. The lowest mean  $EWT_{leaf}$  was observed during the late reproductive stages of maize development, particularly during the R2-R3 stage ( $96.45 \pm 62.15 \text{ gm}^{-2}$ ), while the highest  $EWT_{leaf}$  was at the V8-V10 growth stages ( $274.45 \pm 43.25 \text{ gm}^{-2}$ ) (Table 7-2). The R2-R3 growth stage had the lowest mean  $FMC_{leaf}$  ( $48.59 \pm 14.66\%$ ), while the greatest mean  $FMC_{leaf}$  was observed at the R1-R2 maize growth stage ( $84.48 \pm 2.23\%$ ) (Table 7-2). The results of a Kolmogorov-Smirnov normality test indicated that the distribution of the measured maize  $EWT_{leaf}$  and  $FMC_{leaf}$  were not significantly deviating from a normal distribution curve. Hence a Pearson correlation was conducted to examine the relationship between maize  $EWT_{leaf}$  and  $FMC_{leaf}$ , and rainfall. Based on the Pearson correlation test, there was a statistically significant correlation between maize  $EWT_{leaf}$  and rainfall ( $R^2 = 0.97$ ,  $p < 0.05$ ). Similarly, a correlation test between maize  $FMC_{leaf}$  and rainfall indicated a statistically significant  $R^2$  of 0.77 ( $p < 0.05$ ).

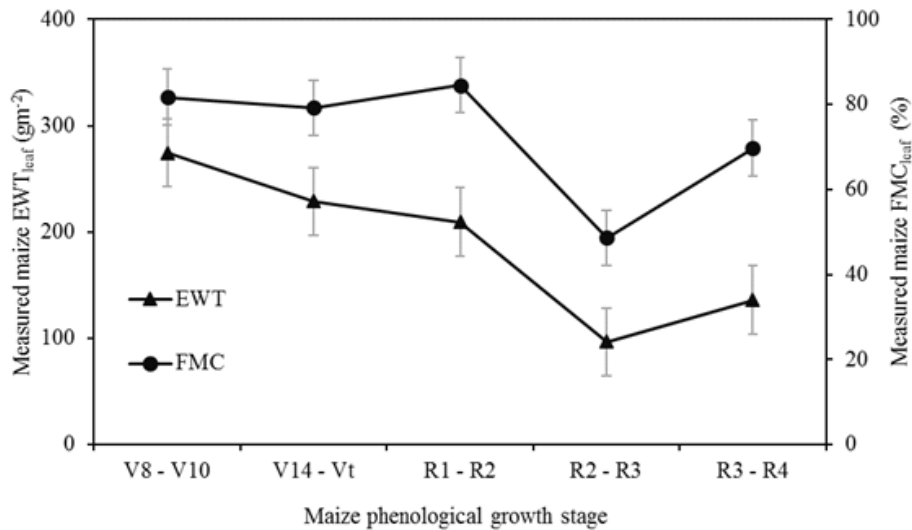


Figure 7-4: Temporal variation of maize EWT<sub>leaf</sub> and FMC<sub>leaf</sub> during the maize growing season

Table 7-2: Descriptive statistics of EWT<sub>leaf</sub> and FMC<sub>leaf</sub> at the different phenological stages

Maize growth stage	Variable	Range (min-max)	Mean	Median	Std.	CV%	SEM
V8-V10	EWT (gm <sup>-2</sup> )	169.35-462.73	274.45	270.47	43.25	15.76	5.45
	FMC (%)	73.72-90.91	81.72	81.63	2.32	2.84	0.29
V14-Vt	EWT (gm <sup>-2</sup> )	154.76-329.33	228.57	229.13	49.67	21.73	6.26
	FMC (%)	69.93-86.05	79.17	79.01	2.89	3.65	0.36
R1-R2	EWT (gm <sup>-2</sup> )	159.86-249.66	209.38	211.34	17	8.12	2.14
	FMC (%)	77.78-91.59	84.48	84.23	2.73	3.24	0.34
R2-R3	EWT (gm <sup>-2</sup> )	11.66-448.71	96.48	91.9	62.15	64.41	7.83
	FMC (%)	8.11-85.98	48.59	50	14.66	30.18	1.85
R3-R4	EWT (gm <sup>-2</sup> )	25.33-360.21	135.7	121.01	62.66	46.17	7.89
	FMC (%)	59.52-82.14	69.72	69.77	4.04	5.79	0.51

### 7.3.2 Estimating maize $EWT_{leaf}$ and $FMC_{leaf}$ throughout the maize growing season

Table 7.3 illustrates the accuracies obtained in estimating maize  $EWT_{leaf}$  and  $FMC_{leaf}$  throughout the growing season based on UAV bands only, vegetation indices (VIs), and the combination of UAV bands and VIs. Generally, UAV bands resulted in relatively lower model accuracies at all maize growth stages. For example, when estimating  $EWT_{leaf}$ , UAV bands exhibited the lowest accuracy at the V14-Vt and R1-R2 growth stages, yielding an RMSE of 47.58  $gm^{-2}$  and  $R^2$  of 0.53 and RMSE of 13.13  $gm^{-2}$  and  $R^2$  of 0.59, respectively. Similarly, in estimating maize  $FMC_{leaf}$ , the lowest RMSEs were obtained when using UAV bands at the R1-R2, R2-R3 and R3-R4 maize growth stage with RMSE of 1.13  $gm^{-2}$  and  $R^2$  of 0.59, RMSE of 11.05  $gm^{-2}$  and  $R^2$  of 0.53, and RMSE of 3.05  $gm^{-2}$  and  $R^2$  of 0.57, respectively.

The use of VIs improved model accuracies of maize  $EWT_{leaf}$  and  $FMC_{leaf}$ . For example, the  $EWT_{leaf}$  model slightly improved by a magnitude of 6.43 from an RMSE of 47.58  $gm^{-2}$  to 41.15  $gm^{-2}$  at the V14-Vt maize growth stage. Again, in estimating  $FMC_{leaf}$ , using VIs improved the model accuracy from 11.05  $gm^{-2}$  to 7.94  $gm^{-2}$  at the R2-R3 growth stage.

Table 7-3: Estimation accuracies of  $EWT_{leaf}$  and  $FMC_{leaf}$  derived using UAV bands, vegetation indices and the combination of both

Maize growth stage	Predictor variables	$EWT_{leaf}$			$FMC_{leaf}$		
		$R^2$	RMSE	rRMSE	$R^2$	RMSE	rRMSE
<b>V8-V10</b>	UAV bands	0.52	14.38	4.89	0.42	2.22	2.69
	Vegetation indices	0.6	14.98	4.91	0.44	2.35	2.85
<b>V14-Vt</b>	UAV bands	0.53	47.58	23.01	0.52	1.93	1.98
	Vegetation indices	0.7	41.15	19.9	0.56	2.15	2.76
<b>R1-R2</b>	UAV bands	0.59	13.13	6.46	0.59	1.13	1.34
	Vegetation indices	0.78	11.17	5.5	0.76	0.9	1.09
<b>R2-R3</b>	UAV bands	0.63	16.71	17.73	0.53	11.05	26.72
	Vegetation indices	0.7	37.21	50.67	0.73	7.94	18.71
<b>R3-R4</b>	UAV bands	0.58	24.49	18.71	0.57	3.05	4.47
	Vegetation indices	0.66	40.39	32.95	0.67	2.68	3.94

The optimal models for predicting maize  $EWT_{leaf}$  and  $FMC_{leaf}$  at all growth stages were determined by combining UAV bands and VIs. For example, when estimating maize  $EWT_{leaf}$ , the combined datasets exhibited the highest model accuracies with an RMSE of  $5.31 \text{ gm}^{-2}$  and  $R^2$  of 0.88 at the R1-R2 growth stage and an RMSE of  $10.28 \text{ gm}^{-2}$  and  $R^2$  of 0.89 at the R2-R3 growth stage. Similarly, when estimating  $FMC_{leaf}$ , the highest model accuracies were obtained when UAV bands and VIs were used (RMSE of  $0.88 \text{ gm}^{-2}$  and  $0.45 \text{ gm}^{-2}$  at the R1-R2 and R2-R3 stages, respectively).

Figure 7-5 illustrates the optimal models for estimating maize  $EWT_{leaf}$  at each growth stage. During the early vegetation growth stages, maize  $EWT_{leaf}$  at the V8-V10 phenological stage was predicted to have an RMSE of  $13.03 \text{ gm}^{-2}$  and  $R^2$  of 0.69. The top-most suitable predictor variables in estimating  $EWT_{leaf}$  at this stage were  $NDVI_{rededge}$ , thermal, rededge, NGRDI,  $CI_{rededge}$ , NDVI, OSAVI, NDRE, NIR, red, NDWI,  $CI_{green}$  and SR, in order of importance (Figure 7-5 (a)). The V14-Vt exhibited the poorest prediction accuracy of maize  $EWT_{leaf}$  during the vegetative stages (RMSE =  $23.99 \text{ gm}^{-2}$  and  $R^2$  of 0.76) using NDVI,  $CI_{rededge}$ , red-edge, NDRE, NDWI,  $CI_{green}$ , NIR, thermal, blue,  $NDVI_{rededge}$ , NGRDI, green and red, in descending order of importance (Figure 7-5 (b)). The most optimal maize growth stage for estimating  $EWT_{leaf}$  was observed in the early reproductive R1-R2 growth stage, which yielded the highest model accuracy across all phenological stages (RMSE of  $5.31 \text{ gm}^{-2}$  and  $R^2$  of 0.88) based on  $NDVI_{rededge}$ , rededge, NIR, NDVI, NDRE, NGRDI, blue,  $CI_{rededge}$ , NDWI, and  $CI_{green}$ , red, thermal and green, in order of importance (Figure 7-5 (c)). Hereafter, a decrease in  $EWT_{leaf}$  model accuracy was observed in all later stages of maize growth. For example, the estimation accuracy of  $EWT_{leaf}$  decreased by  $4.97 \text{ gm}^{-2}$  to an RMSE of  $10.28 \text{ gm}^{-2}$  in the R2-R3 maize growth stage, compared to  $5.31 \text{ gm}^{-2}$  from the R1-R2 stage. Nonetheless, an  $R^2$  of 0.89 was attained from predicting maize  $EWT_{leaf}$  during the R2-R3 growth stage. The influential predictor variables on that model included NDVI, NIR, NDWI,  $CI_{green}$ ,  $NDVI_{rededge}$ , red,  $CI_{rededge}$ , NDRE and NGRDI, accordingly (Figure 7-5 (d)). Furthermore, the maize  $EWT_{leaf}$  model accuracy depreciated at the R3-R4 growth stage, yielding an RMSE of  $12.66 \text{ gm}^{-2}$  and  $R^2$  of 0.77). The optimal from this model were NDVI, NIR, NDWI,  $CI_{green}$ ,  $NDVI_{rededge}$ , and red,  $CI_{rededge}$ , NDRE and NGRDI, in order of descending importance (Figure 7-5 (e)).

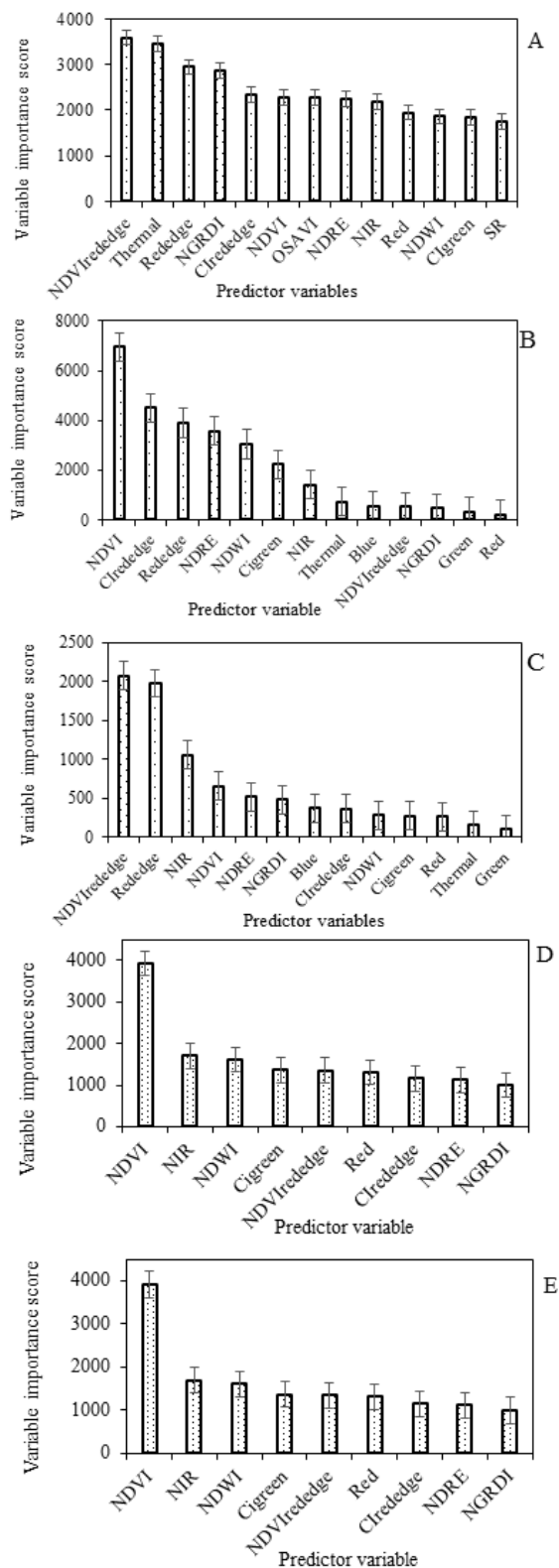
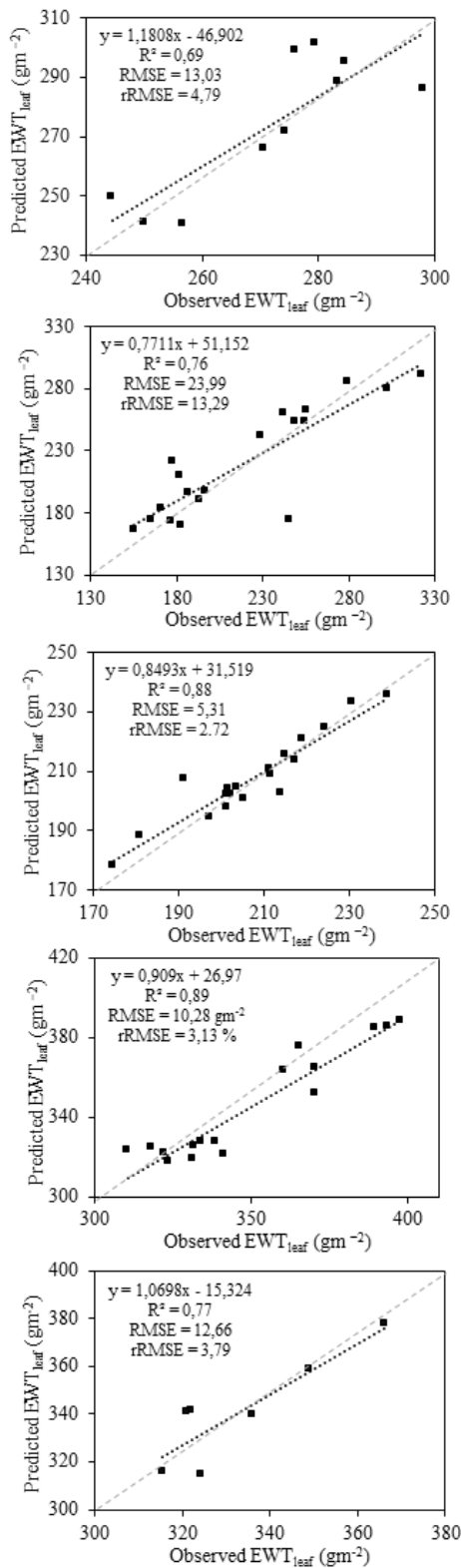


Figure 7-5: Relationship between the predicted and observed maize  $EWT_{leaf}$  at (a), V8-V10, (b) V14-T, (c) R1-R2, (d) R2-R3 and (e) R3-R4 phenological growth stage and the optimal model variable importance scores

Figure 7-6 illustrates the optimal models for estimating maize  $FMC_{leaf}$  across all growth stages. The estimation of maize  $FMC_{leaf}$  at the V8-V10 growth stage yielded a moderate RMSE of 1.13%. However, it exhibited a low  $R^2$  of 0.66 based on NDVI,  $NDVI_{rededge}$ , thermal, red, SR, rededge, NGRDI, green, NDWI, NIR, NDRE, OSAVI,  $CI_{rededge}$ ,  $CI_{green}$  and blue, in order of importance (Figure 7-6 (a)). Meanwhile, at the V14-Vt growth stage, the maize  $FMC_{leaf}$  's yielded an RMSE = 1.44% and an optimal  $R^2 = 0.73$ . The most suitable predictor variables included NDRE, rededge,  $CI_{green}$ , NIR, NDWI,  $CI_{rededge}$ , NDVI,  $NDVI_{rededge}$ , thermal, green, blue, NGRDI and red, in order of decreasing importance (Figure 7-6 (b)).

Meanwhile, the maize  $FMC_{leaf}$  prediction accuracy significantly increased in the early reproductive stages of the maize growing season. For example, the R1-R2 maize growth stage yielded an RMSE of 0.88% and an  $R^2$  of 0.87 using NDVI, rededge,  $NDVI_{rededge}$ , NIR, NDRE,  $CI_{rededge}$ , blue, NGRDI and red, in order of importance (Figure 7-6 (c)). The optimal phenological growth stage for optimally estimating maize  $FMC_{leaf}$  was the R2-R3 growth stage, which yielded the highest model accuracy with an RMSE = 0.45% and  $R^2$  of 0.76. This optimal maize  $FMC_{leaf}$  model was derived based on the NDRE, NIR, NDWI,  $CI_{rededge}$ ,  $NDVI_{rededge}$ , rededge,  $CI_{green}$ , blue, thermal, NDVI, red and green predictor variables (Figure 7-6 (d)).

Meanwhile, the later reproductive growth stages demonstrated the lowest  $FMC_{leaf}$  prediction accuracies. Maize  $FMC_{leaf}$  at the R3-R4 growth stage yielded the poorest prediction accuracy with an RMSE of 1.54% and  $R^2$  of 0.72. Finally, the most optimal variables that were selected in estimating maize  $FMC_{leaf}$  at this growth stage were  $NDVI_{rededge}$ ,  $CI_{rededge}$ , NDRE, NDWI,  $CI_{green}$ , NDVI, red, green, NIR, NGRDI, red-edge, thermal and blue, in order of importance (Figure 7-6 (e)).

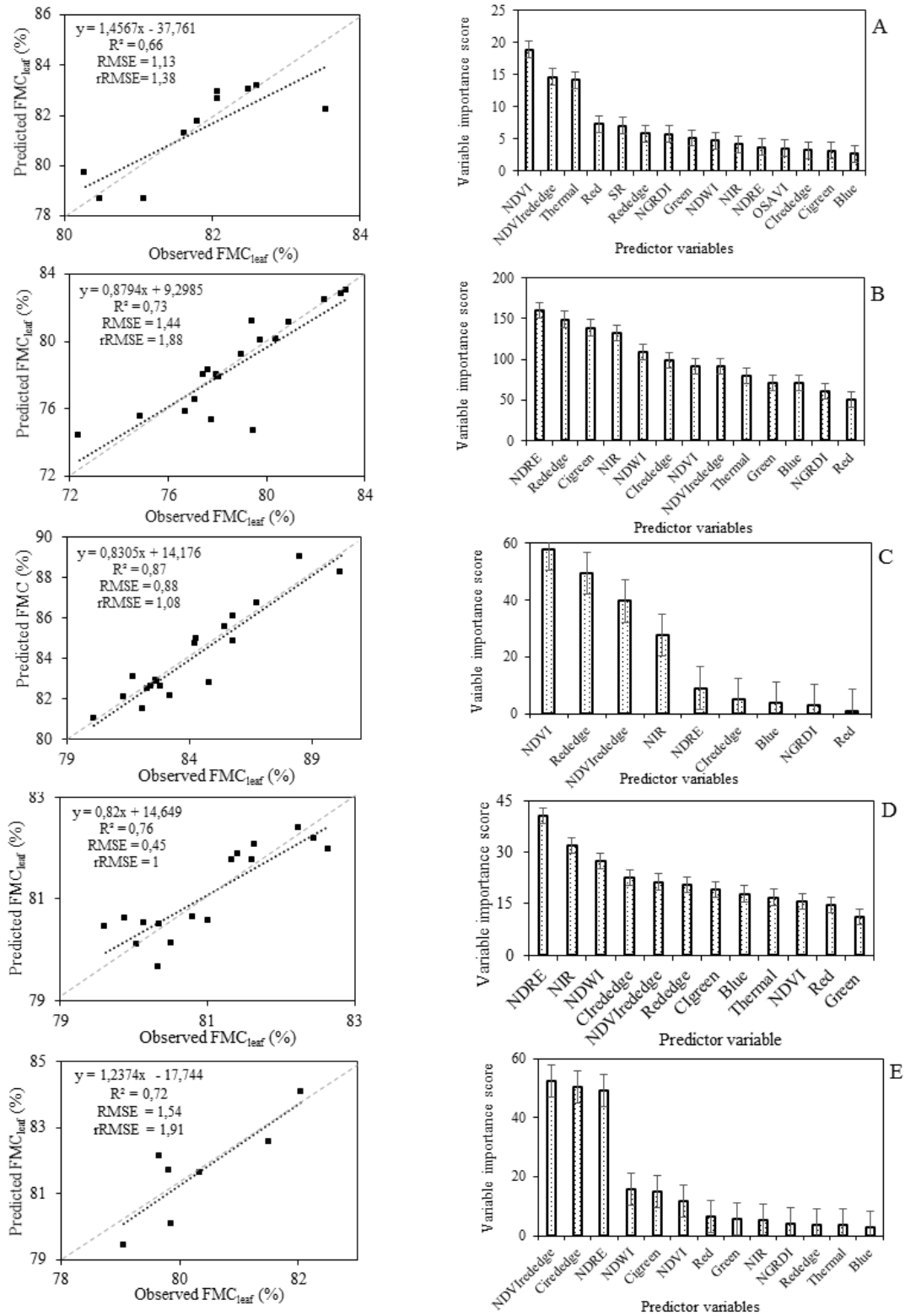


Figure 7-6: Relationship between the predicted and observed maize FMC<sub>leaf</sub> at (a), V8-V10, (b) V14-T, (c) R1-R2, (d) R2-R3 and (e) R3-R4 phenological growth stage and the optimal model variable importance scores

The results show that the prediction accuracy of maize  $EWT_{leaf}$  and  $FMC_{leaf}$  varies for each phenological stage across the growing season. For example, the maize  $FMC_{leaf}$  outperformed  $EWT_{leaf}$  with an rRMSE of 1.38% as opposed to an rRMSE of 4.79% (Figure 7.6 and 7.7 (a)). Similarly, the prediction accuracy of maize  $FMC_{leaf}$  (rRMSE = 1.88%) was significantly higher than that of maize  $EWT_{leaf}$  (13.29%) by a magnitude of 11.41% (Figure 7.6 and 7.7 (b)). Again, at the R1-R2 maize growth stage,  $EWT_{leaf}$  exhibited an rRMSE of 2.72% while  $FMC_{leaf}$  of maize had a higher prediction accuracy with rRMSE of 1.08% (Figure 7.6 and 7.7 (c)). Similarly, model accuracies for predicting maize  $FMC_{leaf}$  were marginally higher than  $EWT_{leaf}$  at the R2-R3 growth stage, with an rRMSE = 1% and 3.13%, respectively. Nonetheless,  $EWT_{leaf}$  at this stage produced the highest  $R^2$  of 0.89 compared to  $FMC_{leaf}$ , which yielded an  $R^2$  of 0.76 (Figure 7.6 and 7.7 (d)). Finally,  $FMC_{leaf}$  produced an rRMSE of 1.91% at the R3-R4 maize growth stage, as compared to the rRMSE of 3.79%, exhibited by the maize  $EWT_{leaf}$  model (Figure 7.6 and 7.7 (e)).

Figures 7-7 and 7-8 illustrate the spatial distribution of maize  $EWT_{leaf}$  and  $FMC_{leaf}$  across the five maize phenological growth stages. It can be observed that maize  $EWT_{leaf}$  and  $FMC_{leaf}$  were higher in the eastern region and decreased towards the western section of the experimental maize plot.

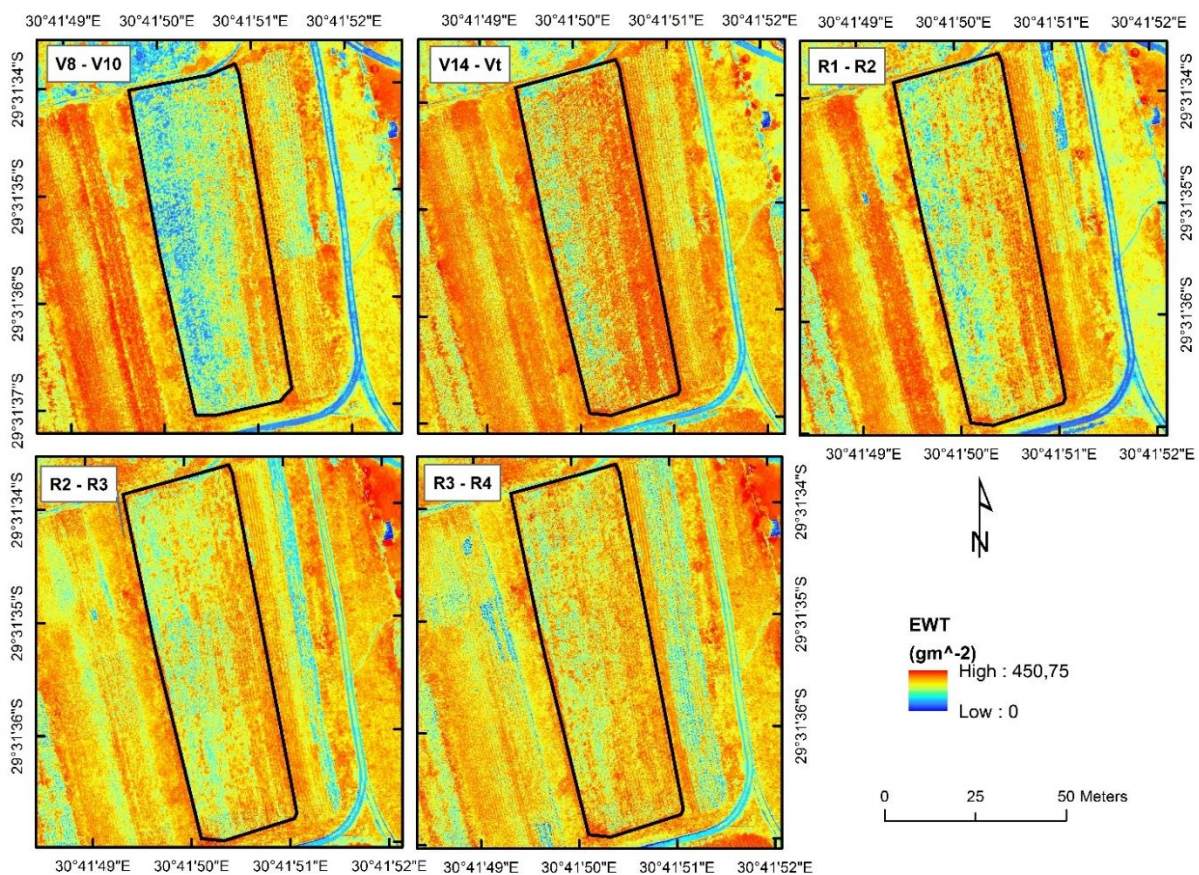


Figure 7-7: Spatial distribution of modelled maize  $EWT_{leaf}$  across the different stages of the growing season

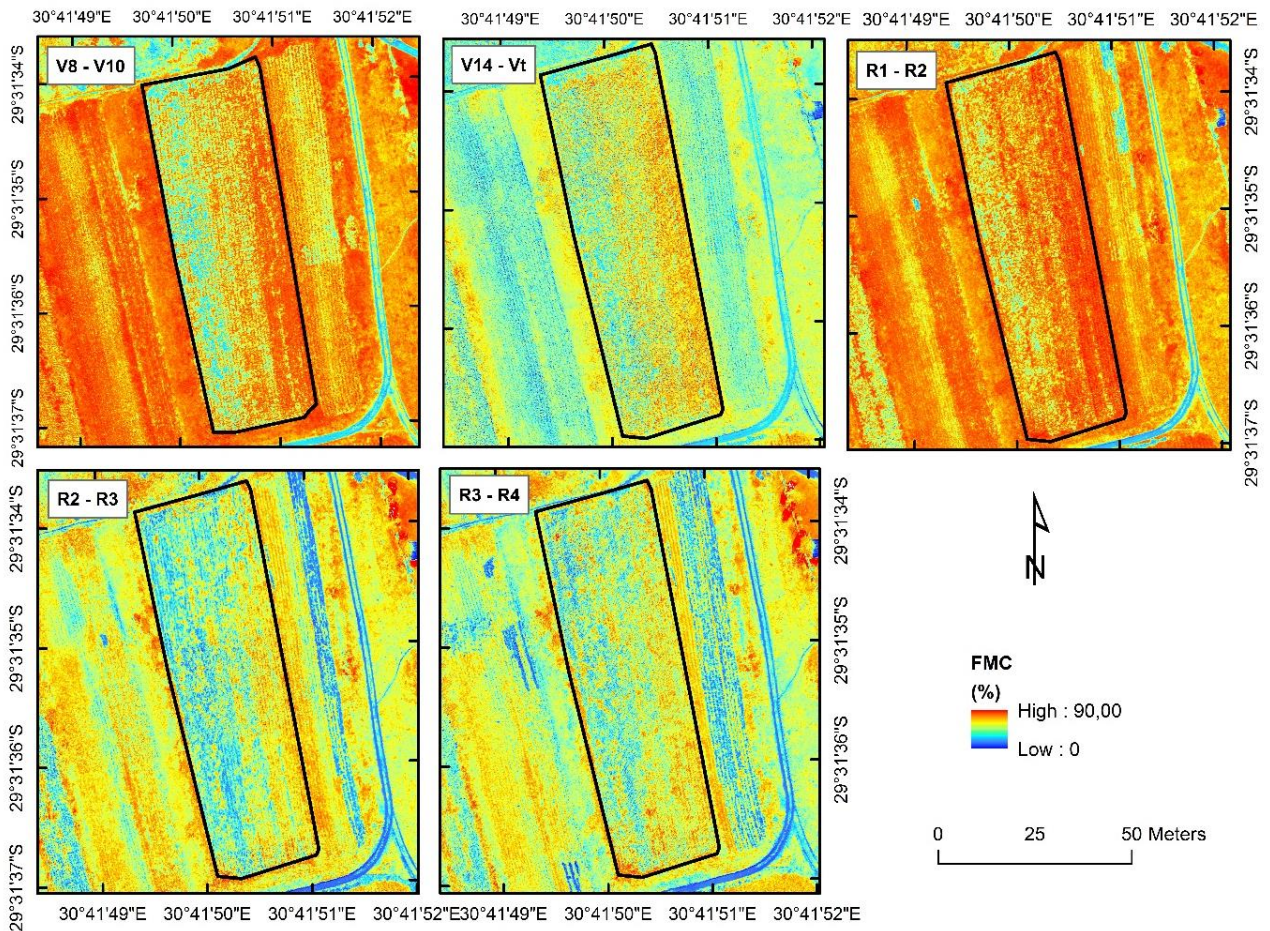


Figure 7-8: Spatial distribution of modelled maize FMCleaf across the different stages of the growing season

## 7.4 Discussion

The emergence of UAV-derived data with a high spatial and temporal resolution presents a valuable tool for monitoring maize moisture content variability throughout the growing season (Chivasa, Mutanga et al., 2020). Reliable determination of spatio-temporal variations in maize moisture is necessary for the early detection of moisture stress and identification of moisture-sensitive growth stages, necessary for developing precision agricultural management practices (Ghooshchi, Seilsepour et al., 2008; Zhang and Zhou, 2015; Wang, Cherkauer et al., 2016).

### 7.4.1 The influence of precipitation on maize moisture content variability

The findings of this study revealed a decreasing trend between precipitation and maize  $EWT_{leaf}$  and  $FMC_{leaf}$  across the growing season. The reduction of maize moisture content across the

growing season, along with the reduction in precipitation received in the study area, implies that a decrease in precipitation results in a reduction in the amount of water available to maize crops (Geneti, 2019; Zhang, Zhang et al., 2019). This finding is supported by a large body of literature suggesting that climatic variables, such as rainfall, influence the amount of foliar moisture and crop growth and development (Zhang, Liu et al., 2018; Geneti, 2019; Bois, Pauthier et al., 2020). Xu, Liu et al. (2012) argued that moisture availability is a serious challenge for rain-fed maize crops. The findings of this study agree with those of Mumo, Yu et al. (2018), who confirmed that a substantial decrease in rainfall resulted in maize moisture deficiency, drastically reducing rain-fed maize yield by 67.53%.

Furthermore, the variation in maize moisture, specifically the decrease of maize  $EWT_{leaf}$  following crop development, can be due to reduced leaf area due to moisture stress (Zhang, Liu et al., 2018). Literature has confirmed that when crops are in a state of water deficit, transpiration of the leaf surface is minimised by reducing leaf area expansion to maintain sufficient moisture levels (Gomez-del-Campo, Ruiz et al., 2002; Song, Jin et al., 2019). This finding supports the rationale of utilising  $EWT_{leaf}$  and  $FMC_{leaf}$  as surrogate measures of crop water stress.

#### **7.4.2 Estimation of maize moisture indicators from UAV-derived spectral reflectance**

Results of this study showed that optimal estimation of  $EWT_{leaf}$  can be obtained at the silking – blister (R1-R2) growth stage of maize ( $R^2 = 0.88$ ,  $RMSE = 5.31 \text{ gm}^{-2}$  and  $rRMSE = 2.72\%$ ) while for  $FMC_{leaf}$  was the blister to milk (R2-R3) stage with an  $R^2 = 0.76$  and  $RMSE = 0.45\%$  ( $rRMSE = 1\%$ ). Literature confirms that the early reproductive growth stages are best suited for detecting physiological characteristics, such as leaf moisture content, using proximal remote sensing techniques (Daughtry, Walthall et al., 2000; Prudnikova, Savin et al., 2019). This is because the transmittance spectra of the fully developed leaves and the canopy have minimal effects on the soil background and maximum reflectance of leaf properties (Daughtry, Walthall et al., 2000; Prudnikova, Savin et al., 2019). Furthermore, Prudnikova, Savin et al. (2019) argued that estimating crop physiology at the early seedling and emergence vegetative growth stages is not optimum because sparse vegetation cover increases the interference of open soil surface reflectance, hence reducing prediction accuracy.

The findings of this study illustrate that vegetation indices (VIs) were the most optimal predictor variables of maize moisture content indicators compared to raw UAV-multispectral bands. This is not surprising since a large and growing body of literature has proven that the use of VIs derived from water-sensitive sections of the electromagnetic spectrum improves prediction accuracies and outperforms conventional bands in estimating crop moisture content indicators (Zhang and Zhou, 2015; Pasqualotto, Delegido et al., 2018; Zhang, Zhang et al., 2019). This is explained by the fact that VIs are derived from a combination of spectral channels which measure reflectance at different wavelengths of the spectrum with different strengths, hence their optimal performance compared to the bands-only model (Sibanda, Onisimo et al., 2021). Furthermore, VIs tend to enhance leaf reflectance while minimising the influence of solar irradiance, atmospheric noise, topology and soil background effects (Xue and Su, 2017; Prudnikova, Savin et al., 2019; Sibanda, Onisimo et al., 2021). This makes them more robust and sensitive to moisture and other plant foliar physiochemical elements.

This study demonstrated that maize moisture indicators were sensitive to VIs derived from the NIR and red-edge wavebands of the electromagnetic spectrum. For example, the estimation of maize  $EWT_{leaf}$  was greatly influenced by  $NDVI_{rededge}$ , rededge, NIR, and NDVI, while NDRE, NIR and NDWI had the highest predictive power in optimally estimating  $FMC_{leaf}$  of smallholder maize crop. The influence of NIR-based indices stems from the fact that this section of the electromagnetic spectrum is highly correlated to the quantity of water in leaf cells (Pasqualotto, Delegido et al., 2018). Literature confirms that the variation in leaf reflectance of turgid vegetation along the NIR wavelength, as a result of the changes in water transmissivity and leaf internal structure, can be used to quantify crop moisture content and detect plants that are in a state of water deficit (Mobasher and Fatemi, 2013; Chemura, Mutanga et al., 2017). Additionally, the sensitivity of the red-edge band in maize moisture prediction can be explained by the fact that the red-edge is closely related to leaf chlorophyll composition and when crops are experiencing moisture stress, there are declines in crop physiochemical characteristics such as foliar pigmentation and leaf area, which are directly linked to leaf water status (Easterday, Kislik et al., 2019; Sibanda, Onisimo et al., 2021). A reduction in moisture content decelerates the photosynthetic activity, reducing the chlorophyll concentrations as the leaf halts its stomatal activities while losing turgidity and pigment (Liu, Peng et al., 2015; Zhang and Zhou 2015). These transitions are then detected from the rededge spectrum, which tends to shift towards the long-wavelength section (Ndlovu, Odindi et al., 2021; Sibanda, Onisimo et al., 2021). This study's results agree with Liu, Zhang et al. (2016), who found that the changes in the vegetation moisture content were spectrally discernible in the NIR spectral reflectance section. In a similar study, Zhang and Zhou (2015) combined the NIR and rededge bands to form the NDRE, which became the most sensitive index to variations in maize moisture content ( $R^2 = 0.75$ ). Furthermore, the results of this study concur with Sow, Mbow et al. (2013), who used NDWI to predict vegetation FMC to an optimal accuracy of  $R^2 = 0.85$ .

Finally, the results of this study also revealed that chlorophyll-based indices such as  $CI_{green}$  and  $CI_{rededge}$  were important predictors of maize moisture content as they were among the most influential spectral variables on V14-Vt and R3-R4 stages when estimating maize  $EWT_{leaf}$  and  $FMC_{leaf}$ . Again, this can be explained by the positive correlation between leaf chlorophyll content and water status, as prolonged moisture stress ultimately reduces chlorophyll pigmentation of maize leaves, thus changing leaf absorbance and reflectance characteristics (Liu, Peng et al., 2015; Zhang, Zhang et al., 2019; Ndlovu, Odindi et al., 2021). In a similar study, Zhang, Zhang et al. (2019) concluded  $CI_{green}$  and  $CI_{rededge}$  to be among the most influential predictors of maize EWT and FMC as they are highly sensitive to crop water variation. Despite the apparent limitations of NDVI as stated in literature (Jackson, Chen et al., 2004; Xue and Su, 2017), this index was an important predictor of maize moisture indicators in this study. This is explained by the fact that the NDVI effectively indicates leaf photosynthetic capacity correlated to leaf greenness and water status (Wijewardana, Alsajri et al., 2019; Ndlovu, Odindi et al., 2021). The results in this study concur with those of Wang, Cherkauer et al. (2016), who successfully used NDVI to monitor maize water variability using a seasonal NDVI time series analysis, while Easterday, Kislik et al. (2019) noted that the NDVI could discriminate variations in vegetation moisture stress and accurately predict leaf water content to an  $R^2$  of 0.89.

### **7.4.3 Implications of the findings**

UAVs are fast becoming a key component of precision agriculture as they provide opportunities for mainstreaming climate-smart agricultural practices into smallholder farming systems for improved crop health monitoring and water resource management. Understanding the spatio-temporal variation in maize moisture can support smallholder agricultural decision-making to facilitate the development of crop-specific management plans to increase maize resilience and reduce the susceptibility of smallholder maize farming systems to the future impacts of climate change. Furthermore, the methods used in this study could be adapted for monitoring the moisture content of other crops within smallholder farming systems. Future studies should assess maize moisture variability across various climates and evaluate the influence of other agronomical factors, such as soil structure and topographic effects on leaf moisture status.

### **7.5 Conclusion**

This study sought to test the utility of UAV-based multispectral data in estimating leaf EWT and FMC of smallholder maize crops across the growing season. The results showed that the UAV-derived multispectral data could be useful in quantifying maize moisture variability at a high spatial and temporal resolution. Therefore, it can be concluded that:

- UAV-derived multispectral data can optimally characterise maize EWT and FMC, foliar moisture, variations using the NIR and red-edge wavelengths of the electromagnetic spectrum, which demonstrated great sensitivity to the variation in maize moisture content
- The phases between silking and milk reproductive growth stage are the most optimal growth stages for predicting maize moisture content using UAV-derived data

This study demonstrates the potential of UAV-based proximal remote sensing techniques in providing near-real-time and spatially explicit information on maize moisture variability across the growing season. Finally, this study will serve as a proxy towards accomplishing sustainable development goal 15, life on land, which seeks to ensure sustainable food security, thus enhancing livelihoods and well-being.

## **8 ASSESSING THE PROSPECTS OF UAV ACQUIRED REMOTELY SENSED DATA IN MAPPING LEAF AREA INDEX AS A PROXY OF YIELD IN SMALLHOLDER CROPLANDS**

Ndlovu HS, Odindi J, Sibanda M, Mutanga O, Clulow A, Chimonyo VGP and Mabhaudhi T

### **8.1 Introduction**

Smallholder agriculture is a critical sector in Sub-Saharan African economies and sustains the livelihoods of most of the region's households (Gollin, 2014). According to Mango, Siziba et al. (2017) and Kamara, Conteh et al. (2019), smallholder croplands support about 70% of households and contribute about 15% and 2.5% to Africa's and South Africa's GDPs, respectively. Maize (*Zea Mays*) is the most important and widely grown grain crop in smallholder farms of Sub-Saharan Africa. In addition, the maize industry plays a significant role in the region's economy due to its contribution to the formal and informal food systems, thus supporting national and household food security (Ndlovu, Odindi et al., 2021). Due to the importance of maize, governments across the region closely monitor crop status to forecast productivity and food security. Often, trained extension officers perform physical crop health assessments at critical phenological stages and productivity. However, these assessments are time-consuming, expensive and at the officer's discretion.

Further to this, due to the remoteness of smallholder farmers, the status and productivity of many maize fields are either estimated through extrapolation or not included in national assessments. Considering the importance of smallholder maize production in localized food systems and their potential to contribute to national food security, there is a dire need to explicitly generate monitoring frameworks for spatially optimizing assessments of maize. Under commercial maize production secondary traits such as leaf area index and chlorophyll content have been used to assess crop health and productivity. These traits could also be applied in smallholder systems.

Generally, crop productivity is evaluated based on its constituents, such as Leaf area index (LAI), chlorophyll content concentration and yield. Amongst these constituents, LAI can be monitored to understand crop health status, canopy physiology and nutritional supply (Luo, Liao et al., 2020). LAI is defined as half the area of all leaves per unit of surface area, and its estimation has long been a research focus for understanding biomass characteristics (Dong, Liu et al., 2019). This is because LAI significantly influences the plant canopy physiological process, which is closely related to crop productivity. In addition, the total accumulation of LAI is strongly related to biomass accumulation and crop yield (Gitelson, Peng et al., 2014). Therefore, monitoring maize LAI in smallholder farms could help assess crop condition and variation across space and time for the detection of crop phenology and to model biomass and yield to optimize the productivity of smallholder farms. Furthermore, monitoring maize LAI is valuable for diagnosing and assessing crop deficiencies like water and plant nutrition, which are necessary for optimizing smallholder productivity (Tunca, Köksal et al., 2018). Hence, monitoring and estimating maize LAI is vital in enhancing productivity, combating food

insecurity, and addressing the sustainable development goals of reducing hunger and poverty (Jin, Azzari et al., 2019; Peng, Li et al., 2019).

Crop LAI can be monitored and estimated through traditional methods like field surveys and point sample measurements (Tunca, Köksal et al., 2018). Despite the high accuracy associated with the traditional methods, they are time-consuming, labour-intensive and lack spatial representativeness (Martínez-Guanter, Egea et al., 2019). In contrast, remote sensing technologies have increasingly become popular in agricultural research as they offer fast and non-destructive ways of monitoring and estimating crop productivity parameters (Yao, Wang et al., 2017). Remote sensing (RS) provides spatial and temporal information on crop responses to dynamic environmental conditions or information that relates directly to LAI. Such RS data has helped derive important crop parameters such as LAI, water use efficiency, chlorophyll and biomass fraction of photosynthetically active radiation (Tumlisan, 2017; Peng, Li et al., 2019).

There are numerous ways of using remotely sensed information to estimate LAI. The simplest is establishing an empirical relationship between the remotely sensed data, such as spectral bands and Vegetation Indices (VIs) and measured LAI (Gao, Yang et al., 2016). Hence, several earth observation sensors have been used to estimate maize LAI with optimal accuracy. These include the Landsat (González-Sanpedro, Le Toan et al., 2008; Su, Huang et al., 2019), moderate resolution imaging spectral radiometer (MODIS) (Kira, Nguy-Robertson et al., 2017; Yu, Yin et al., 2021) and recently Sentinel-2 multispectral instrument (MSI) (Luo, Liao et al., 2020; Amin, Verrelst et al., 2021). Despite the optimal accuracies associated with the data from these satellite-borne sensors in LAI estimation, the trade-off between its spatial and temporal resolution limits its use in capturing crop LAI heterogeneity and dynamics at a farm scale (Martínez-Guanter, Egea et al., 2019). Yang, Gong et al. (2021) notes that medium spatial resolution products, e.g. Landsat and Sentinel-2 have the potential to miss observations at critical growth stages because of their long revisit time (16 and 10 days respectively) as well as their coarser spatial resolution, which is inadequate for smallholder fields of less than 5 Ha. In this regard, there is still a need to assess other sources of spatial data which could be cheaper and flexible, while offering very high spatial resolution data suitable for capturing crop LAI at farm-to-field scales.

The introduction of UAV remote sensing technology offers valuable remotely sensed data for estimating crop productivity constituents such as LAI (Martínez-Guanter, Egea et al., 2019). UAV remote sensing technologies offer maximum flexibility in terms of temporal resolution since the flying times are user-determined. Their ability to fly at low altitudes, portability and generation of very high spatial resolution data of up to 5 cm makes them more suitable for farm-scale research than satellite remotely sensed data (Gao, Yang et al., 2016). It is anticipated that the very high resolution (VHR) spatial resolution, combined with a multispectral resolution covering the red edge section of the electromagnetic spectrum (EMS) renowned for mapping LAI of plants, could optimize the estimation of maize productivity in smallholder croplands. UAVs have been widely used in crop monitoring. For instance, Kanning, Kühling et al. (2018) successfully estimated wheat LAI with an  $R^2$  of 0.79 and an RMSE of 0.18, while Yao, Wang et al. (2017) estimated wheat LAI to an  $R^2$  of 0.80 and an RRMSE of 24% using UAV imagery. Guomin, Yajie et al. (2020) used UAV-derived VIs to estimate maize LAI to an  $R^2$  of 0.83 and RMSE of 0.05. The proven compatibility of unmanned aerial vehicles with multi-spectral sensors enables daily LAI estimation at high resolution.

However, most of these studies have been conducted based on single images in experimental plots outside the third-world smallholder croplands. For an accurate estimation and outlook on a specific crop's productivity and yield, multitemporal images are required to understand the growth trajectory of the crop for informed decision making before the harvesting. Hence, there is need to assess the utility of UAV derived multispectral data in assessing the productivity of staple crops such as maize in smallholder croplands of regions such as southern Africa where hunger and poverty are rife and the need for optimizing crop production is imperative.

The literature illustrates that combining VIs with robust machine learning algorithms improves the accuracy of crop productivity models. VIs depict biophysical parameters of the plant canopy, such as biomass, greenness and LAI and are calculated using the reflectance of two or more spectral bands (Zhang, Lan et al., 2009). VIs enhance the sensitivity to a specific crop parameter while suppressing the influence of other factors, such as leaf and canopy structure (Sun, Qin et al., 2019). Also, VIs counteract the impacts of soil background, atmospheric conditions, leaf pigment and inclination (Ngie and Ahmed, 2018). Several VIs have been proven to be strongly correlated with maize LAI (Sun, Qin et al., 2019) and yield. These include the soil-adjusted VIs (i.e. Soil Adjusted Vegetation Index and Optimized Soil Adjusted Vegetation Index) developed to reduce soil reflectance's impact at low LAI. In recent years, due to the advancement in sensor technologies, Indices such as the red edge band VIs as the Normalized Difference Vegetation Index (NDVI) based on the red edge (NDVIRE), the Normalized Difference Red Edge (NDRE), the Modified Simple Ratio Red Edge (MSRRE) and the red edge-based Chlorophyll Index (CIRE) have been developed (Dong, Liu et al., 2019). These VIs have proven effective in estimating LAI, especially from moderate to high LAI and are less influenced by canopy structures (Martínez-Guanter, Egea et al., 2019). Qiao *et al.* (Qiao, Gao et al., 2022), using red edge-based VIs derived from UAV imagery, estimated maize LAI to an R<sup>2</sup> of 0.94, whilst Tao *et al.* (Tao, Feng et al., 2020) in their study concluded that combining red edge parameters with VIs significantly improves the estimation of LAI. Nevertheless, the effectiveness of these VIs using UAV image data remains largely unexplored.

Hence, this study sought to test the value of using UAV-derived VIs in estimating maize LAI across the growing season and determine its relationship with yield. A robust algorithm, Random Forest (RF) regression, was used to achieve this. This algorithm was chosen based on its popularity in literature due to its ability to resolve overfitting problems and select a subset of variables that best explain crop attributes such as LAI and insensitivity to small sample sizes. Specific objectives of this study were (1) to reliably estimate LAI using a combination of traditional, new and red edge-based VIs in conjunction with the RF algorithm and (2) to produce a model for the estimation of maize LAI at each growth stage based on UAV images and field-collected LAI measurements.

## **8.2 Materials and Methods**

### **8.2.1 Study site**

This study was conducted in a maize crop field on a smallholder farm in Swayimane within the KwaZulu-Natal province, South Africa (29°31'24"S and 30°41'37" E), covering an area of

2699.005 m<sup>2</sup> (Figure 8 1). A sub-humid climate with hot and humid summers and warm and dry winters characterizes the area. According to Miya, Modi et al. (2018), the area is characterized by a uni-modal rainfall pattern from November to March with an average precipitation of 900-1200 mm and an average temperature of 20°C. Major economic activity in the area is small-scale sugarcane and maize farming.

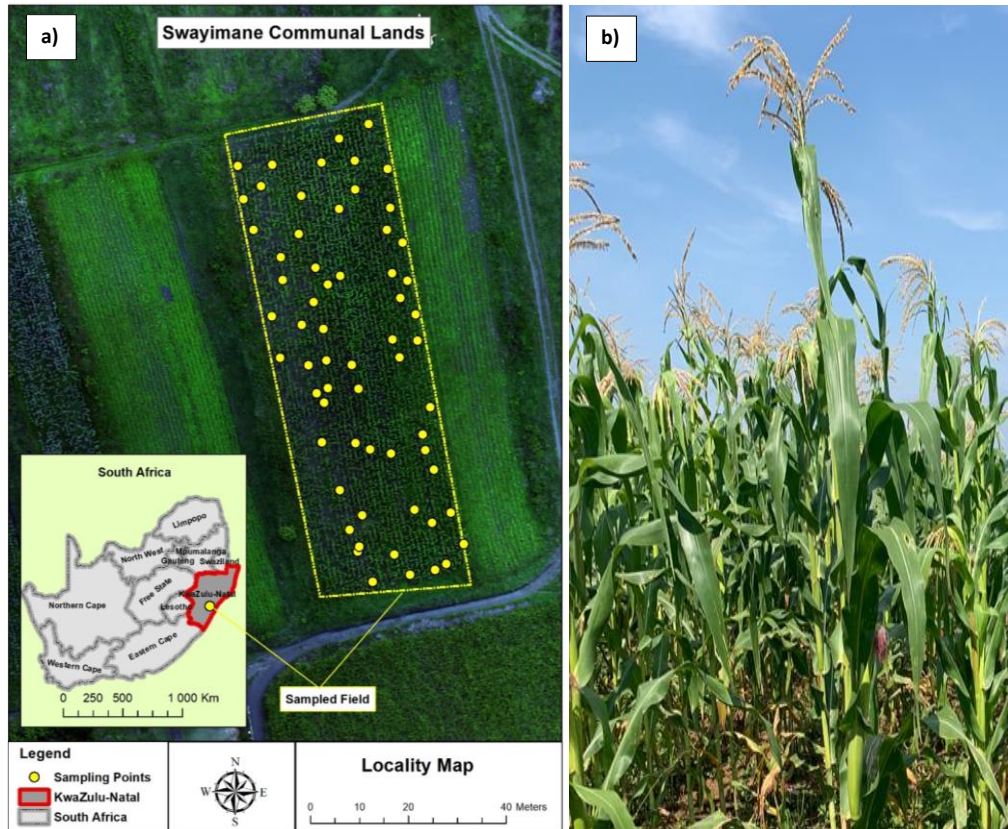


Figure 8-1: a) Location of study site in Swayimane, KwaZulu-Natal, South Africa and b) The maize plot.

The leaves with visible collars were used to discern the maize growth stage. Maize growth stages were divided into two sub-groups; that is, the vegetative (V) and reproductive (R) stages (Coelho and Dale, 1980, Ciampitti, Elmore et al., 2011) (Table 8-1). The V stages began with emergence denoted VE. This stage marks the emergence of coleoptiles from the soil (Ciampitti, Elmore et al., 2011). The following stages were subdivided numerically into V1 to V3. V1, V2 and V3. The development of the first true leaf generally marks V2.

Meanwhile, V3 is characterised by the establishment of the collar of the third leaf between 10-14 days after emergence. The vegetative stages can proceed to V(n) Nth leaf collar depending on the crop variety. The final V stage is the tasselling stage, typically noted by establishing the tassel. The plant at the tasselling stage will have developed to a full height, and all leaves will have emerged. The next stage will be the reproductive and kernel development stages, generally denoted using the letter R (Ciampitti, Elmore et al., 2011). The first reproductive stage is R1, silking. At this stage, silks emerge outside the husks with pollen shed at a rate of 1- to 1.5 inches per day (Coelho and Dale, 1980; Ciampitti, Elmore et al., 2011).

The Blister stage follows this, denoted R2 at approximately 70 after emergence. At this stage, the blisters occur most between 10-4 days after silking. Small watery kernels will be developed while silks will be browning and drying out (Coelho and Dale, 1980). The milk stage (R3) occurs 18 to 22 days after silking. At this stage, the kernel develops a milky fluid inside. The milk stage occurs 91 days after emergence. The dough stage (R4) follows approximately 105 days after the emergence. At this stage, the kernels have a pasty consistency. The dent (R5) occurs about 112 days after emergence. At this point, the cobs would have been developed. This stage can be identified using the milk or starch line (a line separating the solid and the liquid endosperms) which progressively gravitates towards the cob as moisture is being lost and the kernel matures (Coelho and Dale, 1980; Ciampitti, Elmore et al., 2011). The final stage is physiological maturity also referred to as the black layer (R6) and occurs approximately 160 days after emergence. At the black layer stage, the milk line would have progressed to the base of the kernel and a black line would have developed at the kernel base (Coelho and Dale, 1980).

Table 8-1: Maize growth stages.

	<b>Growth stage</b>	<b>Name of growth stage</b>	<b>Days after emergence</b>	<b>Brief description</b>
Vegetative	(VE)	Emergence	0	Germination and Emergence
	V1	First leaf collar		
	V2	Second leaf collar	7	
	V3	Third leaf collar		
	V(n)	Nth leaf collar	21-55	Plant population established, cob development, active growth: cob size determined
	VT	Tassling	56	Pollination
Reproductive	R1	Silking	63	
	R2	Blister	70	Kernel development
	R3	Milk	91	Grain filling: nutrients transported to cob
	R4	Dough	105	
	R5	Dent	112	Physiological maturity and ready for harvest
	R6	Maturity	160	

### **8.2.2 LAI measurements**

A polygon map was generated in Google Earth Pro covering the maize field to estimate the maize LAI. The polygon was imported into ArcMap 10.6 as a keyhole markup language (kml) file and used to generate stratified random sampling points and determine the flight path. A total of 63 points were generated and used for this analysis. These sampling points were loaded into a Trimble handheld Global Positioning System (GPS) with an accuracy of 30 cm and used to locate the sampling points in the plot. At each sample point, a close maize plant was marked for ease of identification and used for further sampling. Five field surveys were conducted during the vegetative (V) and reproductive (R) growth stages, i.e. V8-V10 (18 March 2021), V10-V12 (31 March 2021), VT-R1 (12 April 2021), R2-R3 (28 April 2021) and R3-R4 (14 May 2021). UAV were acquired at each field survey.

The LAI was determined by using the LiCOR 2200C Plant Canopy Analyzer. The LiCOR 2200C has a fisheye optical sensor with five concentric rings centred at zenith angles 7°, 22°, 38°, 52° and 68° measuring radiation above and below the canopy to estimate canopy light interception and transmittance at five angles. The LAI is determined by inverting the Beer-Lambert law.

### **8.2.3 Data analysis**

The UAV bands were used to calculate 57 VIs (Table 8 2). Specifically, traditional, red edge-based and new VIs (nDVI) based on all combinations of the six spectral bands were calculated in geographic information systems (GIS). The UAV-derived VIs were then used to estimate maize LAI across the growing season. The UAV data used in this study are summarized in (Table 8-2). All vegetation indices were loaded in the model computation to estimate LAI, and the RF selected the optimal spectral features as described in section 2.5 below. We then assessed the correlation between LAI and observed yield data.

Table 8-2: UAV-derived VIs were used in this study.

	Vegetation Index	Abbreviation	Formula	Reference	
Traditional	Normalized Difference Vegetation Index	NDVI	$(\text{NIR}-\text{R})/(\text{NIR}+\text{R})$	(Aboelghar, Arafat et al., 2011)	
	Phenological Difference Index	Normalized PNDVI	$(\text{NIR}-(\text{G}+\text{R}+\text{B})) / (\text{NIR}+(\text{G}+\text{R}+\text{B}))$	(Liu, Liu et al., 2019)	
	Red-Blue Vegetation Index	Normalized RBNDVI	$(\text{NIR}-(\text{R}+\text{B})) / (\text{NIR}+(\text{R}+\text{B}))$	(Li, Xu et al., 2020)	
	Enhanced Vegetation Index	Normalized ENDVI	$((\text{NIR}+\text{G})-(2*\text{B})) / ((\text{NIR}+\text{G})+(2*\text{B}))$	(Mditshwa, 2017)	
	Green-Blue Vegetation Index	Normalized GBNDVI	$(\text{NIR}-(\text{G}+\text{B})) / (\text{NIR}+(\text{G}+\text{B}))$	(Peng, Li et al., 2019)	
	Green-Red Vegetation Index	Normalized GRNDVI	$(\text{NIR}-(\text{G}+\text{R})) / (\text{NIR}+(\text{G}+\text{R}))$	(Peng, Li et al., 2019)	
	Generalized Vegetation Index	Difference GDVI	$\text{NIR}-\text{G}$	(Ramos, Osco et al., 2020)	
	Chlorophyll Index	Green CIgreen	$(\text{NIR}/\text{G})-1$	(Stroppiana, Migliazzi et al., 2015)	
	Chlorophyll Index	Vegetation CVI	$\text{NIR}*(\text{R}/(\text{G}* \text{G}))$	(Stroppiana, Migliazzi et al., 2015)	
	Green Leaf Index	GLI	$((2*\text{G})-\text{R}-\text{B}) / ((2*\text{G})+\text{R}+\text{B})$	(Tumlisan, 2017)	
	Enhanced Vegetation Index	EVI	$2,5*((\text{NIR}-\text{R}) / (\text{NIR}+(6*\text{B})-(7,5*\text{B}))+1)$	(Potgieter, Apan et al., 2007)	
	Enhanced Vegetation Index 2	EVI2	$2,4*((\text{NIR}-\text{R}) / (\text{NIR}+\text{R}+1))$	(Zheng, Cheng et al., 2019)	
	Enhanced Vegetation Index 3	EVI3	$2,5*((\text{NIR}-\text{R}) / (\text{NIR}+(2,4*\text{R}+1))$	(Sibanda, Mutanga et al., 2017)	
	Chlorophyll Index	CI	$(\text{R}-\text{B})/\text{B}$	(Yao, Wang et al., 2017)	
	Infrared Vegetation Index	Percentage IPVI	$(\text{NIR}/\text{NIR}+\text{R})/2*(\text{NDVI}+1)$	(Zhang, Zhao et al., 2019)	
	Soil Adjusted Vegetation Index	SAVI	$((\text{NIR}-\text{R}) / (\text{NIR}+\text{R}+0,5))*(1+0,5)$	(Mditshwa, 2017)	
	Optimized Soil Adjusted Vegetation Index	OSAVI	$(\text{NIR}-\text{R}) / (\text{NIR}+\text{R}+0,16)$	(Peng, Li et al., 2019)	
	Simple Ratio	SR	$(\text{NIR}/\text{R})$	(Peng, Li et al., 2019)	
	Red edge based	Normalized Difference Red Edge Chlorophyll Canopy Content Index	NDRE	$(\text{NIR}-\text{RE}) / (\text{NIR}+\text{RE})$	(Sun, Qin et al., 2019)
		Chlorophyll Red Edge Content Index	CI <sub>RE</sub>	$(\text{NIR}/\text{RE})-1$	(Sun, Qin et al., 2019)
Canopy Chlorophyll Content Index		CCCI	$((\text{NIR}-\text{RE}) / (\text{NIR}+\text{RE})) / ((\text{NIR}-\text{R}) / (\text{NIR}+\text{R}))$	(Al-Gaadi, Hassaballa et al., 2016)	
Red Edge based Normalized Difference Vegetation Index		NDVI <sub>RE</sub>	$(\text{RE}-\text{R}) / (\text{RE}+\text{R})$	(Dong, Liu et al., 2019)	
New	-	nDVI	$(\text{R}_{Yi}) - (\text{R}_{Yj}) / (\text{R}_{Yi}) + (\text{R}_{Yj})$	This study	

\*Where R<sub>Yi</sub> and R<sub>Yj</sub> are different Altum spectral bands, including the thermal band.

#### 8.2.4 Maize LAI prediction

Before predicting the LAI using UAVs acquired remotely sensed data, we assessed the magnitude of the relationship between field-measured LAI and field-measured yield of maize based on Pearson's product moments correlation after assessing the data for normality. We sought to evaluate whether a change in LAI (a proxy for biomass accumulation) could be associated with the change in yield. Before conducting the Pearson's correlation test, the LAI estimates measured in the field at different stages were averaged to relate them with grain yield. Grain yield was destructively derived from each sampling plot and measured using a digital scale.

RF algorithm was then used to estimate maize LAI across the growing season. RF is amongst the group of supervised ensemble regression machine learning techniques developed to advance the classification and regression trees algorithm by compiling a huge set of decision trees. RF uses a bootstrap aggregation technique popularly known as bagging. In conducting bagging, RF creates decision trees and then trains each tree using exclusive data samples from the field-measured data (LAI). Data sampling for each tree is conducted with replacement from the main pool. Its popularity is based on optimising the regression trees (*ntree*) method by combining a large set of decision trees. Another hyperparameter of RF, *mtry*, regulates that split-variable randomization feature. This study implemented the RF machine learning technique using the R interface. In R, the *doBest* function was used to optimize the *ntree* and *mtry* parameters to 200 and 5, respectively, as it was the best combination of parameters after testing the *ntree* values in increments of 100 to 2500 and the *mtry* values in increments of 1 to 5. The resulting models of each growth stage were then compared to assess the best-performing model. RF conducted the optimal spectral feature selection, and these optimal features were identified using their relatively high variable importance scores.

#### 8.2.5 Accuracy assessment

To assess the performance of the models, the dataset ( $n = 63$ ) was split into 70% training ( $n = 44$ ) and 30% test ( $n = 19$ ) datasets. The training data was used to train the model, and the test data was used to evaluate the estimation models. The performance of each model in estimating LAI was evaluated using the coefficient of determination, the root mean square error (RMSE) and the relative root mean square error (RRMSE) (see Equations 7-3 and 7-4). The model that yielded a high  $R^2$  and low RMSE was then used to create an LAI map for the study site in ArcMap 10.6. The LAI index mathematical models and the selected optimal spectral variables were then used to create LAI maps using the raster calculator in ArcMap.

### 8.3 Results

#### 8.3.1 Descriptive statistics

Descriptive statistics of LAI measured in the field for all the growth stages (i.e. V8-V10, V10-V12, VT-R1, R2-R3, R3-R4) are shown in Table 8-3. The highest average maize LAI of 3.44 was obtained from the R3-R4 growth stage, and the lowest was observed for the V8-V10 growth stage, which was 1.78. Furthermore, the R3-R4 growth stage had the highest

maximum LAI of 6.29 compared to the rest. The V8-V10 stage had the lowest LAI of 0.47 compared to the rest. The mean LAI increased along with an increase in maize crop productivity. In assessing the general relationship between the maize field measured LAI estimates and the yield, results showed a significant ( $\alpha = 0.05$ ) positive correlation. Specifically, a correlation coefficient ( $r$ ) of 0.74 indicated a strong positive relationship between the yield and the LAI. This implied that an increase in average LAI estimates is associated with a significant increase in yield (Figure 8-2).

Table 8-3: Descriptive statistics of the actual maize LAI

Growth Stage	N	Mean	Std. dev	Min	Max
V8-V10	63	1.78	0.35	0.47	1.37
V12-V14	63	1.82	1.37	1.01	2.93
VT-R1	63	2.07	1.14	2.24	3.46
R2-R3	63	3.29	1.1	2.66	5.15
R3-R4	63	3.44	0.63	3.53	6.29

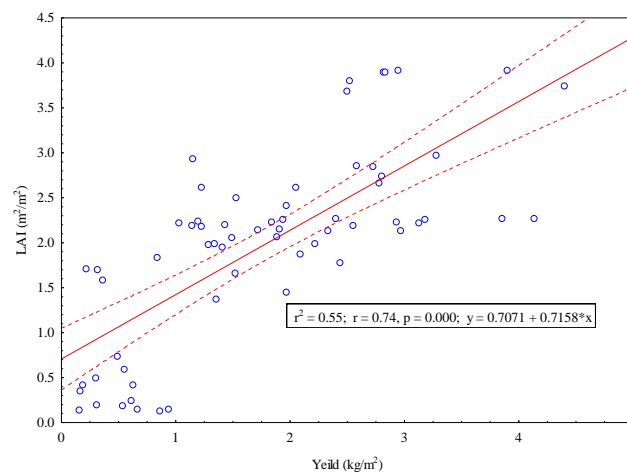


Figure 8-2: Relationship between field-measure Yield and average LAI estimates of maize.

### 8.3.2 Derived Maize LAI prediction models and their accuracies

Figure 8-3 demonstrates the model accuracies obtained in estimating maize LAI based on the RF algorithm. The prediction models' accuracy was moderate to high across the different maize growth stages. For instance, the most optimal model derived in predicting LAI was the V8-V10 growth stage with an  $R^2$  of 0.91, RMSE of 0.15  $m^2/m^2$  and RRMSE of 8.13% (Figure 8-3 (a)) based on  $ndviB\&T$  and  $ndviG\&B$  spectral variables (Figure 8-4 (a)). The V12-V14 growth stage exhibited the second-best model with a maize LAI model that exhibited an  $R^2$  of 0.93, RMSE of 0.17  $m^2/m^2$  and RRMSE of 8.97% (Figure 8-3 b) with BNDVI and  $ndviB\&NIR$  being more influential for the model (Figure 8-4 (b)).

Meanwhile, the VT-R1 growth stage demonstrated a moderate prediction accuracy in estimating maize LAI ( $R^2 = 0.91$ , RMSE = 0.65  $m^2/m^2$  and RRMSE = 19.61%) (Figure 8-3 (c)).

The most suitable predictor variables for this stage included ndviNIR&T and ndviR&T (Figure 8-3 (c)). This was followed by a drastic improvement in the R2-R3 growth stage with an R2 of 0.89, RMSE of 0.19 m<sup>2</sup>/m<sup>2</sup> and RRMSE of 10.78% (Figure 8 3 (d)). CI and ndviB&RE (Figure 8-4 (d)) were the most influential variables for this prediction. The R3-R4 growth stage also yielded the least model with an R<sup>2</sup> = 0.91, RMSE = 0.32 m<sup>2</sup>/m<sup>2</sup> and RRMSE = 15.22% (Figure 8-3 (e)). The most optimal variables for predicting maize LAI at the R3-R4 growth stage were ndviNIR&B and ndviB&NIR (Figure 8-4 (e)).

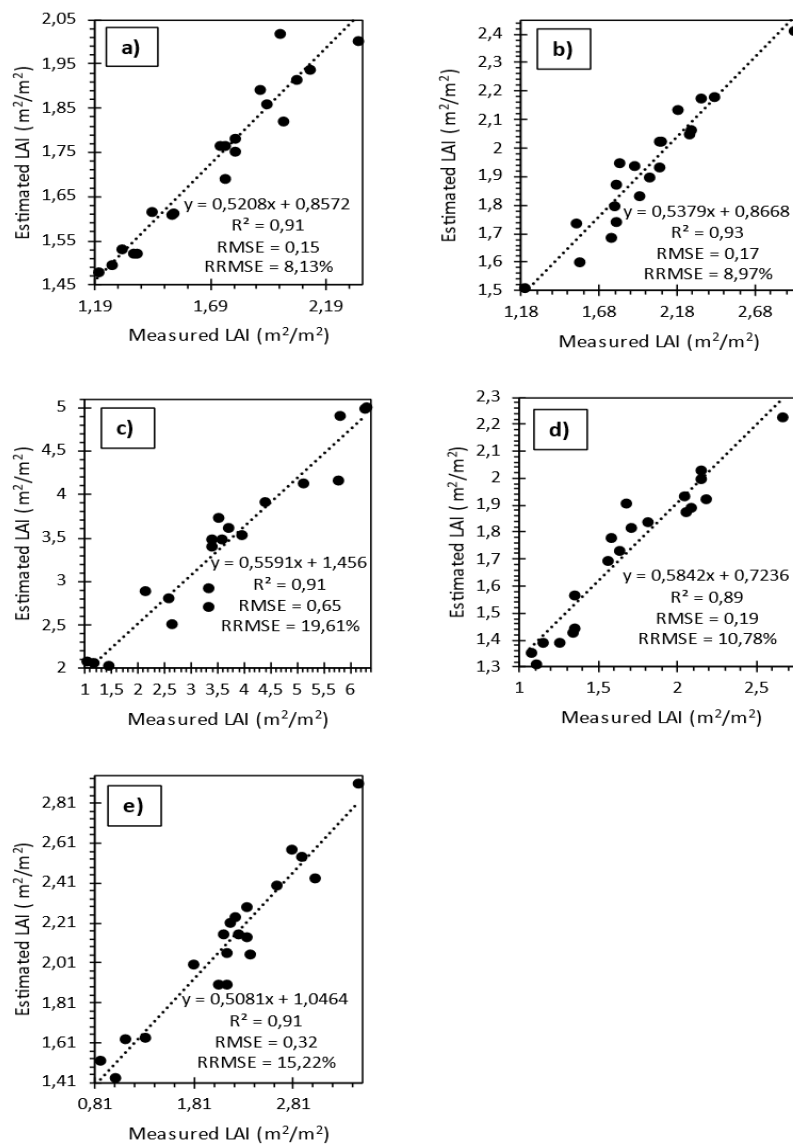


Figure 8-3: Relationship between measured and estimated LAI based on the combination of traditional, red edge-based and new VIs using the RF Model for the a) V8-V10 b) V12-V14 c) VT-R1 d) R2-R3 and e) R3-R4 maize growth stages.

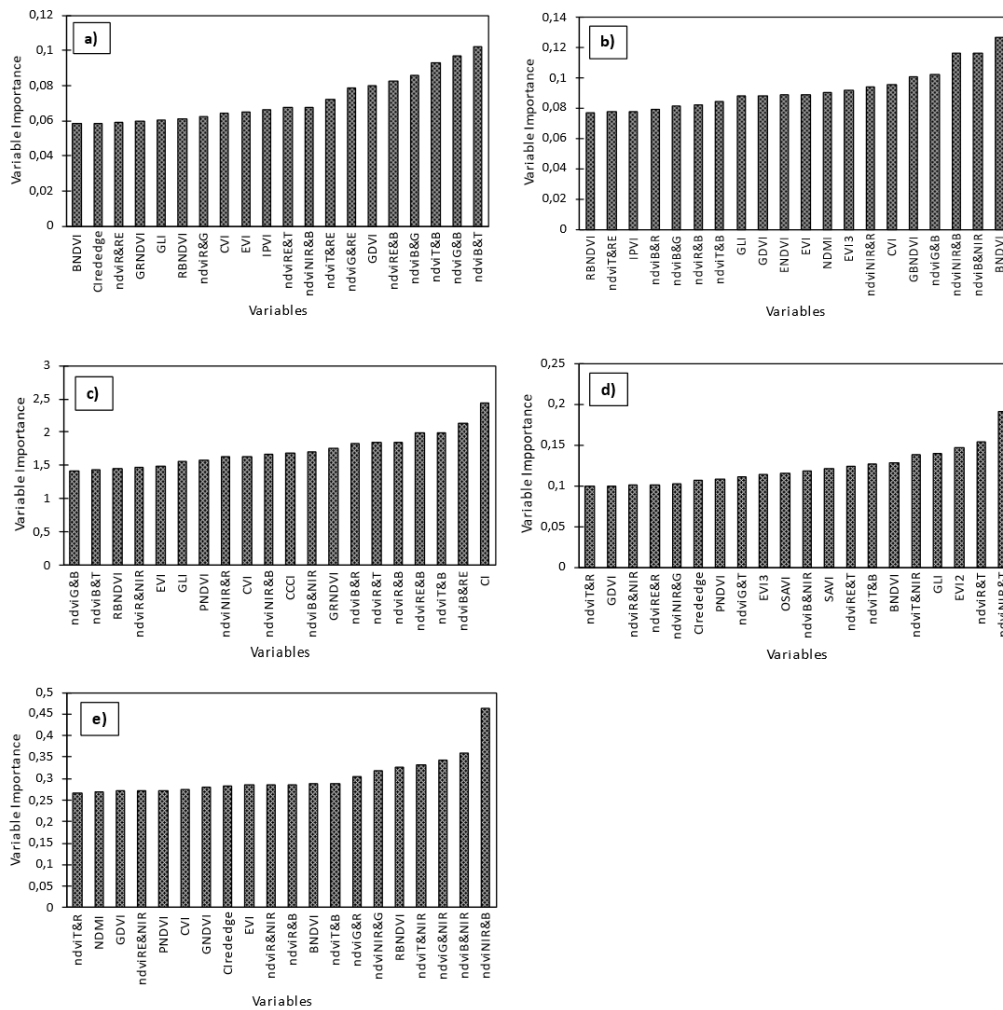


Figure 8-4: The variable importance scores of selected variables that exhibited the highest scores in predicting maize LAI for the a) V8-V10, b) V12-V14, c) VT-R1 d) R2-R3 and e) R3-R4 maize growth stages

Figure 8-5 illustrates the spatial distribution of LAI estimated using UAVs remotely sensed data at different phenological stages. Following the maize development stages considered in this study, the spatial variation of LAI increases with the increase in the growing stages. Across all maps, the eastern section of the field exhibits slightly higher maize LAI estimates in relation to the western section.

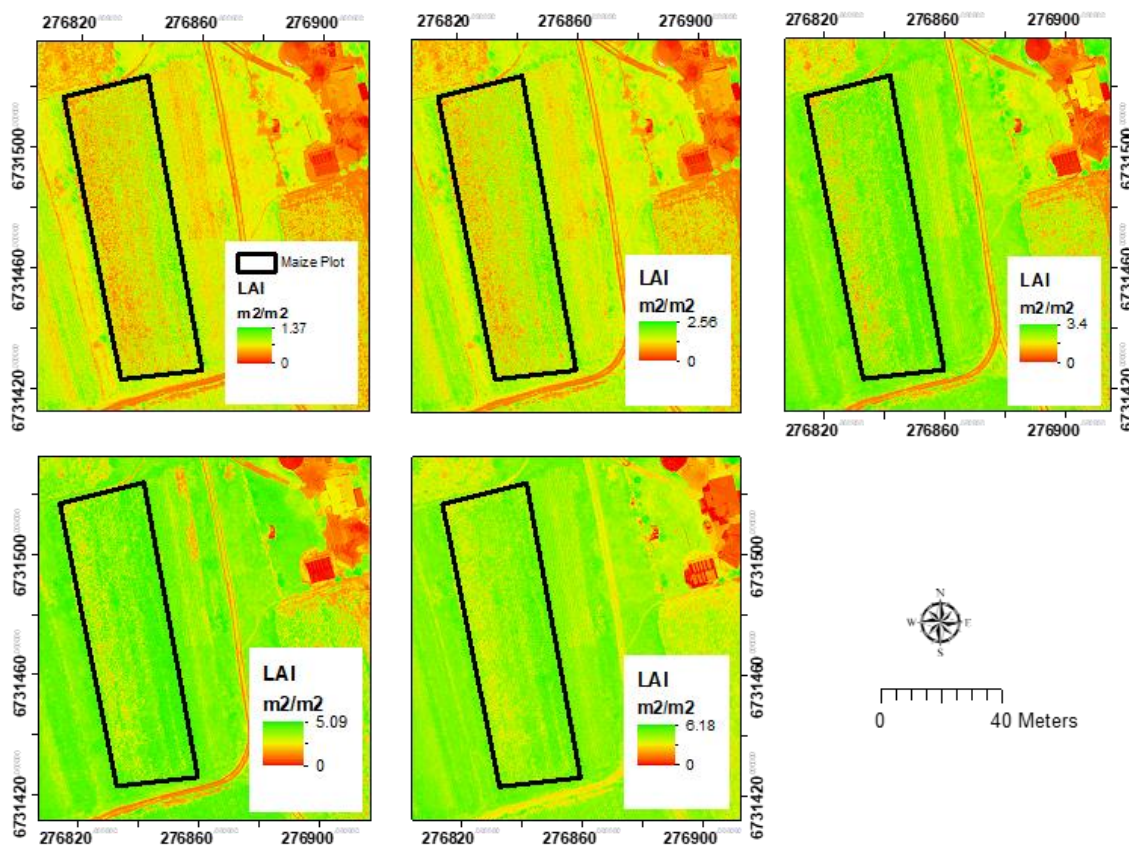


Figure 8-5: The distribution of modelled maize LAI for the a) V8-V10, b) V12-V14, c) VT-R1 d) R2-R3, and e) R3-R4 growth stages based on the RF models.

## 8.4 Discussion

This study sought to test the utility of UAV-derived VIs in estimating maize LAI across the growing season based on the Altum sensor mounted on the DJI Matrice 300 UAV data. Specifically, this study sought to estimate LAI using a combination of UAV-derived traditional, new and red edge-based bands, indices and the RF algorithm across the growing season within a smallholder farm.

### 8.4.1 Predicting maize LAI

The results of this study showed that maize LAI could be optimally estimated at the V8-V10 growth stage to an R2 of 0.91, RMSE of 0.15 m<sup>2</sup>/m<sup>2</sup> and RRMSE of 8.13%, with the most influential variables being the ndviG&B and ndviB&T derived using the green, blue and thermal spectral variables. This finding demonstrates the sensitivity of maize LAI to the blue, green and thermal regions of the EMS in the early growth stages. Literature notes that the blue section of the EMS is sensitive to green vegetation as plants use it during photosynthesis, which results in its absorption by vegetation, hence its influence in predicting LAI (Dou, Niu et al., 2019; Grajek, Ryzdyński et al., 2020). Literature also notes that the presence of bright

green vegetation on the ground during the early stages of plant growth results in a high reflectance in the green region of the EMS, which explains the sensitivity of maize LAI to the green section of the EMS at the V8-V10 stages for this study (Ren and Zhou, 2019; Sharifi and Agriculture, 2020). These findings agree with Motohka, Nasahara et al. (2010), who noticed a decrease in green reflection when leaves changed from bright green in the early to dark green towards the later stages of the season. This is attributed to the end of the formation of new leaves, which was also detected using spectral variables derived from the green section of the EMS. New leaves tend to be thinner and primarily function as a source for plant assimilates. Older leaves are thicker and are actively photosynthesizing functioning as an assimilation source for the cob. In addition, the thermal band was also amongst the most influential spectral predictor variables. This could be explained by the fact that during the V8-V10 growth stage, there is low foliage density. Literature notes that when there is low foliage density, the soil tends to absorb more heat, resulting in a high reflectance of the thermal region from the ground, which explains the sensitivity to the thermal band during this stage for this study (Filgueiras, Mantovani et al., 2019).

In estimating maize LAI during the V12-V14 growth stage, UAV-derived VIs yielded an R<sup>2</sup> of 0.93, an RMSE of 0.17 m<sup>2</sup>/m<sup>2</sup> and an RRMSE of 8.97% based on spectral variables derived from the blue and NIR regions of the EMS (BNDVI). The results of this growth stage signify the sensitivity of maize LAI to the blue and NIR sections of the EMS to maize LAI during the V12-V14 growth stage. As mentioned earlier, the blue region of the EMS plays an important role in the daily plant photosynthetic process, hence the importance of the blue waveband at this growth stage as well (Grajek, Rydzynski et al., 2020). In explaining the sensitivity of maize LAI to the NIR section of the EMS, the literature notes that this section is significant in vegetation monitoring as healthy vegetation tends to reflect highly in this section, hence its influence in estimating LAI (Fu, Yang et al., 2014; Liu, Liu et al., 2019; Martínez-Guanter, Egea et al., 2019). Specifically, maize plants' presence and increased foliage density result in leaves strongly reflecting in the NIR section of the EMS. Correspondingly, studies by He et al. (He, Zhang et al., 2019) and Tunca et al. (Tunca, Köksal et al., 2018) successfully illustrated the use of leaf optical reflectance in the NIR section of the EMS in optimally predicting LAI with an R<sup>2</sup> of 0.83 and 0.77, respectively. Specifically, the presence and increased foliage density due to leaf and stem elongation result in leaves strongly reflecting in the NIR section of the EMS.

In predicting maize LAI at the VT-R1 growth stage, UAV-derived VIs produced a prediction model with an R<sup>2</sup> of 0.91, a RMSE of 0.65 m<sup>2</sup>/m<sup>2</sup> and an RRMSE of 19.61% based on the combination of spectral variables derived from the red and NIR regions of the EMS (ndviR&T and ndviNIR&T). The EMS's red and NIR sections are significant in vegetation monitoring. Specifically, vegetation tends to absorb in the red section strongly and as mentioned earlier, reflect highly in the NIR section explaining the sensitivity of maize LAI to these sections of the EMS. As in this study, *Kanning et al.* (Kanning, Kühling et al., 2018) noted that these red and NIR band-based indices presented a higher sensitivity to crop growth parameters. These sections of the EMS are of great value in explaining LAI because the level of absorption in the red section and reflection in the NIR section reflects on the amount of vegetation present on the ground, and therefore the higher the absorption and reflection in the red and NIR sections respectively, the higher the amount of vegetation on the ground and vice versa (Ramos, Osco et al., 2020).

When predicting maize LAI at the R2-R3 growth stage using UAV-derived VIs, a model with an  $R^2$  of 0.89, an RMSE of  $0.19 \text{ m}^2/\text{m}^2$  and an RRMSE of 10.78% was obtained based on the indices derived using the blue and red wavebands together with the red edge wavebands (ndviB&RE and CI). This indicates maize LAI sensitivity to the EMS's blue, red and red edge sections in the R2-R3 growth stage. The contribution of the red edge could be attributed to the fact that chlorophyll and biomass are sensitive to the red edge (Tumlisan, 2017). Specifically, LAI is correlated to chlorophyll and biomass, hence the influence of the red edge in predicting LAI (Sun, Qin et al., 2019). Finally, in the R3-R4 growth stage, maize LAI was sensitive to the blue and NIR sections of the EMS. These produced an optimal model with an  $R^2$  of 0.91, an RMSE of  $0.32 \text{ m}^2/\text{m}^2$  and an RRMSE of 15.22%. As aforementioned, the influence of the blue and NIR bands in predicting maize LAI could be explained by the blue band's role in photosynthesis and the strong reflection of vegetation in the NIR section of the EMS.

#### **8.4.2 The performance of combining UAV-derived traditional, red edge-based and new VIs in predicting maize LAI**

Results in this study show that combining traditional, red edge-based and new VIs produced good yield prediction models for all the growth stages. This could be due to the sensitivity of the red edge region of the EMS, together with the ability of VIs to enhance vegetation features to the variation in LAI changes (Sun, Qin et al., 2019). Across the growing season, LAI changes, as shown in Table 3. During the early stages (V8-V10 and V12-V14) of the growing season, leaves are small, and as maize grows, so do the leaves. This results in the alteration of LAI across the phenological cycle. Therefore, the red edge section of the EMS better detects the spectral reflectance of these growth stages, which shifts with vegetation growth, expanding on the performance of VIs (Sibanda, Onesimo et al., 2021). Additionally, the red edge region of the EMS is also sensitive to chlorophyll content variability, which increases as maize grows. This also contributes to the high accuracy of estimating maize LAI when VIs is combined with the red edge.

Meanwhile, VIs are sensitive to distinctive spectral properties of green vegetation in the image caused by the reflectance of maize at various growth stages on particular spectral bands such as the red, red edge and NIR (Kanning, Kühling et al., 2018). Furthermore, VIs is highly correlated with LAI. This then boosts the robustness of VIs in estimating LAI. VIs are also sensitive to the LAI variability caused by the different stages of the phenological cycle and the accumulating chlorophyll content throughout the crop's growing season (Leroux, Castets et al., 2019). In this regard, high estimation accuracies of LAI are realized when the traditional, red edge-based and new VIs are combined. In addition, VIs optimize the characterization of spatial information on vegetation while increasing the range of LAI to optimal levels (He, Zhang et al., 2019). The results of this study are consistent with those of Fu, Yang et al. (2014), who reported that models derived from the combination of VIs and band parameters could effectively increase the accuracy of winter wheat biomass estimation compared with the performance of bands or VIs as stand-alone data. Another study by He, Zhang et al. (2019) estimated the rice-LAI based on a new vegetation index and concluded that combining the NIR and red edge bands best-predicted rice LAI ( $R^2 = 0.6$ , RMSE =  $1.41 \text{ m}^2/\text{m}^2$ ).

Although the findings of this experimental study address the overarching objective, the caveats of UAV-derived datasets need to be stated as they negatively impact related studies. For

instance, most studies based on UAV remotely sensed data cover small spatial extents due to the battery power's inhibited duration and weight (Boukoberine, Zhou et al., 2019). Batteries with limited power or are heavy tend to inhibit the flight plan and time to a small area. This limits these earth observation technologies and associated experimental studies to farm or field scales.

## **8.5 Conclusion**

This study sought to test the utility of UAV-derived VIs in estimating maize LAI across the growing season based on the Altum sensor mounted on the DJI Matrice 300 UAV data in a smallholder farm. Based on the findings of this study, it can be concluded that:

- Maize LAI can be optimally estimated using UAV-derived VIs across the growing season.
- The blue, green, red edge and NIR sections of the EMS are influential in estimating Maize LAI
- Combining traditional, red edge-based and new VIs is useful in attaining high LAI estimation accuracies.

Quantitative assessments of maize LAI attained in this study are a step towards developing non-destructive and cost-effective methods for routine and timely monitoring of maize LAI in smallholder farms for improved crop health and productivity estimation. The findings indirectly contribute to a better understanding of maize crop health and crop monitoring efforts for improved food security.

## **9 PREDICTING MAIZE YIELD IN SMALLHOLDER CROPLANDS USING UAVS-DERIVED MULTI-TEMPORAL REMOTELY SENSED DATASETS**

Ndlovu HS, Odindi J, Sibanda M, Mutanga O, Clulow A, Chimonyo VGP and Mabhaudhi T

### **9.1 Introduction**

Agriculture continues to be the mainstay of the economies of most Southern African countries, providing over 35% of their gross domestic product, 70-80% of the available employment opportunities and about 30% foreign exchange. Furthermore, the agricultural sector provides livelihoods to over 70% of the country's population through smallholder farming, which constitutes the majority of food producers (Jin, Azzari et al., 2019). However, despite the sector's fundamental role in the region's economies and food security, like many other regions of the African continent, abject poverty and deepening hunger continue to stall the development prospects. This is demonstrated by, among others, the increasing number of people living below the poverty line and malnourished children. These trends could reduce the region's objective of ending poverty and hunger by 2030 as the current sustainable development goals stipulated. Whereas there are many challenges accelerating food insecurity, the principal cause is the decline in the production of staple crops. Specifically, drastically decreasing yields of critical food crops such as maize are attributed to, among others, the utility of rudimentary farming practices, the low inputs that characterize conventional farming systems, lack of incentives and appropriate technologies to optimize production, especially on smallholder farms (Tan, Zhang et al., 2020). Despite their potential, the characteristic nature of smallholder farming systems has presented a low predisposition to invest in improved agricultural technologies that can optimize agricultural productivity, hence mitigating food insecurity and poverty.

As mentioned, smallholder farming is the most prevalent maize production in southern African countries. In a recent sub-national census, Jin, Azzari et al. (2019) showed that 50% of food calories in the region were produced on farms of less than 5 ha in size. This region's annual demand for maize is expected to increase by 2.4% per annum up to 2025 (Dhau, Adam et al., 2018). Hence, exploring approaches to maximize maize production on smallholder farms is necessary to mitigate poverty and address food and nutritional insecurities. To achieve this, frequent monitoring across the growing season is critical in assessing the value of the adopted techniques and approaches to improve smallholder farm productivity (Tunca, Köksal et al., 2018).

Traditionally, several approaches that include ground observations, surveys and measurements have been adopted in crop monitoring (Mditshwa, 2017). However, these approaches are limited by their high labour and financial costs and, therefore, not ideal for continuous and time-efficient crop monitoring (Jégo, Pattey et al., 2012). Meanwhile, satellite remote sensing has emerged as a better alternative for crop monitoring and yield estimation (Fernandez-Ordoñez and Soria-Ruiz, 2017; Leroux, Castets et al., 2019). For instance,

Aghighi, Azadbakht et al. (2018) demonstrated that Landsat 8 multispectral remotely sensed data could predict silage maize yield with an optimal  $R^2$  of 0.87, while Kayad, Sozzi et al. (2019) utilized Sentinel-2 multispectral instrument derived VIs to estimate corn grain yield spatial variability with an  $R^2$  of 0.6. Despite the successes associated with these studies, the utilization of such multispectral satellite datasets in crop monitoring and yield estimation in smallholder farms is limited by their relatively coarse spatial and temporal resolutions (Stratoulis, Tolpekin et al., 2017). Although numerous satellite images have high spatial resolutions (e.g. SPOT, Worldview and QuickBird and PlanetScope), they are not cost-effective for monitoring smallholder crops. Moreover, they are often associated with processing complexities, making them unsuitable for monitoring and estimating maize yield at a farm scale (Jin, Azzari et al., 2019; Chivasa, Mutanga et al., 2020).

On the other hand, UAVs, also known as drones, have emerged as a prospective alternative source of remotely sensed data suitable for mapping and monitoring crop productivity at a farm-to-field scale (Maes, Huete et al., 2018). With advancements in technology, the weight and size of multispectral cameras have been drastically reduced to ease mounting on UAVs for use in precision agriculture (Candiago, Remondino et al., 2015). UAV systems provide high spatial resolution remotely sensed data at user-defined revisit frequencies and areas of interest, hence time-efficient and cost-effective agricultural applications such as yield modelling (Schut, Traore et al., 2018; Ziliani, Parkes et al., 2018). Furthermore, in estimating maize crop yield using temporal remotely sensed datasets, it is not very clear whether the ultimate plant biomass (inclusive of the grains), the actual grain biomass (excluding the foliage and stem) or the biomass of grain yield as a proportion of ultimate plant biomass exhibits more accurate yield estimates. This has further compounded the challenge in using remotely sensed data to estimate the yield of crops such as maize when compared with crops such as cabbages and spinach (Abdel-Rahman, Mutanga et al., 2014) where biomass is derived from the foliage which in turn directly interacts with the spectral signatures used in yield estimation. In this regard, very few studies have utilized UAV-derived data in estimating maize yield at smallholder farms in Sub-Saharan Africa. Hence, there is a need to test the utility of multispectral and thermal drone-derived remotely sensed datasets to not only estimate maize yield in smallholder farms of the southern African region but also identify the specific yield variables that optimally facilitate the accurate estimation of yield. Testing drone-derived remotely sensed data in estimating maize yield is important for optimizing agricultural production, a challenge using coarse spatial resolution image data. Therefore, this study aimed to test the utility of UAV-derived data in estimating maize yield across the growing season in a smallholder farm. To address this overarching objective, the study sought to; i) predict maize yield using UAV remotely sensed data in conjunction with the RF algorithm and determine the most optimal growth stage for yield prediction, and ii) compare the performance of using the actual grain biomass (excluding the foliage), the ultimate plant biomass (inclusive of the grains and foliage) and the biomass of grain yield as a proportion of ultimate plant biomass in estimating maize yield. To achieve this, the combination of bands and VIs and the RF algorithm regression ensemble was used.

## 9.2 Materials and Methods

### 9.2.1 Study area

This study was conducted on a smallholder farm in Swayimane, KwaZulu-Natal, South Africa. The farm is between 29°31'24"S and 30°41'37" E (Figure 9-1). The area has a sub-humid climate with an average temperature of 20°C and average precipitation of 900-1200 mm per annum (Miya, Modi et al., 2018). The study was conducted on a 2699.005 m<sup>2</sup> maize field where the maize was sown in November with approximately 160 days of the growing season.

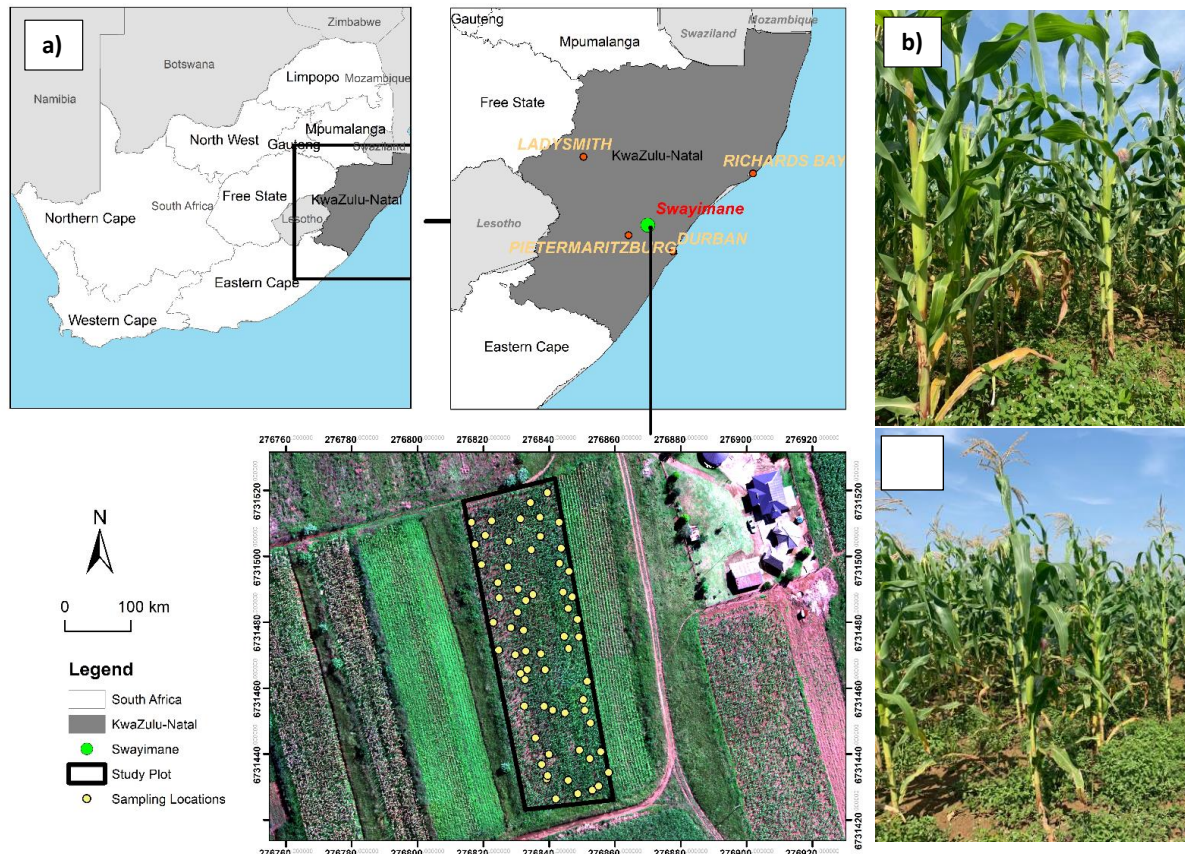


Figure 9-1: a) Location of the experimental field plot in Swayimane, KwaZulu-Natal, South Africa, and b) & c) The maize field.

The maize growth stages were divided into two sub-groups, the vegetative growth stages, which are the early growth stages covering the V8-V10, V12-V14 and VT-R1 growth stages and the reproductive growth stages covering the R2-R3 and R3-R4 growth stages. \*Refer to Table 9-1 in Chapter Two for more details on the growth stages.

### 9.2.2 Agricultural practices

Maize seeds were sown by hand in February 2021, and weeds were constantly hand removed throughout the growing season. Cow manure, instead of chemical fertilizers, were used to optimize soil fertility. The maize crops in the study area were rain-fed.

### **9.2.3 Sampling strategy for yield measurements**

To optimize the sampling procedure, a polygon of the entire experimental field was generated in Google Earth Pro and imported into ArcGIS 10.6. Subsequently, 63-point locations were generated inside the experimental field plot polygon based on stratified random sampling to determine the sampling points for yield data collection. These points were then uploaded into a Trimble handheld GPS with a sub-meter accuracy of 30 cm. The GPS was then used to locate and navigate the sampling points in the field. A square meter plot was established at each location, and maize plants near each sample point were selected for yield estimation. To determine the absolute maize plant biomass, the sample plants (the entire stalk and the cob with the grains) were harvested manually during the reproductive stage R3-R4, which marked the end of the growing season of maize. These were lightly shredded to fit in the brown bags and appropriately labelled. The entire plant biomass was first oven-dried at 60°C for 48 hours and then weighed to determine the entire plant biomass before separating the cobs from the plant. After the separation, the grains were shelled to determine the grain yield biomass. The dry grains were weighed, and grain yield was calculated as the weight in kg/m<sup>2</sup>. The absolute plant biomass divided the dry grains to determine the proportional yield. These weights were then recorded on an Excel spreadsheet, together with the coordinates of each sampling point.

### **9.2.4 Calculation of VIs**

The UAV-derived image bands were used to compute VIs, and both spectral bands and indices were used to predict maize yield. The VIs selected and utilized in this study are summarized in Table 9-1. These VIs were chosen based on their performance in literature (Bala and Islam, 2009; Mditshwa, 2017; Tumlisan, 2017). The indices directly relate to the chlorophyll content of the plant, which indirectly relates to yield.

Table 9-1: VIs used in this study.

Vegetation Index	Abbreviation	Equation	Reference
Normalized Vegetation Index	NDVI	$\frac{NIR-RED}{NIR+RED}$	(Wahab, Hall et al., 2018)
Enhanced Vegetation Index	ENDVI	$\frac{(NIR + GREEN) - (2 \times BLUE)}{(NIR + GREEN) + (2 \times BLUE)}$	(Zhang, Lan et al., 2009)
Soil Adjusted Vegetation Index	SAVI	$\frac{(NIR - RED)}{(NIR + RED + L)} \times (1 + L)$	Ngie and Ahmed (2018)
Optimized Soil Adjusted Vegetation Index	OSAVI	$\frac{(NIR - RED)}{(NIR + RED + 0.16)} \times (1 + 0.16)$	Liu, Liu et al. (2019)
Simple Ratio	SR	$\frac{RED}{NIR}$	Kanning, Kühling et al. (2018)

### 9.2.5 Data Analysis

A correlation between the grain and the biomass data was determined to evaluate whether there was a link between the accumulated biomass and the actual yield at the R3-R4 growth stage. A Pearson product-moment correlation test was conducted in this regard following a data normality test, which indicated that the data did not significantly deviate from the normal distribution.

To test the relationship between biomass, grain yield and proportional yield determined at the R3-R4 stage, the collected 63 yield samples and UAV data (i.e. combination of bands and VIs data) were divided into training (70%) and test (30%) datasets to derive models using the RF algorithm in R statistical package. The RF algorithm was adopted in this study as it is a non-parametric statistical technique that uses a bagging-based approach to build an ensemble of regression trees while ranking important variables that produce an independent measure of prediction error Prasad, Iverson et al. (2006). In R, the *ntree* and *mtry* parameters were optimized using the *doBest* function. The function selected the *ntree* and *mtry* parameters with the lowest RMSE to determine the most influential parameters. These parameters were tuned to 600 for *ntree* and five for *mtry*. In addition, the most optimal growth stage at which the combination of bands and VIs were highly correlated to the yield was assessed to determine the most suitable period to predict maize yield before harvest.

Test data (30%) was used to evaluate the model performance of the derived models. Performance indicators such as  $R^2$ , RMSE and RRMSE (see Equations 7-3 and 7-4) were determined and used to assess the accuracy of each model. The model that yielded a low RMSE and high  $R^2$  at a stage with adequate time before harvest for intervention was set aside and used to predict yield. The most optimal model was then used to create a yield map for the study site in ArcMap 10.6.

## 9.3 Results

### 9.3.1 Descriptive statistics

The highest maize biomass, grain yield and proportional yield were 8.61 kg/m<sup>2</sup>, 4.4 kg m<sup>2</sup> and 0.76 kg/m<sup>2</sup>, and the lowest was 3.24 kg/m<sup>2</sup>, 0.16kg/m<sup>2</sup>, and 0.04 kg/m<sup>2</sup>, respectively. There was considerable variation in maize yield samples in the study. The standard deviation was 1.45, 1.08 and 0.15 for biomass, grain yield and proportional yield, respectively. Furthermore, a strong ( $R^2$  of 0.74) positive correlation between the grain yield samples and the overall biomass of the maize plants was attained. Figure 9-2 shows the relationship between yield and biomass.

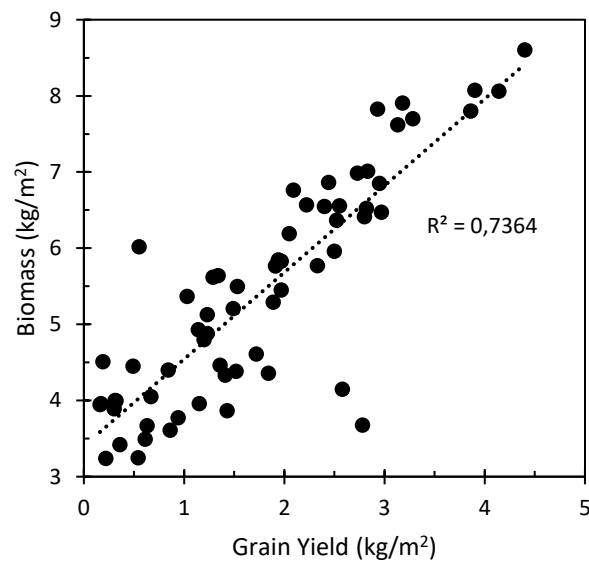


Figure 9-2: Correlation between the grain yield and biomass at the R3-R4 stage using all samples.

### 9.3.2 Derived maize yield prediction models and their accuracies

Figure 9-3 illustrates the model accuracies obtained in predicting the biomass, grain yield and proportional yield based on the RF algorithm. The accuracies of the prediction models varied greatly across the maize growing season. For example, when estimating the absolute plant biomass, the V8-V10 growth stage yielded the poorest model, with an  $R^2$  of 0.80 and RMSE of 0.94 kg/m<sup>2</sup>. The biomass prediction improved in the V12-V14 growth stage model ( $R^2 = 0.85$  an RMSE = 0.72 kg/ m<sup>2</sup>). Similarly, the VT-R1 and R2-R3 models predicted biomass at an improved  $R^2 = 0.89$ , RMSE = 0.77 kg/m<sup>2</sup> and  $R^2 = 0.89$ , RMSE = 0.88 kg/m<sup>2</sup>, respectively. The optimal model in estimating biomass was derived from the R3-R4 model, with an  $R^2$  of 0.91 and RMSE of 0.61 kg/m<sup>2</sup> (Figure 9-3 (e)). The most optimal variables in estimating biomass were ENDVI, the red edge band, NIR and NDVI, in order of importance (Figure 9-4 (e)).

Similarly, the V8-V10 model demonstrated the lowest prediction accuracy in estimating the grain yield ( $R^2 = 0.85$  and RMSE = 0.6 kg/m<sup>2</sup>). V12-V14 and VT-R1 followed this with an  $R^2$  of

0.89, RMSE of 0.12 kg/m<sup>2</sup> and, R<sup>2</sup> of 0.85, RMSE of 0.1 kg/m<sup>2</sup>, respectively. The prediction accuracy increased significantly with the R2-R3 model (R<sup>2</sup> = 0.95 and RMSE = 0.09 kg/m<sup>2</sup>). The R3-R4 model optimally predicted the grain yield with the lowest RMSE = 0.03 kg/m<sup>2</sup> and R<sup>2</sup> = 0.92 (Figure 9-3 (e)). The variables with the highest influence in the grain yield model were ENDVI, NIR, NDVI and the red edge band in ascending order of importance (Figure 9-4(e)).

When predicting the proportional yield, the V12-V14 model produced the lowest prediction accuracy with an R<sup>2</sup> of 0.92 and RMSE of 0.11 kg/m<sup>2</sup>. The prediction of proportional yield improved in the V8-V10, VT-R1 and R2-R3 models with an R<sup>2</sup> of 0.91, RMSE of 0.09 kg/m<sup>2</sup>; R<sup>2</sup> of 0.92, RMSE of 0.06 kg/m<sup>2</sup> and R<sup>2</sup> = 0.92, RMSE = 0.07 kg/m<sup>2</sup>. The optimal model for estimating proportional yield produced an R<sup>2</sup> of 0.95 and RMSE = 0.07 kg/m<sup>2</sup> (Figure 9-3 (e)). The most suitable predictor variables included NDVI, the green, NIR and red edge bands (Figure 9-4 (e)).

The results varied greatly in comparing the performance of the maize biomass, grain yield, and proportional yield variables in predicting yield across all growth stages (Figure 9-3). For example, when estimating yield at the V8-V10 growth stage, the proportional yield model exhibited the poorest prediction accuracy with an RRMSE of 30.43%, followed by the grain yield model with an RRMSE of 27.99%. Comparatively, the most optimal model in estimating yield during the V8-V10 growth stage was the biomass model with an RRMSE of 15.42% (Figure 9-3(a)). The most important variables include the red and blue bands, SAVI and OSAVI (Figure 9-4).

Similarly, the proportional yield model yielded the poorest model with an RRMSE of 39.91%, followed by the biomass model with an RRMSE of 15.37% at the V12-V14 growth stage. The grain yield model optimally predicted maize yield with the lowest RRMSE = 5.44% at the V12-14 (Figure 9-3 (b)). The most optimal variables for this prediction were the green, red edge, red and blue bands (Figure 9-4 (b)).

In predicting yield at the VT-R1 growth stage, the proportional yield model produced the highest RRMSE of 17.56%. The prediction accuracy improved with the biomass and grain yield models (RRMSE = 12.56% and 5.08%, correspondingly) (Figure 9-3 (c)). The variables with the highest influence in the grain yield model were SAVI, NDVI, ENDVI and the green band, in order of importance (Figure 9-4 (c)).

When predicting yield in the R2-R3 growth stage, the highest RRMSE of 22.57% was obtained by the proportional yield model. The biomass model improved the prediction by a magnitude of 8.1%, i.e. RRMSE = 14.47%. Similarly, the grain yield model was optimal for estimating yield at the R2-R3 growth stage (Figure 9-3 (d)). The red-edge band, NDVI, ENDVI and SR were the most influential variables for this model (Figure 9-4(d)).

For the R3-R4 growth stage, the proportional yield exhibited the lowest prediction accuracy with an RRMSE of 21.78%. The prediction of yield improved significantly with the biomass model (RRMSE = 12.97%) and even greater with the grain yield model (RRMSE = 2.21%) (Figure 9-3(e)). The most influential variables for this prediction were NDVI, NIR, ENDVI and the red edge band (Figure 9-4 (e)). Then, Figure 9-5 shows the modelled spatial variation of

biomass, grain yield and proportion of grain yield. Based on the maps, biomass, grain yield, and proportion of grain yield increased from the west to the east of the experimental fields.

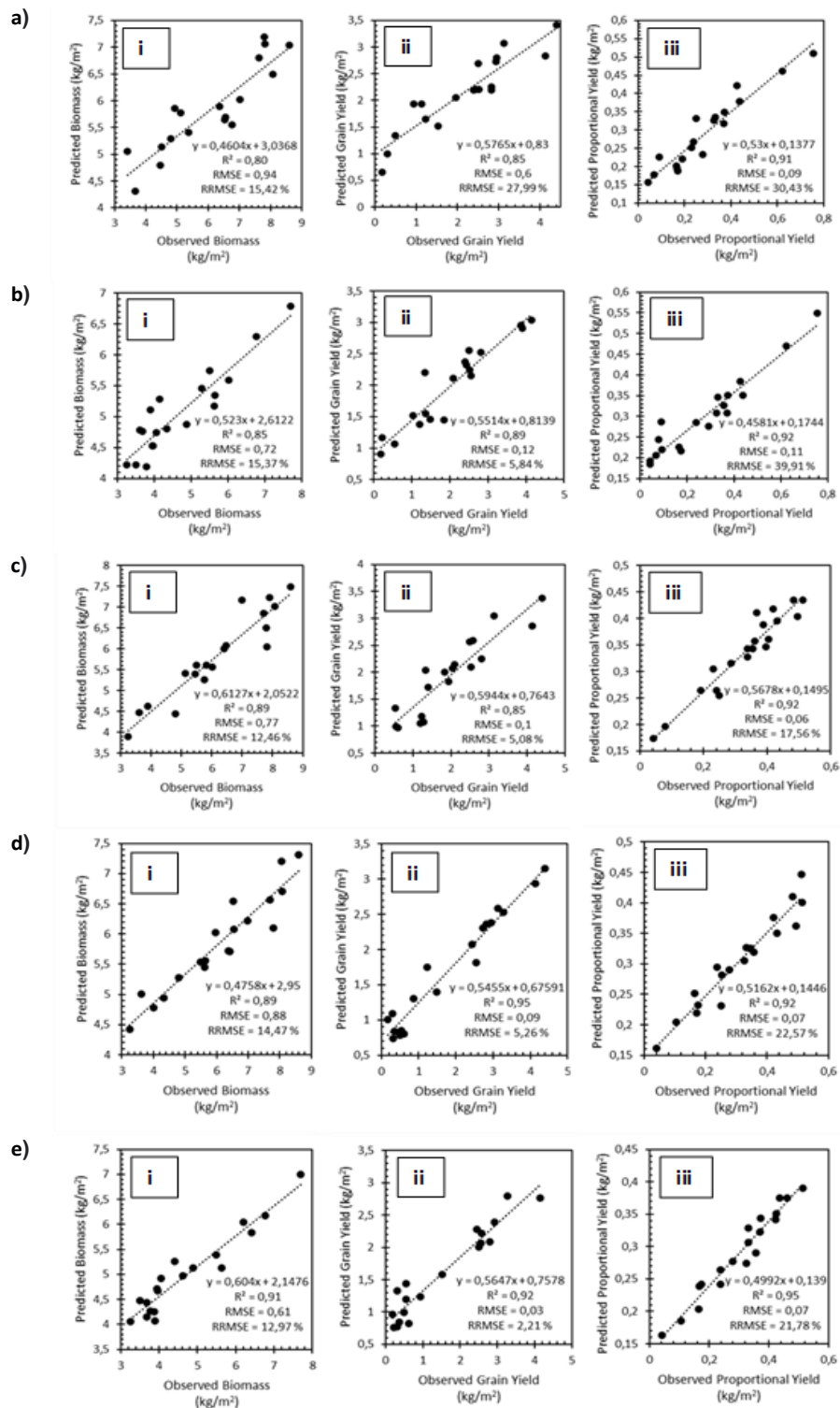


Figure 9-3: Relationship between observed and predicted i) biomass, ii) grain yield and iii) proportional yield based on the combination of bands and VIs using the RF Model for a) V8-V10 b) V12-V14 c) VT-R1 d) R2-R3 and e) R3-R4 maize growth stages.

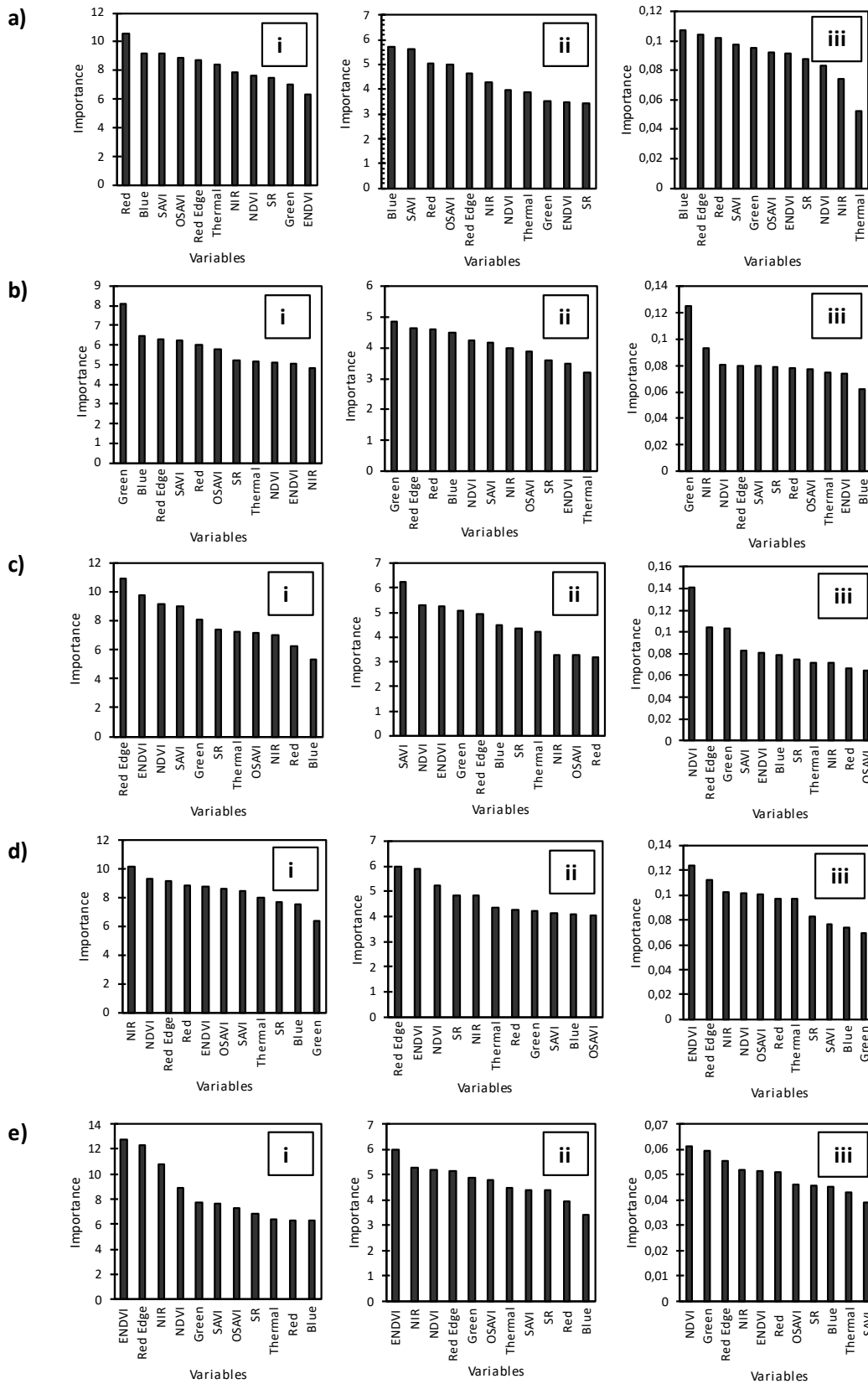


Figure 9-4: The variable importance of the i) biomass, ii) grain yield and iii) proportional yield models for a) V8-V10, b) V12-V14, c) VT-R1, d) R2-R3 and e) R3-R4 maize growth stages.

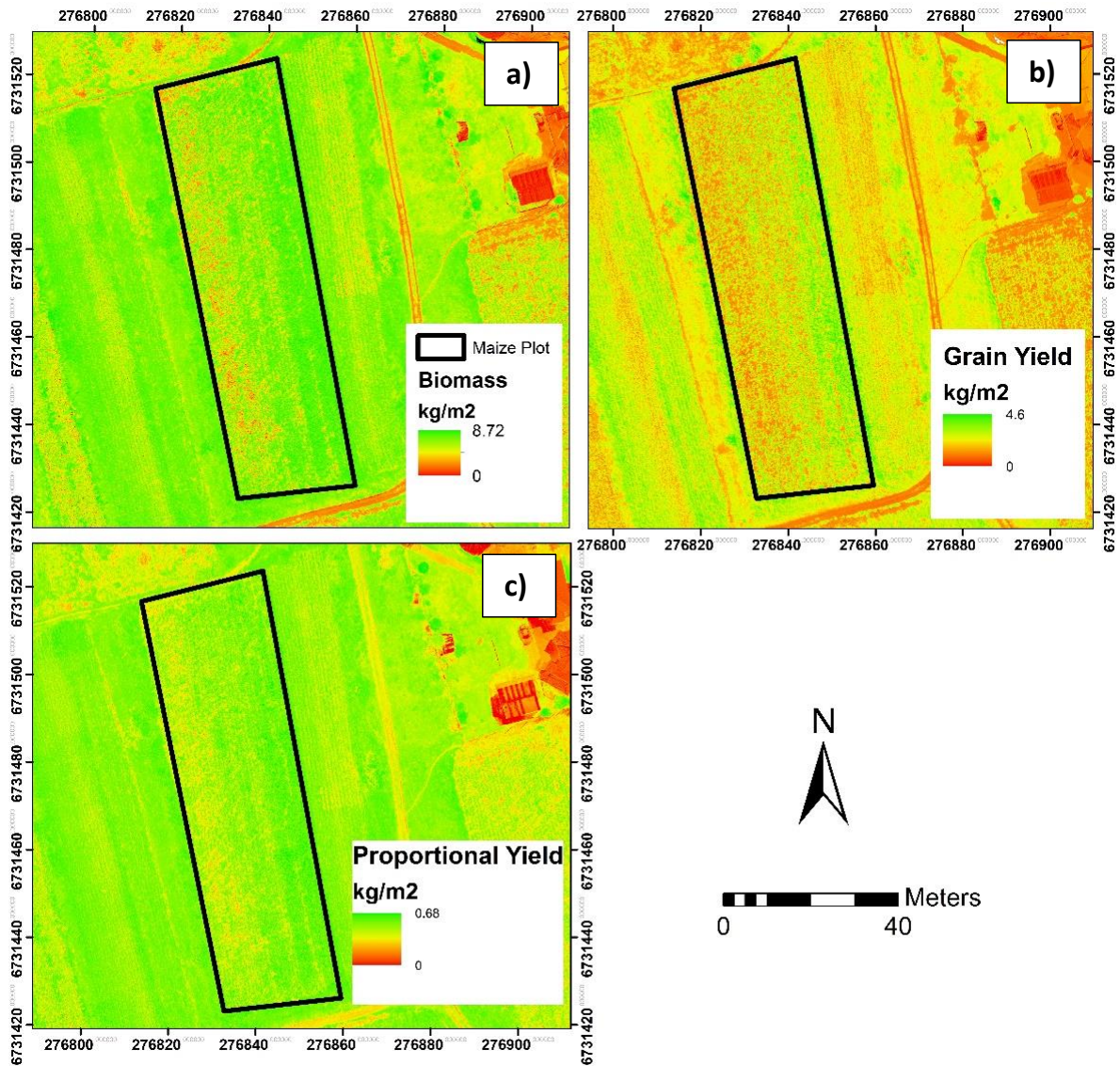


Figure 9-5: The spatial distribution of modelled maize a) biomass, b) grain yield and c) proportional yield based on the most optimal RF models.

## 9.4 Discussion

This study sought to test the capability of UAV-derived data in estimating maize yield across the growing season based on the Altum sensor mounted on the DJI Matrice 300 UAV. Specifically, this study sought to predict maize yield using UAV images and the RF algorithm in smallholder farms.

### 9.4.1 Maize yield prediction models

The results of this study show that the early growth stages of the crop yielded lower overall accuracies for the biomass, grain yield and proportional yield, followed by some improvements

in the later stages of growth (Figure 9-3). Specifically, the V8-V10, V12-V14 and VT-R1 growth stages had lower overall accuracies when compared to the R2-R3 and R3-R4 growth stages. Several studies (Guindin-Garcia, 2010; Son, Chen et al., 2013; Al-Gaadi, Hassaballa et al., 2016; Chivasa, Mutanga et al., 2017) have noted that in the early stages of crop development, vegetation reflectance is affected by the soil background, which explains the low performance of UAV data in predicting maize biomass, grain yield and proportional yield at the early (vegetative growth) stages of this study. At this stage, the maize leaves are not fully grown, exposing the surrounding soil and interfering with the plant's reflectance as the sensor also picks up the soil reflectance (Zhang, Niu et al., 2019).

In contrast, the later growth stages of the crop yielded higher overall accuracies. Specifically, the R2-R3 and R3-R4 growth stages had higher accuracies when compared to the V8-V10, V12-V14 and VT-R1 stages. The high performance of the UAV data in predicting maize yield at the R2-R3 and R3-R4 stages of the growth cycle can be explained by existing literature which has reported significantly high accuracies in the prediction of maize yield at the late (reproductive) stages of the crop (Guindin-Garcia, 2010; Mditshwa, 2017). Literature notes that at this stage, the maize leaves have grown to mid-density, covering the surrounding soil, and therefore crop reflectance is not impacted by the soil background (Mkhabela, Mkhabela et al., 2005; Tumlihan 2017; Tunca, Köksal et al., 2018). When plants have grown to mid-density, there is canopy coverage, meaning the biomass production has reached its most mature stage, making it possible to remotely sense vegetation without any interferences from the ground, such as soil (Kayad, Sozzi et al., 2019). At this stage, when biomass production has reached its peak, it is most closely related to yield, which explains why the model accuracies for these stages were higher than those of the earlier stages of growth (Ngie and Ahmed 2018; Li, Xu et al., 2020).

Regarding model variable importance, SAVI, OSAVI, and the blue and red bands were more important in predicting early stages than in the late stages of the crop phenological cycle. The value of SAVI and OSAVI can be attributed to their ability to suppress soil background, hence better prediction at minimal leaf coverage and soil exposure (Ren and Zhou, 2019; Zhang, Zhang et al., 2019). The importance of the blue and red bands for these models can be explained by soil being more dominant than vegetation in the early stages of the crop resulting in high reflectance in the blue and red region of the EMS (Ngie and Ahmed, 2018).

Comparatively, NDVI, ENDVI, the green, red, red edge and NIR bands were important in the prediction models at the R2-R3 and R3-R4 crop growth stages. The importance of NDVI and ENDVI in these models could be a result of the fact that when the reflectance measurements for the R2-R3 and R3-R4 growth stages were taken, a saturation of the plant canopy had not occurred, the plant canopy had only accumulated to mid-density, and there is a good relationship between NDVI and ENDVI and biomass and yield at mid-density canopies, which characterize the R2-R3 and R3-R4 maize growth stages (Awad, 2019). The importance of the green, red, red edge and NIR bands in the models of the R2-R3 and R3-R4 growth stages for this study can be attributed to the fact that there was a dominance of vegetation which reflects strongly in the green and NIR regions of the EMS and highly absorbs in the red and red edge regions of the EMS (Khaliq, Comba et al., 2019; Marcial-Pablo, Gonzalez-Sanchez et al., 2019).

#### 9.4.2 Determining the most optimal growth stages and variables for yield prediction

The best-fit model for predicting maize biomass and grain yield was obtained at the R3-R4 growth stage, with ENDVI and the red edge band being the most important variables for predicting maize biomass and ENDVI and NDVI being the most important for the prediction of grain yield. The influence of the ENDVI, NDVI and the red edge in the prediction at this stage could be explained by the good relationship between the two indices and biomass and yield at mid-density canopies before saturation (Mutanga, Adam et al., 2012; Tan, Zhang et al., 2020). On the other hand, the literature notes that the red edge section of the EMS is related to chlorophyll and biomass, which directly relates to yield (Dube, Mutanga et al., 2017; Sibanda, Mutanga et al., 2017). Generally, mid-density canopies are characterized by a high amount of biomass, associated with high chlorophyll content and carbon assimilation, which are sensitive to the red edge section of the EMS (Sibanda, Onisimo et al., 2021). Furthermore, a mid-density canopy like in the R3-R4 growth stage results in high ENDVI and NDVI values as well as a strong absorption in the red edge region of the EMS, hence their strong influence in the prediction of biomass and grain yield when compared to the other variables (Raeva, Šedina et al., 2019). In addition, the best-fit model for predicting proportional maize yield was obtained in the VT-R1 growth stage, with NDVI and SAVI being the most important variables for predicting proportional yield. The significance of NDVI and SAVI in the prediction model of maize of proportional yield at this stage can be attributed to the fact that this is the middle stage where the canopy has not grown to mid-density resulting in significant soil exposure (Mditshwa, 2017). This then results in SAVI being important in suppressing the soil background effect and allows NDVI to perform well as it has a good relationship with the biomass and yield at this stage's canopy level because the canopy has not yet reached saturation, as canopy saturation hinders the performance of NDVI (Mutanga, Adam et al., 2012).

The best-fit model for maize biomass and grain yield was obtained at the R3-R4 reproductive development stage and proportional yield at the VT-R1 vegetative development stage (78 and 62 days after emergence) of the growth cycle. Using the R3-R4 growth stage for biomass and grain yield prediction could be late for adopting any effective measure before harvest. A significant relationship was found at the VT-R1 (62 days after emergence) growth stage for biomass and grain yield. Our findings indicate this is the optimal stage at which maize yield could be predicted before harvesting. The most significant variables for the optimal biomass, grain yield and proportional yield prediction models were the red edge band and ENDVI, SAVI and NDVI, ENDVI and the red edge band respectively.

Furthermore, the grain yield produced higher prediction accuracies in estimating maize yield for most of the crop's growth stages (V12-V14, VT-R1, R2-R3 and R3-R4) compared to the absolute plant biomass and the biomass of grain yield as a proportion of ultimate plant biomass. The absolute plant biomass was only optimal in the V8-V10 growth stage, and the proportional yield produced the poorest yield prediction accuracies in all growth stages. Therefore, the grain yield was the most optimal in estimating maize yield.

The obtained validation accuracies and their variable importance match those from previous findings, where the prediction was conducted on maize using different space-borne sensors. For example, Battude, Al Bitar et al. (2016) estimated the biomass and maize yield over a

large area using Sentinel-2 data and concluded that remotely sensed data could accurately predict the biomass and yield throughout the phenological cycle, with prediction accuracies ranging from 0.8-0.9. Ngie and Ahmed (2018) successfully estimated maize grain yield using SPOT 5 data in the Free State province of South Africa, where prediction models with accuracies of 0.92 and 0.9 were achieved using SAVI and NDVI. Mditshwa (2017) used GIS and remote sensing to estimate maize grain yield from the different growth stages and concluded that NDVI and SAVI are good yield predictors. Unlike the current study, which was conducted on a small area using high spatial and temporal resolution datasets, the studies mentioned above were conducted at large spatial extents using Sentinel-2 and Landsat-8. In this study, adopting a sensor mounted on a UAV has demonstrated its value in predicting maize yield in a smallholder farm.

## **9.5 Conclusion**

Based on UAV remotely sensed data, this study aimed to predict maize yield (biomass, grain yield and proportional yield) across the growing season in a smallholder farm. The following conclusions were drawn:

- UAV-derived data optimally predicted maize yield during the R3-R4 growth stage using ENDVI, NDVI and the red edge band.
- The VT-R1 stage was the most optimal stage for the early prediction of maize yields using SAVI, NDVI, ENDVI and the red edge band.
- The grain yield models produced higher accuracies in estimating maize yield compared to the absolute plant biomass and the biomass of grain yield as a proportion of absolute plant biomass models.

The characterised variations in field productivity can assist farmers and decision-makers in identifying low-yield areas within the field to adjust their management practices to maximize farm productivity. These findings highlight the utility of UAV systems in optimizing agricultural production through precision farming on smallholder farms, which is necessary for poverty alleviation and food and nutritional security.

## 10 EXPLORING THE PROSPECTS OF USING LANDSAT, SEBS AND METRIC-EFFLUX MODELS AND A CLOUD COMPUTING INFRASTRUCTURE IN THE ESTIMATION OF $ET_c$ USING UAV MULTI-SPECTRAL IMAGERY

Nyaawose A, Odindi J, Sibanda M, Mutanga O, Clulow A, Chimonyo VGP and Mabhaudhi T

### 10.1 Introduction

Crop evapotranspiration ( $ET_c$ ) is the key water balance component representing crop water requirements.  $ET_c$  can be used to quantify the amount of water required in rain-fed and irrigated agricultural fields to maximize farm and water productivity while mitigating water resource depletion (Bansouleh, Karimi et al., 2015).  $ET_c$  is estimated to assess crop water use or stress, and it can provide invaluable information to facilitate improved agricultural water resource management (Bansouleh, Karimi et al., 2015; Dzikiti, Volschenk et al., 2018). Shortages of water in semi-arid regions during the growing season decrease crop production and yield, especially in small-scale rain-fed agricultural systems (Adetoro, Ngidi et al., 2022).

Rain-fed smallholder farms, the most common communal cropping practice in Southern Africa, generally contribute substantially to food production and improving livelihoods (Masiza, Chirima et al., 2022). Maize (*Zea mays* L) is one of the most produced crops in rain-fed smallholder farms because its production can occur in diverse environments (Masupha and Moeletsi, 2020). Maize is a staple food in Southern African countries and is among the crops whose production needs to be increased to meet the demand of the growing human population (Giller, 2020; Cairns, Chamberlin et al., 2021). The production of maize in rain-fed agriculture is significantly affected by changes and the distribution of precipitation during the growing season (Oluwaranti, Edema et al., 2020). To attain optimum maize crop yield, adequate water is required throughout the physiological development (emergence to maturity) because yield is sensitive to water stress (Masupha and Moeletsi, 2020). The amount of water required by maize depends on the crop's development stage, growth duration, evaporative demand of the environment, and planting density (Song, Jin et al., 2019). Therefore, detailed spatially explicit locally developed crop and water relationships can aid farmers in understanding the variation in crop water use and stress across the growing season for optimising crop production. Estimating  $ET_c$  at different crop growth stages would allow for an improved understanding of water use requirements and aid in informed agricultural management decisions (Quan and Doluschitz, 2021).

Numerous methods have been developed to estimate  $ET_c$ . The most commonly used methods are conventional and remote sensing-based methods. Conventional methods such as the Bowen ratio, Eddy covariance, and lysimeter are efficient and provide accurate  $ET_c$  estimates (Aryalekshmi, Biradar et al., 2021). However, these methods require extensive input data, which is costly and labour-intensive, especially in data-scarce and resource-poor regions such as Southern Africa (Mashaba-Munghemezulu, Chirima et al., 2021). Application of conventional methods in smallholder farms is a challenge because these farms are

fragmented and have heterogeneous fields, whereas these methods are well-suited to uniform, extensive homogenous fields (Giller 2020; Mashaba-Munghemezulu, Chirima et al., 2021). Remote sensing technologies have emerged as a tool that overcomes the limitations of conventional data collection methods. For instance, remote sensing techniques are noninvasive, offer robust time, cost-effective and reliable methods of estimating  $ET_c$ . Many studies successfully utilized remote sensing to estimate  $ET_c$  at various spatial and temporal scales (Reyes-González, Kjaersgaard et al., 2018). Furthermore, the availability and accessibility of some remotely sensed data used in agriculture allow for retrieving  $ET_c$ -related information in resource-poor and data-scarce regions (Reyes-González, Kjaersgaard et al., 2018; Nisa, Khan et al., 2021).

Although satellite-based methods have shown better prospects for estimating  $ET_c$  due to their free access to data policies such as the Moderate-resolution Imaging Spectroradiometer (MODIS) and Landsat fleet. However, some satellite platforms provide multispectral images with a limited spatial or spectral resolution, which limits the applicability of freely available satellite-borne images in smallholder farms (Mashaba-Munghemezulu, Chirima et al., 2021; Rezaei, Ghazaryan et al., 2021). For instance, MODIS and Landsat with medium to coarse spatial resolution (30-1000 m) often mask out the heterogeneity and complexity of smallholder farms, which makes it difficult to obtain finer spatial resolution data suitable to generate information for decision-making in smallholder croplands (Sibanda and Murwira, 2012; Mashaba-Munghemezulu, Chirima et al., 2021). Meanwhile, the Sentinel-2 multispectral instrument (MSI) has a minimum spatial resolution of 10 m with better prospects of capturing smallholder farms. However, its application is limited by its spectral resolution, which does not cover the critical thermal band for characterising land surface temperature for  $ET_c$  estimation (Segarra, Buchailot et al., 2020). Satellite-borne sensors characterised by very high spatial resolutions (>1 m), such as Geo Eye, Rapid Eye, and Pleiades-1A, are associated with exorbitant acquisition costs, which restrict their application in smallholder farms (Stratoulis, Tolpekin et al., 2017). Meanwhile, manned aerial vehicles are not often used in smallholder farms because they are costly (Chivasa, 2020).

Unmanned aerial vehicles (UAVs) also have emerged as a potential source of spatially explicit data that could alternatively estimate crop water use for optimising agricultural productivity at a local scale (Quan and Doluschitz, 2021). UAVs mounted with portable sensors have shown great prospects of providing ultra-high spatial resolution (UHSR) (>1 m) suitable for detecting and mapping crop attributes such as  $ET_c$  and water stress in fragmented heterogeneous cropping environments (Niu, Zhao et al., 2019; Quan and Doluschitz, 2021). UAVs can address the spatiotemporal limitations of readily available spatial datasets. They can be deployed to acquire data on heterogeneous crop types while capturing the complexity of fragmented smallholder farms aided by their high spatial resolution (Marcial-Pablo, Ontiveros-Capurata et al., 2021). Cloud cover does not extensively affect UAVs as they are flown at low heights above sea level. They are flexible to acquire images at user-defined times and in geographically exclusive areas; hence they have a great potential to accurately estimate  $ET_c$  in smallholder croplands. Morandé, Trezza et al. (2017) demonstrated that using UAV-derived data as an input in a remote sensing-based model allows for an improved representation of the spatial variability in  $ET_c$ . Ellsäßer, Stiegler et al. (2021) showed that UAV-derived  $ET_c$  estimates compared favourably against eddy covariance estimates and concluded that UAVs have great prospects of being utilised in estimating crop  $ET_c$  in smallholder farms.

There are various approaches to estimating  $ET_C$  using remotely sensed data, including surface energy balance (SEB) models, vegetation indices (VIs), or a combination of SEB models and VIs. Mapping Evapotranspiration at high Resolution with Internalized Calibration (METRIC) (Allen, Tasumi et al., 2007), Surface Energy Balance System (SEBS) (Su, 2002), and Surface Energy Balance Algorithm for Land (SEBAL) (Bastiaanssen, Menenti et al., 1998) are amongst single source SEB models that have been commonly applied using different satellite images to estimate  $ET_C$  and an evaporative fraction (EF) (Ramoelo, Majozi et al., 2014; Singh and Senay 2016). EF is the ratio between available energy at the land surface and latent heat flux (Liu, Xu et al., 2020). EF is used with VIs to estimate  $ET_C$  when there are gaps in the available dataset due to spatial, spectral, and temporal limitations. SEB models are used with freely available satellite data to estimate  $ET_C$  with limited costs (Aryalekshmi, Biradar et al., 2021). Following the availability of several methods of estimating  $ET_C$ , comparative studies have been conducted to assess the accuracy of  $ET_C$  estimates derived using non-spatially explicit conventional empirical methods in relation to RS-based models. Results of those studies showed that RS-based models could estimate  $ET_C$  to acceptable accuracies comparable to empirical conventional methods (Grosso, Manoli et al., 2018, Niu, Zhao et al., 2019). Specifically, SEBS and METRIC-Efflux have successfully been applied in estimating maize  $ET_C$  (Bansouleh, Karimi et al., 2015). For example, a large and growing body of literature has successfully estimated  $ET_C$  using SEBS in irrigated fields (Bansouleh, Karimi et al., 2015; Jamshidi, Zand-parsa et al., 2019). Huang, Li et al. (2015) successfully estimated  $ET_C$  using SEBS in a semi-arid region.

Meanwhile, there is also a significant number of studies that have demonstrated the potential of utilising METRIC-Efflux in estimating maize  $ET_C$  irrigated fields (de Oliveira Costa, José et al., 2020; Nisa, Khan et al., 2021; Kamyab, Mokhtari et al., 2022). Although these models are commonly used, their application has been mainly on irrigated fields using MODIS and Landsat data. An existing study by Cha, Li et al. (2020) demonstrated that incorporating Landsat with medium resolution into SEB models can provide accurate estimates compared to incorporating MODIS with coarse resolution into SEB models. Considering that many comparative studies have been conducted at large scales, Cha, Li et al. (2020) concluded that a need to evaluate and compare these RS-based models at spatial scales different from those targeted in their development, as their spatial resolution could affect the accuracy of  $ET_C$  estimates.

While these models have been frequently utilized for various scenarios, only a few selected studies have implemented them using UAV-derived inputs (Quan and Doluschitz, 2021). Furthermore, given the spectral limitations of UAV-based sensors, the requisite RS-based inputs may not be available directly from the UAV imagery, similar to when utilising satellite-borne data. Therefore, this study explores and demonstrates a relatively simple approach that utilizes open source and readily available data, models and cloud computing infrastructure to aid in estimating  $ET_C$  using multi-spectral UAV imagery suitable for application in smallholder croplands. Specifically, this study sought to assess the performance of the SEBS and the METRIC-Efflux models combined with UAV-derived multispectral data based on Landsat-derived VIs as a proxy of EF in estimating maize crop  $ET_C$  across the growing season in smallholder croplands in relation to the FAO-56 potential ET as a reference.

## 10.2 Materials and Methods

### 10.2.1 Description of the study area

The study was conducted in the rural community of Swayimane (29°52'S, 30°69'E) in the Kwa-Zulu-Natal province of South Africa (Figure 10-1). The community is dominated by small-scale subsistence farming. The area is characterised by cool temperatures, average annual rainfall, and deep fertile soils (Matungul, Lyne et al., 2001). Swayimane has a mean annual temperature range of 16°C-18°C and receives annual average precipitation of 1000 mm. During the maize growing season of 2020-2021, Swayimane recorded an average air temperature of 23.94°C and an average rainfall of 86.56 mm (Ndlovu, Odindi et al., 2021). The area is characterised by a gentle elevation between 800 and 1000 m above sea level.

Farmers have an average of 2 hectares of fields for cultivating various crops, including maize, sweet potato, amadumbe, sugarcane and vegetable crops such as spinach and cabbage. The variety of maize used in this study is SC701 variety of green mealies. Green mealies are one of the most important crops in Southern Africa regarding their economic value (Chirigo, 2014). SC701 is one of the most nutritious varieties optionally grown under rain-fed agriculture. It is highly recommended for green mealies production in smallholder croplands because of its drought and heat tolerance capabilities (Rezaei, Ghazaryan et al., 2021). In this study, maize was planted in mid-November 2020 and mid-January 2021, and it matured between 138 and 150 days after the planting date. Maize was managed using traditional techniques. Traditional techniques were used for levelling the soil, distributing cow manure, sowing, and harvesting. Weedicides were then used to clear the weeds before planting. From the ET<sub>C</sub> maps of the entire study area maize fields were extracted by masking the other land cover types. The field was divided into 3 plots A, B, and C (Table 10-1), each plot represented a different monthly growth stage.

Table 10-1: Maize growth stages

Picture	Growth Stage	Description
	Vegetative growth stage (V5).	20-25 mm below the surface. 5 leaf – cob and tassel initiation.
	Vegetative growth stage (V12).	Active growth, leaf and cob development. 12 leaf – cob size determined.
	Reproductive growth stage (R1-R2).	Pollination and kernel development.

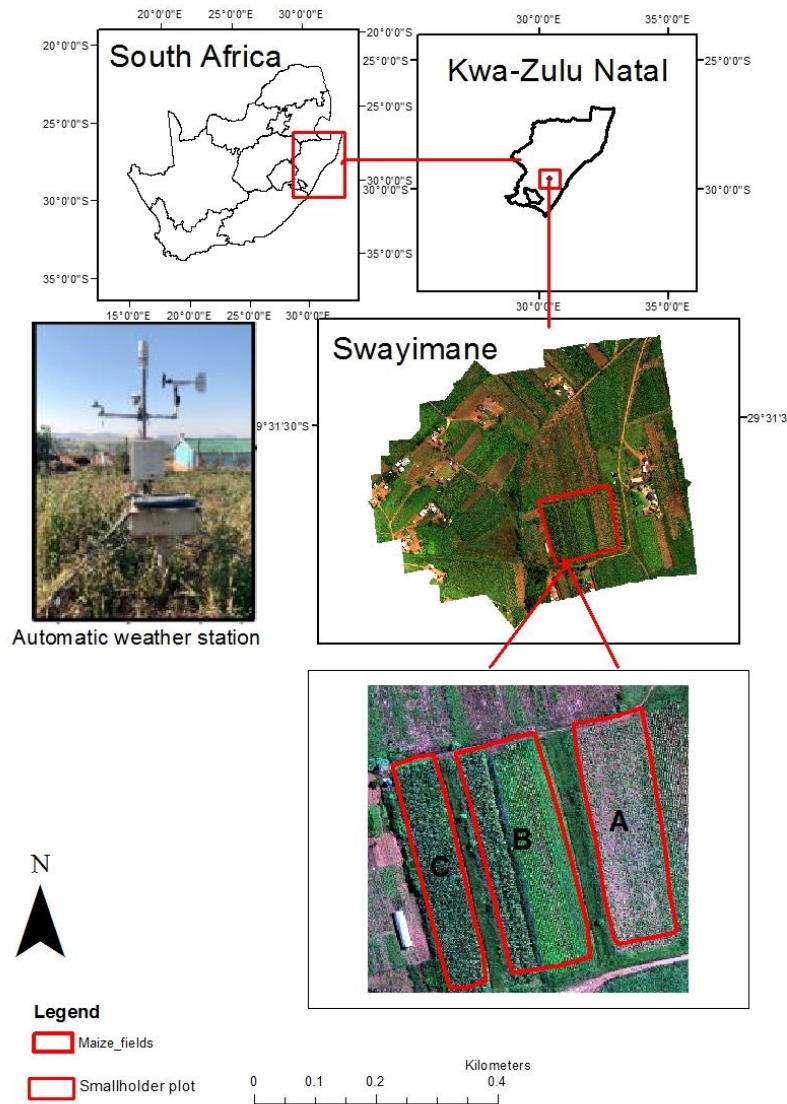


Figure 10-1: Study area and maize fields (A, B, and C)

### 10.2.2 Daily $ET_c$ estimation using UAV imagery, Landsat data, SEB models, and GEE

This study computed maize  $ET_c$  using the formula below using the reference crop evapotranspiration  $ET_o$  and crop coefficient ( $K_c$ ) following the surface energy balance model.

$$ET_c = ET_o \times K_c \quad \text{Equation 10-1}$$

Where  $ET_c$  is the crop evapotranspiration  $\text{mm d}^{-1}$ ;  $ET_o$  is the reference evapotranspiration from the automatic weather station derived using the Penman-Monteith method;  $K_c$  is the maize crop coefficient (dimensionless) from the FAO-56 manual.

Albedo could not be derived from our UAV-derived multispectral image due to the spectral limitation of the sensor used; hence the evaporative fraction (EF) was derived from Landsat

data and used in this study. The literature illustrates that EF is closely related to VIs, crop coefficient ( $K_c$ ), and reference evapotranspiration ( $ET_o$ ) (Parmar and Gontia, 2022). Therefore, it can be used to derive and upscale hourly  $ET_c$  to daily  $ET_c$  as it is assumed to be constant for 24 hours (Parmar and Gontia, 2022). Normalised difference vegetation index (NDVI) is the commonly used VI indicator of land surface vegetation because the magnitude of EF,  $ET_c$  is affected by the vegetation density covering the ground. The EF and NDVI ratio (Equation 10-2) is based on their strong linear relationship and correlation (Cihlar, Laurent et al., 1991). The ratio of EF and NDVI are hypothesized to be equivalent for different sensors; therefore, it was used to downscale EF. Subsequently, UAVs based EF ( $EF_{UAV}$ ) was derived using Equation 10-3 (Singh, Khand et al., 2020). Downscaling is generally conducted to address sensors' spatial, temporal, or spectral limitations (Tan, Wu et al., 2017). Numerous studies used downscaling approach to estimate daily  $ET_c$  using EF (Yang, Chen et al., 2010; Singh, Khand et al., 2020). For instance, Yang, Chen et al. (2010) demonstrated that the EF approach is more accurate than the residual approach.

$$\frac{EF}{NDVI}(Landsat) = \frac{EF}{NDVI}(UAV) \quad \text{Equation 10-2}$$

$$EF_{UAV} = \frac{EF}{NDVI} \times NDVI_{UAV} \quad \text{Equation 10-3}$$

Normalised difference vegetation index (NDVI)

$$NDVI = \frac{NIR - Red}{NIR + Red} \quad \text{Equation 10-4}$$

Where NIR and Red represent near-infrared and red bands, respectively. In UAV, NIR and Red are Bands 5 and 3, respectively. In Landsat 7, NIR and Red are 4 and 3, respectively. In Landsat 8, NIR and Red are Bands 5 and 4, respectively.

SEBS and METRIC-Efflux were used to derive EF based on Landsat 7 and 8 data. EF and NDVI derived from Landsat images were used to estimate  $EF_{UAV}$ . Landsat was used because all SEBS input parameters can be derived from its image; it is freely available. Landsat images with a cloud cover of less than 30% were selected, from the USGS Earth Explorer site, downloaded and used in this study. To calculate the ratio  $\frac{EF}{NDVI}$ , Landsat and UAV images must be acquired on the same date. If the images were not acquired on the same date, the last Landsat image acquired before the UAV image and the first Landsat image acquired after the UAV image must be used. In this study, Landsat and UAV images were not acquired on the same date; therefore, a linear interpolation was applied based on the Landsat images acquired before and after the UAV image acquisition date to calculate  $\frac{EF}{NDVI}(UAV)$  (Equation 10-5).

$$\text{Ratio: } \frac{EF}{NDVI}(UAV) = \left(\frac{EF}{NDVI}\right)_{i-1} + \frac{\left(\frac{EF}{NDVI}\right)_{i+1} - \left(\frac{EF}{NDVI}\right)_{i-1}}{(DOY_{i+1}) - (DOY_{i-1})} \times ((DOY_i) - (DOY_{i-1})) \quad \text{Equation 10-5}$$

Where:  $\left(\frac{EF}{NDVI}\right)_{i-1}$  is the ratio of the Landsat image acquired before the drone image.  $\left(\frac{EF}{NDVI}\right)_{i+1}$  is the ratio of the Landsat image acquired after the drone image.  $DOY_i$  is the day of the year when the drone image was acquired.  $DOY_{i-1}$  is the last Landsat image before the drone image was acquired.  $DOY_{i+1}$  first image of Landsat after the drone image was acquired. The Landsat images were retrieved from the GEE platform by specifying the date range (February to May

2021) and the location of the study site. GEE was selected due to its advanced image processing capabilities and ability to minimize processing errors often associated with image pre-processing.

### 10.2.3 Calculation of EF to NDVI ratio using SEBS

Surface Energy Balance System (SEBS) is a single-source model developed by Su (2002) that is incorporated into free, open-source GIS software Integrated Land and Water Information System (ILWIS). SEBS was selected for this study because it does not require subjective intervention by the user to select hot and cold pixels and does not require professional expertise to develop or build the model (Bansouleh, Karimi et al., 2015). This model is less site-specific as compared to the other models. SEBS input parameters are NDVI, leaf area index (LAI), albedo, emissivity, land surface temperature (LST), and fractional vegetation cover (FVC). These parameters were calculated from Landsat images within GEE using equations Mhawej and Faour (2020) described. Hourly meteorological data used were average air temperature (°C), wind speed (m/s), solar radiation ( $Wm^{-2}$ ), specific humidity (kg/kg), atmospheric pressure (Pa), surface pressure (Pa) and daily air temperature (°C). The meteorological data used was observed on the hour of the satellite overpass. Meteorological data were obtained from the automatic weather stations (AWS) located at Swayimane primary school, approximately 2 km from the study site. AWS was installed following World Meteorological Organization's standards. The meteorological variables were measured at 2 m above the ground using the following sensors: CS215 Temp/RH probe (temperature and relative humidity), CS106 barometric pressure sensor (pressure), RM young 05103 sensors (wind speed and direction), Licor LI2005 pyranometer (solar radiation). The sensor scans every 10 seconds and outputs average data every hour.

The input parameters were manually imported into the model to derive EF and NDVI. EF and NDVI output files were exported from SEBS and imported to ArcGIS 10.6 for further processing. Using ArcGIS 10.6, the ratio was calculated and resampled from 30 m to 0.5 m to match the pixel size of the UAV image. The daily maize  $ET_C$  was calculated on GEE as the product of EF to NDVI ratio,  $NDVI_{UAV}$ , and total daily  $ET_o$  (Equation 10-6). The  $\frac{EF}{NDVI}$  (UAV) was imported to GEE to generate daily  $ET_C$  maps using Equation 10-5.

$$ET_C = \left(\frac{EF}{NDVI}\right)_{Landsat} \times NDVI_{UAV} \times ET_o \quad \text{Equation 10-6}$$

Where  $ET_C$  is the crop evapotranspiration ( $mm\ d^{-1}$ ).  $\frac{EF}{NDVI}$  ratio derived from the Landsat 7/8 data and using the SEB model.  $NDVI_{UAV}$  is derived from drone imagery near-infrared (NIR) and red bands.  $ET_o$  is the total daily reference evapotranspiration calculated from the local weather station based on the Penman-Monteith equation.

### 10.2.4 Calculation of ETrF to NDVI ratio using METRIC-Efflux

The same procedure used to derive EF and NDVI using SEBS was applied using METRIC-Efflux. Earth Engine Evapotranspiration Flux (Efflux) is an automated version of METRIC that operates on the GEE system; it was designed and developed within GEE based on the

METRIC algorithm (de Oliveira Costa, José et al., 2020). METRIC-Efflux uses Landsat 7 and 8 images and meteorological data within the GEE platform to generate intermediate maps such as NDVI, albedo, ETrF, and LST for estimating  $ET_C$ . ETrF is the fraction of maize reference evapotranspiration (ET), equivalent to maize-based Kc. METRIC-Efflux was used in this study because it is an automated open-source software; the user does not manually download and pre-process Landsat images. Automatic pre-processing and generation of intermediate maps are advantageous because it minimizes human errors associated with pre-processing (Allen, Morton et al., 2015). METRIC-Efflux can be applied in resource-poor and data-scarce regions as it does not require field input data and does not require expertise. METRIC-Efflux version 0.20.4, accessed from the website <https://eeflux-level1.appspot.com/>, was used to download and pre-process NDVI and ETrF. The  $\frac{ETrF}{NDVI}$  (UAV) calculated (Equation 10-5) following the same procedure used in SEBS to calculate the ratio.

A total of 25  $ET_C$  values from each plot were randomly extracted from the  $ET_C$  maps, and the average value attained was used to compare SEBS and METRIC-Efflux  $ET_C$  with the FAO-56 potential ET estimates across the study period.

### 10.2.5 Data Validation

$ET_C$  estimates derived from remote-sensing-based models are often validated using conventional methods such as the Bowen ratio, Eddy covariance, and lysimeters (Nisa, Khan et al., 2021). Due to the lack of in-situ monitoring systems at the study site, the FAO-56 Penman-Monteith method was used to validate UAV  $ET_C$  estimates. This method uses  $ET_O$  from a weather station situated at the study site and tabulated FAO-56-based crop coefficient (Kc) for a specific crop to estimate potential ET (equation 10.1) (Parmar and Gontia, 2022). The expected crop coefficient values for different maize growth stages were obtained from the FAO-56 manual using maize estimated height and number of days after the planting date. The Kc values used varied with growth stage in February (A= 0.19, B = 0.7, and C = 1.2), March (A = 0.4, B = 1.0, and C = 1.25) and April (A = 1.3, B = 1.2, and C = 0.95) (Kabanda, 2015; Pereira, Paredes et al., 2021).  $ET_O$  values were 4.157, 4.708, and 2.368  $mm^{-d}$  for February, March, and April, respectively.

## 10.3 Results

### 10.3.1 Spatial distribution of $ET_C$ across the growing season

Figure 10-2 illustrates the distribution of daily  $ET_C$  across different growth stages during the growing season.  $ET_C$  ranged from 0.5-7.5  $mm^{-d}$ , with the lowest  $ET_C$  attained at the initial stage and the highest attained at the matured stage. For both models,  $ET_C$  varied for different growth stages, and an increasing trend of  $ET_C$  with increasing vegetation cover was observed.  $ET_C$  decreased after harvesting the maize. Both models can map  $ET_C$ 's spatial distribution across the growth stages.

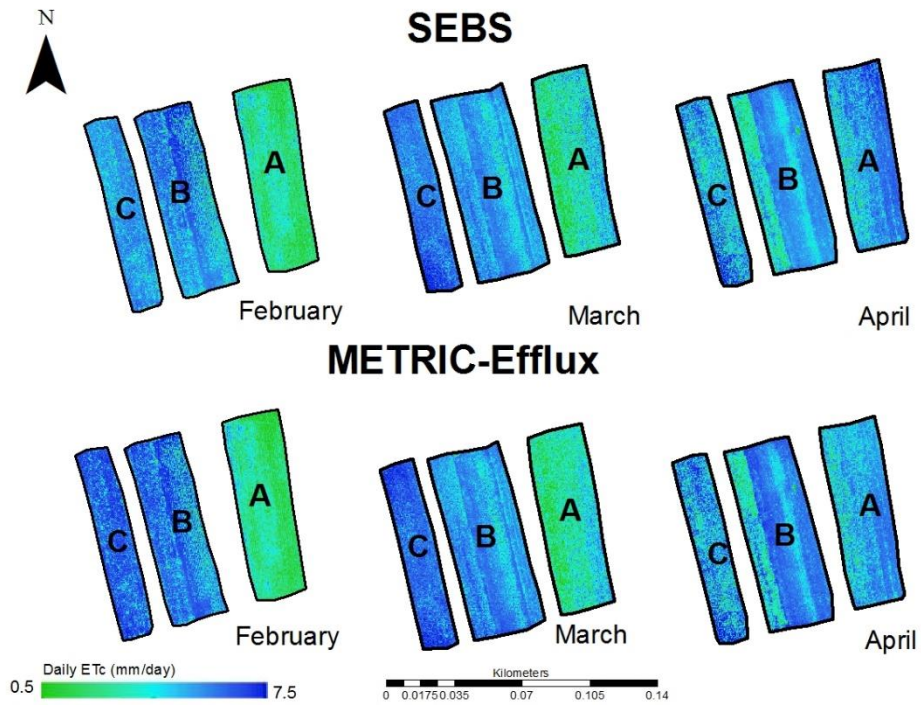


Figure 10-2: Daily distribution of  $ET_c$  across the growing season

### 10.3.2 Comparison of SEBS and METRIC-Efflux daily $ET_c$ estimates with FAO-56 potential ET for maize.

Figure 10-3 graphically presents the maximum  $ET_c$  steatites extracted from derived maps compared to the FAO-56 reference  $ET_c$  for maize. The SEBS estimates were higher than METRIC-Efflux, and FAO-56 estimates throughout the growing season.

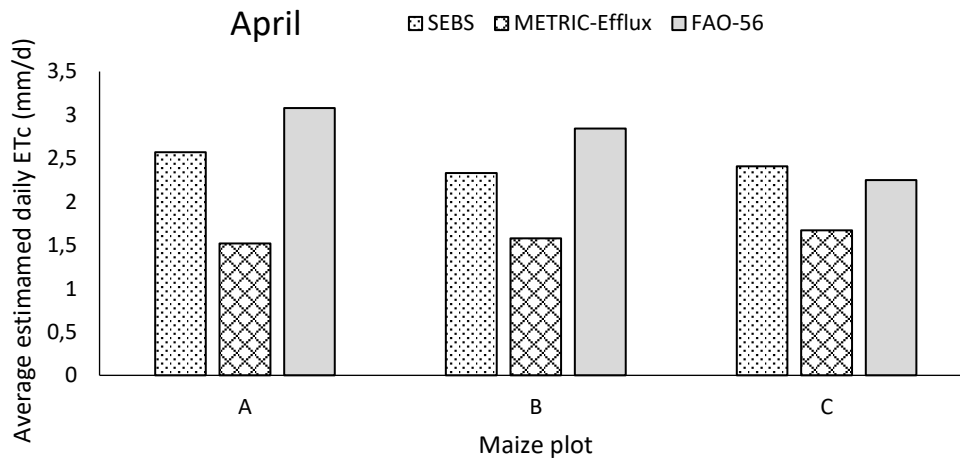
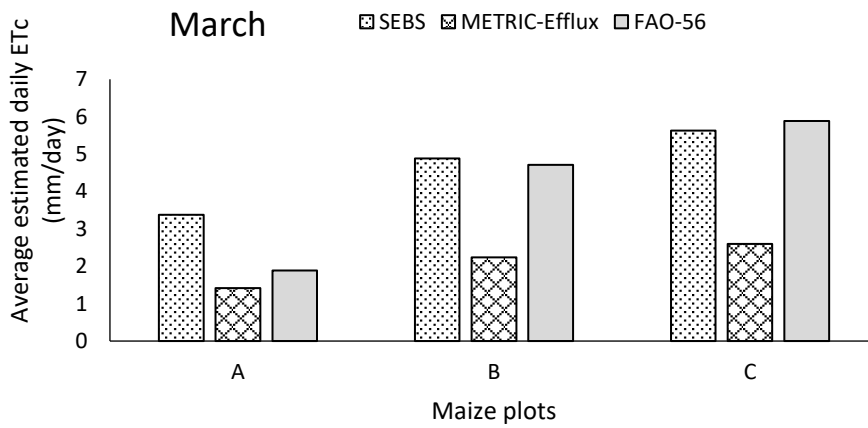
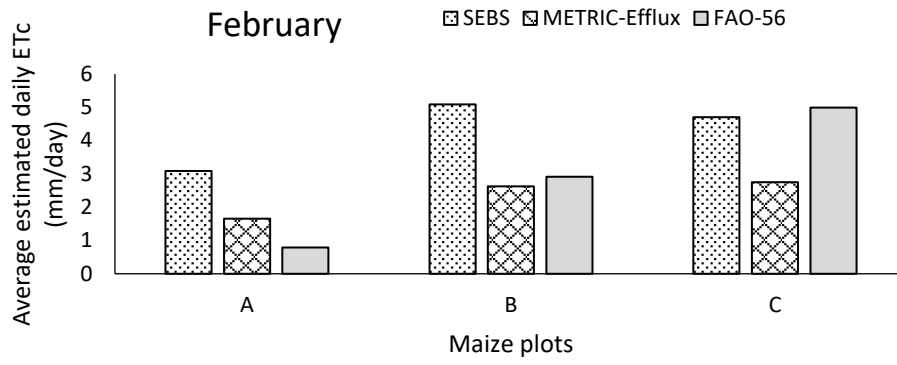


Figure 10-3: Comparison of maximum ET<sub>c</sub> estimates of SEBS, METRIC-Efflux, with FAO-56 across different maize growth stages.

Figure 10-4 illustrates the linear relationship between estimated and potential daily  $ET_c$ . There is a close correlation between  $ET_c$  estimated using METRIC-Efflux and potential  $ET_c$  (B, D, and F) when compared with  $ET_c$  estimated using SEBS (A, C, and E).

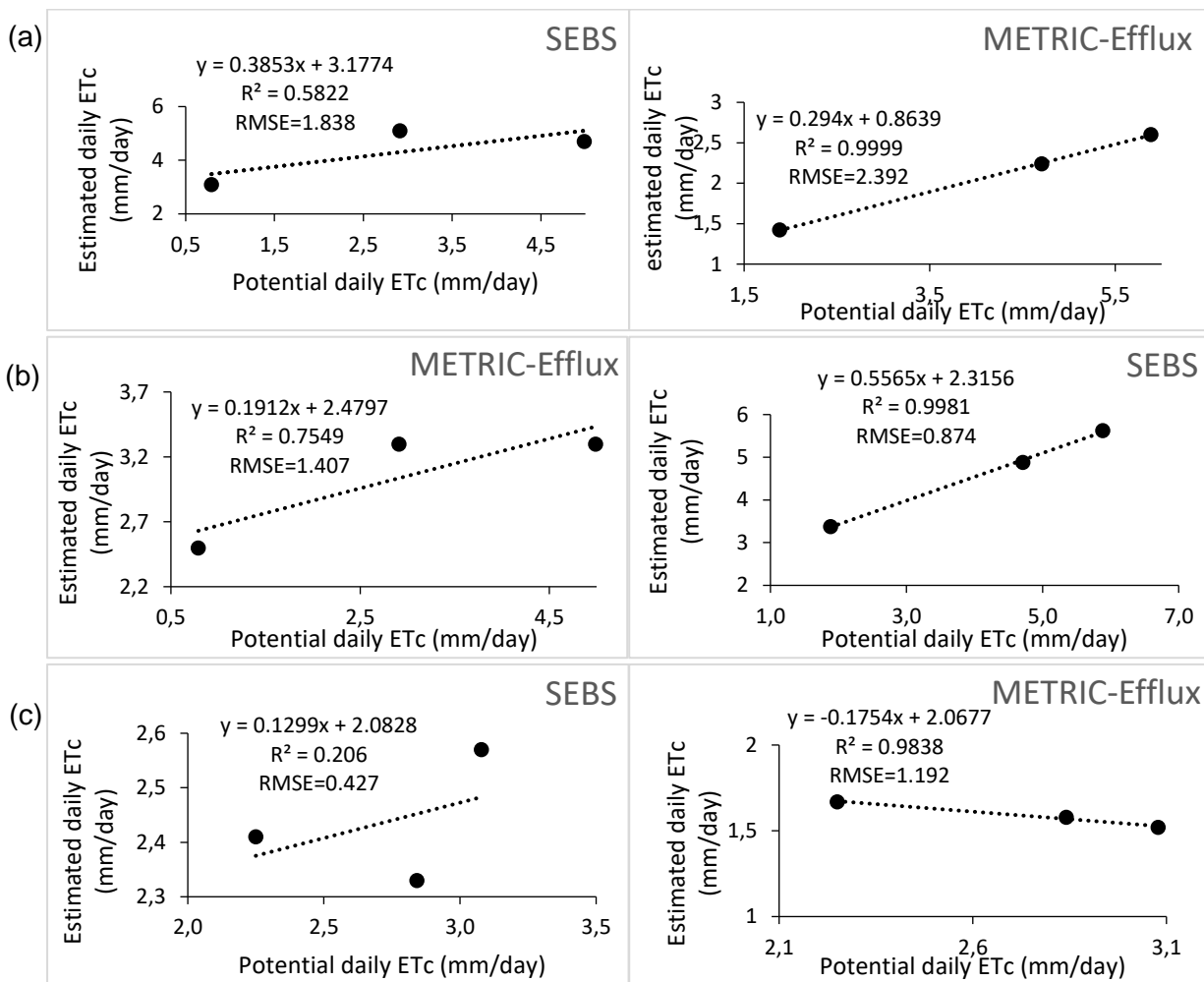


Figure 10-4: Relationship between SEBS & FAO-56  $ET_c$  estimates and METRIC-Efflux & FAO-56 estimates in (a) February, (b) March and (c) April.

## 10.4 Discussion

This study's main objective was to assess the performance of the SEBS and the METRIC-Efflux models combined with UAV-derived multispectral data and Landsat-derived VIs as a proxy of EF in estimating maize crop  $ET_c$  across the growing season in smallholder croplands in relation to the FAO  $ET_c$  as a reference.

#### 10.4.1 Comparison of SEBS and METRIC-Efflux daily $ET_c$ estimates with FAO-56 potential ET for maize.

Results of this study showed that the  $ET_c$  estimates derived following the METRIC-Efflux model ranged between 0.9 and 3.3  $mm\ d^{-1}$ , while the FAO ranged between 0.78 and 5.8  $mm\ d^{-1}$ . Meanwhile, the SEBS model exhibited  $ET_c$  values that ranged between 1.5 and 7.2  $mm\ d^{-1}$ . In this regard, the  $ET_c$  estimates from both models were comparable to those from FAO and in the literature across the growth stages (Bansouleh, Karimi et al., 2015; Kamyab, Mokhtari et al., 2022). For example, Kamyab, Mokhtari et al. (2022) found that  $ET_c$  ranges from 2.3-6.5  $mm\ d^{-1}$  when estimated using METRIC-Efflux in an irrigated field. de Oliveira Costa, José et al. (2020) found that the average daily maize evapotranspiration estimated using METRIC-Efflux was 3.64, 3.59  $mm\ d^{-1}$ , and 3.62  $mm\ d^{-1}$  for initial, development, and matured, respectively. Wagle, Gowda et al., 2016 found that  $ET_c$  ranges from 1.2-7.1  $mm\ d^{-1}$  when estimated using SEBS in an irrigated field. Bansouleh, Karimi et al., 2015 found that SEBS daily maximum  $ET_c$  range from 4.07-7.7  $mm\ d^{-1}$  in irrigated fields. A study that was done by (Kabanda, 2015) in South Africa (North West) found that maize  $ET_c$  ranges from 1.3-1.5  $mm\ d^{-1}$ , 1.8-3.81  $mm\ d^{-1}$ , 3.87-4.5  $mm\ d^{-1}$ , and 1.52-3.33  $mm\ d^{-1}$  in the initial, development, matured, and postharvest growth stages, respectively. Our ranges are similar to all these values, even though most studies were conducted under irrigation conditions.

SEBS had the highest  $ET_c$  estimates because it overestimated  $ET_c$  estimates during February. The fact could explain this during February; the crop foliage will be minimal while the soil background effect will be pronounced. Subsequently, when the vegetation is sparse, SEBS overestimates sensible heat flux (Elhag, Psilovikos et al., 2011; Mohammadian, Arfania et al., 2017). This is typical in February conditions similar to those in arid and semi-arid regions where water is a limiting factor to foliage density and sparse vegetation, SEBS overestimate  $ET_c$  (Huang, Li et al., 2015). Many authors have shown that although tabulated Kc values give reasonable  $ET_c$  estimates, it tends to overestimate  $ET_c$  even when adjusted with local data. This is because Kc values used to calculate  $ET_c$  were developed for standard conditions (Grosso, Manoli et al., 2018). Kc values are available for the initial, development, and matured growth stages; the Kc values are estimated for the other stages. Estimating Kc values for vegetative and postharvest growth stages could impact the estimate because they do not represent the actual crop characteristics (Van der Laan, Jarman et al., 2019).

Furthermore, the difference in the performance of these models could be explained by the fact that they differ in their input requirements, model structure, and assumptions made in the model. This could impact the model output, thus, differences in  $ET_c$  estimates (Acharya & Sharma, 2021). SEBS uses local meteorological data that is recorded on-site. Meanwhile, METRIC-Efflux does not use local meteorological data observed on site. This could impact the final estimates of  $ET_c$  due to the microclimate variability (de Oliveira Costa et al., 2020).

Furthermore, the METRIC-Efflux is automated, and the input files are stored, pre-processed, and processed within the GEE platform. On the other hand, SEBS requires many input parameters derived manually and requires the user to manually input these files (Aryalekshmi et al., 2021). Li et al. (2017) noted that SEBS's uncertainties are associated with input parameterization. Subsequently, SEBS is more subjected to human errors in relation to

METRIC-Efflux, which could contribute to the variation in its performance compared to METRIC-Efflux.

#### **10.4.2 Variability of estimated daily $ET_c$ across different plots**

Results of this study showed significant differences between the  $ET_c$  models across the growing season between plots B, C and A.  $ET_c$  was high at vegetative, reproduction, and matured for both models. This could be explained by the different phenological stages associated with different foliage densities. Plot A was slightly younger than plots B and C. Similarly, the variability of  $ET_c$  across the three months resulted from changes in meteorological and crop characteristics which are factors that influence the rate of  $ET_c$  (Van der Laan, Jarman et al., 2019). The vegetation cover increased from February to March hence the increase in  $ET_c$  with time (Figures 10-2 and 10-3). There are minimal differences in  $ET_c$  estimates in plots B and C because the planting dates for these plots were a few weeks apart. Whereas plot A was planted a month later after plots B and C.  $ET_c$  was high at vegetative, reproduction, and matured because these are identified as the peak crop development stages characterised by higher biomass accumulation and high water demand to sustain the accumulation of biomass and reproduction process (Van der Laan, Jarman et al., 2019).

Maize daily  $ET_c$  increase gradually from the beginning of the growing season to the peak season, then decrease gradually in the late season (Zhou, Wang et al., 2019). The gradual increase of  $ET_c$  is closely related to the increase in leaf area index (LAI) (Zhang, Ming et al., 2021). However, in this study  $ET_c$  decreased from March to April because maize crop leaves were damaged by the hailstorm, reducing the leaf area index and thus reducing  $ET_c$  (Brewer, Clulow et al., 2022). Another factor that might have contributed to April having the least  $ET_c$  estimates is that the microclimate parameters on that day were low compared to the other days because  $ET_c$  is significantly affected by available soil water and radiant energy (Huang, Li et al., 2015). The rate of  $ET_c$  is significantly affected by crop,  $ET_o$ , and weather conditions (Reyes-González, Kjaersgaard et al., 2018).

#### **10.4.3 Implications of the Study**

The results indicate that SEBS and METRIC-Efflux could be used with various remotely sensed images from various sensors, including UAVs with fine spatial resolution under rain-fed farms from the early to the matured stage of maize crops. Therefore, in critical early growth stages, UAVs can aid farmers by providing near-real-time data that would assist in mitigating threats that can drastically reduce potential crop yield (Brewer, Clulow et al., 2022).  $ET_c$  spatial distribution for short crops was a challenge to map due to the high spatial resolution, which is  $>30$  m (Nisa, Khan et al., 2021). The results demonstrate that UAVs can be a reliable tool to map the  $ET_c$  spatial distribution of all crops, including short crops. In addition, using fine resolution for mapping spatial crop traits in subsistence smallholder farms is advantageous because coarse spatial resolution may result in the misclassification of crop type (Chivasa, Mutanga et al., 2017). Misclassification is a major source of error in fields where different crops with similar phonologies are intercropped or grown together (Reyes-González, Kjaersgaard et al., 2018).

#### 10.4.4 Limitations and recommendations

The approach of using EF and NDVI to estimate daily  $ET_C$  was applied successfully using UAV data in rain-fed smallholder farms. It can be used as a reliable method of estimating and mapping  $ET_C$  variability in  $ET_C$  in data-scarce and resource-poor sites. However, the study's limitations include the unavailability of on-site data to validate SEBS, and METRIC-Efflux  $ET_C$  estimates. Due to the lack of on-situ data to validate the estimates from the models, it was a challenge to assess the model's accuracy because both models could overestimate or underestimate  $ET_C$  under different crop and environmental conditions (Xue, Bali et al., 2020). Due to spectral resolution differences between Landsat and UAV downscaling, EF could have impacted the results.

Furthermore, the UAV and Landsat images were not acquired on the same date; hence application of linear interpolation could have affected the performance of the models. In February, the cloud-free Landsat image was acquired two weeks before the UAV image acquisition. In March, the cloud-free Landsat image was acquired four weeks after the acquisition of the UAV image. The huge gap between acquisition dates could significantly impact the final results due to microclimate variability. According to (Singh, Khand et al., 2020) the image acquisition dates of different sensors used must be acquired on the same date. The  $K_c$  values used for validation were designed for irrigated maize fields with standard conditions and were not adjusted for non-irrigated fields.

Therefore, future studies should consider assessing the accuracy of the SEBS and METRIC-Efflux using on-site validation data or adjusting  $K_c$  values to study area specifications. More research is needed on deriving SEBS parameters directly from the sensor type used, which will provide a simpler way of estimating  $ET_C$  using UAVs directly. This study highlighted the strengths and limitations of each model, implying the importance of model comparison for application in different conditions, as the input data type strongly influences the model performance. Future research should consider developing an automated SEBS version within GEE. The automated version should allow users to input local meteorological data due to its significant impact on the rate of  $ET_C$  (Singh and Senay, 2015).

#### 10.5 Conclusion

The essence of the study was to assess the potential of SEBS and METRIC-Efflux in estimating and mapping daily  $ET_C$  using UAV data in rain-fed smallholder farms with limited datasets. Based on the findings of this study, it can be concluded that,

- The utility of unmanned aerial vehicle data in conjunction with Landsat-derived EF and NDVI could comparably and effectively estimate and map spatial variability of maize evapotranspiration at different growth stages throughout the growing season.
- SEBS and METRIC-Efflux can be applied successfully in rain-fed smallholder farms using UAV remotely sensed data to estimate, map and monitor the variability of crop evapotranspiration.

The findings of this study are a step towards establishing smallholder crops' water use monitoring frameworks required to optimise productivity. Especially because it is based on open-source data and software (ILWIS, Efflux level 1, and GEE). The approach used in this study has great prospects of being implemented as a precision agricultural application in farms with limited resources and datasets.

## 11 GENERAL DISCUSSION, CONCLUSION AND RECOMMENDATIONS

### 11.1 General Discussion

Smallholder farming systems contribute significantly to agricultural production, livelihood sustenance, and socio-economic growth in most third-world countries. Regardless of their critical role, smallholder farmers generally lack the resources to maximize their potential. Subsequently, they face challenges in optimising their crop production due to the lack of mechanisms for monitoring the spatial variability of crop health and water use efficiency. Hence, it is imperative to identify and provide smallholder farmers with innovative, objective, low-cost solutions to assist them in optimizing their productivity. Recent precision agricultural developments, such as unmanned aerial vehicles (UAVs) mounted with ultra-high-resolution cameras, provide spatially explicit near real-time information useful in monitoring and assessing farm and plot scale crop growth dynamics. The synergistic use of UAV technology with remote sensing techniques allows for a deeper understanding of crop characteristics that could assist with operational decisions related to crop health at the field level, allowing the timely implementation of remedial solutions to ensure productivity. Maize is one of the crops widely grown in smallholder croplands in South Africa and across southern Africa. In this regard, maize is the staple food in these countries, often affected by climate variability and natural disasters such as storms and drought. In this regard, the project sought to assess the utility of drone technology in monitoring the state of maize crops to improve water use and productivity. Specifically, the project sought to

- To review the literature on specialist drones for crop monitoring and crop-water models that use drone products. This will include an analysis of drones' use to monitor crops, modelling yield and water use, and irrigation scheduling.
- To assess crop health by analysing real-time NDVI derived from drone imagery.
- To monitor crop evapotranspiration at the field scale for a farmer to make on-field decisions.
- To develop high-resolution maps of agriculture fields and irrigated areas and datasets on water use and water productivity, potential yield and evapotranspiration.
- To assess the impact of the application of drones on water use, crop nutrition, and water productivity (yield and quality) for improved livelihoods of smallholder farmers.

In synthesising the literature on using UAVs in the smallholder agriculture sector in developing countries, the review highlights the role of UAV-derived normalised difference vegetation index (NDVI) in assessing crop health, evapotranspiration, water stress and disaster risk reduction. The review's findings showed that UAV technologies could improve the productivity of smallholder agriculture by facilitating access to information on crop biophysical parameters in near real-time for improved preparedness and operational decision-making. Coupled with accurate meteorological data, the technology could allow for precise estimations of crop water requirements and crop evapotranspiration at high spatial resolutions. They offer opportunities for mainstreaming climate-smart and precision agriculture into smallholder farming through improved crop health monitoring and agricultural water management.

A lack of resources and skills has limited their use in smallholder farming to acquire and operate them. Furthermore, the perception that they are expensive has failed to consider the benefits that would be unlocked through their use in smallholder agriculture. While noting the high ownership costs, the review recommended communal ownership of UAVs by smallholder farmers to reduce operational costs, as they can potentially improve agriculture and water productivity. Specifically, the review recommended that drones be targeted as an opportunity to increase youth participation in agriculture, which is a priority in most African countries. The application of UAVs in smallholder agriculture would advance the importance of remote sensing in previously disadvantaged smallholder farmers by providing high-resolution images at user-defined temporal resolution and automating data collection, processing and analysis at low cost. This will improve mapping accuracy, stress classification, irrigation scheduling and yield prediction for smallholder croplands. Applications of UAVs in smallholder agricultural farming could significantly improve input efficiency, environmental sustainability, and nutrition of farmers, as well as farm income and livelihoods. This review informed the methodological procedures we employed in evaluating the utility of drones in mapping maize crop health and productivity in smallholder croplands. In this regard, the project's next objective was to map field boundaries.

The project aimed to demonstrate how GEE can be leveraged to maximize the potential of UAVs for mapping LULC in smallholder farms, with a specific focus on cultivated areas. The results of these investigations demonstrated that LULC could be mapped fairly accurately using UAV imagery and GEE's image classification procedures. Furthermore, the UAV-derived LULC map outperformed other publicly available landcover maps in capturing the spatial heterogeneity within the study area. While these investigations could have benefited from the availability of more training data or higher spectral resolution data, the overall results were quite promising. They can serve as a foundation for developing improved land cover maps for the study area in the future, which in turn can facilitate improved agricultural management. After the field boundaries were delineated, the project sought to assess the utility of crop UAVs in mapping and monitoring crop health and water use proxies.

The project focused on chlorophyll content and leaf area index in predicting maize crop health parameters. The project sought to test the use of UAV-derived multispectral data by estimating maize chlorophyll content over the various stages of phenotyping. This was done using a random forest prediction model, which estimated the chlorophyll concentrations of maize in smallholder farms of Swayimane. Therefore, premised on the findings of the study, it is concluded that:

- Optimal chlorophyll content prediction accuracies were produced during early vegetative growth stages (V5-V10 and V12), late vegetative growth stages (V14-T) and early reproductive growth stages (R1-R3),
- Maize chlorophyll content was optimally estimated through UAV-derived NIR and red-edge wavelengths.

After noting the prospects of accurately mapping chlorophyll content, the project sought to map another productivity attribute, the leaf area index.

In testing the utility of UAV-derived VIs in estimating maize LAI across the growing season based on the Altum sensor mounted on the DJI Matrice 300 UAV data in a smallholder farm. It could be concluded that:

- Maize LAI can be optimally estimated using UAV-derived VIs across the growing season
- The blue, green, red edge and NIR sections of the EMS are influential in estimating Maize LAI
- Combining traditional, red edge-based and new VIs is useful in attaining high LAI estimation accuracies

Overall, the UAV technologies illustrated a great potential for quantifying the spatial variability of crop health at reasonable accuracies. The next segment assessed maize crop water stress and use efficiency.

The project tested the utility of UAV-derived multispectral data in estimating folia temperature and stomatal conductance as proxies of crop water stress and use. These two variables are linked to water loss through evapotranspiration; hence they were selected and used in this project section. Based on the findings of this study, it was concluded that foliar temperature and stomatal conductance are adequate indicators and proxies of crop water stress throughout the growing period. Foliar temperature yielded higher prediction accuracies as compared to stomatal conductance. Nevertheless, the random forest regression model optimally predicted both indicators throughout all phenological stages of maize. Specifically:

- The UAV-derived multispectral data and thermal infrared waveband optimally estimated maize temperature during the mid-vegetative stage to an RMSE = 0.59°C and  $R^2 = 0.81$  (RRMSE = 2.9%) based on the thermal infrared, followed by the NIR, NGRBI, EVI and NDVI, in order of importance,
- The multispectral and thermal infrared data optimally predicted stomatal conductance during the early reproductive stage to an RMSE = 25.9 mmol/m<sup>2</sup> and  $R^2 = 0.85$  (RRMSE = 11.5%) based on the red-edge band, followed by the NIR, green, OSAVI and blue band, in order of importance.

The project then sought to explore and demonstrate a relatively simple approach that utilizes open source and readily available data, models and cloud computing infrastructure to aid in estimating  $ET_c$  using multi-spectral UAV imagery suitable for application in smallholder croplands. Specifically, in this section, the project sought to comparatively assess the performance of the SEBS and the METRIC-Efflux models combined with UAV-derived multispectral data based on Landsat-derived VIs as a proxy of EF in estimating maize crop  $ET_c$  across the growing season in smallholder croplands in relation to the FAO-56 potential ET as a reference. Grounded on the findings of that study was concluded that;

- The utility of unmanned aerial vehicle-acquired data in conjunction with Landsat-derived EF and NDVI could comparably and effectively estimate and map spatial variability of maize evapotranspiration at different growth stages throughout the growing season.

- SEBS and METRIC-Efflux can be applied successfully in rain-fed smallholder farms using UAV remotely sensed data to estimate, map and monitor the variability of crop evapotranspiration.

The findings of this study are a step towards establishing smallholder crops water use monitoring frameworks required to optimise productivity, especially because it is based on open source data and software (ILWIS, Efflux level 1, and GEE). The approach used in this study has great prospects of being implemented as a precision agricultural application in farms with limited resources and datasets.

## 11.2 Limitations of The Study

The project managed to adequately address all the specific objectives. Although the study hypothesised that maize crop evapotranspiration could be adequately estimated using UAV-acquired data, numerous limitations were associated with the procedure. Using evaporative fraction (EF) and Landsat-derived NDVI to estimate daily  $ET_C$  was applied using UAV remotely sensed data in rain-fed smallholder farms, indicating that it can be used as a reliable method of estimating and mapping variability of  $ET_C$  in data-scarce and resource-poor sites. However, this can only be feasible where the target fields are expansive. The moderate spatial resolution of Landsat affects the spatial variability of the derived maps. Due to spectral resolution differences between Landsat and UAV downscaling, the EF derived and used in this study could have possibly impacted the accuracy of our results.

Furthermore, the unavailability of on-site data for validation of SEBS and METRIC-Efflux  $ET_C$  estimates was another major limitation associated with the procedure followed in this project. Despite attempts to compare our modelled evapotranspiration with FAO estimates, it was a challenge to assess the accuracy of the models because both SEBS and METRIC-Efflux seem to overestimate or underestimate  $ET_C$  at different crop and environmental conditions. Furthermore, the UAV and Landsat images were not acquired on the same date. Hence, applying linear interpolation could also have affected the derived  $ET_C$  models' accuracy. In February, the cloud-free Landsat image was acquired two weeks before the UAV image acquisition. In March, the cloud-free Landsat image was acquired four weeks after the acquisition of the UAV imagery. The huge gap between acquisition dates could have significantly impacted the final results due to microclimate variability. Also, the  $K_c$  values used to validate derived  $ET_C$  were designed for irrigated maize fields with standard conditions and were not adjusted for non-irrigated fields. Considering that water use, productivity, and potential yield are derived using evapotranspiration, this study did not estimate these crop attributes. Furthermore, the study was conducted using rainfed crops. Smallholder croplands in Swayimane do not have crop irrigation facilities; hence this aspect of the project was not addressed.

### 11.3 Conclusion

Based on this study's findings, it can be concluded that multispectral data derived using UAVs could be optimally used to map and monitor smallholder crop attributes throughout the growing season. The UAVs technology could improve smallholder agriculture by facilitating access to information on crop biophysical parameters in near real-time for improved preparedness and operational decision-making. Coupled with accurate meteorological data, the technology allows for precise estimations of crop water requirements and crop evapotranspiration at high spatial resolution. Timely access to crop health information helps inform operational decisions at the farm level, thus, enhancing rural livelihoods and well-being. Subsequently, this will help in optimising productivity in smallholder croplands. However, there is still a need to extend the research evaluating the relative contribution of drone technologies in monitoring other climate-smart crops in smallholder croplands. Specifically, there is limited literature on the utilisation of drones in mapping and monitoring neglected and under-utilised crop species, the impact of weeds, and water quality and quantity assessments in smallholder croplands. The successful implementation of drone technologies is a pathway towards offering detailed and spatially explicit information to smallholder farmers on local variations of cropland characteristics and facilitating on-field decisions for optimising productivity. Furthermore, there is a need to assess how drone-derived data could be integrated with other datasets in building strategies and frameworks for monitoring crop health and productivity while informing policy.

### 11.4 Recommendations

Numerous gaps remain regarding using drone remotely sensed data in mapping and monitoring crop health and water use efficiency. In this regard, several recommendations are listed below.

- More efforts need to be extended in assessing the integration of UAV-derived data with the Google Earth engine as well as ancillary data in characterising farm boundaries.
- There is a need to assess the utility of UAV-derived multispectral data in estimating crop health parameters and ecophysiological attributes such as the canopy chlorophyll content and structural attributes of crops in relation to the environmental attributes of the fields.
- Following the exploratory nature of this project, there is a need to exert more efforts toward the estimation of evapotranspiration of crops using UAV-derived data.
- Future studies could assess other techniques, such as the sap flows and on-site measurement of evapotranspiration, in evaluating water use efficiency.
- Research efforts are still needed to estimate water use and water productivity, potential yield and evapotranspiration using drone remotely sensed data.
- Variables such as soil moisture and precipitation need to be integrated into the characterisation of crop health and water use efficiency models.
- Above all, future studies could evaluate the fusion of freely available remotely sensed data sets and UAV-acquired data in mapping and monitoring crop attributes in smallholder croplands.
- Future studies should consider assessing the accuracy of the SEBS and METRIC-Efflux using on-site validation data or adjusting  $K_c$  values to study area specifications.

More research is needed on deriving SEBS parameters directly from the sensor type used, which will provide a simpler way of estimating  $ET_C$  using UAVs directly.

## References

- Abdel-Rahman, E. M., F. B. Ahmed and R. Ismail (2013). "Random forest regression and spectral band selection for estimating sugarcane leaf nitrogen concentration using EO-1 Hyperion hyperspectral data." International Journal of Remote Sensing **34**(2): 712-728.
- Abdel-Rahman, E. M., O. Mutanga, J. Odindi, E. Adam, A. Odindo and R. Ismail (2014). "A comparison of partial least squares (PLS) and sparse PLS regressions for predicting yield of Swiss chard grown under different irrigation water sources using hyperspectral data." Computers and Electronics in Agriculture **106**: 11-19.
- Abdi, A. M. (2020). "Land cover and land use classification performance of machine learning algorithms in a boreal landscape using Sentinel-2 data." GIScience & Remote Sensing **57**(1): 1-20.
- Aboelghar, M., S. Arafat, M. A. Yousef, M. El-Shirbeny, S. Naeem, A. Massoud, N. J. T. E. J. o. R. S. Saleh and S. Science (2011). "Using SPOT data and leaf area index for rice yield estimation in Egyptian Nile delta." **14**(2): 81-89.
- Adam, E., O. Mutanga, D. Rugege and R. Ismail (2012). "Discriminating the papyrus vegetation (*Cyperus papyrus* L.) and its co-existent species using random forest and hyperspectral data resampled to HYMAP." International Journal of Remote Sensing **33**(2): 552-569.
- Adão, T., J. Hruška, L. Pádua, J. Bessa, E. Peres, R. Morais and J. J. Sousa (2017). "Hyperspectral imaging: A review on UAV-based sensors, data processing and applications for agriculture and forestry." Remote sensing **9**(11): 1110.
- Adetoro, A. A., M. S. C. Ngidi, G. Danso-Abbeam, T. O. Ojo and A. A. Ogundeji (2022). "Impact of irrigation on welfare and vulnerability to poverty in South African farming households." Scientific African **16**: e01177.
- Adisa, O. M., C. M. Botai, J. O. Botai, A. Hassen, D. Darkey, E. Tesfamariam, A. F. Adisa, A. M. Adeola and K. P. Ncongwane (2018). "Analysis of agro-climatic parameters and their influence on maize production in South Africa." Theoretical and applied climatology **134**(3): 991-1004.
- Afzal, A. and S.-F. Mousavi (2008). "Estimation of moisture in maize leaf by measuring leaf dielectric constant." Int J Agricul Biol **10**: 66-68.
- Agbugba, I., M. Christian and A. Obi (2020). "Economic analysis of smallholder maize farmers: implications for public extension services in Eastern Cape." South African Journal of Agricultural Extension **48**(2): 50-63.
- Aghighi, H., M. Azadbakht, D. Ashourloo, H. S. Shahrabi, S. J. I. J. o. S. T. i. A. E. O. Radiom and R. Sensing (2018). "Machine learning regression techniques for the silage maize yield prediction using time-series images of landsat 8 OLI." **11**(12): 4563-4577.

Agidew, A.-m. A. and K. Singh (2017). "The implications of land use and land cover changes for rural household food insecurity in the Northeastern highlands of Ethiopia: the case of the Teleyayen sub-watershed." Agriculture & Food Security **6**(1): 1-14.

Al-Gaadi, K. A., A. A. Hassaballa, E. Tola, A. G. Kayad, R. Madugundu, B. Alblewi and F. Assiri (2016). "Prediction of potato crop yield using precision agriculture techniques." PloS one **11**(9).

Alexandratos, N. and J. Bruinsma (2012). World agriculture towards 2030/2050: the 2012 revision, ESA Working paper No. 12-03, Rome, FAO.

Alexandratos, N. and J. Bruinsma (2012). World agriculture towards 2030/2050: The 2012 revision. Rome, Italy, Food and Agriculture Organisation (FAO): 154.

Ali, A. M., R. Darvishzadeh and A. K. Skidmore (2017). "Retrieval of specific leaf area from landsat-8 surface reflectance data using statistical and physical models." IEEE Journal of selected topics in applied earth observations and remote sensing **10**(8): 3529-3536.

Ali, A. M., R. Darvishzadeh, A. K. Skidmore and I. van Duren (2017). "Specific leaf area estimation from leaf and canopy reflectance through optimization and validation of vegetation indices." Agricultural and forest meteorology **236**: 162-174.

Allen, R., A. Irmak, R. Trezza, J. M. Hendrickx, W. Bastiaanssen and J. Kjaersgaard (2011). "Satellite-based ET estimation in agriculture using SEBAL and METRIC." Hydrological Processes **25**(26): 4011-4027.

Allen, R. G., C. Morton, B. Kamble, A. Kilic, J. Huntington, D. Thau, N. Gorelick, T. Erickson, R. Moore and R. Trezza (2015). EEFlux: A Landsat-based evapotranspiration mapping tool on the Google Earth Engine. 2015 ASABE/IA Irrigation Symposium: Emerging Technologies for Sustainable Irrigation-A Tribute to the Career of Terry Howell, Sr. Conference Proceedings, American Society of Agricultural and Biological Engineers.

Allen, R. G., M. Tasumi, A. Morse, R. Trezza, J. L. Wright, W. Bastiaanssen, W. Kramber, I. Lorite and C. W. Robison (2007). "Satellite-based energy balance for mapping evapotranspiration with internalized calibration (METRIC)—Applications." Journal of irrigation and drainage engineering **133**(4): 395-406.

Allen, R. G., M. Tasumi and R. Trezza (2007). "Satellite-based energy balance for mapping evapotranspiration with internalized calibration (METRIC)—Model." Journal of irrigation and drainage engineering **133**(4): 380-394.

Amani, M. and M. R. Mobasheri (2015). "A parametric method for estimation of leaf area index using landsat ETM+ data." GIScience & Remote Sensing **52**(4): 478-497.

Ambrosone, M., A. Matese, S. F. Di Gennaro, B. Gioli, M. Tudoroiu, L. Genesio, F. Miglietta, S. Baronti, A. Maienza and F. Ungaro (2020). "Retrieving soil moisture in rainfed and irrigated fields using Sentinel-2 observations and a modified OPTRAM approach." International Journal of Applied Earth Observation and Geoinformation **89**: 102113.

- Amin, E., J. Verrelst, J. P. Rivera-Caicedo, L. Pipia, A. Ruiz-Verdú and J. Moreno (2021). "Prototyping Sentinel-2 green LAI and brown LAI products for cropland monitoring." Remote Sensing of Environment **255**: 112168.
- Anderson, H. B., L. Nilsen, H. Tømmervik, S. R. Karlsen, S. Nagai and E. J. Cooper (2016). "Using ordinary digital cameras in place of near-infrared sensors to derive vegetation indices for phenology studies of High Arctic vegetation." Remote Sensing **8**(10): 847.
- Andersson, J., A. J. Zehnder, G. P. Jewitt and H. Yang (2009). "Water availability, demand and reliability of in situ water harvesting in smallholder rain-fed agriculture in the Thukela River Basin, South Africa." Hydrology and Earth System Sciences **13**(12): 2329-2347.
- Aparicio, N., D. Villegas, J. Casadesus, J. L. Araus and C. Royo (2000). "Spectral vegetation indices as nondestructive tools for determining durum wheat yield." Agronomy Journal **92**(1): 83-91.
- Aragon, B., K. Johansen, S. Parkes, Y. Malbeteau, S. Al-Mashharawi, T. Al-Amoudi, C. F. Andrade, D. Turner, A. Lucieer and M. F. McCabe (2020). "A calibration procedure for field and UAV-based uncooled thermal infrared instruments." Sensors **20**(11): 3316.
- Aryalekshmi, B., R. C. Biradar, K. Chandrasekar and J. M. Ahamed (2021). "Analysis of various surface energy balance models for evapotranspiration estimation using satellite data." The Egyptian Journal of Remote Sensing and Space Science **24**(3): 1119-1126.
- Avetisyan, D. and G. Cvetanova (2019). "Water Status Assessment in Maize and Sunflower Crops Using Sentinel-2 Multispectral Data." Space, Ecology, Safety: 152-157.
- Awad, M. M. (2019). "Toward precision in crop yield estimation using remote sensing and optimization techniques." Agriculture **9**(3): 54.
- Bae, J. H., J. Han, D. Lee, J. E. Yang, J. Kim, K. J. Lim, J. C. Neff and W. S. Jang (2019). "Evaluation of sediment trapping efficiency of vegetative filter strips using machine learning models." Sustainability **11**(24): 7212.
- Bala, S. and A. J. I. J. o. R. S. Islam (2009). "Correlation between potato yield and MODIS-derived vegetation indices." **30**(10): 2491-2507.
- Ballester, C., J. Brinkhoff, W. C. Quayle and J. Hornbuckle (2019). "Monitoring the effects of water stress in cotton using the green red vegetation index and red edge ratio." Remote Sensing **11**(7): 873.
- Ballesteros, R., J. Ortega, D. Hernández and M. Moreno (2014). "Applications of georeferenced high-resolution images obtained with unmanned aerial vehicles. Part I: Description of image acquisition and processing." Precision Agriculture **15**(6): 579-592.
- Bano, S., M. Aslam, M. Saleem, S. Basra and K. Aziz (2015). "Evaluation of maize accessions under low temperature stress at early growth stages." J. Anim. Plant Sci **25**(2): 392-400.

Bansouleh, B. F., A. R. Karimi and H. Hesadi (2015). "Evaluation of SEBAL and SEBS Algorithms in the Estimation of Maize Evapotranspiration." International Journal of Plant & Soil Science: 350-358.

Bansouleh, B. F., A. R. Karimi, H. J. I. J. o. P. Hesadi and S. Science (2015). "Evaluation of SEBAL and SEBS Algorithms in the Estimation of Maize Evapotranspiration." 350-358.

Bar-Massada, A. and A. Svir (2020). "Utilizing Vegetation and Environmental New Micro Spacecraft (VENμS) Data to Estimate Live Fuel Moisture Content in Israel's Mediterranean Ecosystems." IEEE Journal of Selected Topics in Applied Earth Observations and Remote Sensing **13**: 3204-3212.

Barbedo, J. G. A. (2019). "A review on the use of unmanned aerial vehicles and imaging sensors for monitoring and assessing plant stresses." Drones **3**(2): 40.

Basdew, M., O. Jiri and P. L. Mafongoya (2017). "Integration of indigenous and scientific knowledge in climate adaptation in KwaZulu-Natal, South Africa." Change and Adaptation in Socio-Ecological Systems **3**(1): 56-67.

Basso, B., D. Cammarano and E. Carfagna (2013). Review of crop yield forecasting methods and early warning systems. Proceedings of the First Meeting of the Scientific Advisory Committee of the Global Strategy to Improve Agricultural and Rural Statistics, FAO Headquarters, Rome, Italy, FAO.

Bastiaanssen, W. G., M. Menenti, R. Feddes and A. Holtslag (1998). "A remote sensing surface energy balance algorithm for land (SEBAL). 1. Formulation." Journal of hydrology **212**: 198-212.

Battude, M., A. Al Bitar, D. Morin, J. Cros, M. Huc, C. M. Sicre, V. Le Dantec and V. J. R. S. o. E. Demarez (2016). "Estimating maize biomass and yield over large areas using high spatial and temporal resolution Sentinel-2 like remote sensing data." **184**: 668-681.

Belgiu, M. and L. Dragut (2016). "Random forest in remote sensing: A review of applications and future directions." ISPRS journal of photogrammetry and remote sensing **114**: 24-31.

Bennett, M. K., N. Younes and K. Joyce (2020). "Automating drone image processing to map coral reef substrates using google earth engine." Drones **4**(3): 50.

Berra, E. and M. Peppas (2020). Advances and Challenges of UAV SFM MVS Photogrammetry and Remote Sensing: Short Review. 2020 IEEE Latin American GRSS & ISPRS Remote Sensing Conference (LAGIRS), IEEE.

Böhler, J. E., M. E. Schaepman and M. Kneubühler (2018). "Crop classification in a heterogeneous arable landscape using uncalibrated UAV data." Remote Sensing **10**(8): 1282.

Bois, B., B. Pauthier, L. Brillante, O. Mathieu, J. Leveque, C. Van Leeuwen, T. Castel and Y. Richard (2020). "Sensitivity of Grapevine Soil-Water Balance to Rainfall Spatial Variability at Local Scale Level." Frontiers in Environmental Science **8**(110).

Boken, V. K. and C. F. Shaykewich (2002). "Improving an operational wheat yield model using phenological phase-based Normalized Difference Vegetation Index." International Journal of Remote Sensing **23**(20): 4155-4168.

Bonada, M., V. Sadras, M. Moran and S. Fuentes (2013). "Elevated temperature and water stress accelerate mesocarp cell death and shrivelling, and decouple sensory traits in Shiraz berries." Irrigation Science **31**(6): 1317-1331.

Boukoberine, M. N., Z. Zhou and M. Benbouzid (2019). "A critical review on unmanned aerial vehicles power supply and energy management: Solutions, strategies, and prospects." Applied Energy **255**: 113823.

Boyle, S. A., C. M. Kennedy, J. Torres, K. Colman, P. E. Perez-Estigarribia and U. Noé (2014). "High-resolution satellite imagery is an important yet underutilized resource in conservation biology." PLoS One **9**(1): e86908.

Brenner, C., C. E. Thiem, H.-D. Witzmann, M. Bernhardt and K. Schulz (2017). "Estimating spatially distributed turbulent heat fluxes from high-resolution thermal imagery acquired with a UAV system." International Journal of Remote Sensing **38**(8-10): 3003-3026.

Brewer, K., A. Clulow, M. Sibanda, S. Gokool, V. Naiken and T. Mabhaudhi (2022). "Predicting the Chlorophyll Content of Maize over Phenotyping as a Proxy for Crop Health in Smallholder Farming Systems." Remote Sensing **14**(3): 518.

Brewer, K., A. Clulow, M. Sibanda, S. Gokool, J. Odindi, O. Mutanga, V. Naiken, V. G. P. Chimonyo and T. Mabhaudhi (2022). "Estimation of Maize Foliar Temperature and Stomatal Conductance as Indicators of Water Stress Based on Optical and Thermal Imagery Acquired Using an Unmanned Aerial Vehicle (UAV) Platform." Drones **6**(7): 169.

Broge, N. H. and E. Leblanc (2001). "Comparing prediction power and stability of broadband and hyperspectral vegetation indices for estimation of green leaf area index and canopy chlorophyll density." Remote sensing of environment **76**(2): 156-172.

Burba, G. (2013). Eddy covariance method for scientific, industrial, agricultural and regulatory applications: A field book on measuring ecosystem gas exchange and areal emission rates, LI-Cor Biosciences.

Cai, X., J. Magidi, L. Nhamo and B. van Koppen (2017). Mapping irrigated areas in the Limpopo Province, South Africa. IWMI Working Paper 172. I. W. P. 172. Colombo, Sri Lanka, International Water Management Institute (IWMI), IWMI Working Paper 172. **IWMI Working Paper 172**: 37.

Cairns, J. E., J. Chamberlin, P. Rutsaert, R. C. Voss, T. Ndhlela and C. Magorokosho (2021). "Challenges for sustainable maize production of smallholder farmers in sub-Saharan Africa." Journal of Cereal Science: 103274.

Cakir, R. (2004). "Effect of water stress at different development stages on vegetative and reproductive growth of corn." Field Crops Research **89**(1): 1-16.

Cammarano, D., G. J. Fitzgerald, R. Casa and B. Basso (2014). "Assessing the robustness of vegetation indices to estimate wheat N in Mediterranean environments." Remote Sensing **6**(4): 2827-2844.

Candiago, S., F. Remondino, M. De Giglio, M. Dubbini and M. Gattelli (2015). "Evaluating multispectral images and vegetation indices for precision farming applications from UAV images." Remote sensing **7**(4): 4026-4047.

Cao, Z. and Q. Wang (2017). "Retrieval of leaf fuel moisture contents from hyperspectral indices developed from dehydration experiments." European journal of remote sensing **50**(1): 18-28.

Carroll, D. A., N. C. Hansen, B. G. Hopkins and K. C. DeJonge (2017). "Leaf temperature of maize and Crop Water Stress Index with variable irrigation and nitrogen supply." Irrigation Science **35**(6): 549-560.

Carter, G. A. (1998). "Reflectance wavebands and indices for remote estimation of photosynthesis and stomatal conductance in pine canopies." Remote Sensing of Environment **63**(1): 61-72.

Carter, M., A. de Janvry, E. Sadoulet and A. Sarris (2014). Index-based weather insurance for developing countries: A review of evidence and a set of propositions for up-scaling. Development Policies Working Paper. Paris, France, Fondation pour les études et recherches sur le développement International. **111**: 42.

Castaldi, F., F. Pelosi, S. Pascucci and R. Casa (2017). "Assessing the potential of images from unmanned aerial vehicles (UAV) to support herbicide patch spraying in maize." Precision Agriculture **18**(1): 76-94.

Castellanos-Quiroz, H. O. A., H. M. Ramírez-Daza and Y. Ivanova (2017). "Detection of open-pit mining zones by implementing spectral indices and image fusion techniques." Dyna **84**(201): 42-49.

Castillo, M. J., S. Boucher and M. Carter (2016). "Index insurance: using public data to benefit small-scale agriculture." International Food and Agribusiness Management Review **19**(1030-2016-83144): 93.

Çetinsoy, E., S. Dikyar, C. Hançer, K. Oner, E. Sirimoglu, M. Unel and M. Aksit (2012). "Design and construction of a novel quad tilt-wing UAV." Mechatronics **22**(6): 723-745.

Cha, M., M. Li and X. Wang (2020). "Estimation of Seasonal Evapotranspiration for Crops in Arid Regions Using Multisource Remote Sensing Images." Remote Sensing **12**(15): 2398.

Chemura, A., O. Mutanga and T. Dube (2017). "Remote sensing leaf water stress in coffee (*Coffea arabica*) using secondary effects of water absorption and random forests." Physics and Chemistry of the Earth, Parts A/B/C **100**: 317-324.

Chirigo, K. C. (2014). An analysis of the economic competitiveness of green maize production in smallholder irrigation schemes: a case of Makhathini flats irrigation scheme in KwaZulu-Natal, South Africa.

Chivasa, W. (2020). UAV and field spectrometer based remote sensing for maize phenotyping, varietal discrimination and yield forecasting.

Chivasa, W., O. Mutanga and C. Biradar (2017). "Application of remote sensing in estimating maize grain yield in heterogeneous African agricultural landscapes: a review." International Journal of Remote Sensing **38**(23): 6816-6845.

Chivasa, W., O. Mutanga and C. Biradar (2020). "UAV-based multispectral phenotyping for disease resistance to accelerate crop improvement under changing climate conditions." Remote Sensing **12**(15): 2445.

Chivasa, W., O. Mutanga and C. J. I. J. o. R. S. Biradar (2017). "Application of remote sensing in estimating maize grain yield in heterogeneous African agricultural landscapes: a review." **38**(23): 6816-6845.

Chivasa, W., O. Mutanga and C. J. R. S. Biradar (2020). "UAV-based multispectral phenotyping for disease resistance to accelerate crop improvement under changing climate conditions." **12**(15): 2445.

Chivasa, W., O. Mutanga and J. Burgueño (2021). "UAV-based high-throughput phenotyping to increase prediction and selection accuracy in maize varieties under artificial MSV inoculation." Computers and Electronics in Agriculture **184**: 106128.

Chou, T.-Y., M.-L. Yeh, Y. C. Chen and Y. H. Chen (2010). Disaster monitoring and management by the Unmanned Aerial Vehicle technology. ISPRS TC VII Symposium – 100 Years ISPRS. W. Wagner and B. Székely. Vienna, Austria, International Society for Photogrammetry and Remote Sensing (ISPRS). **XXXVIII, Part 7B**.

Ciampitti, I. A., R. W. Elmore and J. Lauer (2011). "Corn growth and development." Dent **5**(75).

Ciganda, V. S., A. A. Gitelson and J. Schepers (2012). "How deep does a remote sensor sense? Expression of chlorophyll content in a maize canopy." Remote Sensing of Environment **126**: 240-247.

Cihlar, J., L. S.-. Laurent and J. Dyer (1991). "Relation between the normalized difference vegetation index and ecological variables." Remote sensing of Environment **35**(2-3): 279-298.

Clevers, J. G. and A. A. Gitelson (2013). "Remote estimation of crop and grass chlorophyll and nitrogen content using red-edge bands on Sentinel-2 and-3." International Journal of Applied Earth Observation and Geoinformation **23**: 344-351.

Coelho, D. T. and R. F. Dale (1980). "An Energy-Crop Growth Variable and Temperature Function for Predicting Corn Growth and Development: Planting to Silking 1." Agronomy Journal **72**(3): 503-510.

- Colombo, R., M. Meroni, A. Marchesi, L. Busetto, M. Rossini, C. Giardino and C. Panigada (2008). "Estimation of leaf and canopy water content in poplar plantations by means of hyperspectral indices and inverse modeling." Remote sensing of environment **112**(4): 1820-1834.
- Cosgrove, W. J. and D. P. Loucks (2015). "Water management: Current and future challenges and research directions." Water Resources Research **51**(6): 4823-4839.
- Costa, C., L. M. Dwyer, P. Dutilleul, D. W. Stewart, B. L. Ma and D. L. Smith (2001). "Inter-relationships of applied nitrogen, SPAD, and yield of leafy and non-leafy maize genotypes." Journal of plant nutrition **24**(8): 1173-1194.
- Costa, C., D. Frigon, P. Dutilleul, L. M. Dwyer, V. D. Pillar, D. W. Stewart and D. L. Smith (2003). "Sample size determination for chlorophyll meter readings on maize hybrids with a broad range of canopy types." Journal of plant Nutrition **26**(5): 1117-1130.
- Costa, J. d. O., R. D. Coelho, W. Wolff, J. V. José, M. V. Folegatti and S. F. d. B. Ferraz (2019). "Spatial variability of coffee plant water consumption based on the SEBAL algorithm." Scientia Agricola **76**(2): 93-101.
- Cousins, B. (2010). What is a 'smallholder'? Class-analytic perspectives on small-scale farming and agrarian reform in South Africa. Reforming Land and Resource Use in South Africa. P. Hebinck and C. Shackleton. Bellville, South Africa, Routledge: 102-127.
- Craine, J. M. and R. Dybzinski (2013). "Mechanisms of plant competition for nutrients, water and light." Functional Ecology **27**(4): 833-840.
- Cucho-Padin, G., H. Loayza, S. Palacios, M. Balcazar, M. Carbajal and R. Quiroz (2020). "Development of low-cost remote sensing tools and methods for supporting smallholder agriculture." Applied Geomatics **12**(3): 247-263.
- DAFF (2017). "A profile of the South African maize market value chain." Department of agriculture, forestry and fisheries: 1-47.
- Dahms, T., S. Seissiger, C. Conrad and E. Borg (2016). "MODELLING BIOPHYSICAL PARAMETERS OF MAIZE USING LANDSAT 8 TIME SERIES." International Archives of the Photogrammetry, Remote Sensing & Spatial Information Sciences **41**.
- Dai, Y., R. E. Dickinson and Y.-P. Wang (2004). "A two-big-leaf model for canopy temperature, photosynthesis, and stomatal conductance." Journal of climate **17**(12): 2281-2299.
- Dalezios, N. R., N. Dercas and S. S. Eslamian (2018). "Water scarcity management: part 2: satellite-based composite drought analysis." International Journal of Global Environmental Issues **17**(2-3): 262-295.
- Daryanto, S., L. Wang and P.-A. Jacinthe (2016). "Global synthesis of drought effects on maize and wheat production." PloS one **11**(5): e0156362.

Das, B., R. N. Sahoo, S. Pargal, G. Krishna, R. Verma, C. Viswanathan, V. K. Sehgal and V. K. Gupta (2021). "Evaluation of different water absorption bands, indices and multivariate models for water-deficit stress monitoring in rice using visible-near infrared spectroscopy." Spectrochimica Acta Part A: Molecular and Biomolecular Spectroscopy **247**: 119104.

Daughtry, C. S., C. Walthall, M. Kim, E. B. De Colstoun and J. McMurtrey Iii (2000). "Estimating corn leaf chlorophyll concentration from leaf and canopy reflectance." Remote sensing of Environment **74**(2): 229-239.

Davidson, A., S. Wang and J. Wilmshurst (2006). "Remote sensing of grassland-shrubland vegetation water content in the shortwave domain." International Journal of Applied Earth Observation and Geoinformation **8**(4): 225-236.

de Castro, A., J. Peña, J. Torres-Sánchez, F. Jiménez-Brenes and F. López-Granados (2017). "Mapping *Cynodon dactylon* in vineyards using UAV images for site-specific weed control." Advances in Animal Biosciences **8**(2): 267-271.

de Castro, A. I., J. Torres-Sánchez, J. M. Peña, F. M. Jiménez-Brenes, O. Csillik and F. López-Granados (2018). "An automatic random forest-obia algorithm for early weed mapping between and within crop rows using UAV imagery." Remote Sensing **10**(2): 285.

de Oliveira Costa, J., J. V. José, W. Wolff, N. P. R. de Oliveira, R. C. Oliveira, N. L. Ribeiro, R. D. Coelho, T. J. A. da Silva, E. M. Bonfim-Silva and A. F. Schlichting (2020). "Spatial variability quantification of maize water consumption based on Google EEflux tool." Agricultural Water Management **232**: 106037.

DeBell, L., K. Anderson, R. E. Brazier, N. King and L. Jones (2015). "Water resource management at catchment scales using lightweight UAVs: Current capabilities and future perspectives." Journal of Unmanned Vehicle Systems **4**(1): 7-30.

Delavarpour, N., C. Koparan, J. Nowatzki, S. Bajwa and X. Sun (2021). "A technical study on UAV characteristics for precision agriculture applications and associated practical challenges." Remote Sensing **13**(6): 1204.

Delegido, J., J. Verrelst, L. Alonso and J. Moreno (2011). "Evaluation of Sentinel-2 Red-Edge Bands for Empirical Estimation of Green LAI and Chlorophyll Content." Sensors **11**(7): 7063-7081.

Department of Agriculture, F. and Fisheries (2012). A framework for the development of smallholder farmers through cooperatives development, Department of Agriculture, Forestry and Fisheries Pretoria.

Dhau, I., E. Adam, O. Mutanga, K. Ayisi, E. M. Abdel-Rahman, J. Odindi and M. J. G. I. Masocha (2018). "Testing the capability of spectral resolution of the new multispectral sensors on detecting the severity of grey leaf spot disease in maize crop." **33**(11): 1223-1236.

- Di Gennaro, S. F., F. Rizza, F. W. Badeck, A. Berton, S. Delbono, B. Gioli, P. Toscano, A. Zaldei and A. Matese (2018). "UAV-based high-throughput phenotyping to discriminate barley vigour with visible and near-infrared vegetation indices." International Journal of Remote Sensing **39**(15-16): 5330-5344.
- Dobrowski, S., J. Pushnik, P. J. Zarco-Tejada and S. L. Ustin (2005). "Simple reflectance indices track heat and water stress-induced changes in steady-state chlorophyll fluorescence at the canopy scale." Remote sensing of environment **97**(3): 403-414.
- Dong, T., J. Liu, J. Shang, B. Qian, B. Ma, J. M. Kovacs, D. Walters, X. Jiao, X. Geng and Y. J. R. S. o. E. Shi (2019). "Assessment of red-edge vegetation indices for crop leaf area index estimation." **222**: 133-143.
- Dou, H., G. Niu and M. J. H. Gu (2019). "Photosynthesis, morphology, yield, and phytochemical accumulation in basil plants influenced by substituting green light for partial red and/or blue light." **54**(10): 1769-1776.
- Du Plessis, J. (2003). Maize production, Department of Agriculture Pretoria, South Africa.
- Du, T., S. Kang, J. Zhang and W. J. Davies (2015). "Deficit irrigation and sustainable water-resource strategies in agriculture for China's food security." Journal of Experimental Botany **66**(8): 2253-2269.
- Dube, T., O. Mutanga, M. Sibanda, C. Shoko, A. J. P. Chemura and P. A. B. C. Chemistry of the Earth (2017). "Evaluating the influence of the Red Edge band from RapidEye sensor in quantifying leaf area index for hydrological applications specifically focussing on plant canopy interception." **100**: 73-80.
- Duveiller, G., R. López-Lozano and B. Baruth (2013). "Enhanced processing of 1-km spatial resolution fAPAR time series for sugarcane yield forecasting and monitoring." Remote Sensing **5**(3): 1091-1116.
- Dye, M., O. Mutanga and R. Ismail (2011). "Examining the utility of random forest and AISA Eagle hyperspectral image data to predict *Pinus patula* age in KwaZulu-Natal, South Africa." Geocarto International **26**(4): 275-289.
- Dzikiti, S., T. Volschenk, S. Midgley, E. Lötze, N. Taylor, M. B. Gush, Z. Ntshidi, S. Zirebwa, Q. Doko and M. Schmeisser (2018). "Estimating the water requirements of high yielding and young apple orchards in the winter rainfall areas of South Africa using a dual source evapotranspiration model." Agricultural water management **208**: 152-162.
- Easterday, K., C. Kislik, T. E. Dawson, S. Hogan and M. Kelly (2019). "Remotely sensed water limitation in vegetation: insights from an experiment with unmanned aerial vehicles (UAVs)." Remote Sensing **11**(16): 1853.

El-Hendawy, S. E., N. A. Al-Suhaibani, S. Elsayed, W. M. Hassan, Y. H. Dewir, Y. Refay and K. A. Abdella (2019). "Potential of the existing and novel spectral reflectance indices for estimating the leaf water status and grain yield of spring wheat exposed to different irrigation rates." Agricultural Water Management **217**: 356-373.

Elarab, M., A. F. Torres-Rua, W. Kustas, H. Nieto, L. Song, J. G. Alfieri, J. H. Prueger, L. McKee, M. Anderson and L. Sanchez (2015). Use of Aggieair UAS Remote Sensing Data to Estimate Crop ET at High Spatial Resolution. Synergy in Science: Partnering for Solutions 2015 Annual Meeting. Minneapolis, MN, USA, Entomological Society of America.

Elhag, M., A. Psilovikos, I. Manakos and K. Perakis (2011). "Application of the SEBS water balance model in estimating daily evapotranspiration and evaporative fraction from remote sensing data over the Nile Delta." Water Resources Management **25**(11): 2731-2742.

Ellsäßer, F., C. Stiegler, A. Röhl, T. June, A. Knohl and D. Hölscher (2021). "Predicting evapotranspiration from drone-based thermography – a method comparison in a tropical oil palm plantation." Biogeosciences **18**(3): 861-872.

Elsherif, A., R. Gaulton and J. Mills (2019). Measuring Leaf Equivalent Water Thickness of Short-Rotation Coppice Willow Canopy Using Terrestrial Laser Scanning. IGARSS 2019-2019 IEEE International Geoscience and Remote Sensing Symposium, IEEE.

Fan, J., J. Zheng, L. Wu and F. Zhang (2021). "Estimation of daily maize transpiration using support vector machines, extreme gradient boosting, artificial and deep neural networks models." Agricultural Water Management **245**: 106547.

Fan, M., J. Shen, L. Yuan, R. Jiang, X. Chen, W. J. Davies and F. Zhang (2011). "Improving crop productivity and resource use efficiency to ensure food security and environmental quality in China." Journal of experimental botany **63**(1): 13-24.

Fan, S. and C. Rue (2020). The role of smallholder farms in a changing world. The role of smallholder farms in food and nutrition security, Springer, Cham: 13-28.

Fang, Y. and R. Ramasamy (2015). "Current and prospective methods for plant disease detection." Biosensors **5**(3): 537-561.

FAO (2015). The impact of natural hazards and disasters on agriculture and food security and nutrition: A call for action to build resilient livelihoods. World Conference on Disaster Risk Reduction. Sendai, Japan, Food and Agriculture Organisation of the United Nations (FAO): 16.

Fereres, E. and M. A. Soriano (2006). "Deficit irrigation for reducing agricultural water use." Journal of experimental botany **58**(2): 147-159.

Fernandez-Ordoñez, Y. M. and J. Soria-Ruiz (2017). Maize crop yield estimation with remote sensing and empirical models. 2017 IEEE international geoscience and remote sensing symposium (IGARSS), IEEE.

- Filella, I., L. Serrano, J. Serra and J. Penuelas (1995). "Evaluating wheat nitrogen status with canopy reflectance indices and discriminant analysis." Crop Science **35**(5): 1400-1405.
- Filgueiras, R., E. C. Mantovani, S. H. B. Dias, E. I. Fernandes Filho, F. F. da Cunha and C. M. U. J. E. J. o. A. Neale (2019). "New approach to determining the surface temperature without thermal band of satellites." **106**: 12-22.
- Fitzgerald, G., D. Rodriguez and G. O'Leary (2010). "Measuring and predicting canopy nitrogen nutrition in wheat using a spectral index—The canopy chlorophyll content index (CCCI)." Field Crops Research **116**(3): 318-324.
- Flynn, K. C., A. E. Frazier and S. Admas (2020). "Performance of chlorophyll prediction indices for Eragrostis tef at Sentinel-2 MSI and Landsat-8 OLI spectral resolutions." Precision Agriculture: 1-15.
- Fu, Y., G. Yang, J. Wang, X. Song, H. J. C. Feng and E. i. Agriculture (2014). "Winter wheat biomass estimation based on spectral indices, band depth analysis and partial least squares regression using hyperspectral measurements." **100**: 51-59.
- Fuentes, S., R. De Bei, J. Pech and S. Tyerman (2012). "Computational water stress indices obtained from thermal image analysis of grapevine canopies." Irrigation Science **30**(6): 523-536.
- Furuya, D. E. G., J. A. F. Aguiar, N. V. Estrabis, M. M. F. Pinheiro, M. T. G. Furuya, D. R. Pereira, W. N. Gonçalves, V. Liesenberg, J. Li and J. Marcato Junior (2020). "A Machine Learning Approach for Mapping Forest Vegetation in Riparian Zones in an Atlantic Biome Environment Using Sentinel-2 Imagery." Remote Sensing **12**(24): 4086.
- Gago, J., C. Douthe, R. Coopman, P. Gallego, M. Ribas-Carbo, J. Flexas, J. Escalona and H. Medrano (2015). "UAVs challenge to assess water stress for sustainable agriculture." Agricultural Water Management **153**: 9-19.
- Gao, B.-C. (1996). "NDWI—A normalized difference water index for remote sensing of vegetation liquid water from space." Remote sensing of environment **58**(3): 257-266.
- Gao, L., G. Yang, H. Li, Z. Li, H. Feng, L. Wang, J. Dong and P. J. Z. S. N. X. C. J. o. E.-A. He (2016). "Winter wheat LAI estimation using unmanned aerial vehicle RGB-imaging." **24**(9): 1254-1264.
- García, M., E. Chuvieco, H. Nieto and I. Aguado (2008). "Combining AVHRR and meteorological data for estimating live fuel moisture content." Remote Sensing of Environment **112**(9): 3618-3627.
- Ge, T., F. Sui, L. Bai, C. Tong and N. Sun (2012). "Effects of water stress on growth, biomass partitioning, and water-use efficiency in summer maize (*Zea mays* L.) throughout the growth cycle." Acta Physiologiae Plantarum **34**(3): 1043-1053.

- Geneti, T. Z. (2019). "Review on the Effect of Moisture or Rain Fall on Crop Production." Civil and Environmental Research **11**(2224-5790).
- Gerhards, M., M. Schlerf, K. Mallick and T. Udelhoven (2019). "Challenges and future perspectives of multi-/Hyperspectral thermal infrared remote sensing for crop water-stress detection: A review." Remote Sensing **11**(10): 1240.
- Ghooshchi, F., M. Seilsepour and P. Jafari (2008). "Effects of water stress on yield and some agronomic traits of maize (SC 301)." Am-Eurasian J Agric Environ Sci **4**(3): 302-305.
- Gibson, L., C. Jarman, Z. Su and F. Eckardt (2013). "Estimating evapotranspiration using remote sensing and the Surface Energy Balance System – A South African perspective." Water SA **39**(4): 477-484.
- Giller, K. E. (2020). "The food security conundrum of sub-Saharan Africa." Global Food Security **26**: 100431.
- Gitelson, A. A., Y. Peng, T. J. Arkebauer and J. Schepers (2014). "Relationships between gross primary production, green LAI, and canopy chlorophyll content in maize: Implications for remote sensing of primary production." Remote Sensing of Environment **144**: 65-72.
- Gitelson, A. A., Y. Peng and K. F. Huemmrich (2014). "Relationship between fraction of radiation absorbed by photosynthesizing maize and soybean canopies and NDVI from remotely sensed data taken at close range and from MODIS 250 m resolution data." Remote Sensing of Environment **147**: 108-120.
- Göbel, L., H. Coners, D. Hertel, S. Willinghöfer and C. Leuschner (2019). "The role of low soil temperature for photosynthesis and stomatal conductance of three graminoids from different elevations." Frontiers in plant science **10**: 330.
- Godfray, H. C. J., J. R. Beddington, I. R. Crute, L. Haddad, D. Lawrence, J. F. Muir, J. Pretty, S. Robinson, S. M. Thomas and C. Toulmin (2010). "Food security: the challenge of feeding 9 billion people." science **327**(5967): 812-818.
- Gokool, S., K. Chetty, G. Jewitt and A. Heeralal (2016). "Estimating total evaporation at the field scale using the SEBS model and data infilling procedures." Water SA **42**(4): 673-683.
- Gollin, D. J. I. W. P. I., London (2014). "Smallholder agriculture in Africa."
- Gomez-del-Campo, M., C. Ruiz and J. R. Lissarrague (2002). "Effect of water stress on leaf area development, photosynthesis, and productivity in Chardonnay and Airén grapevines." American Journal of Enology and Viticulture **53**(2): 138-143.
- Gomez y Paloma, S., L. Riesgo and K. Louhichi (2020). The Role of Smallholder Farms in Food and Nutrition Security, Springer Nature.
- Gonzalez-Aguilera, D. and P. Rodriguez-Gonzalvez (2017). "Drones—An Open Access Journal." Drones **1**(1): 5.

González-Dugo, M., M. Moran, L. Mateos and R. Bryant (2006). "Canopy temperature variability as an indicator of crop water stress severity." Irrigation Science **24**(4): 233.

González-Sanpedro, M., T. Le Toan, J. Moreno, L. Kergoat and E. Rubio (2008). "Seasonal variations of leaf area index of agricultural fields retrieved from Landsat data." Remote Sensing of Environment **112**(3): 810-824.

Gonzalez, J. A., M. Gallardo, M. B. Hilal, M. D. Rosa and F. E. Prado (2009). "Physiological responses of quinoa (*Chenopodium quinoa*) to drought and waterlogging stresses: dry matter partitioning."

Gorelick, N., M. Hancher, M. Dixon, S. Ilyushchenko, D. Thau and R. Moore (2017). "Google Earth Engine: Planetary-scale geospatial analysis for everyone." Remote sensing of Environment **202**: 18-27.

Govaerts, B. and N. Verhulst (2010). The normalized difference vegetation index (NDVI) Greenseeker (TM) handheld sensor: toward the integrated evaluation of crop management part A: concepts and case studies. Mexico City, Mexico, International Maize and Wheat Improvement Center (CIMMYT): 16.

Govindaraj, M., M. Vetriventhan and M. Srinivasan (2015). "Importance of genetic diversity assessment in crop plants and its recent advances: an overview of its analytical perspectives." Genetics research international **2015**.

Graeb, B. E., M. J. Chappell, H. Wittman, S. Ledermann, R. B. Kerr and B. Gemmill-Herren (2016). "The state of family farms in the world." World Development **87**: 1-15.

Grajek, H., D. Rydzyński, A. Piotrowicz-Cieślak, A. Herman, M. Maciejczyk and Z. J. C. Wieczorek (2020). "Cadmium ion-chlorophyll interaction – Examination of spectral properties and structure of the cadmium-chlorophyll complex and their relevance to photosynthesis inhibition." **261**: 127434.

Greatrex, H., J. Hansen, S. Garvin, R. Diro, M. Le Guen, S. Blakeley, K. Rao and D. Osgood (2015). Scaling up index insurance for smallholder farmers: Recent evidence and insights. Copenhagen, Denmark, CGIAR Research Program on Climate Change, Agriculture and Food Security (CCAFS): 32.

Grosso, C., G. Manoli, M. Martello, Y. H. Chemin, D. H. Pons, P. Teatini, I. Piccoli and F. Morari (2018). "Mapping maize evapotranspiration at field scale using SEBAL: A comparison with the FAO method and soil-plant model simulations." Remote Sensing **10**(9): 1452.

Guindin-Garcia, N. (2010). "Estimating maize grain yield from crop biophysical parameters using remote sensing."

Guo, Y., G. Yin, H. Sun, H. Wang, S. Chen, J. Senthilnath, J. Wang and Y. Fu (2020). "Scaling Effects on Chlorophyll Content Estimations with RGB Camera Mounted on a UAV Platform Using Machine-Learning Methods." Sensors **20**(18): 5130.

- Guomin, S., W. Yajie and H. J. S. A. Wenting (2020). "Estimation Method of Leaf Area Index for Summer Maize Using UAV-Based Multispectral Remote Sensing." **2**(3): 118.
- Haarhoff, S. J., T. N. Kotzé and P. A. Swanepoel (2020). "A prospectus for sustainability of rainfed maize production systems in South Africa." Crop Science **60**(1): 14-28.
- Haboudane, D., J. R. Miller, N. Tremblay, P. J. Zarco-Tejada and L. Dextraze (2002). "Integrated narrow-band vegetation indices for prediction of crop chlorophyll content for application to precision agriculture." Remote sensing of environment **81**(2-3): 416-426.
- Hackney, C. and A. Clayton (2015). Unmanned Aerial Vehicles (UAVs) and their application in geomorphic mapping. Geomorphological Techniques. L. Clarke. London, UK, British Society for Geomorphology (BSG): 12.
- Haghighian, F., S. Yousefi and S. Keesstra (2020). "Identifying tree health using sentinel-2 images: a case study on Tortrix viridana L. infected oak trees in Western Iran." Geocarto International: 1-11.
- Hall, C., T. Dawson, J. Macdiarmid, R. Matthews and P. Smith (2017). "The impact of population growth and climate change on food security in Africa: looking ahead to 2050." International Journal of Agricultural Sustainability **15**(2): 124-135.
- Han, L., G. Yang, H. Dai, B. Xu, H. Yang, H. Feng, Z. Li and X. Yang (2019). "Modeling maize above-ground biomass based on machine learning approaches using UAV remote-sensing data." Plant Methods **15**(1): 1-19.
- Han, L., G. Yang, H. Dai, H. Yang, B. Xu, H. Feng, Z. Li and X. Yang (2019). "Fuzzy Clustering of Maize Plant-Height Patterns Using Time Series of UAV Remote-Sensing Images and Variety Traits." Frontiers in Plant Science **10**(926).
- Handiganoor, M. G., S. Patil and S. Vasudevan (2018). "Effect of Seed Coating Polymer and Micronutrients on Stomatal Conductance and Resistance at Different Growth Stages of Pigeonpea." Advances in Research: 1-8.
- Hasanuzzaman, M., K. Nahar, M. Alam, R. Roychowdhury and M. Fujita (2013). "Physiological, biochemical, and molecular mechanisms of heat stress tolerance in plants." International journal of molecular sciences **14**(5): 9643-9684.
- Hassanijalilian, O., C. Igathinathane, C. Doetkott, S. Bajwa, J. Nowatzki and S. A. H. Esmaeili (2020). "Chlorophyll estimation in soybean leaves infield with smartphone digital imaging and machine learning." Computers and Electronics in Agriculture **174**: 105433.
- Hatfield, J. L. and J. H. Prueger (2010). "Value of using different vegetative indices to quantify agricultural crop characteristics at different growth stages under varying management practices." Remote Sensing **2**(2): 562-578.
- Haxeltine, A. and I. Prentice (1996). "A general model for the light-use efficiency of primary production." Functional Ecology: 551-561.

He, J., N. Zhang, X. Su, J. Lu, X. Yao, T. Cheng, Y. Zhu, W. Cao and Y. J. R. S. Tian (2019). "Estimating leaf area index with a new vegetation index considering the influence of rice panicles." **11**(15): 1809.

Hernández-Clemente, R., A. Hornero, M. Mottus, J. Peñuelas, V. González-Dugo, J. Jiménez, L. Suárez, L. Alonso and P. J. Zarco-Tejada (2019). "Early diagnosis of vegetation health from high-resolution hyperspectral and thermal imagery: Lessons learned from empirical relationships and radiative transfer modelling." Current forestry reports **5**(3): 169-183.

Hoffmann, H., R. Jensen, A. Thomsen, H. Nieto, J. Rasmussen and T. Friborg (2016). "Crop water stress maps for an entire growing season from visible and thermal UAV imagery." Biogeosciences **13**(24): 6545-6563.

Hoffmann, H., R. Jensen, A. Thomsen, H. Nieto, J. Rasmussen and T. Friborg (2016). "Crop water stress maps for an entire growing season from visible and thermal UAV imagery."

Hu, H., M. Siala, E. Hebrard and M.-J. Huguet (2020). Learning optimal decision trees with MaxSAT and its integration in AdaBoost. IJCAI-PRICAI 2020, 29th International Joint Conference on Artificial Intelligence and the 17th Pacific Rim International Conference on Artificial Intelligence.

Hu, P., S. C. Chapman and B. Zheng (2021). "Coupling of machine learning methods to improve estimation of ground coverage from unmanned aerial vehicle (UAV) imagery for high-throughput phenotyping of crops." Functional Plant Biology.

Huang, C., Y. Chen, S. Zhang and J. Wu (2018). "Detecting, extracting, and monitoring surface water from space using optical sensors: A review." Reviews of Geophysics **56**(2): 333-360.

Huang, C., Y. Li, J. Gu, L. Lu and X. Li (2015). "Improving estimation of evapotranspiration under water-limited conditions based on SEBS and MODIS data in arid regions." Remote Sensing **7**(12): 16795-16814.

Huang, J., H. Wang, Q. Dai and D. Han (2014). "Analysis of NDVI Data for Crop Identification and Yield Estimation." IEEE Journal of Selected Topics in Applied Earth Observations and Remote Sensing **7**(11): 4374-4384.

Huete, A. R. (1988). "A soil-adjusted vegetation index (SAVI)." Remote sensing of environment **25**(3): 295-309.

Hunt Jr, E. R. and C. S. Daughtry (2017). "What good are unmanned aircraft systems for agricultural remote sensing and precision agriculture?" International Journal of Remote Sensing: 1-32.

Hunt Jr, E. R. and C. S. Daughtry (2018). "What good are unmanned aircraft systems for agricultural remote sensing and precision agriculture?" International journal of remote sensing **39**(15-16): 5345-5376.

- Hussain, S., K. Gao, M. Din, Y. Gao, Z. Shi and S. Wang (2020). "Assessment of UAV-Onboard Multispectral Sensor for non-destructive site-specific rapeseed crop phenotype variable at different phenological stages and resolutions." Remote Sensing **12**(3): 397.
- Hutton, J., G. Lipa, D. Baustian, J. Sulik and R. Bruce (2020). "High Accuracy Direct Georeferencing of the Altum Multi-Spectral Uav Camera and its Application to High Throughput Plant Phenotyping." The International Archives of Photogrammetry, Remote Sensing and Spatial Information Sciences **43**: 451-456.
- Igbadun, H. E., H. F. Mahoo, A. K. Tarimo and B. A. Salim (2006). "Crop water productivity of an irrigated maize crop in Mkoji sub-catchment of the Great Ruaha River Basin, Tanzania." Agricultural water management **85**(1-2): 141-150.
- Ihuoma, S. O. and C. A. Madramootoo (2017). "Recent advances in crop water stress detection." Computers and Electronics in Agriculture **141**: 267-275.
- Ishihara, M., Y. Inoue, K. Ono, M. Shimizu and S. Matsuura (2015). "The impact of sunlight conditions on the consistency of vegetation indices in croplands—Effective usage of vegetation indices from continuous ground-based spectral measurements." Remote Sensing **7**(10): 14079-14098.
- IWMI (2015). Irrigated area map of Asia (2000-2010) and Africa (2010). Colombo, Sri Lanka, International Water Management Institute (IWMI).
- Jackson, R. D., S. Idso, R. Reginato and P. Pinter Jr (1981). "Canopy temperature as a crop water stress indicator." Water resources research **17**(4): 1133-1138.
- Jackson, T. J., D. Chen, M. Cosh, F. Li, M. Anderson, C. Walthall, P. Doriaswamy and E. R. Hunt (2004). "Vegetation water content mapping using Landsat data derived normalized difference water index for corn and soybeans." Remote Sensing of Environment **92**(4): 475-482.
- Jamshidi, S., S. Zand-Parsa and D. Niyogi (2021). "Assessing crop water stress index of citrus using in-situ measurements, Landsat, and Sentinel-2 Data." International Journal of Remote Sensing **42**(5): 1893-1916.
- Jamshidi, S., S. Zand-parsa, M. Pakparvar and D. Niyogi (2019). "Evaluation of evapotranspiration over a semiarid region using multiresolution data sources." Journal of Hydrometeorology **20**(5): 947-964.
- Jayanthi, H., G. J. Husak, C. Funk, T. Magadzire, A. Chavula and J. P. Verdin (2013). "Modeling rain-fed maize vulnerability to droughts using the standardized precipitation index from satellite estimated rainfall—Southern Malawi case study." International Journal of Disaster Risk Reduction **4**: 71-81.
- Jégo, G., E. Pattey and J. J. F. C. R. Liu (2012). "Using Leaf Area Index, retrieved from optical imagery, in the STICS crop model for predicting yield and biomass of field crops." **131**: 63-74.

Jeong, J. H., J. P. Resop, N. D. Mueller, D. H. Fleisher, K. Yun, E. E. Butler, D. J. Timlin, K.-M. Shim, J. S. Gerber and V. R. Reddy (2016). "Random forests for global and regional crop yield predictions." PLoS One **11**(6): e0156571.

Jin, X., S. Liu, F. Baret, M. Hemerlé and A. Comar (2017). "Estimates of plant density of wheat crops at emergence from very low altitude UAV imagery." Remote Sensing of Environment **198**: 105-114.

Jin, X., C. Shi, C. Y. Yu, T. Yamada and E. J. Sacks (2017). "Determination of Leaf Water Content by Visible and Near-Infrared Spectrometry and Multivariate Calibration in Miscanthus." Frontiers in Plant Science **8**(721).

Jin, Z., G. Azzari, C. You, S. Di Tommaso, S. Aston, M. Burke and D. B. J. R. S. o. E. Lobell (2019). "Smallholder maize area and yield mapping at national scales with Google Earth Engine." **228**: 115-128.

Jones, H. G. (2004). "Irrigation scheduling: advantages and pitfalls of plant-based methods." Journal of experimental botany **55**(407): 2427-2436.

Jones, T. (2017). International Commercial Drone Regulation and Drone Delivery Services. Santa Monica, California, USA, Rand Corporation. **RR-1718/3-RC**.

Jovanovic, N. and S. Israel (2012). Critical review of methods for the estimation of actual evapotranspiration in hydrological models. Evapotranspiration-Remote Sensing and Modeling, InTech: 24.

Jurdao, S., M. Yebra, J. P. Guerschman and E. Chuvieco (2013). "Regional estimation of woodland moisture content by inverting Radiative Transfer Models." Remote Sensing of Environment **132**: 59-70.

Kabanda, T. (2015). "An approach to land capability evaluation for agriculture using remote sensing and GIS in Barberspan, North West Province of South Africa." African Journal of Science, Technology, Innovation and Development **7**(6): 453-461.

Kamali, M. I. and R. Nazari (2018). "Determination of maize water requirement using remote sensing data and SEBAL algorithm." Agricultural Water Management **209**: 197-205.

Kamara, A., A. Conteh, E. R. Rhodes and R. A. Cooke (2019). "The relevance of smallholder farming to African agricultural growth and development." African Journal of Food, Agriculture, Nutrition and Development **19**(1): 14043-14065.

Kamyab, A. D., S. Mokhtari and R. Jafarinia (2022). "A comparative study in quantification of maize evapotranspiration for Iranian maize farm using SEBAL and METRIC-1 EEFLux algorithms." Acta Geophysica: 1-14.

Kanning, M., I. Kühling, D. Trautz and T. Jarmer (2018). "High-resolution UAV-based hyperspectral imagery for LAI and chlorophyll estimations from wheat for yield prediction." Remote Sensing **10**(12): 2000.

- Kanning, M., I. Kühling, D. Trautz and T. J. R. S. Jarmer (2018). "High-resolution UAV-based hyperspectral imagery for LAI and chlorophyll estimations from wheat for yield prediction." **10**(12): 2000.
- Kayad, A., M. Sozzi, S. Gatto, F. Marinello and F. J. R. S. Pirotti (2019). "Monitoring within-field variability of corn yield using Sentinel-2 and machine learning techniques." **11**(23): 2873.
- Kayet, N., K. Pathak, A. Chakrabarty and S. Sahoo (2016). "Urban heat island explored by co-relationship between land surface temperature vs multiple vegetation indices." Spatial Information Research **24**(5): 515-529.
- Keen, S. and H. Winkler (2020). "Enhanced Direct Access finance in South Africa: SANBI and the Adaptation Fund."
- Ketema, H., W. Wei, A. Legesse, Z. Wolde, H. Temesgen, F. Yimer and A. Mamo (2020). "Quantifying smallholder farmers' managed land use/land cover dynamics and its drivers in contrasting agro-ecological zones of the East African Rift." Global Ecology and Conservation **21**: e00898.
- Khaliq, A., L. Comba, A. Biglia, D. Ricauda Aimonino, M. Chiaberge and P. J. R. S. Gay (2019). "Comparison of satellite and UAV-based multispectral imagery for vineyard variability assessment." **11**(4): 436.
- Khan, Z., V. Rahimi-Eichi, S. Haefele, T. Garnett and S. J. Miklavcic (2018). "Estimation of vegetation indices for high-throughput phenotyping of wheat using aerial imaging." Plant methods **14**(1): 1-11.
- Khan, Z., V. Rahimi-Eichi, S. Haefele, T. Garnett and S. J. Miklavcic (2018). "Estimation of vegetation indices for high-throughput phenotyping of wheat using aerial imaging." Plant methods **14**(1): 20.
- Kijne, J. W., R. Barker and D. J. Molden (2003). Water productivity in agriculture: limits and opportunities for improvement, Comprehensive Assessment of Water Management in Agriculture Series 1. CABI International, UK.
- Kim, H. W., K. Hwang, Q. Mu, S. O. Lee and M. Choi (2012). "Validation of MODIS 16 global terrestrial evapotranspiration products in various climates and land cover types in Asia." KSCE Journal of Civil Engineering **16**(2): 229-238.
- Kira, O., A. L. Nguy-Robertson, T. J. Arkebauer, R. Linker and A. A. Gitelson (2017). "Toward generic models for green LAI estimation in maize and soybean: Satellite observations." Remote Sensing **9**(4): 318.
- Kooistra, L. and J. G. Clevers (2016). "Estimating potato leaf chlorophyll content using ratio vegetation indices." Remote Sensing Letters **7**(6): 611-620.

- Kprienbaareh, D., X. Sun, J. Wang, I. Luginaah, R. Bezner Kerr, E. Lupafya and L. Dakishoni (2021). "Crop type and land cover mapping in northern Malawi using the integration of sentinel-1, sentinel-2, and planetscope satellite data." Remote Sensing **13**(4): 700.
- Krishna, G., R. N. Sahoo, P. Singh, V. Bajpai, H. Patra, S. Kumar, R. Dandapani, V. K. Gupta, C. Viswanathan and T. Ahmad (2019). "Comparison of various modelling approaches for water deficit stress monitoring in rice crop through hyperspectral remote sensing." Agricultural Water Management **213**: 231-244.
- Krishna, G., R. N. Sahoo, P. Singh, H. Patra, V. Bajpai, B. Das, S. Kumar, R. Dhandapani, C. Vishwakarma and M. Pal (2019). "Application of thermal imaging and hyperspectral remote sensing for crop water deficit stress monitoring." Geocarto International: 1-18.
- Lary, D. J., A. H. Alavi, A. H. Gandomi and A. L. Walker (2016). "Machine learning in geosciences and remote sensing." Geoscience Frontiers **7**(1): 3-10.
- Leroux, L., M. Castets, C. Baron, M.-J. Escorihuela, A. Bégué and D. L. J. E. J. o. A. Seen (2019). "Maize yield estimation in West Africa from crop process-induced combinations of multi-domain remote sensing indices." **108**: 11-26.
- Levidow, L., D. Zaccaria, R. Maia, E. Vivas, M. Todorovic and A. Scardigno (2014). "Improving water-efficient irrigation: Prospects and difficulties of innovative practices." Agricultural Water Management **146**: 84-94.
- Li, B., X. Xu, L. Zhang, J. Han, C. Bian, G. Li, J. Liu, L. J. I. J. o. P. Jin and R. Sensing (2020). "Above-ground biomass estimation and yield prediction in potato by using UAV-based RGB and hyperspectral imaging." **162**: 161-172.
- Li, F., S. Kang and J. Zhang (2004). "Interactive effects of elevated CO<sub>2</sub>, nitrogen and drought on leaf area, stomatal conductance, and evapotranspiration of wheat." Agricultural Water Management **67**(3): 221-233.
- Li, H., W. Yang, J. Lei, J. She and X. Zhou (2021). "Estimation of leaf water content from hyperspectral data of different plant species by using three new spectral absorption indices." PloS one **16**(3): e0249351.
- Li, X., X. Liu, M. Liu, C. Wang and X. Xia (2015). "A hyperspectral index sensitive to subtle changes in the canopy chlorophyll content under arsenic stress." International Journal of Applied Earth Observation and Geoinformation **36**: 41-53.
- Li, X., Y. Zhang, Y. Bao, J. Luo, X. Jin, X. Xu, X. Song and G. Yang (2014). "Exploring the best hyperspectral features for LAI estimation using partial least squares regression." Remote Sensing **6**(7): 6221-6241.
- Li, Z.-L., R. Tang, Z. Wan, Y. Bi, C. Zhou, B. Tang, G. Yan and X. Zhang (2009). "A review of current methodologies for regional evapotranspiration estimation from remotely sensed data." Sensors **9**(5): 3801-3853.

- Liakos, K. G., P. Busato, D. Moshou, S. Pearson and D. Bochtis (2018). "Machine learning in agriculture: A review." Sensors **18**(8): 2674.
- Liang, L., L. Di, T. Huang, J. Wang, L. Lin, L. Wang and M. Yang (2018). "Estimation of leaf nitrogen content in wheat using new hyperspectral indices and a random forest regression algorithm." Remote Sensing **10**(12): 1940.
- Lickley, M. and S. Solomon (2018). "Drivers, timing and some impacts of global aridity change." Environmental Research Letters **13**(10): 104010.
- Lim, J., N. Watanabe, R. Yoshitoshi and K. Kawamura (2020). "Simple in-field evaluation of moisture content in curing forage using normalized difference vegetation index (NDVI)." Grassland Science **66**(4): 238-248.
- Ling, Q., W. Huang and P. Jarvis (2011). "Use of a SPAD-502 meter to measure leaf chlorophyll concentration in Arabidopsis thaliana." Photosynthesis research **107**(2): 209-214.
- Liu, H., J. Zhang, Y. Pan, G. Shuai, X. Zhu and S. Zhu (2018). "An Efficient Approach Based on UAV Orthographic Imagery to Map Paddy With Support of Field-Level Canopy Height From Point Cloud Data." IEEE Journal of Selected Topics in Applied Earth Observations and Remote Sensing.
- Liu, J., J. R. Williams, A. J. Zehnder and H. Yang (2007). "GEPIC-modelling wheat yield and crop water productivity with high resolution on a global scale." Agricultural systems **94**(2): 478-493.
- Liu, L., S. Zhang and B. Zhang (2016). "Evaluation of hyperspectral indices for retrieval of canopy equivalent water thickness and gravimetric water content." International Journal of Remote Sensing **37**(14): 3384-3399.
- Liu, S., Y. Peng, W. Du, Y. Le and L. Li (2015). "Remote estimation of leaf and canopy water content in winter wheat with different vertical distribution of water-related properties." Remote Sensing **7**(4): 4626-4650.
- Liu, X., J. Xu, X. Zhou, W. Wang and S. Yang (2020). "Evaporative fraction and its application in estimating daily evapotranspiration of water-saving irrigated rice field." Journal of Hydrology **584**: 124317.
- Liu, Y., S. Liu, J. Li, X. Guo, S. Wang and J. Lu (2019). "Estimating biomass of winter oilseed rape using vegetation indices and texture metrics derived from UAV multispectral images." Computers and Electronics in Agriculture **166**: 105026.
- Livingston, G., S. Schonberger and S. Delaney (2011). Saharan Africa: The state of smallholders in agriculture. Rome, Italy, International Fund for Agricultural Development (IFAD): 36.
- Losing, V., H. Wersing and B. Hammer (2018). Enhancing very fast decision trees with local split-time predictions. 2018 IEEE international conference on data mining (ICDM), IEEE.

Lowder, S. K., J. Skoet and S. Singh (2014). "What do we really know about the number and distribution of farms and family farms in the world? Background paper for The State of Food and Agriculture 2014."

Lu, B. and Y. He (2019). "Evaluating Empirical Regression, Machine Learning, and Radiative Transfer Modelling for Estimating Vegetation Chlorophyll Content Using Bi-Seasonal Hyperspectral Images." Remote Sensing **11**(17): 1979.

Lu, H.-d., J.-q. Xue and D.-w. Guo (2017). "Efficacy of planting date adjustment as a cultivation strategy to cope with drought stress and increase rainfed maize yield and water-use efficiency." Agricultural Water Management **179**: 227-235.

Luan, J., C. Zhang, B. Xu, Y. Xue and Y. Ren (2020). "The predictive performances of random forest models with limited sample size and different species traits." Fisheries Research **227**: 105534.

Luo, P., J. Liao and G. Shen (2020). "Combining spectral and texture features for estimating leaf area index and biomass of maize using Sentinel-1/2, and Landsat-8 data." IEEE Access **8**: 53614-53626.

Luo, P., J. Liao and G. J. I. A. Shen (2020). "Combining spectral and texture features for estimating leaf area index and biomass of maize using Sentinel-1/2, and Landsat-8 data." **8**: 53614-53626.

Ma, L., T. Fu, T. Blaschke, M. Li, D. Tiede, Z. Zhou, X. Ma and D. Chen (2017). "Evaluation of feature selection methods for object-based land cover mapping of unmanned aerial vehicle imagery using random forest and support vector machine classifiers." ISPRS International Journal of Geo-Information **6**(2): 51.

Mabhaudhi, T., T. Chibarabada and A. Modi (2016). "Water-food-nutrition-health nexus: Linking water to improving food, nutrition and health in Sub-Saharan Africa." International journal of environmental research and public health **13**(1): 107.

Madugundu, R., K. A. Al-Gaadi, E. Tola, A. A. Hassaballa and V. C. Patil (2017). "Performance of the METRIC model in estimating evapotranspiration fluxes over an irrigated field in Saudi Arabia using Landsat-8 images." Hydrology and Earth System Sciences **21**(12): 6135-6151.

Maes, W. H., A. R. Huete, M. Avino, M. M. Boer, R. Dehaan, E. Pendall, A. Griebel and K. R. S. Steppe (2018). "Can UAV-based infrared thermography be used to study plant-parasite interactions between mistletoe and eucalypt trees?" Remote Sensing **10**(12): 2062.

Maes, W. H., A. R. Huete, M. Avino, M. M. Boer, R. Dehaan, E. Pendall, A. Griebel and K. J. R. S. Steppe (2018). "Can UAV-based infrared thermography be used to study plant-parasite interactions between mistletoe and eucalypt trees?" **10**(12): 2062.

Maes, W. H. and K. Steppe (2019). "Perspectives for remote sensing with unmanned aerial vehicles in precision agriculture." Trends in plant science **24**(2): 152-164.

- Mahomed, M., A. D. Clulow, S. Strydom, T. Mabhaudhi and M. J. Savage (2021). "Assessment of a Ground-Based Lightning Detection and Near-Real-Time Warning System in the Rural Community of Swayimane, KwaZulu-Natal, South Africa." Weather, Climate, and Society **13**(3): 605-621.
- Manfreda, S., M. McCabe, P. Miller, R. Lucas, V. Pajuelo Madrigal, G. Mallinis, E. Ben Dor, D. Helman, L. Estes and G. Ciralo (2018). "On the use of unmanned aerial systems for environmental monitoring." Remote sensing **10**(4): 641.
- Manfreda, S., M. F. McCabe, P. E. Miller, R. Lucas, V. Pajuelo Madrigal, G. Mallinis, E. Ben Dor, D. Helman, L. Estes and G. Ciralo (2018). "On the use of unmanned aerial systems for environmental monitoring." Remote sensing **10**(4): 641.
- Mango, N., S. Siziba and C. Makate (2017). "The impact of adoption of conservation agriculture on smallholder farmers' food security in semi-arid zones of southern Africa." Agriculture & Food Security **6**(1): 1-8.
- Mangus, D. L., A. Sharda and N. Zhang (2016). "Development and evaluation of thermal infrared imaging system for high spatial and temporal resolution crop water stress monitoring of corn within a greenhouse." Computers and Electronics in Agriculture **121**: 149-159.
- Marcial-Pablo, M. d. J., A. Gonzalez-Sanchez, S. I. Jimenez-Jimenez, R. E. Ontiveros-Capurata and W. J. I. j. o. r. s. Ojeda-Bustamante (2019). "Estimation of vegetation fraction using RGB and multispectral images from UAV." **40**(2): 420-438.
- Marcial-Pablo, M. d. J., R. E. Ontiveros-Capurata, S. I. Jiménez-Jiménez and W. Ojeda-Bustamante (2021). "Maize Crop Coefficient Estimation Based on Spectral Vegetation Indices and Vegetation Cover Fraction Derived from UAV-Based Multispectral Images." Agronomy **11**(4): 668.
- Markwell, J., J. C. Osterman and J. L. Mitchell (1995). "Calibration of the Minolta SPAD-502 leaf chlorophyll meter." Photosynthesis research **46**(3): 467-472.
- Martínez-Guanter, J., G. Egea, M. Pérez-Ruiz and O. Apolo-Apolo (2019). Estimation of the leaf area index in maize based on UAV imagery using deep learning techniques. Precision agriculture'19, Wageningen Academic Publishers: 1304.
- Mashaba-Munghemezulu, Z., G. J. Chirima and C. Munghemezulu (2021). "Mapping smallholder maize farms using multi-temporal sentinel-1 data in support of the sustainable development goals." Remote Sensing **13**(9): 1666.
- Masiza, W., J. G. Chirima, H. Hamandawana, A. M. Kalumba and H. B. Magagula (2022). "A Proposed Satellite-Based Crop Insurance System for Smallholder Maize Farming." Remote Sensing **14**(6): 1512.
- Masupha, T. E. and M. E. Moeletsi (2020). "The use of Water Requirement Satisfaction Index for assessing agricultural drought on rain-fed maize, in the Luvuvhu River catchment, South Africa." Agricultural Water Management **237**: 106142.

Matese, A., P. Toscano, S. F. Di Gennaro, L. Genesio, F. P. Vaccari, J. Primicerio, C. Belli, A. Zaldei, R. Bianconi and B. Gioli (2015). "Intercomparison of UAV, aircraft and satellite remote sensing platforms for precision viticulture." Remote Sensing **7**(3): 2971-2990.

Matthews, S. (2013). "Dead fuel moisture research: 1991-2012." International Journal of Wildland Fire **23**(1): 78-92.

Matungul, P. M., M. C. Lyne and G. F. J. D. S. A. Ortmann (2001). "Transaction costs and crop marketing in the communal areas of Impendle and Swayimana, KwaZulu-Natal." **18**(3): 347-363.

McEvoy, J. F., G. P. Hall and P. G. McDonald (2016). "Evaluation of unmanned aerial vehicle shape, flight path and camera type for waterfowl surveys: disturbance effects and species recognition." PeerJ **4**: e1831.

McNairn, H., C. Champagne, J. Shang, D. Holmstrom and G. Reichert (2009). "Integration of optical and Synthetic Aperture Radar (SAR) imagery for delivering operational annual crop inventories." ISPRS Journal of Photogrammetry and Remote Sensing **64**(5): 434-449.

Mditshwa, S. (2017). Estimating Maize Grain Yield from Crop Growth Stages Using Remote Sensing and GIS in the Free State Province, South Africa, University of Fort Hare.

Mee, C. Y., S. K. Balasundram and A. H. M. Hanif (2017). "Detecting and Monitoring Plant Nutrient Stress Using Remote Sensing Approaches: A Review." Asian Journal of Plant Sciences **16**: 1-8.

Meroni, M., E. Marinho, N. Sghaier, M. Verstrate and O. Leo (2013). "Remote sensing based yield estimation in a stochastic framework—Case study of durum wheat in Tunisia." Remote Sensing **5**(2): 539-557.

Messina, G. and G. Modica (2020). "Applications of UAV thermal imagery in precision agriculture: State of the art and future research outlook." Remote Sensing **12**(9): 1491.

Mhawej, M. and G. Faour (2020). "Open-source Google Earth Engine 30-m evapotranspiration rates retrieval: The SEBALIGEE system." Environmental Modelling & Software **133**: 104845.

Mi, N., F. Cai, Y. Zhang, R. Ji, S. Zhang and Y. Wang (2018). "Differential responses of maize yield to drought at vegetative and reproductive stages." Plant, Soil and Environment **64**(6): 260-267.

Miao, Y., D. J. Mulla, G. W. Randall, J. A. Vetsch and R. Vintila (2009). "Combining chlorophyll meter readings and high spatial resolution remote sensing images for in-season site-specific nitrogen management of corn." Precision Agriculture **10**(1): 45-62.

Miller, I. J., B. Schieber, Z. De Bey, E. Benner, J. D. Ortiz, J. Girdner, P. Patel, D. G. Coradazzi, J. Henriques and J. Forsyth (2020). Analyzing crop health in vineyards through a multispectral imaging and drone system. 2020 Systems and Information Engineering Design Symposium (SIEDS), IEEE.

- Mink, R., A. Dutta, G. G. Peteinatos, M. Sökefeld, J. J. Engels, M. Hahn and R. Gerhards (2018). "Multi-Temporal Site-Specific Weed Control of *Cirsium arvense* (L.) Scop. and *Rumex crispus* L. in Maize and Sugar Beet Using Unmanned Aerial Vehicle Based Mapping." *Agriculture* **8**(5): 65.
- Miya, S. P., A. T. Modi, S. Z. Tesfay, T. J. S. A. J. o. P. Mabhaudhi and Soil (2018). "Maize grain soluble sugar and protein contents in response to simulated hail damage." **35**(5): 377-383.
- Mkhabela, M. S., M. S. Mkhabela, N. N. J. A. Mashinini and F. Meteorology (2005). "Early maize yield forecasting in the four agro-ecological regions of Swaziland using NDVI data derived from NOAA's-AVHRR." **129**(1-2): 1-9.
- Mobasheri, M. R. and S. B. Fatemi (2013). "Leaf Equivalent Water Thickness assessment using reflectance at optimum wavelengths." *Theoretical and Experimental Plant Physiology* **25**(3): 196-202.
- Mohammadian, M., R. Arfania and H. Sahour (2017). "Evaluation of SEBS algorithm for estimation of daily evapotranspiration using landsat-8 dataset in a semi-arid region of Central Iran." *Open Journal of Geology* **7**(3): 335-347.
- Mokhtari, M., B. Ahmad, H. Hoveidi and I. Busu (2013). "Sensitivity analysis of METRIC-based evapotranspiration algorithm." *International Journal of Environmental Research* **7**(2): 407-422.
- Molden, D., T. Oweis, P. Steduto, P. Bindraban, M. A. Hanjra and J. Kijne (2010). "Improving agricultural water productivity: between optimism and caution." *Agricultural Water Management* **97**(4): 528-535.
- Möller, M., V. Alchanatis, Y. Cohen, M. Meron, J. Tspiris, A. Naor, V. Ostrovsky, M. Sprintsin and S. Cohen (2006). "Use of thermal and visible imagery for estimating crop water status of irrigated grapevine." *Journal of experimental botany* **58**(4): 827-838.
- Monteith, J. (1972). "Solar radiation and productivity in tropical ecosystems." *Journal of Applied Ecology* **9**(3): 747-766.
- Morandé, J. A., R. Trezza, A. Anderson, K. Tha, Y. Paw, Y. Chen, J. Viers and J. Medellín-Azuara (2017). "Appendix K. Evapotranspiration Estimation from Unmanned Aerial Vehicles." UC Water Secur. Sustain. Res. Initiat. Interim Report.
- Morison, J. I., N. R. Baker, P. M. Mullineaux and W. J. Davies (2008). "Improving water use in crop production." *Philosophical Transactions of the Royal Society of London B: Biological Sciences* **363**(1491): 639-658.
- Motohka, T., K. N. Nasahara, H. Oguma and S. Tsuchida (2010). "Applicability of Green-Red Vegetation Index for Remote Sensing of Vegetation Phenology." **2**(10): 2369-2387.
- Mulla, D. J. (2013). "Twenty five years of remote sensing in precision agriculture: Key advances and remaining knowledge gaps." *Biosystems engineering* **114**(4): 358-371.

- Mumo, L., J. Yu and K. Fang (2018). "Assessing impacts of seasonal climate variability on maize yield in Kenya." International Journal of Plant Production **12**(4): 297-307.
- Mungai, L. M., S. Snapp, J. P. Messina, R. Chikowo, A. Smith, E. Anders, R. B. Richardson and G. Li (2016). "Smallholder farms and the potential for sustainable intensification." Frontiers in Plant Science **7**: 1720.
- Mutanga, O., E. Adam and M. A. Cho (2012). "High density biomass estimation for wetland vegetation using WorldView-2 imagery and random forest regression algorithm." International Journal of Applied Earth Observation and Geoinformation **18**: 399-406.
- Mutanga, O., T. Dube and O. Galal (2017). "Remote sensing of crop health for food security in Africa: Potentials and constraints." Remote Sensing Applications: Society and Environment **8**: 231-239.
- Muzari, W., W. Gatsi and S. Muvhunzi (2012). "The impacts of technology adoption on smallholder agricultural productivity in sub-Saharan Africa: A review." Journal of Sustainable Development **5**(8): 69.
- Naito, H., S. Ogawa, M. O. Valencia, H. Mohri, Y. Urano, F. Hosoi, Y. Shimizu, A. L. Chavez, M. Ishitani and M. G. Selvaraj (2017). "Estimating rice yield related traits and quantitative trait loci analysis under different nitrogen treatments using a simple tower-based field phenotyping system with modified single-lens reflex cameras." ISPRS Journal of Photogrammetry and Remote Sensing **125**: 50-62.
- Naumann, G., L. Alfieri, K. Wyser, L. Mentaschi, R. Betts, H. Carrao, J. Spinoni, J. Vogt and L. Feyen (2018). "Global changes in drought conditions under different levels of warming." Geophysical Research Letters **45**(7): 3285-3296.
- Ndlovu, H. S., J. Odindi, M. Sibanda, O. Mutanga, A. Clulow, V. G. Chimonyo and T. Mabhaudhi (2021). "A Comparative Estimation of Maize Leaf Water Content Using Machine Learning Techniques and Unmanned Aerial Vehicle (UAV)-Based Proximal and Remotely Sensed Data." Remote Sensing **13**(20): 4091.
- Ndlovu, H. S., J. Odindi, M. Sibanda, O. Mutanga, A. Clulow, V. G. Chimonyo and T. J. R. S. Mabhaudhi (2021). "A Comparative Estimation of Maize Leaf Water Content Using Machine Learning Techniques and Unmanned Aerial Vehicle (UAV)-Based Proximal and Remotely Sensed Data." **13**(20): 4091.
- Ndlovu, P., J. Thamaga-Chitja and T. Ojo (2021). "Factors influencing the level of vegetable value chain participation and implications on smallholder farmers in Swayimane KwaZulu-Natal." Land Use Policy **109**: 105611.
- Nejad, T. S. (2011). "Effect of drought stress on stomata resistance changes in corn." Journal of American Science **7**(9): 27-31.

Nembilwi, N., H. Chikoore, E. Kori, R. B. Munyai and T. C. Manyanya (2021). "The Occurrence of Drought in Mopani District Municipality, South Africa: Impacts, Vulnerability and Adaptation." Climate **9**(4): 61.

Ngie, A. and F. J. S. A. J. o. G. Ahmed (2018). "Estimation of Maize grain yield using multispectral satellite data sets (SPOT 5) and the random forest algorithm." **7**(1): 11-30.

Ngoune Tandzi, L. and C. S. Mutengwa (2020). "Estimation of maize (*Zea mays* L.) yield per harvest area: Appropriate methods." Agronomy **10**(1): 29.

Nhamo, L., T. Mabhaudhi and M. Magombeyi (2016). "Improving Water Sustainability and Food Security through Increased Crop Water Productivity in Malawi." Water **8**(9): 411.

Nhamo, L., T. Mabhaudhi and A. Modi (2019). "Preparedness or repeated short-term relief aid? Building drought resilience through early warning in southern Africa." Water SA **45**(1): 75-85.

Nhamo, L., T. Mabhaudhi and A. Modi (2019). "Preparedness or repeated short-term relief aid? Building drought resilience through early warning in southern Africa." Water SA **45**(1): 20.

Nhamo, L., J. Magidi, A. Nyamugama, A. D. Clulow, M. Sibanda, V. G. Chimonyo and T. Mabhaudhi (2020). "Prospects of Improving Agricultural and Water Productivity through Unmanned Aerial Vehicles." Agriculture **10**(7): 256.

Nhamo, L., J. Magidi, A. Nyamugama, A. D. Clulow, M. Sibanda, V. G. P. Chimonyo and T. Mabhaudhi (2020). "Prospects of Improving Agricultural and Water Productivity through Unmanned Aerial Vehicles." Agriculture **10**(256).

Nhamo, L., G. Matchaya, T. Mabhaudhi, S. Nhlengethwa, C. Nhemachena and S. Mpandeli (2019). "Cereal production trends under climate change: Impacts and adaptation strategies in southern Africa." Agriculture **9**(2): 30.

Nhamo, L., R. van Dijk, J. Magidi, D. Wiberg and K. Tshikolomo (2018). "Improving the Accuracy of Remotely Sensed Irrigated Areas Using Post-Classification Enhancement Through UAV Capability." Remote Sensing **10**(5): 712.

Nicholls, C. I., M. A. Altieri, A. Dezanet, M. Lana, D. Feistauer and M. Ouriques (2004). "A rapid, farmer-friendly agroecological method to estimate soil quality and crop health in vineyard systems." Biodynamics: 33-39.

Niinemets, Ü. (2001). "Global-scale climatic controls of leaf dry mass per area, density, and thickness in trees and shrubs." Ecology **82**(2): 453-469.

Nisa, Z., M. S. Khan, A. Govind, M. Marchetti, B. Lasserre, E. Magliulo and A. Manco (2021). "Evaluation of SEBS, METRIC-EEFlux, and QWaterModel Actual Evapotranspiration for a Mediterranean Cropping System in Southern Italy." Agronomy **11**(2): 345.

Nisa, Z., M. S. Khan, A. Govind, M. Marchetti, B. Lasserre, E. Magliulo and A. J. A. Manco (2021). "Evaluation of SEBS, METRIC-EEFlux, and QWaterModel Actual Evapotranspiration for a Mediterranean Cropping System in Southern Italy." **11**(2): 345.

Niu, H., T. Zhao, D. Wang and Y. Chen (2019). Estimating evapotranspiration with UAVs in agriculture: A review. 2019 ASABE Annual International Meeting, American Society of Agricultural and Biological Engineers.

Niu, H., T. Zhao, D. Wang and Y. Chen (2019). "Evapotranspiration estimation with UAVs in agriculture: a review."

Noi, P. T., J. Degener and M. Kappas (2017). "Comparison of multiple linear regression, cubist regression, and random forest algorithms to estimate daily air surface temperature from dynamic combinations of MODIS LST data." Remote Sensing **9**(5): 398.

Nouri, H., S. Beecham, F. Kazemi and A. M. Hassanli (2013). "A review of ET measurement techniques for estimating the water requirements of urban landscape vegetation." Urban Water Journal **10**(4): 247-259.

Okonya, J. S., K. Syndikus and J. Kroschel (2013). "Farmers' perception of and coping strategies to climate change: Evidence from six agro-ecological zones of Uganda." Journal of agricultural science **5**(8): 252.

Okunlola, G. O., O. A. Olatunji, R. O. Akinwale, A. Tariq and A. A. Adelusi (2017). "Physiological response of the three most cultivated pepper species (*Capsicum* spp.) in Africa to drought stress imposed at three stages of growth and development." Scientia Horticulturae **224**: 198-205.

Oluwaranti, A., R. Edema, S. Ajayi, C. Atkinson, G. Asea and D. Kwemoyi (2020). "Climate Variability and Its Impacts on the Performance of Elite Uganda Maize Parental Lines." Handbook of Climate Change Management: Research, Leadership, Transformation: 1-18.

Onoda, Y., J. B. Saluñga, K. Akutsu, S. i. Aiba, T. Yahara and N. P. Anten (2014). "Trade-off between light interception efficiency and light use efficiency: implications for species coexistence in one-sided light competition." Journal of Ecology **102**(1): 167-175.

Osakabe, Y., K. Osakabe, K. Shinozaki and L.-S. P. Tran (2014). "Response of plants to water stress." Frontiers in plant science **5**: 86.

Ozelkan, E. (2020). "Water body detection analysis using NDWI indices derived from landsat-8 OLI." Polish Journal of Environmental Studies **29**(2): 1759-1769.

Panda, S. S., D. P. Ames and S. Panigrahi (2010). "Application of vegetation indices for agricultural crop yield prediction using neural network techniques." Remote Sensing **2**(3): 673-696.

Panigrahi, N. and B. Das (2018). "Canopy spectral reflectance as a predictor of soil water potential in rice." Water Resources Research **54**(4): 2544-2560.

- Park, S., D. Ryu, S. Fuentes, H. Chung, E. Hernández-Montes and M. O'Connell (2017). "Adaptive estimation of crop water stress in nectarine and peach orchards using high-resolution imagery from an unmanned aerial vehicle (UAV)." Remote Sensing **9**(8): 828.
- Parmar, H. and N. Gontia (2022). "Evapotranspiration estimation using surface energy balance-based evaporative fraction for water management in canal irrigation command." Journal of the Indian Society of Remote Sensing **50**(2): 373-384.
- Pasqualotto, N., J. Delegido, S. Van Wittenberghe, J. Verrelst, J. P. Rivera and J. Moreno (2018). "Retrieval of canopy water content of different crop types with two new hyperspectral indices: Water Absorption Area Index and Depth Water Index." International journal of applied earth observation and geoinformation **67**: 69-78.
- Pavlovic, D., B. Nikolic, S. Djurovic, H. Waisi, A. Andjelkovic and D. Marisavljevic (2015). "Chlorophyll as a measure of plant health: Agroecological aspects." Pesticides and Phytomedicine **29**(1): 14.
- Pekel, E. (2020). "Estimation of soil moisture using decision tree regression." Theoretical and Applied Climatology **139**(3): 1111-1119.
- Peng, Y., Y. Li, C. Dai, S. Fang, Y. Gong, X. Wu, R. Zhu, K. J. A. Liu and F. Meteorology (2019). "Remote prediction of yield based on LAI estimation in oilseed rape under different planting methods and nitrogen fertilizer applications." **271**: 116-125.
- Peñuelas, J., I. Filella, C. Biel, L. Serrano and R. Save (1993). "The reflectance at the 950-970 nm region as an indicator of plant water status." International journal of remote sensing **14**(10): 1887-1905.
- Pereira, L., P. Paredes, D. Hunsaker, R. López-Urrea and Z. M. Shad (2021). "Standard single and basal crop coefficients for field crops. Updates and advances to the FAO56 crop water requirements method." Agricultural Water Management **243**: 106466.
- Perez-Priego, O., T. S. El-Madany, M. Migliavacca, A. S. Kowalski, M. Jung, A. Carrara, O. Kolle, M. P. Martín, J. Pacheco-Labrador and G. Moreno (2017). "Evaluation of eddy covariance latent heat fluxes with independent lysimeter and sapflow estimates in a Mediterranean savannah ecosystem." Agricultural and forest meteorology **236**: 87-99.
- Pimentel, D., B. Berger, D. Filiberto, M. Newton, B. Wolfe, E. Karabinakis, S. Clark, E. Poon, E. Abbett and S. Nandagopal (2004). "Water Resources: Agricultural and Environmental Issues." BioScience **54**(10): 909-918.
- Pinter Jr, P. J., J. L. Hatfield, J. S. Schepers, E. M. Barnes, M. S. Moran, C. S. Daughtry and D. R. Upchurch (2003). "Remote sensing for crop management." Photogrammetric Engineering & Remote Sensing **69**(6): 647-664.
- Pongnumkul, S., P. Chaovalit and N. Surasvadi (2015). "Applications of smartphone-based sensors in agriculture: a systematic review of research." Journal of Sensors **2015**.

Potgieter, A. B., A. Apan, P. Dunn and G. Hammer (2007). "Estimating crop area using seasonal time series of Enhanced Vegetation Index from MODIS satellite imagery." Australian Journal of Agricultural Research **58**(4): 316-325.

Prakash, A. (2000). "Thermal remote sensing: concepts, issues and applications." International Archives of Photogrammetry and Remote Sensing **33**(B1; PART 1): 239-243.

Prasad, A. M., L. R. Iverson and A. Liaw (2006). "Newer classification and regression tree techniques: bagging and random forests for ecological prediction." Ecosystems **9**(2): 181-199.

Prudnikova, E., I. Savin, G. Vindeker, P. Grubina, E. Shishkonakova and D. Sharychev (2019). "Influence of soil background on spectral reflectance of winter wheat crop canopy." Remote Sensing **11**(16): 1932.

Psirofonia, P., V. Samaritakis, P. Eliopoulos and I. Potamitis (2017). "Use of unmanned aerial vehicles for agricultural applications with emphasis on crop protection: Three novel case-studies." International Journal of Agricultural Science and Technology **5**(1): 30-39.

Qiao, L., D. Gao, R. Zhao, W. Tang, L. An, M. Li, H. J. C. Sun and E. i. Agriculture (2022). "Improving estimation of LAI dynamic by fusion of morphological and vegetation indices based on UAV imagery." **192**: 106603.

Qiu, Z., H. Xiang, F. Ma and C. Du (2020). "Qualifications of rice growth indicators optimized at different growth stages using unmanned aerial vehicle digital imagery." Remote Sensing **12**(19): 3228.

Quan, X. and R. Doluschitz (2021). "Unmanned aerial vehicle (UAV) technical applications, standard workflow, and future developments in maize production-water stress detection, weed mapping, nutritional status monitoring and yield prediction." LANDTECHNIK **76**(1).

Radoglou-Grammatikis, P., P. Sarigiannidis, T. Lagkas and I. Moscholios (2020). "A compilation of UAV applications for precision agriculture." Computer Networks **172**: 107148.

Raeva, P. L., J. Šedina and A. Dlesk (2019). "Monitoring of crop fields using multispectral and thermal imagery from UAV." European Journal of Remote Sensing **52**(sup1): 192-201.

Ramoelo, A., N. Majazi, R. Mathieu, N. Jovanovic, A. Nickless and S. Dziki (2014). "Validation of global evapotranspiration product (MOD16) using flux tower data in the African savanna, South Africa." Remote Sensing **6**(8): 7406-7423.

Ramos, A. P. M., L. P. Osco, D. E. G. Furuya, W. N. Gonçalves, D. C. Santana, L. P. R. Teodoro, C. A. da Silva Junior, G. F. Capristo-Silva, J. Li and F. H. R. Baio (2020). "A random forest ranking approach to predict yield in maize with uav-based vegetation spectral indices." Computers and Electronics in Agriculture **178**: 105791.

- Ramos, A. P. M., L. P. Osco, D. E. G. Furuya, W. N. Gonçalves, D. C. Santana, L. P. R. Teodoro, C. A. da Silva Junior, G. F. Capristo-Silva, J. Li, F. H. R. J. C. Baio and E. i. Agriculture (2020). "A random forest ranking approach to predict yield in maize with uav-based vegetation spectral indices." **178**: 105791.
- Raper, T. and J. Varco (2015). "Canopy-scale wavelength and vegetative index sensitivities to cotton growth parameters and nitrogen status." Precision Agriculture **16**(1): 62-76.
- Rebelo, A. J., S. Gokool, P. B. Holden and M. G. New (2021). "Can Sentinel-2 be used to detect invasive alien trees and shrubs in Savanna and Grassland Biomes?" Remote Sensing Applications: Society and Environment **23**: 100600.
- Ren, H. and G. J. E. I. Zhou (2019). "Estimating green biomass ratio with remote sensing in arid grasslands." **98**: 568-574.
- Reyes-González, A., J. Kjaersgaard, T. Trooien, C. Hay and L. Ahiablame (2018). "Estimation of crop evapotranspiration using satellite remote sensing-based vegetation index." Advances in Meteorology **2018**.
- Rezaei, E. E., G. Ghazaryan, J. González, N. Cornish, O. Dubovyk and S. Siebert (2021). "The use of remote sensing to derive maize sowing dates for large-scale crop yield simulations." International Journal of Biometeorology **65**(4): 565-576.
- Riaño, D., P. Vaughan, E. Chuvieco, P. J. Zarco-Tejada and S. L. Ustin (2005). "Estimation of fuel moisture content by inversion of radiative transfer models to simulate equivalent water thickness and dry matter content: analysis at leaf and canopy level." IEEE Transactions on Geoscience and Remote Sensing **43**(4): 819-826.
- Rockstrom, J. (2000). "Water resources management in smallholder farms in Eastern and Southern Africa: An overview." Physics and Chemistry of the Earth, Part B: Hydrology, Oceans and Atmosphere **25**(3): 275-283.
- Romero-Trigueros, C., P. A. Nortes, J. J. Alarcón, J. E. Hunink, M. Parra, S. Contreras, P. Droogers and E. Nicolás (2017). "Effects of saline reclaimed waters and deficit irrigation on Citrus physiology assessed by UAV remote sensing." Agricultural water management **183**: 60-69.
- Rostami, M., A. R. Koocheki, M. N. Mahallati and M. Kafi (2008). "Evaluation of chlorophyll meter (SPAD) data for prediction of nitrogen status in corn (Zea mays L.)." American-Eurasian Journal Agriculture Science **3**(1): 79-85.
- Ruwaimana, M., B. Satyanarayana, V. Otero, A. M. Muslim, M. Syafiq, S. Ibrahim, D. Raymaekers, N. Koedam and F. Dahdouh-Guebas (2018). "The advantages of using drones over space-borne imagery in the mapping of mangrove forests." PloS one **13**(7): e0200288.
- Sade, N., E. Galkin and M. Moshelion (2015). "Measuring arabidopsis, tomato and barley leaf relative water content (RWC)." Bio-protocol **5**(8): 1451.

- Sade, N., E. Galkin and M. Moshelion (2015). "Measuring Arabidopsis, tomato and barley leaf relative water content (RWC)." Bio-protocol **5**(8): e1451-e1451.
- Sah, R., M. Chakraborty, K. Prasad, M. Pandit, V. Tudu, M. Chakravarty, S. Narayan, M. Rana and D. Moharana (2020). "Impact of water deficit stress in maize: Phenology and yield components." Scientific reports **10**(1): 1-15.
- Salami, A., A. B. Kamara and Z. Brixiova (2010). Smallholder agriculture in East Africa: Trends, constraints and opportunities, African Development Bank Tunis.
- Salamí, E., C. Barrado and E. Pastor (2014). "UAV flight experiments applied to the remote sensing of vegetated areas." Remote Sensing **6**(11): 11051-11081.
- Sandbrook, C. (2015). "The social implications of using drones for biodiversity conservation." Ambio **44**(4): 636-647.
- Sankaran, S., J. M. Maja, S. Buchanon and R. Ehsani (2013). "Huanglongbing (citrus greening) detection using visible, near infrared and thermal imaging techniques." Sensors **13**(2): 2117-2130.
- Saseendran, S., T. Trout, L. Ahuja, L. Ma, G. McMaster, D. Nielsen, A. Andales, J. Chávez and J. Ham (2015). "Quantifying crop water stress factors from soil water measurements in a limited irrigation experiment." Agricultural Systems **137**: 191-205.
- Schut, A. G., P. C. S. Traore, X. Blaes and A. J. F. C. R. Rolf (2018). "Assessing yield and fertilizer response in heterogeneous smallholder fields with UAVs and satellites." **221**: 98-107.
- Scott, G. and A. Rajabifard (2017). "Sustainable development and geospatial information: a strategic framework for integrating a global policy agenda into national geospatial capabilities." Geo-spatial Information Science **20**(2): 59-76.
- Segarra, J., M. L. Buchailot, J. L. Araus and S. C. Kefauver (2020). "Remote sensing for precision agriculture: Sentinel-2 improved features and applications." Agronomy **10**(5): 641.
- Sepulcre-Cantó, G., P. Zarco-Tejada, J. Sobrino, J. Jiménez-Muñoz and F. Villalobos (2005). "Spatial variability of crop water stress in an olive grove with high-spatial thermal remote sensing imagery." Proc. Precision Agric: 267-272.
- Sevara, C., M. Wieser, M. Doneus and N. Pfeifer (2019). "Relative Radiometric Calibration of Airborne LiDAR Data for Archaeological Applications." Remote Sensing **11**(8): 945.
- Shafiee, S., L. M. Lied, I. Burud, J. A. Dieseth, M. Alsheikh and M. Lillemo (2021). "Sequential forward selection and support vector regression in comparison to LASSO regression for spring wheat yield prediction based on UAV imagery." Computers and Electronics in Agriculture **183**: 106036.

Shakhatreh, H., A. H. Sawalmeh, A. Al-Fuqaha, Z. Dou, E. Almaita, I. Khalil, N. S. Othman, A. Khreishah and M. Guizani (2019). "Unmanned Aerial Vehicles (UAVs): A Survey on Civil Applications and Key Research Challenges." IEEE Access **7**: 48572-48634.

Shamshiri, R. R., I. A. Hameed, S. K. Balasundram, D. Ahmad, C. Weltzien and M. Yamin (2018). Fundamental research on unmanned aerial vehicles to support precision agriculture in oil palm plantations. Agricultural Robots-Fundamentals and Applications, IntechOpen.

Sharifi, A. J. J. o. t. S. o. F. and Agriculture (2020). "Remotely sensed vegetation indices for crop nutrition mapping." **100**(14): 5191-5196.

Shelestov, A., M. Lavreniuk, N. Kussul, A. Novikov and S. Skakun (2017). "Exploring Google Earth Engine platform for big data processing: Classification of multi-temporal satellite imagery for crop mapping." frontiers in Earth Science **5**: 17.

Shi, Y., J. A. Thomasson, S. C. Murray, N. A. Pugh, W. L. Rooney, S. Shafian, N. Rajan, G. Rouze, C. L. Morgan and H. L. Neely (2016). "Unmanned aerial vehicles for high-throughput phenotyping and agronomic research." PloS one **11**(7): e0159781.

Sibanda, M. and A. Murwira (2012). "The use of multi-temporal MODIS images with ground data to distinguish cotton from maize and sorghum fields in smallholder agricultural landscapes of Southern Africa." International Journal of Remote Sensing **33**(16): 4841-4855.

Sibanda, M., O. Mutanga, T. Dube and P. L. Mafongoya (2020). "Spectrometric proximally sensed data for estimating chlorophyll content of grasslands treated with complex fertilizer combinations." Journal of Applied Remote Sensing **14**(2): 024517.

Sibanda, M., O. Mutanga, T. Dube, J. Odindi and P. L. Mafongoya (2019). "The Utility of the Upcoming HypsIRI's Simulated Spectral Settings in Detecting Maize Gray Leafy Spot in Relation to Sentinel-2 MSI, VENμS, and Landsat 8 OLI Sensors." Agronomy **9**(12): 846.

Sibanda, M., O. Mutanga, M. Rouget and L. Kumar (2017). "Estimating biomass of native grass grown under complex management treatments using worldview-3 spectral derivatives." Remote Sensing **9**(1): 55.

Sibanda, M., O. Mutanga, M. Rouget and L. J. R. S. Kumar (2017). "Estimating biomass of native grass grown under complex management treatments using worldview-3 spectral derivatives." **9**(1): 55.

Sibanda, M., M. Onisimo, T. Dube and T. Mabhaudhi (2021). "Quantitative assessment of grassland foliar moisture parameters as an inference on rangeland condition in the mesic rangelands of southern Africa." International Journal of Remote Sensing **42**(4): 1474-1491.

Sibanda, M., M. Onisimo, T. Dube and T. J. I. J. o. R. S. Mabhaudhi (2021). "Quantitative assessment of grassland foliar moisture parameters as an inference on rangeland condition in the mesic rangelands of southern Africa." **42**(4): 1474-1491.

Simic Milas, A., J. J. Sousa, T. A. Warner, A. C. Teodoro, E. Peres, J. A. Gonçalves, J. Delgado Garcia, R. Bento, S. Phinn and A. Woodget (2018). "Unmanned Aerial Systems (UAS) for environmental applications special issue preface." International Journal of Remote Sensing **39**(15-16): 4845-4851.

Singh, R. K., K. Khand, S. Kagone, M. Schauer, G. B. Senay and Z. Wu (2020). "A novel approach for next generation water-use mapping using Landsat and Sentinel-2 satellite data." Hydrological Sciences Journal **65**(14): 2508-2519.

Singh, R. K. and G. B. Senay (2015). "Comparison of four different energy balance models for estimating evapotranspiration in the Midwestern United States." Water **8**(1): 9.

Singha, C. and K. C. Swain (2016). "Land suitability evaluation criteria for agricultural crop selection: A review." Agricultural reviews **37**(2).

Singhal, G., B. Bansod, L. Mathew, J. Goswami, B. Choudhury and P. Raju (2019). "Chlorophyll estimation using multi-spectral unmanned aerial system based on machine learning techniques." Remote Sensing Applications: Society and Environment **15**: 100235.

Sinha, P., A. E. Gaughan, F. R. Stevens, J. J. Nieves, A. Sorichetta and A. J. Tatem (2019). "Assessing the spatial sensitivity of a random forest model: Application in gridded population modeling." Computers, Environment and Urban Systems **75**: 132-145.

Sishodia, R. P., R. L. Ray and S. K. Singh (2020). "Applications of remote sensing in precision agriculture: A review." Remote Sensing **12**(19): 3136.

Slattery, R. A., B. J. Walker, A. P. Weber and D. R. Ort (2018). "The impacts of fluctuating light on crop performance." Plant physiology **176**(2): 990-1003.

Solh, M. and M. van Ginkel (2014). "Drought preparedness and drought mitigation in the developing world's drylands." Weather and Climate Extremes **3**: 62-66.

Son, N., C. Chen, C. Chen, L. Chang, H. Duc and L. J. I. J. o. R. S. Nguyen (2013). "Prediction of rice crop yield using MODIS EVI- LAI data in the Mekong Delta, Vietnam." **34**(20): 7275-7292.

Song, L., J. Jin and J. He (2019). "Effects of severe water stress on maize growth processes in the field." Sustainability **11**(18): 5086.

Song, Y., C. Birch, S. Qu, A. Doherty and J. Hanan (2010). "Analysis and modelling of the effects of water stress on maize growth and yield in dryland conditions." Plant Production Science **13**(2): 199-208.

Sow, M., C. Mbow, C. Hély, R. Fensholt and B. Sambou (2013). "Estimation of herbaceous fuel moisture content using vegetation indices and land surface temperature from MODIS data." Remote Sensing **5**(6): 2617-2638.

S

Stratoulas, D., V. Tolpekin, R. A. de By, R. Zurita-Milla, V. Retsios, W. Bijker, M. A. Hasan and E. Vermote (2017). "A Workflow for Automated Satellite Image Processing: from Raw VHRS Data to Object-Based Spectral Information for Smallholder Agriculture." Remote sensing **9**(10): 1048.

Stratoulas, D., V. Tolpekin, R. A. De By, R. Zurita-Milla, V. Retsios, W. Bijker, M. A. Hasan and E. J. R. s. Vermote (2017). "A workflow for automated satellite image processing: From raw VHRS data to object-based spectral information for smallholder agriculture." **9**(10): 1048.

Stroppiana, D., M. Migliazzi, V. Chiarabini, A. Crema, M. Musanti, C. Franchino and P. Villa (2015). Rice yield estimation using multispectral data from UAV: A preliminary experiment in northern Italy. 2015 IEEE International Geoscience and Remote Sensing Symposium (IGARSS), IEEE.

Su, W., J. Huang, D. Liu and M. Zhang (2019). "Retrieving corn canopy leaf area index from multitemporal Landsat imagery and terrestrial LiDAR data." Remote Sensing **11**(5): 572.

Su, Z. (2002). "The Surface Energy Balance System (SEBS) for estimation of turbulent heat fluxes." Hydrology and earth system sciences **6**(1): 85-100.

Sun, Y., Q. Qin, H. Ren, T. Zhang, S. J. I. T. o. G. Chen and R. Sensing (2019). "Red-edge band vegetation indices for leaf area index estimation from sentinel-2/msi imagery." **58**(2): 826-840.

Sylvester, G. (2018). E-agriculture in action: Drones for agriculture. Bangkok, Thailand, Food and Agriculture Organization of the United Nations (FAO) and International Telecommunication Union (ITU): 126.

Taghizadeh-Mehrjardi, R., M. Mahdianpari, F. Mohammadimanesh, T. Behrens, N. Toomanian, T. Scholten and K. Schmidt (2020). "Multi-task convolutional neural networks outperformed random forest for mapping soil particle size fractions in central Iran." Geoderma **376**: 114552.

Taghvaeian, S., J. L. Chávez, W. C. Bausch, K. C. DeJonge and T. J. Trout (2014). "Minimizing instrumentation requirement for estimating crop water stress index and transpiration of maize." Irrigation Science **32**(1): 53-65.

Tahir, M. N., S. Z. A. Naqvi, Y. Lan, Y. Zhang, Y. Wang, M. Afzal, M. J. M. Cheema and S. Amir (2018). "Real time estimation of chlorophyll content based on vegetation indices derived from multispectral UAV in the kinnow orchard." International Journal of Precision Agricultural Aviation **1**(1).

Tan, C.-W., P.-P. Zhang, X.-X. Zhou, Z.-X. Wang, Z.-Q. Xu, W. Mao, W.-X. Li, Z.-Y. Huo, W.-S. Guo and F. J. S. r. Yun (2020). "Quantitative monitoring of leaf area index in wheat of different plant types by integrating NDVI and Beer-Lambert law." **10**(1): 1-10.

Tan, S., B. Wu, N. Yan and W. Zhu (2017). "An NDVI-based statistical ET downscaling method." Water **9**(12): 995.

Tang, J., W. Han and L. Zhang (2019). "UAV Multispectral Imagery Combined with the FAO-56 Dual Approach for Maize Evapotranspiration Mapping in the North China Plain." Remote Sensing **11**(21): 2519.

Tanriverdi, C., A. Atilgan, H. Degirmenci and A. Akyuz (2017). "Comparasion of Crop Water Stress Index (CWSI) and Water Deficit Index (WDI) by using Remote Sensing (RS)." Infrastruktura i Ekologia Terenów Wiejskich(III/1): 879--894.

Tao, H., H. Feng, L. Xu, M. Miao, H. Long, J. Yue, Z. Li, G. Yang, X. Yang and L. J. S. Fan (2020). "Estimation of crop growth parameters using UAV-based hyperspectral remote sensing data." **20**(5): 1296.

Tefera, T., F. Kanampiu, H. De Groote, J. Hellin, S. Mugo, S. Kimenju, Y. Beyene, P. M. Boddupalli, B. Shiferaw and M. Banziger (2011). "The metal silo: An effective grain storage technology for reducing post-harvest insect and pathogen losses in maize while improving smallholder farmers' food security in developing countries." Crop protection **30**(3): 240-245.

Terashima, I., T. Fujita, T. Inoue, W. S. Chow and R. Oguchi (2009). "Green light drives leaf photosynthesis more efficiently than red light in strong white light: revisiting the enigmatic question of why leaves are green." Plant and cell physiology **50**(4): 684-697.

Thorp, K., A. Thompson, S. Harders, A. French and R. Ward (2018). "High-Throughput Phenotyping of Crop Water Use Efficiency via Multispectral Drone Imagery and a Daily Soil Water Balance Model." Remote Sensing **10**(11): 1682.

Tian, H., T. Wang, Y. Liu, X. Qiao and Y. Li (2020). "Computer vision technology in agricultural automation—A review." Information Processing in Agriculture **7**(1): 1-19.

Tilling, A. K., G. J. O'Leary, J. G. Ferwerda, S. D. Jones, G. J. Fitzgerald, D. Rodriguez and R. Belford (2007). "Remote sensing of nitrogen and water stress in wheat." Field Crops Research **104**(1-3): 77-85.

Tilly, N., D. Hoffmeister, H. Schiedung, C. Hütt, J. Brands and G. Bareth (2014). "Terrestrial laser scanning for plant height measurement and biomass estimation of maize." International Archives of the Photogrammetry, Remote Sensing & Spatial Information Sciences.

Tilman, D., C. Balzer, J. Hill and B. L. Befort (2011). "Global food demand and the sustainable intensification of agriculture." Proceedings of the National Academy of Sciences **108**(50): 20260-20264.

Torres-Sánchez, J., J. M. Peña, A. I. de Castro and F. López-Granados (2014). "Multi-temporal mapping of the vegetation fraction in early-season wheat fields using images from UAV." Computers and Electronics in Agriculture **103**: 104-113.

Townshend, J. R. and C. Justice (1986). "Analysis of the dynamics of African vegetation using the normalized difference vegetation index." International Journal of Remote Sensing **7**(11): 1435-1445.

Tsouros, D. C., S. Bibi and P. G. Sarigiannidis (2019). "A review on UAV-based applications for precision agriculture." Information **10**(11): 349.

Tumlisan, G. Y. (2017). Monitoring growth development and yield estimation of maize using very high-resolution UAV-images in Gronau, Germany, University of Twente.

Tumlisan, G. Y. (2017). Monitoring growth development and yield estimation of maize using very high-resolution UAV-images in Gronau, Germany. Masters, University of Twente

Tunca, E., E. S. Köksal, S. Çetin, N. M. Ekiz, H. J. E. m. Balde and assessment (2018). "Yield and leaf area index estimations for sunflower plants using unmanned aerial vehicle images." **190**(11): 1-12.

Ubisi, N. R., P. L. Mafongoya, U. Kolanisi and O. Jiri (2017). "Smallholder farmer's perceived effects of climate change on crop production and household livelihoods in rural Limpopo province, South Africa." Change and Adaptation in Socio-Ecological Systems **3**(1): 27-38.

Uddling, J., J. Gelang-Alfredsson, K. Piikki and H. Pleijel (2007). "Evaluating the relationship between leaf chlorophyll concentration and SPAD-502 chlorophyll meter readings." Photosynthesis research **91**(1): 37-46.

Unganai, L. S. and A. Murwira (2010). Challenges and opportunities for climate change adaptation among smallholder farmers in southeast Zimbabwe. 2nd International Conference: Climate, Sustainability and Development in Semi-arid Regions, Ceará Convention Center, Fortaleza.

Ustin, S. L. and S. Jacquemoud (2020). How the optical properties of leaves modify the absorption and scattering of energy and enhance leaf functionality. Remote sensing of plant biodiversity, Springer, Cham: 349-384.

Ustin, S. L., D. Riaño and E. R. Hunt (2012). "Estimating canopy water content from spectroscopy." Israel Journal of Plant Sciences **60**(1-2): 9-23.

Van der Laan, M., C. Jarman, E. Bastidas-Obando, J. Annandale, M. Fessehazion and D. Haarhoff (2019). "Are water footprints accurate enough to be useful? A case study for maize (*Zea mays* L.)." Agricultural water management **213**: 512-520.

Van der Vyver, C. and S. Peters (2017). "How do plants deal with dry days?" Front. Young Minds **5**: 58.

Vanlauwe, B., D. Coyne, J. Gockowski, S. Hauser, J. Huising, C. Masso, G. Nziguheba, M. Schut and P. Van Asten (2014). "Sustainable intensification and the African smallholder farmer." Current Opinion in Environmental Sustainability **8**(0): 15-22.

Veysi, S., A. A. Naseri, S. Hamzeh and H. Bartholomeus (2017). "A satellite based crop water stress index for irrigation scheduling in sugarcane fields." Agricultural water management **189**: 70-86.

- Vincini, M. and E. Frazzi (2011). "Comparing narrow and broad-band vegetation indices to estimate leaf chlorophyll content in planophile crop canopies." Precision Agriculture **12**(3): 334-344.
- Vitrack-Tamam, S., L. Holtzman, R. Dagan, S. Levi, Y. Tadmor, T. Azizi, O. Rabinovitz, A. Naor and O. Liran (2020). "Random Forest Algorithm Improves Detection of Physiological Activity Embedded within Reflectance Spectra Using Stomatal Conductance as a Test Case." Remote Sensing **12**(14): 2213.
- Vriet, C., E. Russinova and C. Reuzeau (2012). "Boosting crop yields with plant steroids." The Plant Cell **24**(3): 842-857.
- Wagle, P., P. H. Gowda, X. Xiao and K. Anup (2016). "Parameterizing ecosystem light use efficiency and water use efficiency to estimate maize gross primary production and evapotranspiration using MODIS EVI." Agricultural and Forest Meteorology **222**: 87-97.
- Wahab, I., O. Hall and M. Jirström (2018). "Remote Sensing of Yields: Application of UAV Imagery-Derived NDVI for Estimating Maize Vigor and Yields in Complex Farming Systems in Sub-Saharan Africa." Drones **2**(3): 28.
- Wahab, I., O. Hall and M. J. D. Jirström (2018). "Remote sensing of yields: Application of uav imagery-derived ndvi for estimating maize vigor and yields in complex farming systems in sub-saharan africa." **2**(3): 28.
- Wahbi, A. and W. Avery (2018). In Situ Destructive Sampling. Cosmic Ray Neutron Sensing: Estimation of Agricultural Crop Biomass Water Equivalent, Springer, Cham: 5-9.
- Walker, B. J., D. T. Drewry, R. A. Slattery, A. VanLoocke, Y. B. Cho and D. R. Ort (2018). "Chlorophyll can be reduced in crop canopies with little penalty to photosynthesis." Plant Physiology **176**(2): 1215-1232.
- Walker, N. and R. Schulze (2006). "An assessment of sustainable maize production under different management and climate scenarios for smallholder agro-ecosystems in KwaZulu-Natal, South Africa." Physics and Chemistry of the Earth, Parts A/B/C **31**(15-16): 995-1002.
- Wang, L., Y. Lan, Y. Zhang, H. Zhang, M. N. Tahir, S. Ou, X. Liu and P. Chen (2019). "Applications and Prospects of Agricultural Unmanned Aerial Vehicle Obstacle Avoidance Technology in China." Sensors **19**(3): 642.
- Wang, R., K. Cherkauer and L. Bowling (2016). "Corn response to climate stress detected with satellite-based NDVI time series." Remote Sensing **8**(4): 269.
- Wang, S. and V. P. Singh (2017). "Spatio-Temporal Variability of Soil Water Content under Different Crop Covers in Irrigation Districts of Northwest China." Entropy **19**(8): 410.
- Waring, R. and J. Landsberg (2011). "Generalizing plant-water relations to landscapes." Journal of Plant Ecology **4**(1-2): 101-113.

- Watts, A. C., V. G. Ambrosia and E. A. Hinkley (2012). "Unmanned aircraft systems in remote sensing and scientific research: Classification and considerations of use." Remote Sensing **4**(6): 1671-1692.
- Whitford, W. G., A. G. De Soyza, J. W. Van Zee, J. E. Herrick and K. M. Havstad (1998). "Vegetation, soil, and animal indicators of rangeland health." Environmental Monitoring and Assessment **51**(1): 179-200.
- Wijewardana, C., F. A. Alsajri, J. T. Irby, L. J. Krutz, B. Golden, W. B. Henry, W. Gao and K. R. Reddy (2019). "Physiological assessment of water deficit in soybean using midday leaf water potential and spectral features." Journal of Plant Interactions **14**(1): 533-543.
- Williams, G. (2011). Decision trees. Data Mining with Rattle and R, Springer: 205-244.
- Wiratmoko, D., A. E. Prasetyo, R. H. Jatmiko, M. A. Yusuf and S. Rahutomo (2018). "Identification of Ganoderma boninense infection levels on oil palm using vegetation index." International Journal of Oil Palm **1**(3): 110-120.
- Woche, M., K. Berger, M. Danner, W. Mauser and T. Hank (2018). "Physically-based retrieval of canopy equivalent water thickness using hyperspectral data." Remote Sensing **10**(12): 1924.
- Wolfenson, K. D. M. (2013). "Coping with the food and agriculture challenge: smallholders' agenda." Food and Agriculture Organisation of the United Nations, Rome.
- Wu, B., J. Meng, Q. Li, N. Yan, X. Du and M. Zhang (2014). "Remote sensing-based global crop monitoring: experiences with China's CropWatch system." International Journal of Digital Earth **7**(2): 113-137.
- Wu, C., Z. Niu, Q. Tang and W. Huang (2008). "Estimating chlorophyll content from hyperspectral vegetation indices: Modeling and validation." Agricultural and forest meteorology **148**(8-9): 1230-1241.
- Xiang, H. and L. Tian (2011). "Development of a low-cost agricultural remote sensing system based on an autonomous unmanned aerial vehicle (UAV)." Biosystems engineering **108**(2): 174-190.
- Xu, C., J. J. Qu, X. Hao, M. H. Cosh, Z. Zhu and L. Gutenberg (2020). "Monitoring crop water content for corn and soybean fields through data fusion of MODIS and Landsat measurements in Iowa." Agricultural Water Management **227**: 105844.
- Xu, M., C. Lacey and S. Armstrong (2018). "The feasibility of satellite remote sensing and spatial interpolation to estimate cover crop biomass and nitrogen uptake in a small watershed." Journal of Soil and Water Conservation **73**(6): 682-692.
- Xu, Q., S. Liu, X. Wan, C. Jiang, X. Song and J. Wang (2012). "Effects of rainfall on soil moisture and water movement in a subalpine dark coniferous forest in southwestern China." Hydrological Processes **26**(25): 3800-3809.

- Xue, J., K. M. Bali, S. Light, T. Hessels and I. Kisekka (2020). "Evaluation of remote sensing-based evapotranspiration models against surface renewal in almonds, tomatoes and maize." *Agricultural Water Management* **238**: 106228.
- Xue, J. and B. Su (2017). "Significant remote sensing vegetation indices: A review of developments and applications." *Journal of Sensors* **2017**.
- Yang, D., H. Chen and H. Lei (2010). "Estimation of evapotranspiration using a remote sensing model over agricultural land in the North China Plain." *International Journal of Remote Sensing* **31**(14): 3783-3798.
- Yang, G., J. Liu, C. Zhao, Z. Li, Y. Huang, H. Yu, B. Xu, X. Yang, D. Zhu and X. Zhang (2017). "Unmanned Aerial Vehicle Remote Sensing for Field-Based Crop Phenotyping: Current Status and Perspectives." *Frontiers in plant science* **8**: 1111.
- Yang, J. and X. Du (2017). "An enhanced water index in extracting water bodies from Landsat TM imagery." *Annals of GIS* **23**(3): 141-148.
- Yang, K., Y. Gong, S. Fang, B. Duan, N. Yuan, Y. Peng, X. Wu and R. J. R. S. Zhu (2021). "Combining Spectral and Texture Features of UAV Images for the Remote Estimation of Rice LAI throughout the Entire Growing Season." **13**(15): 3001.
- Yao, D., J. Yang and X. Zhan (2013). "An improved random forest algorithm for class-imbalanced data classification and its application in PAD risk factors analysis." *The Open Electrical & Electronic Engineering Journal* **7**(1).
- Yao, H., R. Qin and X. Chen (2019). "Unmanned aerial vehicle for remote sensing applications—A review." *Remote Sensing* **11**(12): 1443.
- Yao, X., N. Wang, Y. Liu, T. Cheng, Y. Tian, Q. Chen and Y. J. R. S. Zhu (2017). "Estimation of wheat LAI at middle to high levels using unmanned aerial vehicle narrowband multispectral imagery." **9**(12): 1304.
- Yeganefar, A., S. A. Niknam and R. Asadi (2019). "The use of support vector machine, neural network, and regression analysis to predict and optimize surface roughness and cutting forces in milling." *The International Journal of Advanced Manufacturing Technology* **105**(1): 951-965.
- Yi, Q., F. Wang, A. Bao and G. Jiapaer (2014). "Leaf and canopy water content estimation in cotton using hyperspectral indices and radiative transfer models." *International Journal of Applied Earth Observation and Geoinformation* **33**: 67-75.
- Yordanov, I., T. Tsonev, V. Goltsev, L. Kruleva and V. Velikova (1997). "Interactive effect of water deficit and high temperature on photosynthesis of sunflower and maize plants. 1. Changes in parameters of chlorophyll fluorescence induction kinetics and fluorescence quenching." *Photosynthetica* **33**(3): 391-402.

- Yu, H., G. Yin, G. Liu, Y. Ye, Y. Qu, B. Xu and A. Verger (2021). "Validation of Sentinel-2, MODIS, CGLS, SAF, GLASS and C3S Leaf Area Index Products in Maize Crops." Remote Sensing **13**(22): 4529.
- Yuan, H., G. Yang, C. Li, Y. Wang, J. Liu, H. Yu, H. Feng, B. Xu, X. Zhao and X. Yang (2017). "Retrieving soybean leaf area index from unmanned aerial vehicle hyperspectral remote sensing: Analysis of RF, ANN, and SVM regression models." Remote Sensing **9**(4): 309.
- Yue, J., H. Feng, X. Jin, H. Yuan, Z. Li, C. Zhou, G. Yang and Q. Tian (2018). "A comparison of crop parameters estimation using images from UAV-mounted snapshot hyperspectral sensor and high-definition digital camera." Remote Sensing **10**(7): 1138.
- Yue, J., H. Feng, G. Yang and Z. Li (2018). "A comparison of regression techniques for estimation of above-ground winter wheat biomass using near-surface spectroscopy." Remote Sensing **10**(1): 66.
- Yun, S. K., S. J. Kim, E. Y. Nam, J. H. Kwon, Y. S. Do, S.-Y. Song, M. Kim, Y. Choi, G. Kim and H. Shin (2020). "Evaluation of water stress using canopy temperature and crop water stress index (CWSI) in peach trees." Protected Horticulture and Plant Factory **29**(1): 20-27.
- Zarco-Tejada, P. J., V. González-Dugo and J. A. Berni (2012). "Fluorescence, temperature and narrow-band indices acquired from a UAV platform for water stress detection using a micro-hyperspectral imager and a thermal camera." Remote sensing of environment **117**: 322-337.
- Zarco-Tejada, P. J., J. Pushnik, S. Dobrowski and S. Ustin (2003). "Steady-state chlorophyll a fluorescence detection from canopy derivative reflectance and double-peak red-edge effects." Remote Sensing of Environment **84**(2): 283-294.
- Zhang, C., J. Liu, J. Shang and H. Cai (2018). "Capability of crop water content for revealing variability of winter wheat grain yield and soil moisture under limited irrigation." Science of the Total Environment **631**: 677-687.
- Zhang, C., E. Pattey, J. Liu, H. Cai, J. Shang and T. Dong (2017). "Retrieving leaf and canopy water content of winter wheat using vegetation water indices." IEEE Journal of Selected Topics in Applied Earth Observations and Remote Sensing **11**(1): 112-126.
- Zhang, F. and G. Zhou (2015). "Estimation of canopy water content by means of hyperspectral indices based on drought stress gradient experiments of maize in the north plain China." Remote Sensing **7**(11): 15203-15223.
- Zhang, F. and G. Zhou (2019). "Estimation of vegetation water content using hyperspectral vegetation indices: A comparison of crop water indicators in response to water stress treatments for summer maize." BMC ecology **19**(1): 18.
- Zhang, F. and G. Zhou (2019). "Estimation of vegetation water content using hyperspectral vegetation indices: A comparison of crop water indicators in response to water stress treatments for summer maize." BMC ecology **19**(1): 1-12.

- Zhang, G., B. Ming, D. Shen, R. Xie, P. Hou, J. Xue, K. Wang and S. Li (2021). "Optimizing grain yield and water use efficiency based on the relationship between leaf area index and evapotranspiration." *Agriculture* **11**(4): 313.
- Zhang, H., Y. Lan, R. Lacey, W. Hoffmann and Y. Huang (2009). "Analysis of vegetation indices derived from aerial multispectral and ground hyperspectral data." *International Journal of Agricultural and Biological Engineering* **2**(3): 33-40.
- Zhang, J., B. Basso, R. F. Price, G. Putman and G. Shuai (2018). "Estimating plant distance in maize using Unmanned Aerial Vehicle (UAV)." *PloS one* **13**(4): e0195223.
- Zhang, L., Y. Niu, H. Zhang, W. Han, G. Li, J. Tang and X. Peng (2019). "Maize canopy temperature extracted from UAV thermal and RGB imagery and its application in water stress monitoring." *Frontiers in plant science* **10**: 1270.
- Zhang, L., Y. Niu, H. Zhang, W. Han, G. Li, J. Tang and X. J. F. i. p. s. Peng (2019). "Maize canopy temperature extracted from UAV thermal and RGB imagery and its application in water stress monitoring." **10**: 1270.
- Zhang, L., H. Zhang, Y. Niu and W. Han (2019). "Mapping Maize Water Stress Based on UAV Multispectral Remote Sensing." *Remote Sensing* **11**(6): 605.
- Zhang, L., H. Zhang, Y. Niu and W. J. R. S. Han (2019). "Mapping maize water stress based on UAV multispectral remote sensing." **11**(6): 605.
- Zhang, L., Z. Zhou, G. Zhang, Y. Meng, B. Chen and Y. Wang (2012). "Monitoring the leaf water content and specific leaf weight of cotton (*Gossypium hirsutum* L.) in saline soil using leaf spectral reflectance." *European Journal of Agronomy* **41**: 103-117.
- Zhang, X., Y. He, C. Wang, F. Xu, X. Li, C. Tan, D. Chen, G. Wang and L. Shi (2019). "Estimation of Corn Canopy Chlorophyll Content Using Derivative Spectra in the O2-A Absorption Band." *Frontiers in plant science* **10**: 1047.
- Zhang, X., J. Zhao, G. Yang, J. Liu, J. Cao, C. Li, X. Zhao and J. J. R. S. Gai (2019). "Establishment of Plot-Yield Prediction Models in Soybean Breeding Programs Using UAV-Based Hyperspectral Remote Sensing." **11**(23): 2752.
- Zhao, L., Shi, Y, Liu, B, Hovis, C, Duan, Y Shi, Z. 2019 (2019). "Finer Classification of Crops by Fusing UAV Images and Sentinel-2A Data." *Remote sensing* **11**.
- Zhao, X., C. Tong, X. Pang, Z. Wang, Y. Guo, F. Du and R. Wu (2012). "Functional mapping of ontogeny in flowering plants." *Briefings in bioinformatics* **13**(3): 317-328.
- Zheng, H., T. Cheng, M. Zhou, D. Li, X. Yao, Y. Tian, W. Cao and Y. J. P. A. Zhu (2019). "Improved estimation of rice aboveground biomass combining textural and spectral analysis of UAV imagery." **20**(3): 611-629.

Zhou, H., G. Zhou, Q. He, L. Zhou, Y. Ji and M. Zhou (2020). "Environmental explanation of maize specific leaf area under varying water stress regimes." Environmental and Experimental Botany **171**: 103932.

Zhou, L., Y. Wang, Q. Jia, R. Li, M. Zhou and G. Zhou (2019). "Evapotranspiration over a rainfed maize field in northeast China: How are relationships between the environment and terrestrial evapotranspiration mediated by leaf area?" Agricultural Water Management **221**: 538-546.

Zhou, X., H. Zheng, X. Xu, J. He, X. Ge, X. Yao, T. Cheng, Y. Zhu, W. Cao and Y. Tian (2017). "Predicting grain yield in rice using multi-temporal vegetation indices from UAV-based multispectral and digital imagery." ISPRS Journal of Photogrammetry and Remote Sensing **130**: 246-255.

Zhu, Y., K. Liu, L. Liu, S. W. Myint, S. Wang, H. Liu and Z. He (2017). "Exploring the potential of worldview-2 red-edge band-based vegetation indices for estimation of mangrove leaf area index with machine learning algorithms." Remote Sensing **9**(10): 1060.

Ziliani, M. G., S. D. Parkes, I. Hoteit and M. F. J. R. S. McCabe (2018). "Intra-season crop height variability at commercial farm scales using a fixed-wing UAV." **10**(12): 2007.

## APPENDICES

### Appendix A: List of Publications

1. Buthelezi, S., Mutanga, O., Sibanda, M., Odindi, J., Clulow, A.D., Chimonyo, V.G. and Mabhaudhi, T., 2023. Assessing the Prospects of Remote Sensing Maize Leaf Area Index Using UAV-Derived Multi-Spectral Data in Smallholder Farms across the Growing Season. *Remote Sensing*, 15(6), p.1597.
2. Brewer, K., Clulow, A., Sibanda, M., Gokool, S., Odindi, J., Mutanga, O., Naiken, V., Chimonyo, V.G. and Mabhaudhi, T., 2022. Estimation of maize foliar temperature and stomatal conductance as indicators of water stress based on optical and thermal imagery acquired using an Unmanned Aerial Vehicle (UAV) platform. *Drones*, 6(7), p.169.
3. Brewer, K., Clulow, A., Sibanda, M., Gokool, S., Naiken, V. and Mabhaudhi, T., 2022. Predicting the chlorophyll content of maize over phenotyping as a proxy for crop health in smallholder farming systems. *Remote Sensing*, 14(3), p.518.
4. Ndlovu, H.S., Odindi, J., Sibanda, M., Mutanga, O., Clulow, A., Chimonyo, V.G. and Mabhaudhi, T., 2021. A comparative estimation of maize leaf water content using machine learning techniques and unmanned aerial vehicle (UAV)-based proximal and remotely sensed data. *Remote Sensing*, 13(20), p.4091.
5. Nhamo, L., Magidi, J., Nyamugama, A., Clulow, A.D., Sibanda, M., Chimonyo, V.G. and Mabhaudhi, T., 2020. Prospects of improving agricultural and water productivity through unmanned aerial vehicles. *Agriculture*, 10(7), p.256.

## Appendix B: List of Conferences Presentations

- 1) Sibanda, M., Ndlovu, H., Brewer RK., Buthelezi, S., Odindi, J. Mutanga, O., Clulow, A., Chimonyo, V., and Mabhaudhi, T. (2022). Detecting the impact of hail damage on maize crops in smallholder farms using Unmanned aerial vehicles derived from multispectral data. 13th African Association for Remote Sensing of the Environment. 29th November – 1st of December 2021, Kigali Conference and Exhibition Village, Kigali, Rwanda.
- 2) Ndlovu, H., Odindi, J. Sibanda, M., Mutanga, O., Clulow, A., Chimonyo, V., and Mabhaudhi, T. (2022). Comparative Estimation of Maize Leaf Water Content Using Machine Learning Techniques and Unmanned Aerial Vehicle (UAV)-Based Proximal and Remotely Sensed Data. 13th African Association for Remote Sensing of the Environment. 24th – 28th October 2022, Kigali Conference and Exhibition Village, Kigali, Rwanda.
- 3) Sibanda, M., Ndlovu, H., Brewer RK., Buthelezi, S., Odindi, J. Mutanga, O., Clulow, A., Chimonyo, V., and Mabhaudhi, T. (2022). Detecting the impact of hail damage on maize crops in smallholder farms using Unmanned aerial vehicles derived from multispectral data. 2nd Drone Users Conference: Conservation and Agriculture. 9th – 1st of December 2021, Elsenburg, Stellenbosch, Western Cape, South Africa.
- 4) Ndlovu, H., Odindi, J. Sibanda, M., Mutanga, O., Clulow, A., Chimonyo, V., and Mabhaudhi, T. (2021). A Comparative Estimation of Maize Leaf Water Content Using Machine Learning Techniques and Unmanned Aerial Vehicles (UAV)-Based Proximal and Remotely Sensed Data. 2nd Drone Users Conference: Conservation and Agriculture. 9th – 1st of December 2021, Elsenburg, Stellenbosch, Western Cape, South Africa.
- 5) Buthelezi, S., Mutanga, O., Sibanda, M, Odindi, J. Clulow, A., Chimonyo, V., and Mabhaudhi, T. (2021). Estimating Leaf Area Index of Maize Crops using Unmanned Aerial Vehicles (UAV) Acquired Remotely Sensed Data. 2nd Drone Users Conference: Conservation and Agriculture. 9th – 1st of December 2021, Elsenburg, Stellenbosch, Western Cape, South Africa.

### Appendix C: List of Post Doctoral Fellows and Graduated Students

<b>Name</b>	<b>Degree Programme</b>	<b>University</b>	<b>Year</b>
Yola Kamteni	Honours in Geography	University of the Western Cape	2021
Kiara R Brewer	MSc Agrometeorology	University of KwaZulu-Natal	2022
Helen S Ndlovu	MSc Environmental Science	University of KwaZulu-Natal	2022
Siphiwokuhle Buthelezi	MSc Environmental Science	University of KwaZulu-Natal	2022
Dr T Matongera	Environmental Science	University of KwaZulu-Natal	2023
Dr S Gokool	Hydrology	University of KwaZulu-Natal	2022
Dr M Sibanda	Environmental Science	University of KwaZulu-Natal	2020
Dr V G P Chimonyo	Crop Science	University of KwaZulu-Natal	2020

## Appendix D: List of Continuing Students

<b>Student Name</b>	<b>Degree Programme</b>	<b>University</b>	<b>Estimated Year of Completion</b>
Mpho S Kapari	MA Environmental Studies	University of the Western Cape	2023
Amanda N Nyawose	MSc Hydrology	University of KwaZulu-Natal	2023